Title
Experimental Study of Water Droplet Vaporization on Nanostructured Surfaces

Author
Padilla, Jorge

Publication Date
2014

Peer reviewed|Thesis/dissertation

Experimental Study of Water Droplet Vaporization on Nanostructured Surfaces

by

Jorge Padilla, Jr.

A dissertation submitted in partial satisfaction of the

requirements for the degree of

Doctor of Philosophy

in

Engineering - Mechanical Engineering

and the Designated Emphasis

in

Energy Science and Technology

in the

Graduate Division

of the

University of California, Berkeley

Committee in charge:

Professor Van P. Carey, Chair
Adjunct Professor Samuel S. Mao
Professor Ralph Greif
Professor Per Peterson

Fall 2014

Experimental Study of Water Droplet Vaporization on Nanostructured Surfaces

Abstract

Experimental Study of Water Droplet Vaporization on Nanostructured Surfaces

by

Jorge Padilla, Jr.

Doctor of Philosophy in Engineering - Mechanical Engineering

University of California, Berkeley

Professor Van P. Carey, Chair

This dissertation summarizes results of an experimental exploration of heat transfer during vaporization of a water droplet deposited on a nanostructured surface at a temperature approaching and exceeding the Leidenfrost point for the surface and at lower surface temperatures, 10{40° above the saturated temperature of the water droplet at approximately 101 kPa. The results of these experiments were compared to those performed on bare smooth copper and aluminum surfaces in this and other studies.

The nanostructured surfaces were composed of a vast array of zinc oxide (ZnO) nanocrystals grown by hydrothermal synthesis on a smooth copper substrate having an average surface roughness of approximately 0.06μm. Various nanostructured surface array geometries were produced on the copper substrate by performing the hydrothermal synthesis for 4, 10 and 24 hours. The individual nanostructures were randomly-oriented and, depending on hydrothermal synthesis time, had a mean diameter of about 500{700 nm, a mean length of 1.7{3.3 μm and porosities of approximately 0.04{0.58.

Surface wetting was characterized by macroscopic measurements of contact angle based on the droplet pro le and calculations based on measurements of liquid lm spread area. Scanning electron microscope imaging was used to document the nanoscale features of the surface before and after the experiments. The nanostructured surfaces grown by hydrothermal synthesis for 4 and 24 hours exhibited contact angles of approximately 10°, whereas the surfaces grown for 10 hours were superhydrophilic, exhibiting contact angles typically less than 3°.

In single droplet deposition experiments at 101 kPa, a high-speed video camera was used to document the droplet-surface interaction. Distilled and degassed water droplets ranging in size from 2.5{4.0 mm were deposited onto the surface from heights ranging from approximately 0.2{8.1 cm, such that Weber numbers spanned a range of approximately 0{99. Heat transfer coe cients were determined from thermal measurements in the test apparatus. All experiments were conducted inside an ISO Class 5 clean room enclosure

It was observed that when a liquid water droplet impinged upon the ZnO nanostructured at surface temperatures less than 140°C, the nominally spherical droplet spread into a thin

lm over the surface. The lm thickness depended on many parameters but in general it measured approximately 100{400 m. As a result it was found that the droplet evaporated by lm evaporation without initiaing nucleate boiling. At wall superheat levels of 10{20°C, it was found in some cases that the heat transfer coe cients were nearly 4 times greater than for those of nucleate boiling at the same superheat level. For these conditions, no bubble nucleation was observed visually, and, nevertheless, extremely high heat transfer coe cients resulting from rapid evaporation of the thin liquid lm formed by the spreading droplet were observed.

At high wall superheat levels, the vaporization process exhibited Leidenfrost droplet vaporization. The extreme wetting of the nanostructured surfaces resulted in high Leidenfrost transition temperatures in the range of 310{376°C, among the highest in the literature, exceeding those exhibited by bare metal surfaces by 100°C or more. The Leidenfrost transition was detected from a recording of the acoustic signal generated from each experiment during the deposition and subsequent evaporation process. It was de ned as the rst point for which there is no disturbance to the acoustical signal in the form of a sizzling sound beyond the initial violent popping generated during the droplet deposition. The results document a trend of increasing Leidenfrost temperature with decreasing contact angle, which is consistent with earlier studies. The results of this study are compared with earlier work in this area and the implications for applications are discussed.

A mis padres...

cuyo amor abnegado por sus hijos siempre ha sido su mayor motivo para trabajar y vivir. Les dedico esta tesis como una pequeña muestra del agradecimiento e infinito amor que siento por ustedes. Gracias, Mama y Papa. Dios los bendiga.

Contents

List of Figures

List of Tables

Acknowledgments

Many, many thanks to my research advisor and dissertation committee chair, Professor Van P. Carey for his guidance, patience and mentorship throughout my masters and doctoral research. It has been a great honor and privilege to work with you and I look forward to our future collaboration.

Many thanks to Professor Ernest G. Cravalho of the Department of Mechanical Engineering at the Massachusetts Institute of Technology. Thank you for your mentorship, friendship and financial support of this research. You first inspired my love of the thermal sciences in 2.005 in the fall semester of 2003. Your commitment to service to society continues to inspire my work to this day. Go Bears!

Thanks to the members of my dissertation committee, Professor Ralph Greif, Professor Sam Mao and Professor Per Peterson for your review and feedback. Your assistance was invaluable.

Financial support of this research from the A. Richard Newton Chair of Engineering, the Alfred P. Sloan Foundation Graduate Scholarship Program, the California Legislative Grant, the Department of Mechanical Engineering at UC Berkeley, the College of Engineering at UC Berkeley, the Chancellor's Fellowship for Graduate Study and the Ralph A. Seban Heat Transfer Fellowship is gratefully acknowledged.

Many thanks as well to the current and former staff of the Department of Mechanical Engineering at UC Berkeley including Yawo Dagbevi Akpawu, Isabel Blanco, Donna Craig, Pat Giddings, and Shareena Samson. Your help and patience throughout the years is greatly appreciated.

A very special thanks to the staff in the Mechanical Engineering Student Machine Shop at UC Berkeley including Mick Franssen, Dennis Lee, Gordon Long and Jesse Lopez. Your technical support and guidance were indispensable to the completion of this research project.

My deepest gratitude to my family, friends and loved ones, including my parents, my brother, Oscar, Rosailda Perez, Miguel Amaya, Hector Mendoza, Kenneth Armijo, Reynaldo Guerra, Roberto Rangel, Eugenio Urquiza, Esther Zeledon, Yu Gan, Sara Beaini, David Lettieri, Maritza Ruiz, Vince Romanin, Michael Toulouse, Beatriz Lopez Flores, Adam Luftman and Maestro David Milnes and the UC Berkeley Symphony Orchestra.

Finally, thanks and glory be to God, through whom all is possible.

Chapter 1

Introduction - Water droplet vaporization from nanostructured surfaces at low and high superheats

The mechanisms for vaporization of a liquid water droplet deposited on a heated solid surface depend primarily on the wetting characteristics of the surface, the surface morphology, and the surface temperature [1]. This dissertation summarizes results of an experimental exploration of heat transfer during vaporization of water droplets deposited on hydrophilic and superhydrophilic nanostructured surfaces at temperatures approaching and exceeding the Leidenfrost point and at lower surface temperatures, 10{40°C above the saturated temperature of water at 101 kPa. In this study surfaces exhibiting contact angles less than 5° are considered superhydrophilic.

For hydrophilic surfaces, at moderate to high surface temperatures, deposited droplets tend to wet and quickly spread over the solid surface rather than bounce or shatter. At low surface superheat temperatures that are below the onset of nucleate boiling temperature, droplets spread and liquid is converted to vapor in a liquid lm evaporation process. At wall temperatures above the Leidenfrost transition, deposited droplets initially touch, or come into close proximity to the surface and then spontaneously form a stable vapor lm under the droplet. This typically results in slower evaporation driven by a lm boiling process in which heat is transferred across the vapor lm under the droplet. At wall superheats above the onset of nucleate boiling temperature, but below the Leidenfrost temperature, a deposited droplet generally spreads on the solid surface and vaporizes by the combined mechanisms of lm evaporation and nucleate boiling. Of the three regimes of droplet evaporation described above, the hydrophilic and superhydrophilic nature of the surfaces considered in this study is expected to have the most impact on vaporization at superheat levels below the onset of nucleate boiling, and on the Leidenfrost transition conditions for incipient lm boiling.

The vaporization of water droplets at low surface superheats due to liquid lm evaporation is a process that is important in a variety of applications that require heat removal from solid surfaces. Important applications of this type include spray cooling of metal forgings and

castings, re suppression, core re- ooding in water-cooled nuclear reactor accident scenarios, and spray cooling augmentation of Rankine power plant air-cooled condensers. In most applications of interest, water spray cooling is applied to surfaces that are moderately wetted to poorly wetted. Moderate wetting is typical of water droplets on common metallic surfaces at low temperatures, whereas more poorly wetted behavior is typical of low surface energy and fabricated hydrophobic surfaces and surfaces at temperatures above the Leidenfrost point. Given the importance of these circumstances to applications, it is not surprising that virtually all of the prior studies of the physics of droplet impingement and vaporization mechanisms associated with spray cooling have focused on moderately wetted or poorly wetted surfaces with contact angles between 20 and 180 (see, for example [2]{[26]). For such circumstances, studies have demonstrated that the dynamic deformation of droplets that impinge and spread on a solid surface can result in oscillation of the droplet pro le, droplet bouncing, or breakup of the droplet into smaller droplets that are ejected away from the surface [18]{[26].

In hybrid air-cooled condensers for power plants, water spray cooling is intermittently used to enhance the performance of the condenser to lower steam condensing temperature in the Rankine cycle and enhance cycle performance to compensate for temporary increases of ambient air temperatures in hot weather, or to increase power output during high demand periods. Increasingly, power plant operators want to minimize the use of water for this purpose because increasing water demand for cities and agriculture is expected to reduce its availability at many power plant locations. Water may also be intrinsically scarce at solar Rankine thermal power generation sites built in arid locations to maximize solar radiation availability.

To maximize the e ectiveness and minimize the use of water in spray cooling of condensers, an ideal system would deliver the water to the heat exchanger air surfaces so that it spreads on the surface and evaporates there without droplet splashing and/or breakup that result in some of the water being carried away by the air ow without evaporating and cooling the surface. Such carryover water is wasted since it does not contribute to evaporative cooling of the condenser air-side surface. For this application, it is desirable to avoid bouncing of droplets or breakup production of secondary droplets that may be entrained into the air ow and carried away without evaporating on the surface to enhance cooling. If the power plant condenser air-side surfaces are coated with a superhydrophilic coating, i.e. a surface which exhibits contact angles less than 5, when droplets impinge on the coating, interfacial tension and wetting forces will tend to spread the droplet rapidly over the surface, forming a thin liquid layer that will rapidly evaporate. This will tend to diminish the tendency for droplet oscillations, break-up or bouncing that can occur at conventional surfaces with higher contact angles.

Because previous studies have generally focused on droplet evaporation on moderate to poorly wetted surfaces, the physics of droplet impingement and evaporation on superhydrophilic surfaces have not been thoroughly explored. However, for superhydrophilic surfaces, the nature of such surfaces suggests that impinging droplets will tend to rapidly spread into a thin liquid lm, allowing rapid transfer of heat across the liquid lm and rapid vapor-

ization of liquid at the liquid-gas interface. In addition to the resulting strong heat transfer performance, the rapid spread of the droplet into a very thin liquid lm due to liquid-solid attractive forces is likely to reduce the tendency for an impinging droplet to splash, bounce, or breakup and eject droplets. This will tend to reduce the probability that liquid will entrain and be carried away by the air ow through the condenser, and make it more likely that droplets will rapidly evaporate on the surface without loss of liquid due to entrainment. This suggests that spray cooling of power plant condensers can be enhanced, and carryover losses of water for the process can be signi cantly reduced by coating the air-side surface with a thin superhydrophilic layer that conducts heat e ciently.

In this study, the exploration of heat transfer for water droplets deposited on superhydrophilic surfaces at low superheat levels is motivated by the potential use of such surfaces to enhance water spray cooling in power plant condensers and other low temperature spray cooling applications. In some spray cooling applications, such as quenching of forged aluminum parts and re suppression, surface temperatures may be close to the Leidenfrost transition. In this study, the exploration of the thermophysics of the Leidenfrost transition on superhydrophilic surfaces is motivated by a desire to better understand how this transition is a ected by the extreme wettability of such surfaces.

In an experimental study and literature review, Bernardin and Mudawar summarize the results of research on the Leidenfrost point in the last half-century [27] . Much of the research described in that study focuses on the wide variation and often con icting information resulting from Leidenfrost experiments. In general, investigators of the Leidenfrost phenomenon concentrated on the role of many parameters that include, but are not limited to, surface material, nish, cleanliness, wettability, liquid droplet size, contact angle, subcooling and pressure.

More recently, various micro- and nanofabrication techniques and surface material substrates have been employed to understand the e ects of surface roughness, nanoporosity and surface wettability on the Leidenfrost point [28]{[32]. In general, it has been found that Leidenfrost point increases with surface wettability and decreases with increasingly non-wetting surfaces. The ability to produce superhydrophilic and superhydrophobic surfaces from micro- and nanofabrication techniques has shifted research e orts toward investigating the e ect of the extreme wetting and non-wetting on the Leidenfrost phenomenon. Kim et al. [30] fabricated microposts on a silicon substrate to vary surface roughness, sputtered gold (100 nm thick) and SiO_2 (20 nm thick) to vary wettability and deposited SiO_2 nanoparticles (600 nm thick) on a silicon substrate to study the e ect of nanoporosity. They found that only the nanoporous surface, which exhibited a contact angle of approximately 0°, to have a signi cant e ect on the Leidenfrost point, elevating it to 359°C. The other surfaces they studied yielded Leidenfrost points in the range of 264{274°C which is typical of many surfaces previously studied [27]. Furthermore, Kruse et al. [31] produced nanostructured and nanoporous surfaces on a 304 stainless steel surface by femtosecond laser surface processing. The contact angles of the surfaces varied from 0{15°. A surface with pyramid microstructures 14 μm tall with 25 μm separation distance and self-assembled nanoparticles resulted in a Leidenfrost temperature of 455°C compared with 280°C for polished stainless steel.

The results of these studies indicate that highly wetting, superhydrophilic nanostructured surfaces may exhibit Leidenfrost transition temperatures well above the plateau temperature range of 250{300°C often observed for common surfaces with moderate contact angles [27].

In this study, the e ect of hydrophilic and superhydrophilic nanostructured surfaces on the Leidenfrost transition and low superheat temperature was further investigated experimentally. In contrast to some of the most recent studies which use semiconductor substrates, the substrate material of choice is copper due to its practicality as a metal in common heat transfer equipment. Zinc oxide (ZnO) nanocrystals are synthesized on a smooth R_a ($\approx$ 0.056 μm) copper substrate by a low temperature (90{95°C) hydrothermal method mod- i ed slightly from that developed by Yang et al. [33]. In contrast with previous studies, therefore, the nanostructured surfaces are composed of two classes of materials, a metal, i.e. the copper substrate and a semiconductor, i.e. the ZnO nanostructures. The resulting surfaces are hydrophilic and superhydrophilic, which is consistent with the observations of Lee et al. [34]. From a practical perspective, the hydrothermal synthesis method used to generate the ZnO nanostructures is scalable such that it can be used potentially to produce nanostructured surfaces on large surface areas such as those used in industrial and power generation applications. Furthermore, prior to this study, the hydrothermal synthesis method had not been attempted on a metallic surface for practical heat transfer applications of the nature investigated in this dissertation. Thus, the results of this investigation e ort are aimed at expanding the fundamental understanding of droplet vaporization from nanostructured surfaces as well as demonstrating their potential for use in practical engineering applications.

In order to properly assess the e ect of ZnO nanostructured surfaces on droplet vaporization, a wide parametric study was conducted in which surface geometry, wall superheat and Weber number were varied. Nanostructure surface geometry was varied by varying the lenght of hydrothermal synthesis time from 4{24 hours. The nanostructured surface temperature was controlled in order to vary wall superheat between a low superheat temperature regime of 10{40 °C and at wall superheats exceeding 200{250°C for the Leidenfrost transition investigation. A Weber number range of 0{99 was achieved by varying water droplet diameter from 2.5{4.0 mm and by depositing droplets onto the surface from heights of 0.2{8.1 cm. In order to assess the potential for using the ZnO nanostructured surfaces in practical heat transfer applications, the surface wetting characteristics and morphology were documented before and after heat transfer experiments through macroscopic measurements of contact angle and microscopically through scanning electron microscope imaging. Furthermore, X-ray di raction was used to con rm the composition of the ZnO nanostructures. Finally, heat transfer experiments at low and high superheat levels were also conducted on smooth, bare copper and aluminum surfaces for comparison with the nanostructured surfaces.

A detailed description of the surface fabrication methodology and results of the explorations of droplet vaporization on hydrophilic and superhydrophilic nanostructured surfaces at low surface superheat temperatures and temperatures near the Leidenfrost transition are described in the remainder of this dissertation.

Chapter 2

Fabrication and experimental methods

The nanostructured surfaces were fabricated by a hydrothermal synthesis method on a copper substrate. The wettability of the resulting nanostructured surfaces was characterized by measuring the contact angle by the sessile drop method or by calculating e ective contact angles from measurements of the wetted area of the superhydrophilic surfaces. One experimental apparatus was used for both the Leidenfrost and low superheat experiments. The nanostructure fabrication and experimental methods are described in the following chapter.

2.1 Copper surface preparation

A copper substrate was chosen for the test surfaces due to its favorable thermal properties in heat transfer applications. The copper (alloy 145) test surface was produced by a computer numerical control (CNC) lathe and subsequently polished to a near mirror nish. The copper test piece is cylindrical with a height of 2.54 cm and 2.52 cm diameter. For the Leidenfrost transition experiments, one of the at surfaces of the cylindrical test piece was designated for the hydrothermal synthesis of ZnO nanowires. A recession was machined into this surface by a CNC lathe. The resulting geometry was that of a at circular center with a diameter of 1 cm and 0.5 mm deep. The surrounding surface sloped up linearly out to the 2.52 cm diameter of the cylindrical test piece. Next, the surface was hand polished with sand papers of increasingly ner grit. The surface was cleaned with isopropyl alcohol between successive sandpapers. The sandpaper material was silicon carbide and grit sizes correspond to the Coated Abrasives Manufacturers Institute (CAMI) standard, which has been approved and adopted by the American National Standards Institute (ANSI). The grit numbers and the corresponding average particle diameter are listed in Table 2.1.

The resulting surface is very near mirror- nish, with few minor surface imperfections visible to the naked eye. The average surface roughness, S_a, of the polished surfaces was measured by a confocal microscope and is approximately 0.056 μm. The resulting surface

Table 2.1: CAMI standard grid sizes and corresponding average particle diameter used to polish copper substrates.

Grit number	Average particle size (μm)
600	16
1000	9.2
1200	6.5
1500	3
2000	1
2500	< 1
3000	< 1

and geometry are pictured in Figure 2.1. The test surface for the low superheat experiments was at and polished in the manner described above.

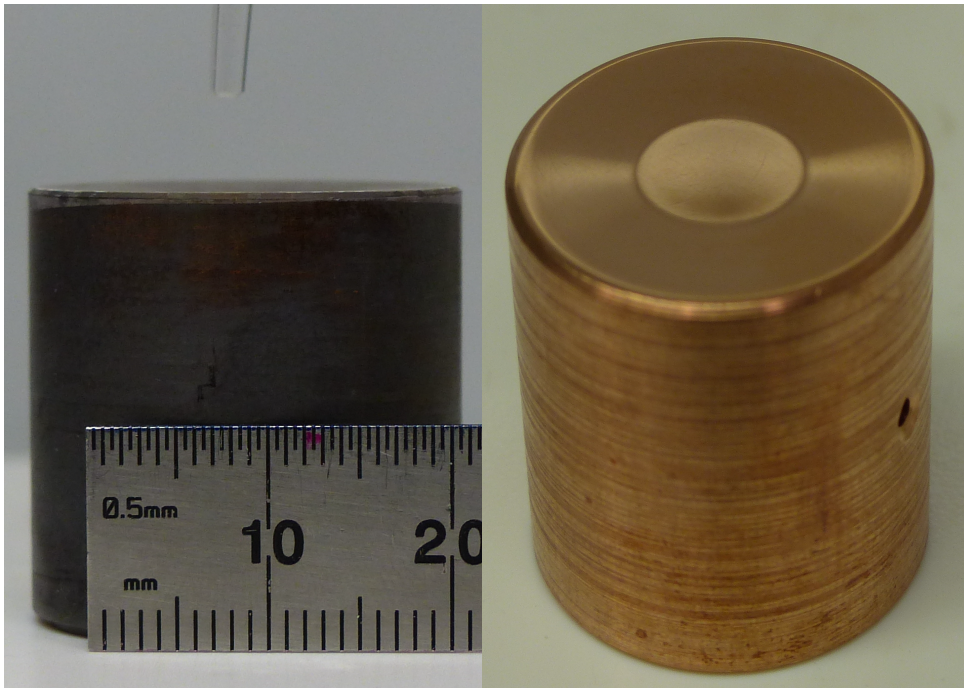

Figure 2.1: Surface geometry and scale of the copper test sample used in Leidenfrost transition experiments.

2.2 Hydrothermal method for ZnO nanocrystal synthesis on smooth copper substrate

The copper test piece was first cleaned in preparation for the hydrothermal synthesis by three consecutive, 15-minute ultrasonic baths of acetone, isopropyl alcohol and distilled water in the order listed. The solvents and parts were placed inside a loosely covered beaker, which was then placed inside the ultrasonic bath of distilled water. The beaker was loosely covered to avoid any pressure build-up by fumes that are generated during the cleaning. Once the copper test piece was cleaned, the ZnO quantum dot solution was prepared.

For this method, the copper substrate was seeded by drop casting with ZnO quantum dots purchased from Meliorum Technologies, approximately 6 nm, in a 30 mL ethanol solution at a concentration of approximately 0.409 M [35]. As sold, the ZnO quantum dot solution concentration is too high for the purposes of this experiment. High concentrations of seeding solution lead to non-uniform growth of ZnO nanowires [36]. Therefore, for the preparation of one ZnO nanostructured test surface, 100 μL were extracted from the 0.409 M quantum dot solution with a micropipette and diluted to 0.0409 M with 1 μL of ethanol in a separate container. It must be noted that before the 100 μL of quantum dot solution were extracted, the entire 0.409 M solution was placed, in its container, in an ultrasonic bath of distilled water for 15 minutes to ensure that the dots were well mixed in solution. The newly diluted 0.0409 M solution was placed, in its container, in an ultrasonic bath of distilled water for about 10 minutes to ensure adequate mixing of the nanoparticles in the diluted solution.

Next, the diluted ZnO quantum dot solution was drop casted on the copper surface at room temperature [35]{[39]. For this method, 5 drops of solution each of 10 μL were deposited on the copper surface. Next, the test piece was rotated slowly by hand until the entire top surface was coated with solution. The test piece was rotated until the ethanol evaporated completely, resulting in a uniform ZnO nanoparticle coating over the entire surface as perceived by the naked eye. This process was repeated four (4) more times so that a total of 25 drops were deposited on the surface. Next, the drop casted piece was placed in an oven at 120°C for 20{25 minutes to anneal the ZnO nanoparticles. The substrate was placed in the oven such that the seeded surface was facing upward, without physically contacting any solid surface.

ZnO nanostructures were synthesized on the copper substrate in aqueous solution by the hydrothermal method [33], [40]{[51]. The aqueous solution was prepared at room temperature and consisted of 25 mM zinc nitrate hexahydrate [$Zn(NO_3)_2 \cdot 6H_2O$] and 25 mM hexamethylenetetramine [$C_6H_{12}N_4$] [34]{[39]. The solution was mixed continuously with a cylindrical magnetic stir bar 1 inch long and 1/4 inch diameter at approximately 600 rpm for approximately 2 hours in a beaker. A crystallizing dish could also be used in place of a beaker. Next, the seeded substrate was completely immersed in the aqueous solution with the seeded surface facing downward. The seeded surface was about 2 cm above the bottom surface of the beaker containing the aqueous solution.

One of the main parameters that was varied in both the Leidenfrost and low superheat

studies was the surface geometry. Varying lengths and surface density of the nanostructures can be grown by varying the time that the copper substrate is subjected to the hydrothermal synthesis. In this study, the hydrothermal synthesis was performed for 4, 10 and 24 hours depending on the desired e ect. The surface density of nucleated nanostructures increases with time of hydrothermal synthesis, although not inde nitely. Longer nanostructures also result from longer hydrothermal synthesis times. In any case, for all hydrothermal syntheses, the beaker with immersed substrate was placed in a standard laboratory gravity convection oven at 90{95°C for either 4, 10 or 24 hours. Finally, the test piece was removed from the solution and rinsed gently but thoroughly with distilled water at room temperature. The test piece was then dried for approximately 30 minutes in air at a temperature of approximately 70 °C. For surfaces grown for 24 hours, the substrates were removed from the solution after about 12 hours, rinsed and dried as described above and immersed into a fresh aqueous solution of the 25 mM zinc nitrate hexahydrate and 25 mM hexamethylenetetramine for the remaining 12 hours of synthesis time [35].

2.3 Contact angle determination

Surface wettability by water on the bare copper and aluminum surfaces was determined by measuring the static contact angle of a drop of distilled water resting on the surface. The contact angle was determined by the sessile drop method, in which a single 2{10 μL distilled water droplet is gently deposited onto the surface by a micropipette. Next, a high resolution digital photograph was taken of the droplet resting on the surface. The contact angle was calculated from analysis of the photograph by the public domain, Java-based image processing program, ImageJ. The reported contact angle for each surface represents the average with standard deviation of the contact angles of many drops deposited over the entire surface.

Due to the superhydrophilicity of the nanostructured surfaces, it was di cult to visually measure a nite contact angle of the thin lms that result from the droplet deposition. Thus, an e ective contact angle was calculated based on the drop spread area that results from the deposition. The deposition and subsequent spreading process were captured by a video camera recording at a rate of 240 frames per second (fps). A schematic diagram of the apparatus used to perform this task is shown in Figure 2.3. The area of the maximum spread was computed from an analysis by the ImageJ software of a still image extracted from the high speed video of the droplet deposition. ImageJ converts a known reference length in a picture into pixels. In these experiments, the known reference length is a metric machinists rule, which is placed directly next to and on the same plane as the test surface plane for the photographs.

Next, for the calculation of the e ective contact angle, the thin lm shape is idealized to be a spherical cap of volume corresponding to the droplet volume, V_l, and the cap base corresponding to the solid-liquid contact area, A_{sl} measured by the ImageJ software. From the known values of V_l and A_{sl}, the radius of curvature, R and e ective contact angle, θ can

be determined by solving

$$V_l = \frac{\pi R^3}{3}(2 - 3\cos\theta - \cos^3\theta) \tag{2.1}$$

and

$$A_{sl} = \pi R^2(1 - \cos^2\theta) \tag{2.2}$$

simultaneously. The geometrical con guration used for the calculation of the e ective contact angle is depicted in Figure 2.2.

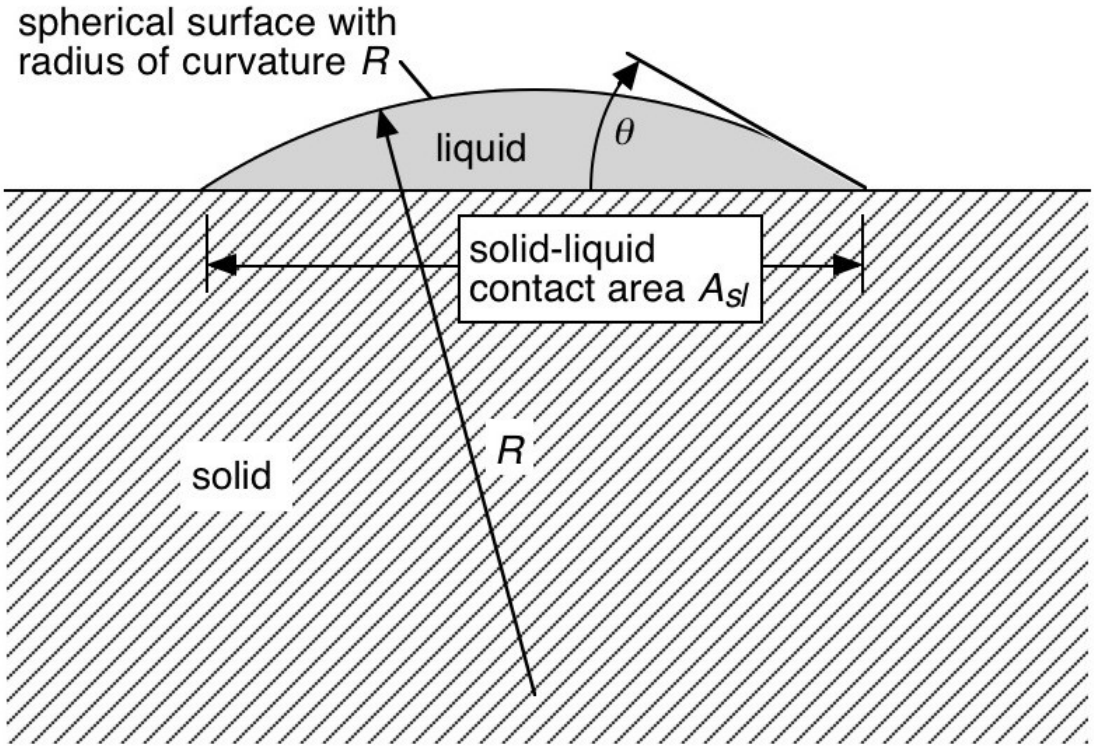

Figure 2.2: Spherical cap idealization of liquid droplet on a solid surface used to calculate e ective contact angle.

2.4 Experimental apparatus and procedure

A schematic diagram of the experimental apparatus for both the Leidenfrost and low superheat experiments is shown in Figure 2.3. The apparatus was placed inside an ISO Class 5 clean room enclosure. The copper substrate measures 2.54 cm in height and 2.52 cm in diameter. The substrate was wrapped in high temperature ceramic blanket insulation measuring nearly 5 cm in thickness in order to maintain a constant temperature throughout the

substrate. The temperature of the substrate was measured at the centroid of the substrate by a K-type thermocouple (TC). Due to the high conductivity of the copper, the lack of forced convection and the very small volumes of distilled water that are deposited on the substrate, it is assumed that there are minimal temperature gradients inside the copper substrate and, thus, the surface temperature over which the evaporation occurs is approximated to be the measured temperature at the center. A second K-type TC was placed half a radius away from and on the same horizontal plane as the TC at the centroid to verify that the substrate was isothermal. The K-type TCs were connected to a data acquisition card furnished by National Instruments (NI) and temperature data were recorded by using the NI LabVIEW software. The uncertainty of the temperature measurements was estimated to be 2.2 °C or 0.75% of the reading in Celsius, whichever was greater. The difference between the two TC readings never exceeded the measurement uncertainty.

To begin either a Leidenfrost or low superheat experiment, the metal substrate (e.g. copper or aluminum) was placed directly over the hot plate as shown in Figure 2.3 and the temperature was set to the desired value. A hypodermic needle was used to deposit distilled and degassed water droplets of a known diameter gently over the heated copper surface. All droplets were deposited at 101 kPa. The ambient air temperature inside the clean room was not controlled and was approximately 21–23°C for all experiments.

For both the Leidenfrost and low superheat experiments one of the parameters that was controlled and varied was the droplet size. Distilled water droplets of varying size are generated by changing the hypodermic needle tip. Three hypodermic needles measuring 16, 22 and 30 ga. were used to generate droplets of approximately 3.9–4.1 mm, 3.0–3.4 mm and 2.5–2.6 mm in diameter, respectively. The droplet diameter is calculated from the known dispensed volume from the hypodermic needle. The calculated values of droplet diameter were also compared to droplet diameters measured from an ImageJ analysis for every experiment. The droplets detached from the needle tip due to their own weight and fell from a known distance above the test surface.

Video of every experiment was recorded at 240 fps. The camera location and angle were adjustable. The camera was placed directly above the test surface such that the camera lens plane was parallel to the test surface plane. The hypodermic needle was removed from the viewing area of the camera lens immediately after the deposition. Effective contact angles were determined from the recorded videos for each surface. Droplet evaporation times were measured from the videos as well.

2.4.1 Leidenfrost experiments

For the Leidenfrost experiments distelled water droplets fell onto the surface from a release height of approximately 0 cm + droplet radius, where release height is defined as the distance from the surface plane to the center of the droplet. The droplet did not touch the surface before it was completely detached from the hypodermic needle tip.

In contrast with previous studies that employed the droplet lifetime method, the Leidenfrost point was determined in this study by heating the surface and measuring the acoustic

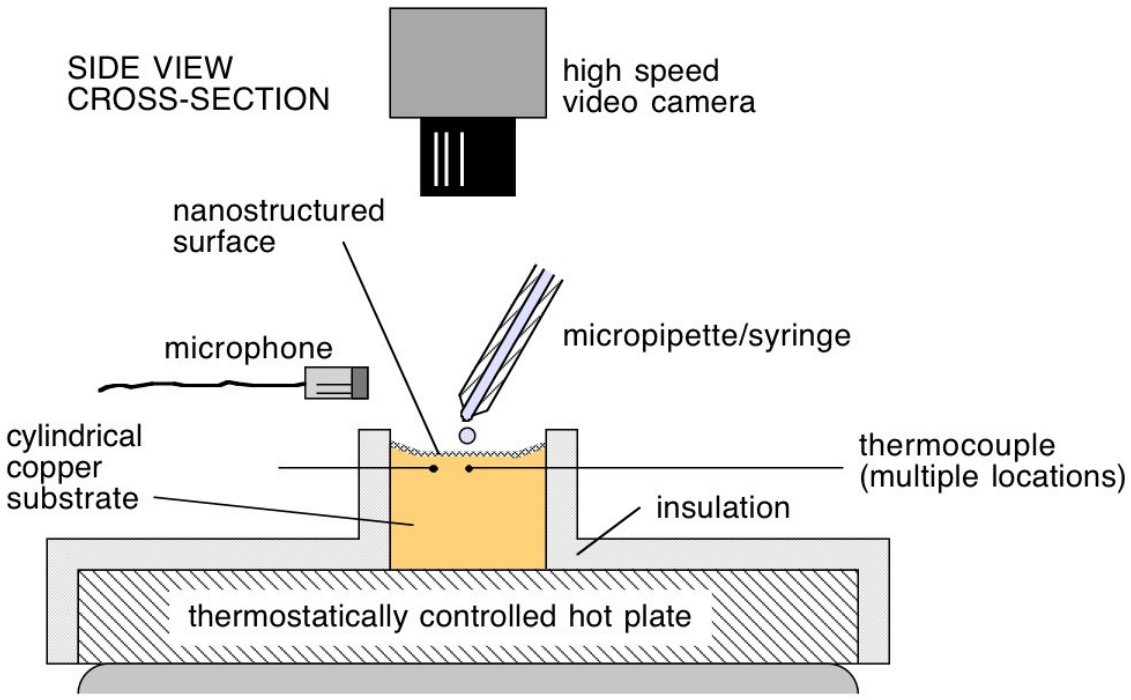

Figure 2.3: Schematic diagram of experimental apparatus for both Leidenfrost and low superheat experiments. The copper substrate in the schematic diagram was the type used in the Leidenfrost experiments, which is evident from the receded nanostructured surface. The top surface of the substrates used in the low superheat experiments was at.

signal produced during droplet deposition and subsequent evaporation process. By this metric, the Leidenfrost point is achieved when, after the initial deposition, the droplet hovers completely silently above the solid surface for the entirety of the evaporation process.

Once the surface temperature corresponding to the rst incidence of silent evaporation was reached, the surface was cooled and heated cyclically by progressively smaller temperature increments, generating noisy and silent evaporations, in order to narrow in on the transition point to within the range of the accuracy of the thermocouple.

Sound from the experiment was detected by a microphone and the resulting signal was recorded by the Audacity software. The Leidenfrost transition was determined from the acoustic signal recordings that were generated during the deposition and subsequent evaporation process. The transition is de ned as the rst point for which there is no disturbance to the acoustical signal in the form of a popping or sizzling sound beyond the initial violent popping generated during the droplet deposition. This metric for establishing the Leidenfrost point is explained further in the results section. An experiment was considered complete when it was veri ed visually that the water droplet had evaporated completely.

2.4.2 Low superheat experiments

For the low superheat experiments droplets fell onto the surface from a release heights of 0 cm + droplet radius, 3.9$\pm$ 0.1 cm and 8.1$\pm$ 0.4 cm where release height is de ned as the distance from the surface plane to the center of the droplet. Four di erent wall superheat temperatures corresponding to 10°C, 20 °C, 30 °C and 40 °C were tested. Wall superheat, T_{wall} is de ned as the di erence in the controlled surface temperature of the substrate, T_{wall} and the saturation temperature of water,T_{sat} at 101 kPa, 100°C. Experiments were performed near sea level at an elvation of approximately 100 m, such that atmospheric pressure is assumed to be 101 kPa.

$$T_{wall} = T_{wall} - T_{sat} \tag{2.3}$$

One complete experiment consisted of depositing a single droplet from a single needle and a single release height over a surface at one level of superheat until the liquid was evaporated. The entire deposition and evaporation process was captured by video at 240 fps in the same method as in the Leidenfrost experiments. Video recordings were used to determine evaporation time, calculate heat transfer coe cient, measure the ight time of the droplet between release from the needle and impact with the surface and measure maximum droplet spread area in conjunction with the ImageJ software and observe whether the droplet evaporated by lm evaporation or by nucleate boiling. Neglecting air friction, the measured droplet ight time was used to calculate the velocity of the droplet upon impact with the surface,V_{impact} given by

$$V_{impact} = gt_{flight} \tag{2.4}$$

where g is the acceleration due to gravity equivalent to 9.81 m/s^2 and t_{flight} is the measured droplet ight time. The impact velocity, V_{impact} was used to calculate the Weber number given by

$$We = \frac{\rho_l V_{impact}^2 D_{drop}}{\sigma_l} \tag{2.5}$$

where ρ_l is the liquid density, D_{drop} is the characteristic length taken to be the droplet diameter and σ_l is the surface tension between the liquid and vapor phases.

Chapter 3

Results and discussion of surface structure and wettability

In order to properly assess the effect of ZnO nanostructured surfaces on droplet vaporization it was necessary to realize various surface characterization techniques on the nanostructured surfaces and bare metal substrates. The ZnO nanostructures were characterized by X-ray diffraction, by scanning electron microscopy, by macroscopic measurements of contact angle from water droplet profile and by measurements of the wetted area of a droplet spreading on the surface. Furthermore, bare, smooth copper and aluminum surfaces were also characterized for comparison with the ZnO nanostructured surfaces. Contact angles from droplet profiles were measured on the bare metal surfaces. A confocal microscope and scanning electron microscope were used to evaluate the surface topography of the bare copper substrates used for the hydrothermal syntheses. The results of the surface characterization study are summarized in the following chapter.

3.1 Bare copper surface for hydrothermal synthesis

An Olympus LEXT OLS3000 3D Laser Confocal Microscope located in the Marvell Nanofabrication Laboratory at UC Berkeley was used to measure the average surface roughness of the bare copper surface. The measured average surface roughness, R_a, was 0.056 μm.

$$R_a = 0.056\,\mu\text{m} \tag{3.1}$$

Furthermore, a LEO 1550, Schottky field emission scanning electron microscope (SEM) located in the Marvell Nanofabrication Laboratory at UC Berkeley was also used to confirm the smoothness of the bare copper surface. A micrograph obtained with the SEM is shown in Figure 3.1.

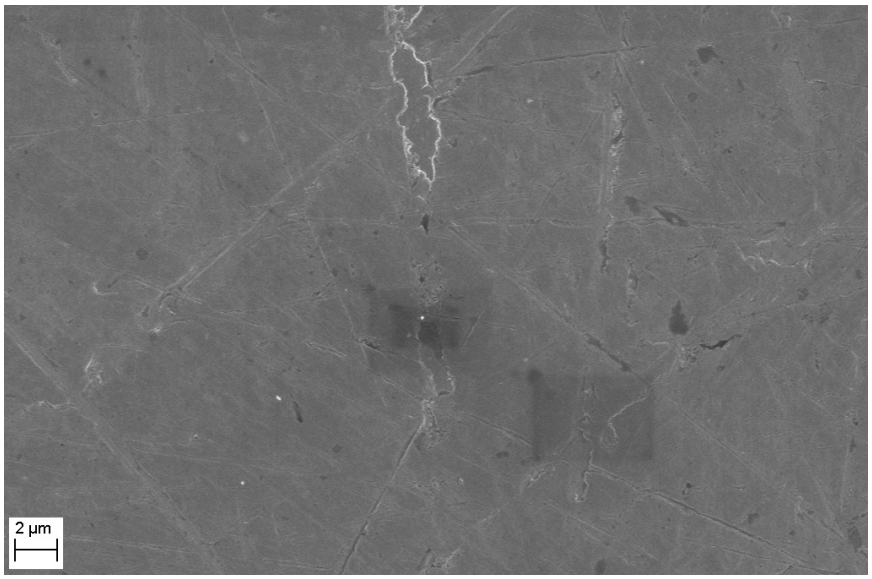

Figure 3.1: SEM image of bare, smooth copper used for hydrothermal syntheses of ZnO nanostructures.

3.2 ZnO nanocrystal structure

A Siemens D5000 X-ray di ractometer located in the Marvell Nanofabrication Laboratory at UC Berkeley was used to characterize the material properties of the ZnO nanostructures on the copper substrates. The di ractometer uses copper K-alpha (Cu K_α) radiation with a weighted average wavelength of 0.154184 nm (Cu $K_{\alpha 1}$ = 0.154056, Cu $K_{\alpha 2}$ 0.154439 nm). The X-ray power supply has an idling condition of 20 kV and 5 mA. Normal operating conditions during measurements are 40 kV and 30 mA. The X-ray di raction (XRD) pattern for the ZnO nanostructures grown for 10 hours by hydrothermal synthesis on a copper substrate is shown in Figure 3.2. The X-ray di raction was performed after the test sample had been heated once to approximately 300 °C for 60 minutes in order to evaporate any contaminants that may had adsorbed on the surface. The test sample had not yet been subjected to any distilled water droplet experiments.

The di raction peaks in Figure 3.2 for the ZnO nanostructures located at approximately 32°, 34.5°, 36.5°, 47.5°, 56.5° and 63° correspond to the planes of hexagonal wurtzite ZnO, which is consistent with findings in the literature [34]–[38], [52], [53]. The di raction peaks in Figure 3.2 located at approximately 43.5°, 50.6° and 74.3° correspond to the copper substrate [54]–[61].

The hexagonal geometry of the ZnO nanocrystals is confirmed visually by micrographs obtained by a scanning electron microscope, which will be shown in Section 3.4. Furthermore, data on thermal properties of nanoscale wurtzite ZnO are limited. The thermal conductivity of nanoscale ZnO is on the order of 1-9 W/m·K [62]. For reference, bulk wurtzite ZnO has a density of 5660 kg/m^3.

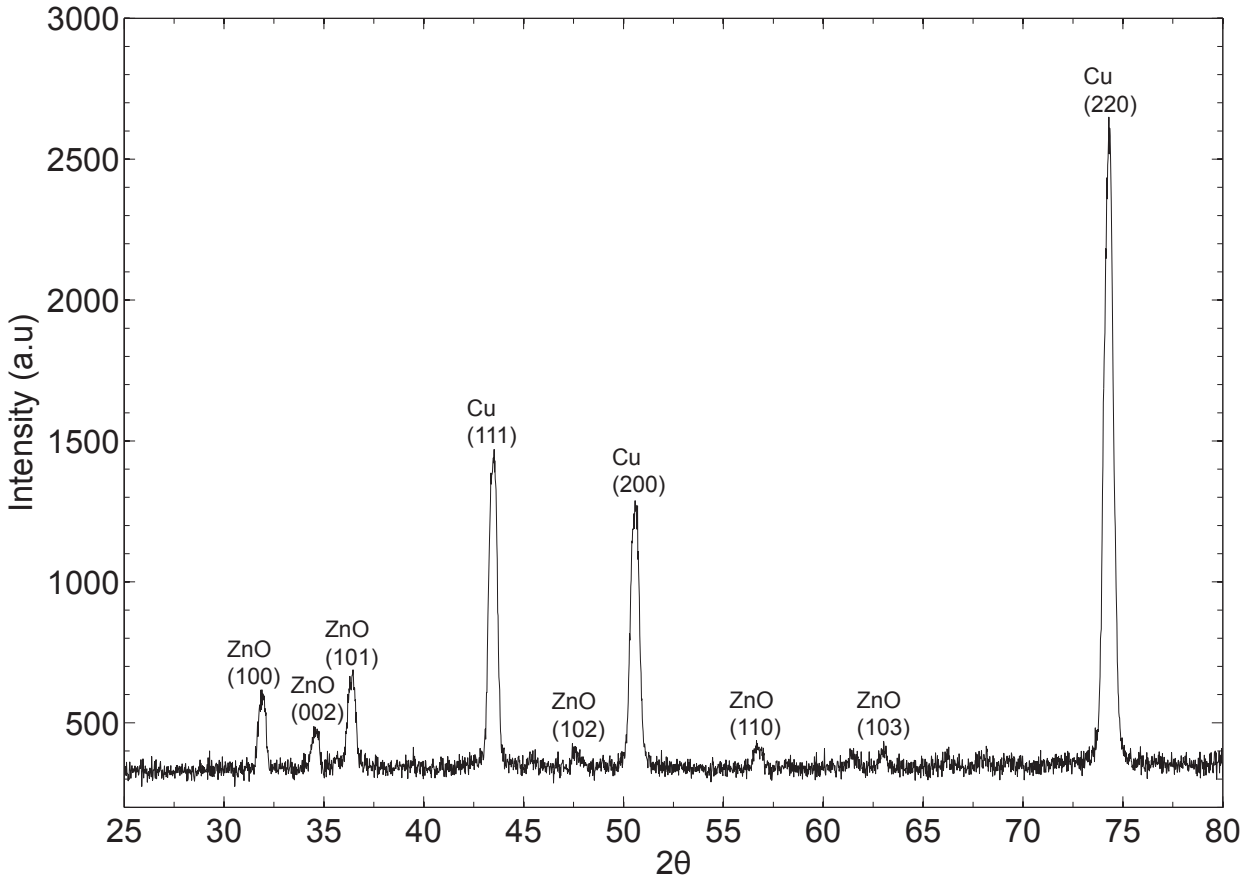

Figure 3.2: XRD pattern for ZnO nanostructures grown by hydrothermal synthesis for 10 hours on a copper (Cu) substrate. The diffraction peaks for the ZnO and Cu are indicated with the corresponding Miller indices in the graph individually. The angle between the projection of the X-ray source and the detector is given by θ2 The X-ray diffraction pattern was obtained before any evaporation tests.

3.3 Rapid spreading of water on superhydrophilic nanostructured surface

When a liquid water droplet impinged upon the superhydrophilic ZnO nanostructured surface it was observed that the nominally spherical droplet spread into a thin film over the surface. The rapid spreading of a single water droplet on one of the superhydrophilic ZnO nanostructured surfaces grown for 10 hours by hydrothermal synthesis used in this study is captured in a series of photographs depicted in Figure 3.3. Beginning on the left-most photograph in Figure 3.3, a single 35 μL distilled water droplet at 20 $^{\circ}$C of approximately 4 mm diameter is gently deposited over a surface at 20 $^{\circ}$C. The process is captured at 240 fps and the photographs in Figure 3.3 are shown in 0.025 s intervals. The spreading process is

complete in less than 0.075 s.

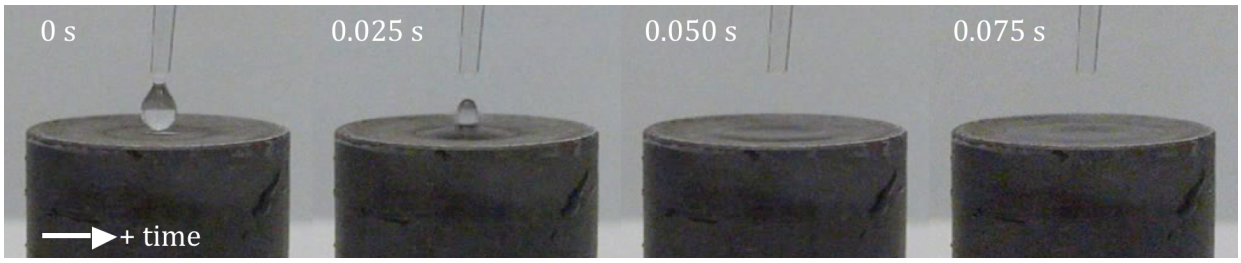

Figure 3.3: Rapid spreading of a single water droplet of approximately 4 mm diameter on ZnO nanostructured surface at 20°C grown by hydrothermal synthesis for 10 hours.

3.4 SEM images of ZnO nanostructured surfaces

Micrographs of the ZnO nanostructured surfaces were captured before and after experiments with a LEO 1550, Schottky field emission scanning electron microscope (SEM) located in the Marvell Nanofabrication Laboratory at UC Berkeley. Micrographs for the ZnO nanostructured surfaces grown by hydrothermal synthesis for 4 hours, 10 hours and 24 hours are found in Figures 3.4–3.6.

From the micrographs in Figures 3.4–3.6 it was possible to measure the average nanocrystal side length, measured from substrate to tip of the nanocrystal, L_{side} and the average crystal hexagon side length, L_{hex} in order to calculate the average nanocrystal surface area, A_{ZnO} which was available to interact with the liquid droplets. For calculation purposes, the top face of an individual ZnO nanocrystal is assumed to form a regular hexagon, such that the length of each of all six sides is equivalent to L_{hex}. The area, A_{hex} of the top face of the ZnO nanocrystal is given by,

$$A_{hex} = \frac{3\sqrt{3}}{2} L_{hex}^2. \tag{3.2}$$

Therefore, surface area of one individual ZnO nanocrystal is given by

$$A_{ZnO} = A_{hex} + 6\, L_{hex} L_{side}. \tag{3.3}$$

Furthermore it was possible to measure the surface area of the substrate that was not covered by ZnO nanocrystals, $A_{un-nucleated}$, i.e. the base area of the substrate, $A_{substrate}$, over which no clearly distinct ZnO nanocrystals nucleated. From these measurements it was possible to determine the porosity, ε given by

$$\varepsilon = 1 - \frac{A_{substrate} - A_{un-nucleated}}{A_{substrate}} = 1 - \frac{A_{nucleated}}{A_{substrate}} \tag{3.4}$$

Table 3.1: Average geometrical parameters with standard deviation of ZnO nanostructured surfaces grown for a hydrothermal synthesis time, t, of 4, 10 and 24 hours. L_{hex} is the hexagon side length, L_{side} is the length of the nanocrystal measured from the substrate to the tip of the nanocrystal, A_{ZnO} is total wetted surface area of one ZnO nanocrystal and ω is wetted surface area ratio.

t (hr)	L_{hex} (μm)	L_{side} (μm)	A_{ZnO} (μm^2)	ε	ω
4	0.28 $\pm$ 0.06	1.70 $\pm$ 0.34	3.08 $\pm$ 0.98	0.58 $\pm$ 0.08	15.6
10	0.34 $\pm$ 0.10	2.66 $\pm$ 0.65	5.73 $\pm$ 2.30	0.16 $\pm$ 0.03	19.3
24	0.77 $\pm$ 0.15	3.25 $\pm$ 0.96	16.73 $\pm$ 5.99	0.04 $\pm$ 0.005	10.8

where $A_{nucleated}$ is the area of the base substrate that is covered by ZnO nanocrystals. It was not possible to determine whether the un-nucleated area was bare copper or simply ZnO nanoparticles that were annealed onto the copper substrate but did not serve as a nanocrystal nucleation site. In any case, from the calculated ZnO nanocrystal surface area, A_{ZnO} and measured un-nucleated substrate surface area, $A_{un-nucleated}$, it was possible to determine the total average surface area that could potentially interact with liquid, i.e. the total average wetted surface area, $A_{wetted,total}$ given by,

$$A_{wetted,total} = \eta A_{ZnO} + A_{un-nucleated} \tag{3.5}$$

where η is the total estimated number of nanocrystals within a given substrate area, $A_{substrate}$, which is given by,

$$\eta = \frac{A_{substrate}}{A_{hex}}. \tag{3.6}$$

Therefore, per unit of substrate area, the wetted surface area ratio, ω, is given by,

$$\omega = \frac{A_{wetted,total}}{A_{substrate}} = \frac{\eta A_{ZnO} + A_{un-nucleated}}{A_{substrate}}. \tag{3.7}$$

which can be simplified further to,

$$\omega = 1 + \frac{4h}{\sqrt{3}L_{hex}} + \varepsilon. \tag{3.8}$$

The geometrical measurements are listed in Table 3.1.

3.4.1 Discussion of surface geometry as a function of hydrothermal synthesis time

From Figures 3.4–3.6 it is evident that the time of hydrothermal synthesis had a significant impact on the geometry of the nanostructured surfaces. In general, an increase in

synthesis time resulted in an increased area coverage of the base copper substrate surfaceby nucleated ZnO nanocrystals. For a hydrothermal synthesis time of 4 hours, ZnO nanocrystals nucleated on approximately 40% of the surface area of the copper substrate. For an increase in nucleation time from 4 to 10 hours, the nucleated area more than doubled, resulting in approximately 84% of the copper surface area covered by ZnO nanocrystals. For a synthesis time of 24 hours, approximately 96% of the copper substrate surface area was covered by ZnO nanocrystals.

For an increase in nucleation time from 4 to 10 hours, the hexagonal area, i.e. the top face of the crystal increased by approximately 50%, from 0.20 μm^2 to 0.30 μm^2, and the length, measured from the substrate to the tip of the crystal, increased by about 55% from 1.7 μm to 2.7 μm. An increase in synthesis time from 10 to 24 hours resulted in even greater gains in hexagonal surface area, approximately 400%, as the hexagonal surface area increased from about 0.30 μm^2 to nearly 1.6 μm^2.

In terms of total wetted surface area of one ZnO nanocrystal, A_{ZnO}, an increase in synthesis time from 4 to 10 hours resulted in an approximate increase of 65%, 3.53 μm^2 to 5.82 μm^2. An increase in synthesis time from 10 to 24 hours resulted in increase in A_{ZnO} of about 185%, from 5.82 μm^2 to 16.65 μm^2. An increase in synthesis time from 4 to 24 hours resulted in increase in A_{ZnO} of about 370%, from 3.53 μm^2 to 16.65 μm^2.

3.4.2 ZnO surface - hydrothermal synthesis time = 4 hours

Micrographs of the ZnO nanostructured surface grown for 4 hours by hydrothermal synthesis are shown in Figure 3.4.

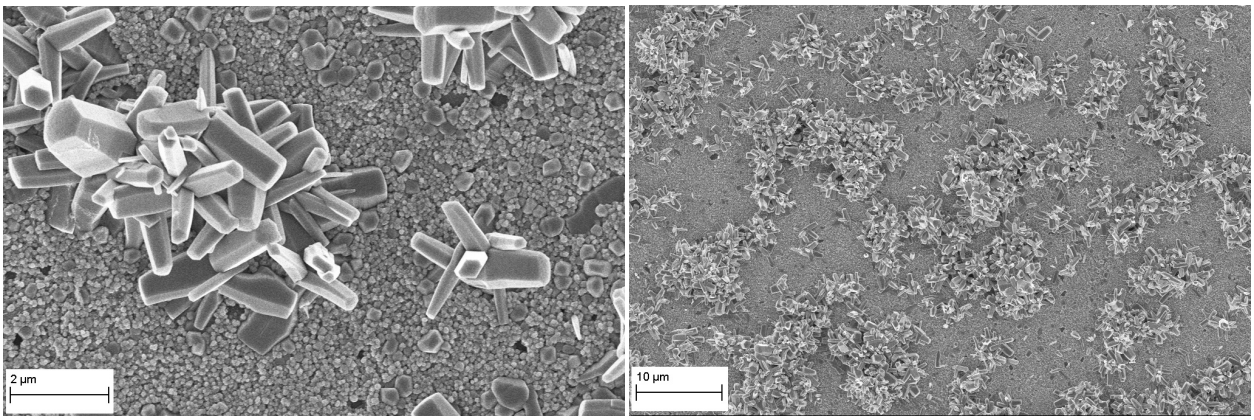

Figure 3.4: SEM images of ZnO nanostructures synthesized on the smooth copper surface for 4 hours before experiments. The image on the right shows the general array of the ZnO nanocrystals on the substrate. The left image is shows the hexagonal wurtzite structure of the ZnO nanocrystals.

From Figure 3.4 the average nanocrystal length was measured to be approximately 1.70

0.34 μm and the average crystal hexagon side length was measured to be approximately 0.28 $\pm$ 0.06 μm. The un-nucleated surface area was about 5 $\pm$ 8% of the total base substrate surface area. Therefore the total wetted area per unit substrate area was approximately 3.53 $\pm$ 0.73 μm^2 per μm^2 of substrate area. The measurement data for this surface are summarized in Table 3.1 along with those of the other two surfaces.

3.4.3 ZnO surface - hydrothermal synthesis time = 10 hours

Micrographs of the ZnO nanostructured surface grown for 10 hours by hydrothermal synthesis are shown in Figure 3.5.

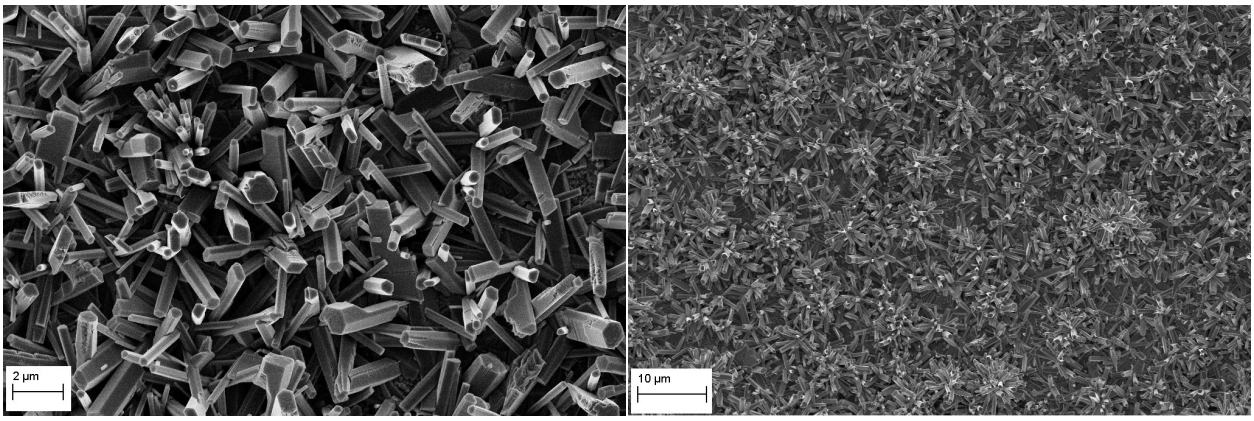

Figure 3.5: SEM images of ZnO nanostructures synthesized on the smooth copper surface for 10 hours before experiments. The image on the right shows the general array of the ZnO nanocrystals on the substrate. The left image is shows the hexagonal wurtzite structure of the ZnO nanocrystals.

From Figure 3.5 the average nanocrystal length was measured to be approximately 2 $\pm$ 0.65 μm and the average crystal hexagon side length was measured to be approximately 0.34 $\pm$ 0.10 μm. The un-nucleated surface area was about 16 $\pm$ 3% of the total base substrate surface area. Therefore the total wetted area per unit substrate area was approximately 5.82 $\pm$ 1.08 μm^2 per μm^2 of substrate area. The measurement data for this surface are summarized in Table 3.1 along with those of the other two surfaces.

3.4.4 ZnO surface - hydrothermal synthesis time = 24 hours

Micrographs of the ZnO nanostructured surface grown for 24 hours by hydrothermal synthesis are shown in Figure 3.6. From Figure 3.6 the average nanocrystal length was measured to be approximately 3.25 $\pm$ 0.96 μm and the average crystal hexagon side length was measured to be approximately 0.77 $\pm$ 0.15 μm. The un-nucleated surface area was about 4 $\pm$ 0.5% of the total base substrate surface area. Therefore the total wetted area per

unit substrate area was approximately 16.65 ± 1.73 μm^2 per μm^2 of substrate area. The measurement data for this surface are summarized in Table 3.1 along with those of the other two surfaces.

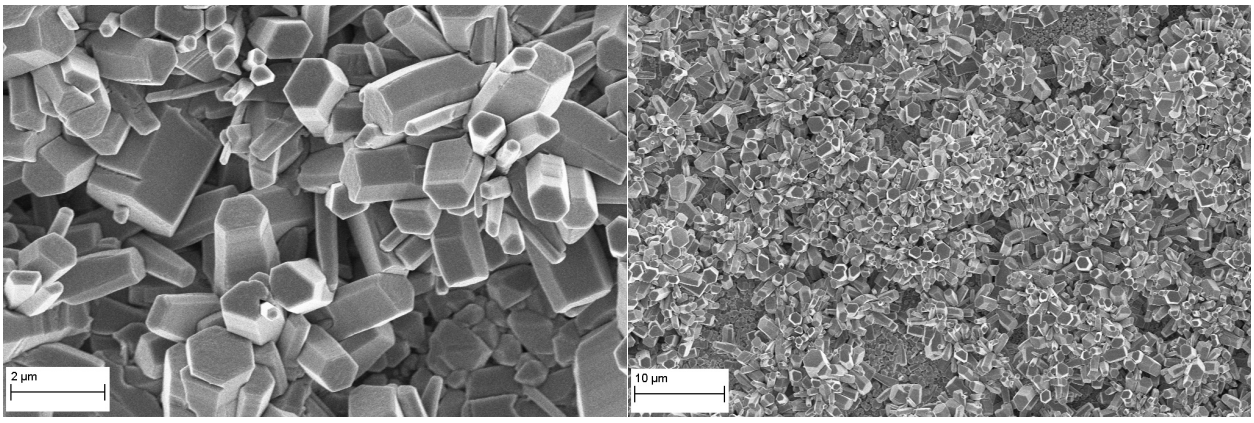

Figure 3.6: SEM images of ZnO nanostructures synthesized on the smooth copper surface for 24 hours before experiments. The image on the right shows the general array of the ZnO nanocrystals on the substrate. The left image is shows the hexagonal wurtzite structure of the ZnO nanocrystals.

3.4.5 Geometrical idealizations for explaining nanostructured surface wettability

From the measurements in Table 3.1 it was possible to make some idealizations of the geometry in order to gain a better understanding of the nature of the liquid-solid nanostructure interactions. If it is assumed that the ZnO nanocrystals are uniformly spaced out in a square array over the base area of the copper substrate, $A_{substrate}$, and grow normal to the substrate surface, the pitch, P, i.e. the center-to-center distance between nanocrystals, can be calculated from the measured porosity, ε, of the nanostructured array and the calculated hexagonal surface area, A_{hex}, of each individual nanocrystal given by,

$$P = 2\left[\frac{2}{3\sqrt{3}}\left(\frac{-A_{hex}}{\varepsilon - 1}\right)\right]^{1/2} \tag{3.9}$$

where A_{hex} was given previously by equation 3.2.

Note that in the calculation of the pitch, P, it is assumed that the center-to-center distance which is the length of the side of a square, is equivalent to twice the length of the side of a regular hexagon. Although it can clearly be seen from Figures 3.4{3.6 that the nanocrystals do not grow normal to the substrate surface, they are generally randomly oriented and not uniformly spaced on the substrate surface, it is still possible to gain some

insight as to their wetting characteristics through these idealizations. In a recent study, Ishino et al. [63] described the wetting of a forest of micropillars by a spreading liquid as a function of the driving capillary and resistive viscous forces. By balancing the driving capillary and viscous forces, the position, z of the meniscus which is drawn into the micropillar forest is predicted by the Washburn law [64], $z \sim (Dt)^{1/2}$, where D is a dynamic coe cient that depends on the liquid surface tension, σ_l and dynamic viscosity, μ_l and the radius, b of the micropillars, such that $D \sim \sigma_l b/\mu_l$. Unlike this study, in the study by Ishino, et al. the pillar radius, height and pitch were individually controlled using techniques from photolithograpy and deep reactive ion etching on a silicon wafer such that the entire test sample was composed of a single material. Nevertheless, the results of the study by Ishino et al. are illuminating and can be applied to those of this study. Ishino et al. studied two regimes of micropillar array geometry, one which was for short pillars, such that $h < P$, where h is the pillar height, and the other was for tall pillars, such that $h > P$. The ZnO nanocrystal height and idealized pitch in this study are in the transition regime between short and tall pillars in the study by Ishino et al. The driving capillary force is given by

$$F_{cap} = 2\pi\sigma_l \frac{bh}{P^2} \tag{3.10}$$

where it is assumed that the liquid wets the surface completely such that the contact angle approaches zero. The viscous forces arise primarily from friction between the liquid and the bottom substrate surface and the micropillars. Although viscous forces are due to friction with both the bottom surface and the micropillars, for short pillar arrays, $h < P$ viscous forces per unit width of spreading liquid lm, $F_{visc,1}$ are primarily due to friction between the liquid and the bottom surface such that

$$F_{visc,1} \sim \mu_l \frac{V}{h} z. \tag{3.11}$$

where V is the velocity of the spreading liquid front. For tall pillar arrays, $h > P$ viscous forces per unit width of spreading liquid lm, $F_{visc,2}$ are due primarily to friction between the liquid and the micropillars such that

$$F_{visc,2} \sim \frac{\mu_l V h z}{P^2 \ln(P/b)}. \tag{3.12}$$

From the balance of the capillary force and the viscous force per unit width of liquid lm, it is possible to determine the dynamic wicking coe cient, D which has units of length^2/time and is a measure of the spreading or di usion of the liquid into the micropillar array such that, from the Washburn law,

$$z^2 = Dt. \tag{3.13}$$

For the transition regime between short and tall pillars the dynamic coe cient that results from balancing the driving force with either one of the viscous forces is approximately the same. Therefore, applying the analysis of Ishino et al. to this study, the dynamic coe cient

Table 3.2: Comparison between capillary driving forces and viscous forces for ZnO nanostructured surface grown for hydrothermal synthesis times t, of 4, 10 and 24 hours. P is the pitch of the idealized square array of nanocrystals D is the dynamic liquid spreading coefficient.

t (hrs)	P (μm^2)	$D \times 10^3$ (m^2/s)
4	0.86	1.0
10	0.74	3.8
24	1.58	2.9

is calculated by balancing F and $F_{visc,1}$ and applying the Pouiseuille law such that the dynamic coefficient, D_1 is found to be

$$D_1 = \frac{4\pi}{3}\frac{\sigma_l}{\mu_l}\frac{h^2 L_{hex}}{P^2} \tag{3.14}$$

where L_{hex} replaces b from the analysis by Ishino et al. The numerical results of the application of the analysis by Ishino to this study are found in Table 3.2.

The results in Table 3.2 indicate that the surface grown by hydrothermal synthesis for 10 hours should be the most wetting of the three ZnO nanostructured surfaces since it exhibits the greatest dynamic coefficient, D of all the surfaces. Indeed, as will be shown in the remaining sections in this chapter, the surface grown for 10 hours exhibited the lowest calculated effective contact angle of all the surfaces. Although this analysis was adapted from the results of a study in which the geometry was controlled very precisely and the surface was composed of one single material, the physical arguments were shown to be applicable to this study. The relative magnitude of the results between surfaces in Table 3.2 agrees with the observations in the experiments in this study.

3.5 SEM images of ZnO nanostructured surfaces before and after experiments

Micrographs of the ZnO nanostructured surface grown for 10 hours by hydrothermal synthesis taken before and after a Leidenfrost experiment are shown in Figure 3.7. In this particular Leidenfrost experiment the nanostructured surface and copper substrate were heated from 20°C to 400 °C over a period of approximately 5.2 hours of testing. As it is evident in Figure 3.7, the surface exhibited some minor degradation. However, as will be shown in Section 3.6, the wetting characteristics of most of the ZnO nanostructured surfaces did not change significantly due to experimentation. Furthermore, while wurtzite ZnO exhibits a coefficient of thermal expansion (CTE) of approximately 2.5–7.5 $\times 10^{-6}$/ °C over a temperature range of 25-430°C and copper alloy 145 exhibits a CTE of approximately

$17.8 \times 10^{-6}/^{\circ}$C for a temperature range of 20{300°C, a factor decreasing from 7 to 2 di er-ence in CTE between the two materials, there is nearly negligible di erence in the surface topography before and after the experiment. Therefore, it is concluded that the surfaces exhibited negligible degradation and that ZnO nanocrystals were well adhered to the copper substrate. Thus, the surfaces were more than su ciently robust for the purposes of this study. Nevertheless, in order to gain a better understanding as to the nature of these types of surfaces, it is recommended that the durability and robustness of these types of surfaces be the main subject of a future study.

Figure 3.7: SEM images of ZnO nanostructures synthesized on the smooth copper surface for 10 hours. The left image represents the surface before experiments. The image on the right represents the surface after experiments.

3.6 Contact angle measurements and calculations

Static contact angles were measured and calculated, immediately after the hydrothermal synthesis and immediately before and after each experiment for each nanostructured surface. All contact angle testing was performed at room temperature, approximately 20°C. For the smooth aluminum and copper surfaces a single μL droplet was gently deposited by the sessile drop method described previously.

3.6.1 Wetting characterization of ZnO nanostructured surfaces

Due to the superhydrophilicity of some of the ZnO nanostructured surfaces, determining the contact angle on the ZnO nanostructured surfaces was not possible from the droplet pro le. Therefore, for all of the ZnO nanostructured surfaces a single μL distilled water droplet was gently deposited and the subsequent spreading was captured by the camera

directly above and parallel to the test surface at 240 fps. One example of a liquid droplet spreading to maximum diameter on one of the ZnO nanostructured surfaces is depicted in Figure 3.8. Maximum droplet spread areas like the one depicted in Figure 3.8, were measured with the ImageJ software in order to calculate an e ective contact angle.

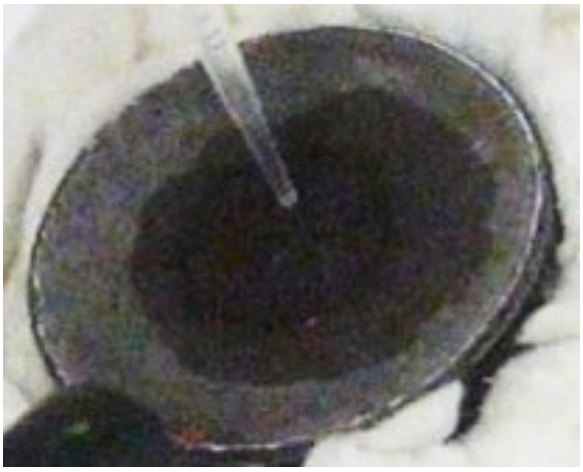

Figure 3.8: Water droplet spread area on ZnO nanostructured surface for e ective contact angle calculation. The photograph is taken at an angle for demonstration purposes only and does not re ect the actual position of the camera during experiments.

3.6.2 Storage of test samples

Furthermore, due to the delicate nature of the nanostructured surfaces it was necessary to store the test samples securely in order to protect and preserve the wetting characteristics of the surfaces. In addition to its a nity for water, the hydrophilicity of the ZnO nanostructured surfaces and other high energy surfaces also encourages wetting by other ambient contaminants. In order to minimize contamination and preserve the surface characteristics, all test samples, including the bare metal samples, were stored in clean glass beakers which were sealed with clean, new aluminum foil. The beakers were stored inside the clean room enclosure, although clean room conditions were only achieved during the evaporation experiments.

3.6.3 Nanostructured surface desorption

In order to remove contaminants that may have been adsorbed onto the nanostructures it was necessary to perform various desorption procedures on the test samples. The rst desorption procedure was performed immediately after the hydrothermal synthesis. This rst desorption procedure was performed after removing the substrate from the aqueous solution and rinsing with distilled water. The sample was then placed into an oven at 70{90

°C for approximately 30 minutes. After the part was removed from the oven and it was allowed to cool down, the contact angle measurements were performed by the sessile drop method and the results were documented.

In many cases, the ZnO nanostructured surfaces were not superhydrophilic immediately after the hydrothermal synthesis and the first desorption procedure. Thus it was assumed that further surface desorption was necessary before droplet evaporation experiments. Therefore a second desorption procedure was performed immediately before any droplet evaporation experiments. It was found that heating the substrate up to about 275{300°C for about 45-60 minutes sufficiently desorbed any adsorbed surface contaminants for the purposes of the droplet evaporation experiments. For most nanostructured surfaces the second desorption resulted in a significant decrease in contact angle. Furthermore, the SEM images in Figure 3.9, taken immediately after the first and second desorption procedures, but before any experiments, do not reveal any significant change in surface topography. However, as can be seen in Figure 3.10 the sample tends to darken and exhibits some asperities after one complete test cycle. One full test cycle consisted of distilled water droplet vaporization experiments across all parameters per surface, i.e. all droplet diameters, release heights and wall superheat levels. Several hundred droplets were evaporated from the surface without any significant alteration to its structure and wettability.

Figure 3.9: SEM images of ZnO nanostructures synthesized on the smooth copper surface for 10 hours. The left image represents the surface after hydrothermal synthesis and subsequent first desorption procedure. The image on the right represents the surface after the second desorption procedure.

In general the wettability of the surfaces increased after each desorption procedure as well as after experiments. Evidence of the increased wettability of the nanostructured surface is shown in the series of photographs in Figure 3.11. The wettability exhibited by the surface after the evaporation experiments represents the maximum wettability observed for the surfaces, meaning there were no further gains in wettability from any further heating. Furthermore, the maximum surface wettability was sustained throughout the testing life

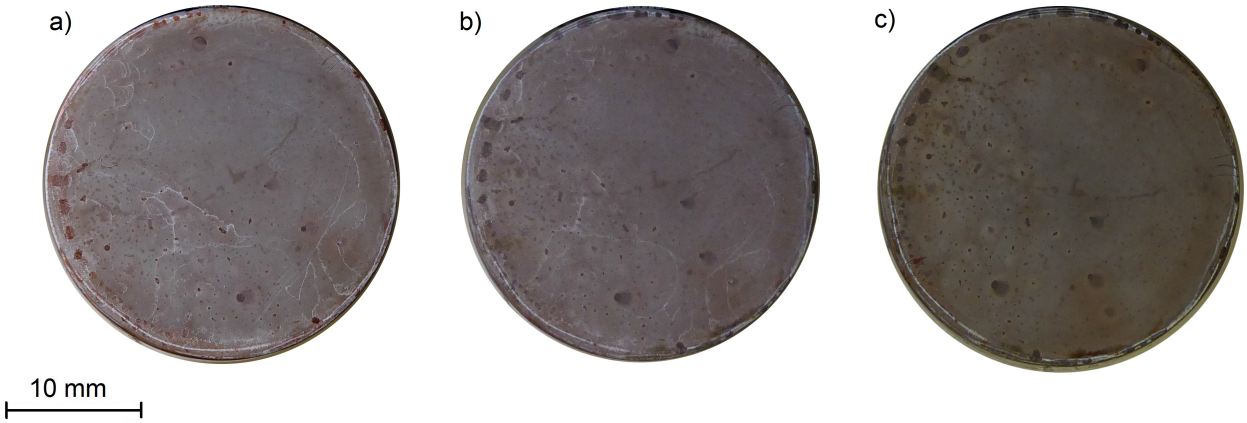

Figure 3.10: Series of photographs which span one full test cycle for a nanostructured surface grown by hydrothermal synthesis for 10 hours. a)After hydrothermal synthesis and first desorption. b)After second desorption, before experiments. c)After one evaporation experiment.

cycle of the experiments. One full test cycle consisted of distilled water droplet vaporization experiments across all parameters per surface, i.e. all droplet diameters, release heights and wall superheat levels. This observation was confirmed microscopically by SEM imaging (see Figure 3.7).

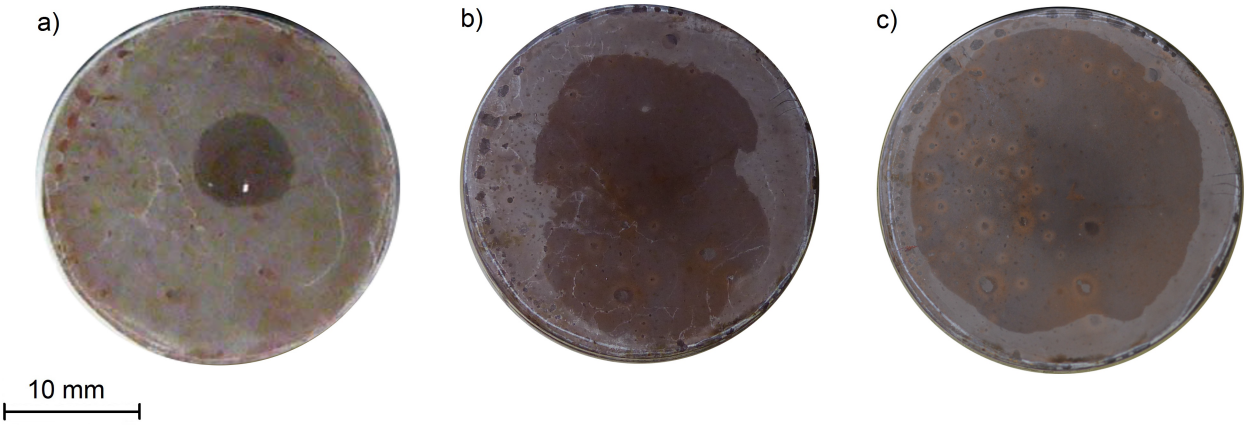

Figure 3.11: Series of photographs which span one full test cycle for a nanostructured surface grown by hydrothermal synthesis for 10 hours. a)Wetting after hydrothermal synthesis and first desorption. b)Wetting after second desorption, before experiments. c)Wetting after one evaporation experiment.

From Figure 3.11 the impact on surface wettability due to the second desorption procedure for this particular surface is clear. Although the series of photographs in Figure

3.11 represent only one surface, the trend of increasing wettability was observed for all the nanostructured surfaces to varying degrees as will be shown in Sections 3.6.6{3.6.7. Results of the contact angle evaluations for the bare metal and nanostructured surfaces used for the Leidenfrost and low superheat experiments are summarized in the remainder of this section.

3.6.4 Contact angle of bare metal surfaces

Experiments were performed with bare metal surfaces for comparison with the ZnO nanostructured surfaces. Surface wettability of the bare metal surfaces was characterized from the contact angle measured from the droplet pro le before and after experiments. Droplet evaporation experiments with the bare metal surfaces were performed as quickly as possible to minimize oxidation as a result of surface heating, which tends to increase the wettability of the surface. The water contact angle on the bare metal surfaces after the experiment was less than the contact angle measured before the experiment due to the oxidation. The average of the contact angle before the experiment, $\theta_{initial}$, and after experiments, θ_{final}, for all aluminum surfaces in this study was approximately $36.4^{\circ} \pm 12.3^{\circ}$. The average of the contact angle before the experiment, $\theta_{initial}$, and after experiments, θ_{final}, for all copper surfaces in this study was approximately $47.0^{\circ} \pm 16.9^{\circ}$. The resulting contact angles for both the copper and aluminum surfaces are typical of metallic surfaces, which are generally hydrophilic as a result of high surface energy. Complete results of contact angle measurements for the bare metal surfaces are found in Table 3.3.

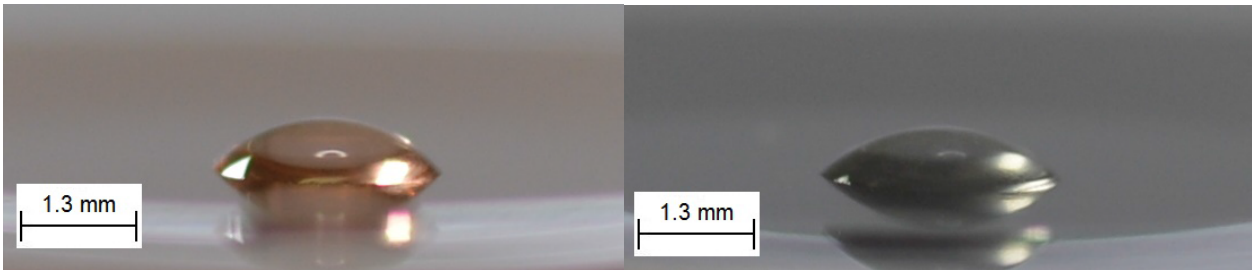

Figure 3.12: Water droplet pro le on copper (left) and aluminum (right) surfaces for contact angle measurement.

3.6.5 Wetting of ZnO nanostructured surfaces - general observations

Generally for droplets exhibiting contact angles greater than approximately 10° it was possible to measure the contact angle directly from the droplet pro le. The contact angle measurement from the droplet pro le was con rmed by an e ective contact angle calculation based on the measurement of the droplet liquid-solid contact area, i.e. the droplet spread

Table 3.3: Contact angles measured before experiments, $\theta_{initial}$, and after experiments, θ_{final}, for bare copper (Cu) and aluminum (Al) surfaces used for low superheat (LSH) and Leidenfrost (Leid) experiments.

Surface	$\theta_{initial}$	θ_{final}
Al (LSH)	$44.0^\circ \pm 4.8^\circ$	$12.9^\circ \pm 3.1^\circ$
Cu (LSH)	$53.6^\circ \pm 2.3^\circ$	$45.8^\circ \pm 4.4^\circ$
Al (Leid)	$50.4^\circ \pm 5.9^\circ$	$30.0^\circ \pm 4.9^\circ$
Al (Leid)	$43.4^\circ \pm 2.4^\circ$	$38.0^\circ \pm 6.5^\circ$
Cu (Leid)	$67.5^\circ \pm 5.9^\circ$	$21.0^\circ \pm 1.1^\circ$

area. For superhydrophilic surfaces exhibiting contact angles less than 5°, the reported contact angle in Table 3.4 was calculated exclusively from measurement of the droplet spread area.

The resulting contact angle measurements and calculations shown in Table 3.4 indicate that the duration of the hydrothermal synthesis on each surface resulted in a signi cant impact on surface wettability as characterized by contact angle and measurements of the droplet spread area. Interestingly, contact angle measurements and calculations indicate that increasing hydrothermal synthesis time does not increase surface wettability inde nitely. Furthermore, as indicated by the measurements and calculations in Tables 3.4{3.5 and visually by Figure 3.11, surface wettability was greatly enhanced by desorption. Finally, from Figure 3.11b) and c) it is acknowledged that the droplet spread area is not perfectly circular such that it would represent a spherical cap. However, for surfaces that exhibit droplet spread areas like those shown in Figure 3.11, assuming that the actual geometry is represented by a spherical cap for calculating e ective contact angles has a negligible e ect. The calculated e ective contact angles for surfaces of the nature exhibited in Figure 3.11 are extremely low, usually less than 1°, which is characteristic of superhydrophilic surfaces.

The ZnO nanostructured surfaces grown for 4 hours exhibited average contact angles of approximately 39.3° after the rst desorption, 22.2° after the second desorption and 11.1° after the evaporation experiments. The ZnO nanostructured surfaces grown for 10 hours exhibited average contact angles of approximately 24.1° after the rst desorption, 2.8° after the second desorption and 0.8° after the evaporation experiments. The ZnO nanostructured surfaces grown for 24 hours exhibited average contact angles of approximately 18.6° after the rst desorption, 13.5° after the second desorption and 10.9° after the evaporation experiments.

The e ect of increasing wettability for all ZnO nanostructured surface after desorption and experiments is evident for all surfaces. The surface grown for 24 hours was the least a ected by the test cycle as its contact angle decreased by approximately 40% from its value after the rst desorption. The contact angle for the surface grown for 4 hours decreased by approximately 75% over the course of the testing cycle. Finally, the surface grown for

10 hours exhibited a contact angle reduction of nearly 97% over the course of the testing cycle. Clearly, the testing cycle tends to increase the wettability of the surface. However, the variation in surface geometry that is achieved by di erent hydrothermal synthesis times is also very important as evidenced by the results summarized in Tables 3.4{3.5.

For the ZnO nanostructured surfaces in this study, the surface wettability, characterized by contact angle, peaks for a hydrothermal synthesis time of 10 hours, for every step in the test cycle. After the rst desorption, the contact angle for the surface grown for 10 hours is approximately 40% and 30% less than the surfaces grown for 4 and 24 hours, respectively. After the second desorption, the contact angle for the surface grown for 10 hours is approximately 87% and 80% less than the surfaces grown for 4 and 24 hours, respectively. After the experiment, the contact angle for the surface grown for 10 hours is approximately 92% less than the surfaces grown for 4 and 24 hours. The di erence in contact angles between the surfaces grown for 4 and 24 hours decreases from about 50% to less than 3% from the rst desorption to the end of the experiments.

Compared with bare copper, the presence of the nanostructures on the copper substrate reduces the contact angle as a result of Wenzel wetting. The presence of nanostructures enhances wetting by a nanoscale roughening of the surface which increases the solid surface area and surface energy of an already high energy metallic substrate. The extreme wetting is a result of the thermodynamic requirement that surface free energy be minimized. In order to minimize the surface free energy, the droplet must spread even further over the nanostructured surface, compared with a bare metallic surface, until the surface free energies of the copper, ZnO and liquid water have been minimized. Furthermore, the somewhat porous geometry of the ZnO nanocrystal array further aids in the spreading of the liquid through capillary action. Experimental results indicate that the geometry of the surface grown for 10 hours is formed in such a way that it promotes extreme wetting of liquid. The surfaces grown for 4 and 24 hours are also very highly wetting, especially compared to the bare metal surfaces. However, recalling that ZnO nanocrystals nucleated uniformly on only about 40% of the base substrate for a 4 hour hydrothermal synthesis, it is possible that this relatively low nanocrystal density weakened capillary e ects and, thus, liquid spreading was not as easily achieved compared with the surface grown for 10 hours whose un-nucleated surface area was only about 15% of the total base subtrate area. Furthermore, it is possible that the nucleated surface area for a 24 hour hydrothermal synthesis, approximately 96% of the total base substrate area, was too high for optimizing liquid spreading. Based on measurements and visual evidence of relatively high nanocrystal density from the SEM images in Figure 3.6, it is possible to conclude that the surface grown for 24 hours behaved more like a thin uniform lm of nanoscale roughness than a porous nanocrystal matrix capable of promoting capillary action and liquid spreading like that exhibited by the surface grown for 10 hours shown in Figure 3.5.

Finally, the geometries of the nanostructured surfaces grown for 4 and 24 hours promoted a stable wetting state which depicted a transition between the Wenzel and lm wetting states. This scenario is shown in Figure 3.13 for a surface grown for 24 hours by hydrothermal synthesis.

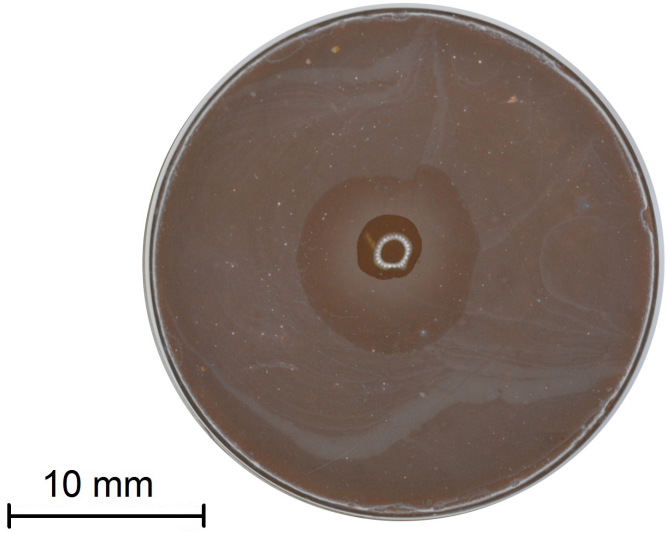

Figure 3.13: Water droplet exhibiting the transition from Wenzel-to- lm wetting state on a ZnO nanostructured surface grown for 24 hours.

For nanostructured surfaces which exhibited droplets in the transition from Wenzel-to- lm wetting states, Tables 3.4{3.5 represent the contact angle of the main bulk droplet as θ_{inner} and the corresponding projected solid-liquid contact area as A_{inner}. The e ective contact angle, θ_{outer} of the liquid lm surrounding the inner droplet is based on, A_{outer}, the spread area of the lm surrounding the liquid droplet.

3.6.6 Contact angle of ZnO nanostructured surfaces used in Leidenfrost experiments

Seven ZnO nanostructured surfaces were produced for the Leidenfrost study, one grown for 4 hours, ve grown for 10 hours and one grown for 24 hours. Complete results of measured and/or calculated contact angles for the surfaces used in the Leidenfrost experiments are found in Table 3.4. The surfaces in Table 3.4 are identi ed by the duration of the hydrothermal synthesis. In particular, since there were ve surfaces grown for 10 hours they are simply identi ed by a number indicating the order in which it was tested, e.g. 10-1 was the rst surface grown for 10 hours that was tested, 10-2 was the second surface grown for 10 hours that was tested and so on.

3.6.7 Contact angle of ZnO nanostructured surfaces used in low superheat experiments

Three ZnO nanostructured surfaces were produced for the low superheat study, one grown for 4 hours, one grown for 10 hours and one grown for 24 hours. Complete results

Table 3.4: Contact angles measured on ZnO nanostructured surfaces grown by hydrothermal synthesis for times, t, lasting 4, 10 and 24 hours for Leidenfrost experiments. θ_{inner} is the contact angle of the inner droplet, where applicable. A_{inner} is the solid-liquid contact area corresponding to the inner droplet. θ_{outer} is the calculated effective contact angle of the liquid film surrounding the inner droplet, where applicable, A_{outer} is the spread area of the film surrounding the liquid droplet. N.A. indicates that the property was not exhibited by the surface. The final column on the right indicates the moment after which the contact angle measurements were taken throughout the desorption and experiment cycles for the surface.

t (hrs)	θ_{inner}	A_{inner} (μm^2)	θ_{outer}	A_{outer} (μm^2)	Measured after...
4	44.2° ± 19.5°	8.5 ± 4.7	N.A.	N.A.	1st desorp.
4	29.9° ± 13.9°	12.3 ± 3.2	N.A.	N.A.	2nd desorp.
4	12.0° ± 3.6°	17.0 ± 3.5	N.A.	N.A.	experiment.
10-1	32.6° ± 8.4°	8.2 ± 4.5	N.A.	N.A.	1st desorp.
10-1	0.2° ± 0.0°	219.6 ± 5.3	N.A.	N.A.	2nd desorp.
10-1	0.2° ± 0.0°	226.1 ± 5.0	N.A.	N.A.	experiment
10-2	0.9° ± 0.1°	428.7 ± 21.0	N.A.	N.A.	experiment
10-3	3.2° ± 0.8°	40.5 ± 4.0	N.A.	N.A.	experiment
10-4	41.9° ± 4.6°	6.8 ± 0.6	9.7° ± 4.3°	20.3 ± 5.1	1st desorp.
10-4	38.4° ± 1.3°	7.3 ± 0.2	10.4° ± 0.4°	18.2 ± 0.5	2nd desorp.
10-4	0.1° ± 0.0°	392.0 ± 36.5	N.A.	N.A.	experiment
10-5	18.0° ± 6.1°	13.1 ± 3.2	1.3° ± 0.2°	72.5 ± 8.0	1st desorp.
10-5	0.5° ± 0.0°	130.7 ± 6.6	N.A.	N.A.	2nd desorp.
10-5	0.4° ± 0.0°	161.8 ± 11.8	N.A.	N.A.	experiment
24	21.2° ± 8.0°	12.9 ± 4.9	5.6° ± 1.6°	44.9 ± 36.8	1st desorp.
24	18.2° ± 4.9°	13.7 ± 3.3	4.9° ± 1.9°	31.5 ± 8.3	2nd desorp.
24	12.4° ± 1.3°	16.2 ± 1.1	3.1° ± 0.4°	41.0 ± 3.3	experiment

of measured and/or calculated contact angles for the surfaces used in the low superheat experiments are found in Table 3.5. The surfaces in Table 3.5 are identified by the duration of the hydrothermal synthesis.

Table 3.5: Contact angles measured on ZnO nanostructured surfaces grown by hydrothermal synthesis for times, t, lasting 4, 10 and 24 hours for low superheat experiments. θ_{inner} is the contact angle of the inner droplet, where applicable, A_{inner} is the solid-liquid contact area corresponding to the inner droplet, θ_{outer} is the calculated effective contact angle of the liquid film surrounding the inner droplet, where applicable, A_{outer} is the spread area of the film surrounding the liquid droplet. N.A. indicates that the property was not exhibited by the surface. The final column on the right indicates the moment after which the contact angle measurements were taken throughout the desorption and experiment cycles for the surface.

t (hrs)	θ_{inner}	A_{inner} (μm^2)	θ_{outer}	A_{outer} (μm^2)	Measured after...
4	34.4° ± 9.9°	9.0 ± 2.1	14.2° ± 0.5°	14.8 ± 1.5	1st desorp.
4	14.5° ± 0.2°	14.5 ± 1.5	12.2° ± 0.2°	16.3 ± 1.5	2nd desorp.
4	10.3° ± 1.0°	18.4 ± 1.2	3.3° ± 0.0°	39.1 ± 0.2	experiment
10	3.7° ± 0.3°	36.5 ± 1.5	N.A.	N.A.	1st desorp.
10	0.2° ± 0.0°	266.0 ± 10.8	N.A.	N.A.	2nd desorp.
10	0.1° ± 0.0°	335.7 ± 11.5	N.A.	N.A.	experiment
24	16.1° ± 7.3°	15.1 ± 6.1	2.4° ± 0.1°	48.4 ± 1.5	1st desorp.
24	8.9° ± 1.1°	20.4 ± 1.6	0.9° ± 0.1°	95.6 ± 9.5	2nd desorp.
24	9.3° ± 1.9°	19.8 ± 2.7	1.5° ± 0.1°	67.5 ± 3.1	experiment

Chapter 4

Results and discussion of low superheat experiments

A parametric study was conducted in order to determine the effect of the ZnO nanostructured surfaces on droplet evaporation at low superheat levels. Four parameters were varied in this study which included liquid droplet size, wall superheat, droplet release height and nanostructured surface geometry. Distilled water droplets having diameters of 1.52 ± 0.2 mm, 3.0 ± 0.4 mm and 3.9 ± 0.3 mm were deposited on the surface. Wall superheat levels were equivalent to 10°C, 20 °C, 30 °C and 40 °C. Droplets were released onto the surface from heights equivalent to the droplet radius, 1.9 ± 0.1 cm and 8.1 ± 0.4 cm, where height is measured from the plane of the surface to the center of the droplet. Three different nanostructured surface geometries were produced by performing the hydrothermal synthesis process for varying lengths of time. The surfaces were generated by hydrothermal synthesis times of 4, 10 and 24 hours. The surfaces are identified by the length of hydrothermal synthesis time. The results of the parametric study are summarized in this chapter.

4.1 Droplet spread area on ZnO nanostructured surfaces

When a liquid water droplet impinged upon the ZnO nanostructured surface it was observed that the nominally spherical droplet spread into a thin film over the surface. This was due to the Wenzel wetting effect [65]. The film thickness depends on many parameters, as will be shown in this chapter, but in general it measures approximately 100–500 μm. To determine the effect of wall superheat on the liquid spreading process over the surface, droplets of three different sizes were each deposited onto the surface from three different distances each onto three different surfaces at four different superheat levels.

During an experiment, the surface area wetted by the spreading droplet increased from a minimum area of approximately $\pi(D_{drop}/2)^2$ upon the time of droplet impact to a maximum spread area, A_{spread} before receding as a result of evaporation. Therefore, the reported mea-

surements are for the maximum area wetted by the spreading droplet during the evaporation experiments. The lm thickness, L_{film} can be estimated from knowledge of the measured initial droplet volume, V_{drop} and the measured A_{spread}, and is given by,

$$L_{film} = \frac{V_{drop}}{A_{spread}}. \quad (4.1)$$

It is assumed that the droplet begins to evaporate immediately upon impact with the surface, therefore at the time that the lm achieves the maximum spread area some liquid has already evaporated. As a result, Equation 4.1 overestimates the liquid lm thickness. Nevertheless, the evaporated liquid during the rapid droplet spreading process is assumed to be negligible such that the estimated L_{film} is appropriate for the purposes of this study. Finally, in an e ort to determine surface reliability and durability, the results that are reported in this study span the testing life cycle of the surface, i.e. the same surface was subjected to several hundred distilled water droplet experiments. The results of this parametric study are summarized in the following sections.

4.1.1 Spread area on ZnO nanostructured surface grown by a hydrothermal synthesis time of 4 hours

Results for experiments performed on the ZnO nanostructured surface grown by hydrothermal synthesis for 4 hours are depicted graphically in Figure 4.1.

In general, for this surface the maximum spread area increased with droplet volume at any given release height and wall superheat. Furthermore, for all droplet sizes, the maximum droplet spread area increased with increasing wall superheat. However, the magnitude of the increase in maximum spread area due to wall superheat also increased with droplet size. Results of droplet spread area measurements, with standard deviation, on the surface grown by hydrothermal synthesis for 4 hours as a function of droplet diameter, release height and wall superheat are listed in Table 4.1. Results of estimated liquid lm thickness as a function of droplet diameter, release height and wall superheat are listed in Table 4.2.

30 ga droplet - 2.5 mm diameter

For droplet release heights of 1.25 mm and 3.9 cm, the maximum spread areas for the 2.5 mm droplet are within 7% of one another for wall superheats of 10{30 °C. For a wall superheat of 10 °C, all 2.5 mm droplet spread areas are within approximately 7% of one another, 59.3{62.8 mm^2 for the three droplet release heights. Furthermore, for wall superheats of 10{30 °C, the droplet spread areas for all release heights increased approximately linearly as a function of temperature, about 2.5 mm^2/ °C. Beyond the wall superheat of 30 °C the droplet spread area increase rate appears to plateau. For the 2.5 mm droplet deposited from 1.25 mm the maximum spread area decreased slightly, by approximately 5% from 98.4 mm^2 to 93.1 mm^2 for a wall superheat increase from 30 °C to 40 °C. A similar trend is observed when the 2.5 mm droplet is released from 8.1 cm, as the maximum spread area decreased

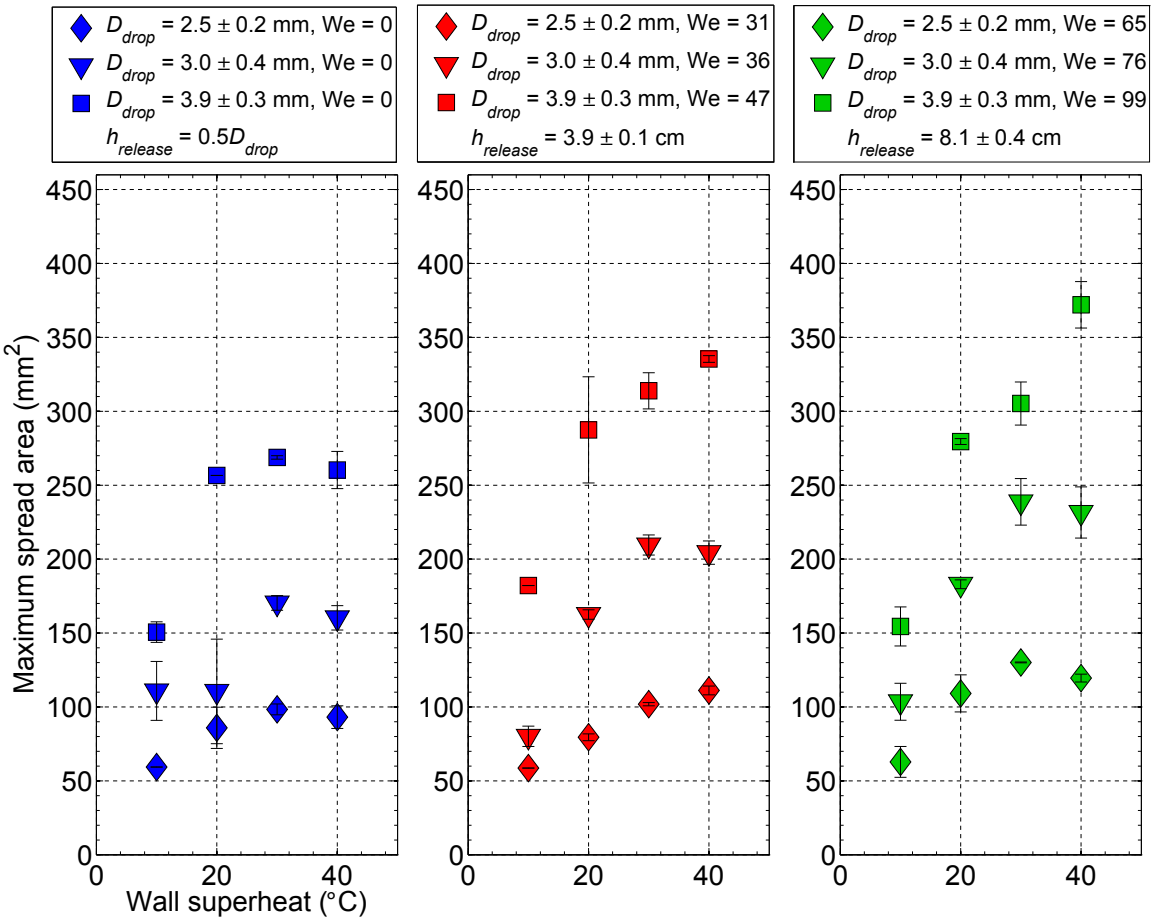

Figure 4.1: Droplet spread area as a function of wall superheat, droplet size and release height for ZnO nanostructured surface generated by hydrothermal synthesis for 4 hours.

by approximately 8% from 130 to 119 mm^2 for a wall superheat increase from 30 °C to 40 °C. The spread area increased by about 9% from about 102 mm^2 to 111 mm^2 for a a wall superheat increase from 30 °C to 40 °C and a release height of 3.9 cm, which is less than a third of the rate of spread area increase resulting from wall superheat increases from 10 °C to 30 °C.

For a droplet release height of 8.1 cm, the maximum spread area is noticeably greater, by an average of about 20%, than that of droplets released from 1.25 mm and 3.9 cm for superheats of 20 °C, 30 °C and 40 °C.

In summary, the maximum spread area for the 2.5 mm droplet increased as a function of wall superheat by an approximate average of 2.5 mm^2/°C up to 30 °C of superheat. Beyond 30 °C of superheat, the spread area increase plateaus. Only the 8.1 cm droplet release height produced a signi cant increase in maximum spread area, 20% on average, compared with the minimum and 3.9 cm release heights and at superheats of 20 °C and greater.

Table 4.1: Results of maximum droplet spread area measurements, with standard deviation, on surface grown for 4 hours D is the droplet diameter, A is the maximum droplet spread area, H is the droplet release height and T is the wall superheat.

		T = 10 °C	T = 20 °C	T = 30 °C	T = 40 °C
D (mm)	H (cm)	A (mm^2)	A (mm^2)	A (mm^2)	A (mm^2)
2.5	0.12	59.3 ± 0.0	85.9 ± 14.0	98.4 ± 3.7	93.1 ± 7.7
2.5	3.9	58.7 ± 0.0	79.5 ± 2.3	101.9 ± 1.1	111.2 ± 3.0
2.5	8.1	62.8 ± 10.4	109.2 ± 12.6	130.1 ± 0.3	119.5 ± 2.7
3.0	0.15	110.9 ± 19.9	110.5 ± 35.4	170.4 ± 4.9	160.3 ± 8.2
3.0	3.9	80.1 ± 6.9	162.5 ± 3.2	209.6 ± 6.8	204.4 ± 7.9
3.0	8.1	103.5 ± 12.5	183.0 ± 3.0	238.7 ± 15.7	231.6 ± 17.3
3.9	0.20	150.7 ± 7.0	256.6 ± 0.0	268.8 ± 1.2	260.3 ± 12.6
3.9	3.9	182.1 ± 0.0	287.4 ± 35.9	313.9 ± 12.2	335.4 ± 2.3
3.9	8.1	154.4 ± 13.2	279.5 ± 2.0	305.3 ± 14.6	372.1 ± 15.7

Table 4.2: Estimated liquid lm thickness based on initial droplet volume and the measured maximum droplet spread area on surface grown for 4 hours D is the droplet diameter, L_{film} is the lm thickness, H is the droplet release height and T is the wall superheat.

		T = 10 °C	T = 20 °C	T = 30 °C	T = 40 °C
D (mm)	H (cm)	L_{film} (μm)	L_{film} (μm)	L_{film} (μm)	L_{film} (μm)
2.5	0.12	110.2	136.0	92.0	91.1
2.5	3.9	144.1	74.6	81.9	53.7
2.5	8.1	172.2	101.8	100.3	65.6
3.0	0.15	141.3	158.9	146.7	112.3
3.0	3.9	151.5	156.7	142.0	98.2
3.0	8.1	163.9	156.0	130.3	97.6
3.9	0.20	127.1	93.7	103.8	128.6
3.9	3.9	151.2	109.8	82.7	92.3
3.9	8.1	170.4	95.1	83.7	80.9

22 ga droplet - 3.0 mm diameter

For 3.0 mm diameter droplets released from all three test heights, it is immediately evident that an increase in wall superheat from 30°C to 40 °C has a minimal e ect on the spread area, which was also observed for the smaller 2.5 mm droplet. For all three release heights, the maximum spread area of the 3.0 mm droplet actually decreases from its value at a wall superheat of 30°C by approximately 6% or less to its value at a superheat of 40 °C. Neglecting the release height of 1.5 mm, the 3.0 mm droplet, like the 2.5 mm droplet,

experiences its greatest percentage increase in spread area as a result of a wall superheat increase from 10°C to 20 °C. For a wall superheat increase from 10°C to 20 °C and a release height of 3.9 cm, the spread area for the 3.0 mm droplets increased by approximately 100% from 80 mm^2 to 160 mm^2. For a wall superheat increase from 10°C to 20 °C and release height of 8.1 cm, the spread area for the 3.0 mm droplets increased by approximately 75% from about 100 mm^2 to 180 mm^2. A superheat increase of 20°C to 30 °C results in only about 30% spread area increase, from about 160 mm^2 to 210 mm^2 for a release height of 3.9 cm. For a superheat increase from 20 to 30°C and a release height of 8.1 cm, the spread area for the 3.0 mm droplet also only increases by about 30%, from 180 mm^2 to 240 mm^2.

Furthermore, an increase in release height generally increased the magnitude of the maximum spread area, which was observed as well for the 2.5 mm droplet. As was also the case for the 2.5 mm droplet, the maximum spread area of the 3.0 mm droplet depends more strongly on wall superheat changes than on changes in release height for wall superheats below 30°C. For example, for a wall superheat of 30°C, the maximum spread area for a 3.0 mm droplet released from 8.1 cm was 240 mm^2, which is about 14% greater than the spread area, about 210 mm^2 for the same size droplet released from 3.9 cm. In comparison, the maximum spread area for the 3.0 mm droplet increased by approximately 30% for release heights of 3.9 cm and 8.1 cm, from about 160 mm^2 to 210 mm^2 and 180 mm^2 to 140 mm^2, respectively, due to a wall superheat increase from 20°C to 30 °C. Beyond a wall superheat of 30 °C, any further increases in spread area area result from increases in droplet release height, which was also observed for the 2.5 mm droplet.

In summary, maximum spread area for the 3.0 mm droplet, increased as a function of wall superheat up to 30°C. The greatest rate of change as a function of superheat occurred for a change of 10°C to 20 °C of superheat. Beyond 30°C of superheat the spread area increase plateaus. The droplet spread area generally increased with increasing release height, although it was more strongly a ected by increases in superheat up to 30°C. Beyond 30°C, any further increases in spread area were due to droplet release height.

16 ga droplet - 3.9 mm diameter

As was observed for the two smaller droplets, the 3.9 mm droplet experiences its greatest change in maximum spread area as a result of a wall superheat increase from 10°C to 20 °C for all release heights. For a release height of approximately 0.2 cm and a wall superheat increase from 10°C to 20 °C, the spread area increased by 70% from about 150 mm^2 to 256 mm^2. For a wall superheat increase from 20°C to 30 °C, the spread area increased by only about 5%, from about 256 to 268 mm^2 and decreased by about 3% to 260 mm^2 for a wall superheat increase to 40°C. Similarly, a release height of 3.9 cm, the 3.9 mm droplet spread area increased by nearly 60% from about 180 mm^2 to nearly 290 mm^2 for a superheat increase from 10°C to 20 °C. A superheat increase from 20°C to 30 °C, results in only about a 10% increase in spread area from about 287 mm^2 to 314 mm^2 and a 7% increase to 335 mm^2 for an increase to a wall superheat of 40°C. A similar trend is observed for a release height of 8.1 cm, where a wall superheat increase from 10°C to 20 °C results in an

80% increase in droplet spread area from about 154 mm^2 to about 280 mm^2. A further wall superheat increase to 30°C resulted in a 9% increase in spread area to about 305 mm^2. In contrast to trend observed for the other two release heights, for a release height of 8.1 cm an increase in wall superheat from 30°C to 40 °C results in an increase in spread area from about 305 mm^2 to 372 mm^2, about 22%.

Furthermore, up to a wall superheat of 30°C, the magnitude of maximum spread area is more strongly sensitive to changes in wall superheat than on droplet release height. For a wall superheat of 10°C the 3.9 mm droplet spread area increases by about 20% from 150 mm^2 to 180 mm^2 due to an release height increase of 0.2 cm to 3.9 cm. In comparison, it has already been shown that a wall superheat increase of 10 to 20 °C, the spread area increased by approximately 70% and nearly 60% for droplets released from 0.2 cm and 5 cm, respectively. For a wall superheat of 20°C, the 3.9 mm droplet spread area increased by about only 12% from 256 mm^2 to 287 mm^2 due to an increase in release height from 0.2 cm to 3.9 cm. This is the general trend up to a superheat of 30°C.

More interestingly, for release heights of 3.9 and 8.1 cm and superheats of 30 and greater, the plateauing effect observed for the smaller droplets is absent. For this droplet size, increases in release height beyond 3.9 of wall superheat result in increases in maximum spread area. For wall superheat changes from 30 to 40 °C and release height increases from 3.9 cm to 8.1 cm, the effect of each parameter was more balanced, with neither parameter clearly resulting in the increase in wall superheat.

For the 0.2 cm release height, the droplet spread area does appeared to plateau beyond a wall superheat of 20°C and even decreased for a wall superheat of 40. This was generally observed as well for the smaller droplets.

In summary, maximum spread area for the 3.9 mm droplet increased as a function of wall superheat for all superheat levels tested when it is released from 3.9 and 8.1 cm. For release heights of 0.2 cm, the droplet maximum spread area increased as a function of superheat up to 30 °C after which it decreased. As was true of the smaller droplets, the greatest rate of change as a function of superheat occurred for an increase of 10 to 20 °C of superheat. The droplet spread area generally increased with increasing release height, although it was more strongly affected by increases in superheat up to 30°C. For release heights of 3.9 cm and 8.1 cm, beyond 30°C increases in spread area were due to a balanced combined effect of increases in both release height and wall superheat.

4.1.2 Discussion of greatest spread area increase for wall superheat of 10 to 20 °C

It is noteworthy that for this particular surface the onset of nucleation was visually observed to be approximately 11 ± 3 °C. As a result vapor bubbles were generated at the surface for wall superheat temperatures greater than and equal to 11. Since the vapor specific density is approximately 1000 times greater than the liquid density, the generation of bubbles that occurs during a wall superheat increase from 10 to 20 °C, may explain the

rapid increase in maximum spread area that is observed for all three droplet sizes released from all three test heights. In e ect, as the vapor bubbles nucleate and grow they do work on the surrounding liquid, pushing it radially outward causing it to spread it over the surface. This experimental observation is similar to those found by other investigators [66].

4.1.3 Discussion of plateauing for small droplets vs large droplets

It was visually observed that there was vigorous nucleate boiling and subsequently signi cant satellite droplet ejection resulting from nucleate boiling for wall superheats greater than and equal to 30°C. Since these satellite droplets represent a greater percentage of the total volume of the two smaller droplets measuring 2.5 and 3.0 mm, this may be the reason that a smaller maximum spread area is observed for these droplet sizes at a superheat of 40 °C. Furthermore, this may also explain the plateauing e ect that is observed for the smaller droplets. The volume of the 3.9 mm droplet is roughly 120% and 250% greater than the volume of the 3.0 mm and 2.5 mm droplets, respectively, which may mean that that any e ect from satellite droplet ejection from the larger droplets is relatively negligible and, furthermore, the maximum droplet spread area continues to increase with further increases in wall superheat.

4.1.4 ZnO surface - hydrothermal synthesis time = 10 hours

Results for experiments performed on the ZnO nanostructured surface grown by hydrothermal synthesis for 10 hours are depicted graphically in Figure 4.2.

In general, for this surface the maximum spread area increased with droplet volume at any given release height and wall superheat. Furthermore, for all droplet sizes, the maximum droplet spread area increased with increasing wall superheat. However, the magnitude of the increase in maximum spread area due to wall superheat also increased with droplet size. Finally, increases in the droplet release height also tended to result in an increase in the maximum spread area. Based on visual observation from the video recordings, the onset of nucleate boiling occurred between superheat levels of 30 to 40 °C. Results of droplet spread area measurements, with standard deviation, on the surface grown by hydrothermal synthesis for 10 hours as a function of droplet diameter, release height and wall superheat are listed in Table 4.3. Results of estimated liquid lm thickness as a function of droplet diameter, release height and wall superheat are listed in Table 4.4.

30 ga droplet - 2.5 mm diameter

Similar to the 2.5 mm droplets deposited on the surface generated by hydrothermal synthesis for 4 hours, for all release heights, the 2.5 mm droplets deposited over a surface grown for 10 hours of hydrothermal synthesis exhibit a more gradual rate of increase in maximum spread area compared with the rate of spread area increase exhibited by the 3.0 mm and 3.9 mm droplets. The maximum spread area rate of increase as a function of wall

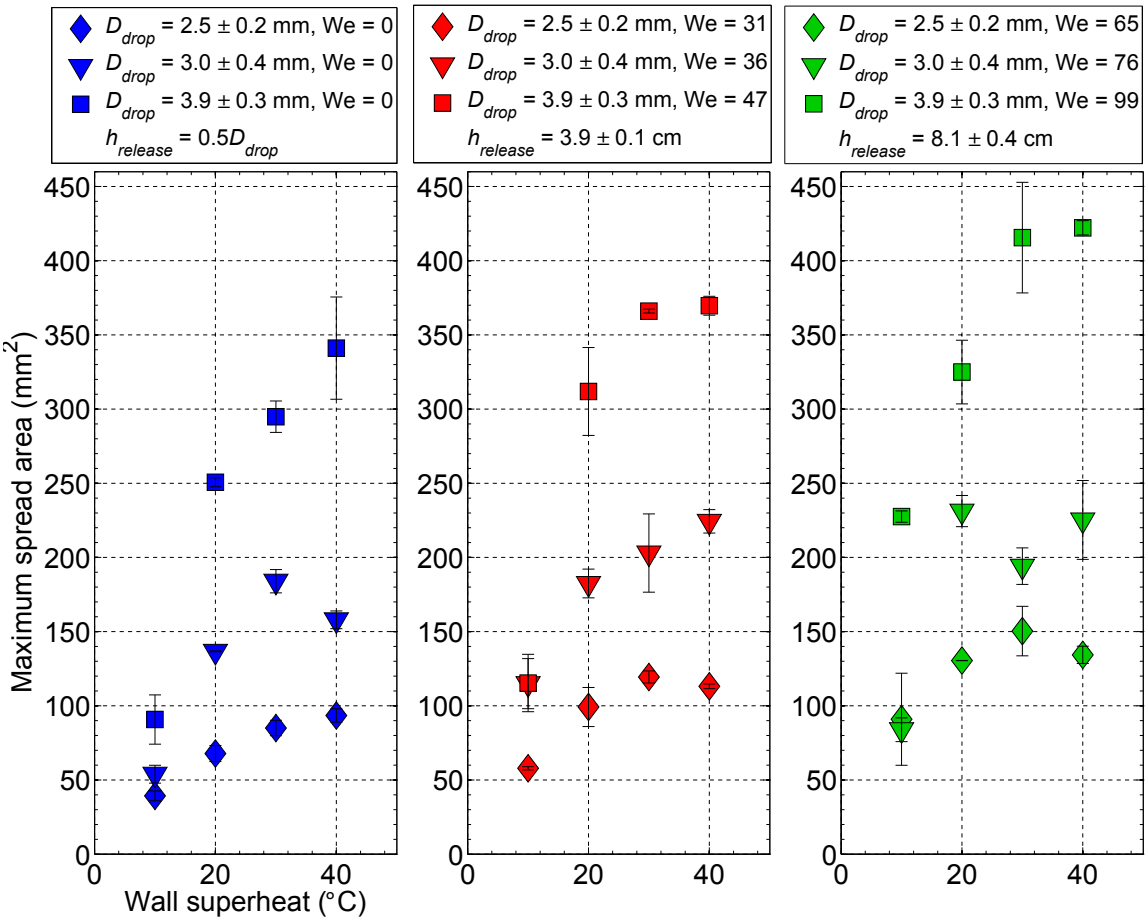

Figure 4.2: Droplet spread area as a function of wall superheat, droplet size and release height for ZnO nanostructured surface generated by hydrothermal synthesis for 10 hours.

superheat temperature was approximately 2{4 mm^2/°C for wall superheats of 10{30°C, which was, on average, approximately half of the rate of spread area increase for the 3.0 mm droplet and one third of the rate of spread area increase for the 3.9 mm droplets. The rate of maximum spread area increase was positive for the lowest droplet release height, 1.25 mm, for all superheat levels, however it slowed signi cantly with increasing wall superheat, especially beyond 30°C. For 2.5 mm droplets released from 3.9 and 8.1 cm, the maximum spread area increased as a function of temperature up to a wall superheat of 30°C, after which it decreased at a wall superheat of 40°C. This phenomenon was also observed on the ZnO surface grown by hydrothermal synthesis for 4 hours. Similarly, there was a plateauing e ect that is most apparent beyond 30°C of wall superheat.

Furthermore, the 2.5 mm droplet experienced the greatest percentage change in spread area for a wall superheat increase from 10°C to 20 °C for all release heights. For a wall superheat increase from 10 to 20 °C and a release height of 1.25 mm, the maximum spread

Table 4.3: Results of maximum droplet spread area measurements, with standard deviation, on surface grown for 10 hours. D is the droplet diameter, A is the maximum droplet spread area, H is the droplet release height and T is the wall superheat.

		T = 10 °C	T = 20 °C	T = 30 °C	T = 40 °C
D (mm)	H (cm)	A (mm^2)	A (mm^2)	A (mm^2)	A (mm^2)
2.5	0.12	39.3 ± 3.3	67.8 ± 5.4	85.0 ± 5.2	93.4 ± 4.5
2.5	3.9	57.9 ± 1.1	99.2 ± 13.1	119.4 ± 4.1	113.1 ± 1.5
2.5	8.1	90.9 ± 31.1	130.4 ± 0.1	150.4 ± 16.7	134.3 ± 5.8
3.0	0.15	53.9 ± 6.0	136.7 ± 0.3	184.0 ± 7.9	158.0 ± 6.0
3.0	3.9	114.9 ± 16.9	182.4 ± 9.7	203.0 ± 26.4	224.3 ± 7.9
3.0	8.1	83.9 ± 8.0	231.3 ± 10.5	194.1 ± 12.3	225.3 ± 26.6
3.9	0.20	90.8 ± 7.0	250.7 ± 0.0	294.9 ± 1.2	341.1 ± 12.6
3.9	3.9	115.4 ± 0.0	311.9 ± 35.9	366.1 ± 12.2	369.7 ± 2.3
3.9	8.1	227.5 ± 13.2	325.0 ± 2.0	415.6 ± 14.6	422.2 ± 15.7

Table 4.4: Estimated liquid film thickness based on initial droplet volume and the measured maximum droplet spread area on surface grown for 10 hours. D is the droplet diameter, L_{film} is the film thickness, H is the droplet release height and T is the wall superheat.

		T = 10 °C	T = 20 °C	T = 30 °C	T = 40 °C
D (mm)	H (cm)	L_{film} (μm)	L_{film} (μm)	L_{film} (μm)	L_{film} (μm)
2.5	0.12	297.8	129.6	104.4	128.0
2.5	3.9	217.1	112.0	96.4	94.9
2.5	8.1	122.4	93.5	78.7	104.1
3.0	0.15	205.6	136.9	102.5	116.5
3.0	3.9	238.1	101.9	95.7	84.6
3.0	8.1	322.1	89.1	121.9	100.5
3.9	0.20	272.0	133.0	127.6	121.0
3.9	3.9	415.2	102.1	100.1	109.0
3.9	8.1	171.9	114.2	122.8	109.5

area increased by approximately 70% from about 40 mm^2 to 68 mm^2. Similarly, for a wall superheat increase from 10 to 20 °C and a release height of 3.9 cm the spread area increased from about 58 mm^2 to 99 mm^2, approximately 70%. For a wall superheat increase from 10 ° to 20 °C and a release height of 8.1 cm the spread area increased by about 40% from 91 mm^2 to 130 mm^2. In comparison, for all release heights, the maximum spread area increased by only about 20% from its value at a superheat of 20 °C to 30 °C. As was described earlier, only the droplet released from 1.25 mm experienced an increase in maximum spread area,

approximately 10%, from 85 mm^2 to 93 mm^2, for a superheat increase from 30 °C to 40 °C. For release heights of 3.9 cm and 8.1 cm, the droplet maximum spread area decreased for a superheat increase of 30 °C to 40 °C. The 2.5 mm droplet deposited on this surface exhibited diminishing returns in maximum spread area increase as a function of wall superheat.

In general, for the 2.5 mm droplet deposited on this surface, the maximum spread area increased with increasing release height. Although the increase in maximum spread area was a result of the combined effect of increasing release height and wall superheat, the maximum spread area was more sensitive to changes in temperature at lower superheat levels. For example, a 2.5 mm droplet impinging on a surface at a superheat of 10 °C exhibited a spread area increase of about 47%, from 39 mm^2 to 58 mm^2, due to a release height increase from 1.25 mm to 3.9 cm. At the same superheat level of 10 °C, the spread area of the 2.5 mm droplet increased by about 57%, from 58 mm^2 to 91 mm^2, for a release height increase from 3.9 cm to 8.1 cm.

For a surface at a superheat level of 20 °C, a release height increase from 1.25 mm to 3.9 cm resulted in a spread area increase of about 46%, from 69 mm^2 to 99 mm^2, and an increase of about 30%, from 99 mm^2 to 130 mm^2, for an increase in release height from 3.9 cm to 8.1 cm. In contrast, for a wall superheat increase from 10 °C to 20 °C, the 2.5 mm droplet spread area increased by approximately 70%, from 39 mm^2 to 68 mm^2, for a release height of 1.25 mm. Similarly, for a release height of 3.9 cm and a wall superheat increase from 10 °C to 20 °C, the 2.5 mm droplet spread area increased by approximately 70% as well, from 58 mm^2 to 99 mm^2. For both release heights of 1.25 mm and 3.9 cm the 70% increase in spread as a function of an increase from 10 °C to 20 °C was greater than the effect due to an increase in release height at superheat levels of 10 °C and 20 °C. However, for a droplet release height of 8.1 cm the maximum spread area increased by only about 43%, from 90 mm^2 to 130 mm^2, as a result of a wall superheat increase from 10 °C to 20 °C. In comparison, at a wall superheat level of 10 °C, the spread area increased by approximately 57%, from 58 mm^2 to 91 mm^2, for a release height increase from 3.9 cm to 8.1 cm. At a wall superheat of 20 °C, the spread area increased by about 30%, from 99 mm^2 to 130 mm^2, as a result of a release height increase from 3.9 cm to 8.1 cm.

Whereas for the lower superheat levels, changes in temperature dominate the increase in droplet spreading, at the higher superheat levels of 30 °C and especially 40 °C, increases in spread area are dominated by release height. For example, only the droplet released from a height of 1.25 mm droplet experienced an increase in spread area, a moderate 10%, from 85 mm^2 to 93 mm^2 when the surface is heated from a superheat of 30 °C to 40 °C . In contrast, at a superheat of 30 °C, increasing the droplet height from 1.25 mm to 3.9 cm resulted in a spread area increase of approximately 40%, from 85 mm^2 to 119 mm^2. At a superheat of 30 °C, an increase in release height from 3.9 cm to 8.1 cm resulted in a spread area increase of about 25%, from 119 mm^2 to 150 mm^2. For a superheat level of 40 °C increasing the droplet height from 1.25 mm to 3.9 cm results in a spread area increase of approximately 20%, from 93 mm^2 to 113 mm^2. An increase in height from 3.9 cm to 8.1 cm also resulted in a spread increase of approximately 20% from about 113 mm^2 to 134 mm^2.

It is interesting to note that for this droplet size, in general the effect of maximum

spread area increase that results from increases in height also diminished, although not quite so drastically as the e ect of increasing surface temperature. Furthermore, the e ect of increasing release height also diminished with increasing wall superheat. Clearly, the maximum spread area depends on both combined e ect of changes in the parameters of wall superheat and release height.

In summary, for the 2.5 mm droplet deposited over the surface grown by hydrothermal synthesis for 10 hours, the maximum spread area increased with increasing wall superheat up to 30 °C. Beyond a superheat of 30°C, only droplets released from the minimum height of 1.25 mm resulted in increases in spread area, a modest 10 %. The maximum spread area decreased for a wall superheat increase from 30°C to 40 °C for release heights of 3.9 cm and 8.1 cm. The spread area plateauing e ect as a function of wall superheat was observed. In general, increasing the release height resulted in an increase in maximum spread area for all superheat levels. An increase from 1.25 mm to 3.9 cm in release height generally resulted in a greater percentage increase in spread area than an increase from 3.9 to 8.1 cm. There were diminishing returns from an increase in release height, although not quite as signi cant as for those observed from increasing wall superheat.

22 ga droplet - 3.0 mm diameter

Some of the data for the 3.0 mm droplet deposited over the surface grown by hydrothermal synthesis for 10 hours exhibit some anomolous behavior relative to that shown by the other droplet sizes. Nevertheless, general trends can still be identi ed. The 3.0 mm droplets released from all test heights over this surface, experienced the greatest percentage change in maximum spread area, compared with all other parameters, as a result of a wall superheat increase of 10°C to 20 °C. For a wall superheat increase of 10°C to 20 °C, the spread area increased by approximately 150%, from 53 mm^2 to 137 mm^2, for a release height of 1.5 mm; by approximately 60%, from 115 mm^2 to 182 mm^2, for a release height of 3.9 cm; and by approximately 175%, from 84 mm^2 to 231 mm^2, for a release height of 8.1 cm. However, a wall superheat increase from 20°C to 30 °C had a much lesser e ect on increasing spread area. For a wall superheat increase from 20°C to 30 °C and a release height of 1.5 mm, the spread area increased by only about 35%, from 137 mm^2 to 184 mm^2. For a release height of 3.9 cm, the spread area increased by only about 10%, from 182 mm^2 to 203 mm^2, and decreased by 16%, from 231 mm^2 to 194 mm^2 for a release height of 8.1 cm and the same wall superheat increase from 20°C to 30 °C.

An additional wall superheat increase to 40°C further diminishes the spread area percentage increase to 10{15% from its value at a superheat of 30°C for all release heights. Similar to the smaller droplet deposited over this surface and all the droplets deposited over the ZnO nanostructured surface grown for 4 hours, increases in wall superheat resulted in a diminishing percentage increase in maximum spread area.

The maximum spread area increased continuously as a function of wall superheat for a release height of 3.9 cm. However, neglecting the anomalous point at a wall superheat level of 30 °C for the droplet released from 8.1 cm, for release heights of 1.5 mm and 8.1 cm the

maximum spread area decreased beyond superheat levels of 30 °C. This was also observed for the smaller 2.5 mm diameter droplet.

With two exceptions, in general, an increase in release height resulted in an increase in maximum spread area of the droplet. Furthermore, increasing the release height from 1.5 mm to 3.9 cm generally produced a signi cantly greater percentage increase in maximum spread area compared with increasing the release height from 3.9 to 8.1 cm. For example at a wall superheat level of 10 °C, increasing the release height from 1.5 mm to 3.9 cm increased the maximum spread area by approximately 110%, from 54 mm^2 to 115 mm^2, whereas the droplet spread area decreased by 27%, from 115 mm^2 to 84 mm^2, for a release height increase from 3.9 to 8.1 cm. At a superheat level of 20 °C, the maximum spread area increased by about 33%, from 137 mm^2 to 182 mm^2, for a release height increase from 1.5 mm to 3.9 cm and only by about 27%, from 182 mm^2 to 231 mm^2, for a release height increase from 3.9 to 8.1 cm. In this particular example it also evident that increasing height and wall superheat simultaneously may have a combined e ect on the spread area. In any case, it is concluded for this droplet size and surface combination that, like with wall superheat, increasing droplet release height yields diminishing increases in maximum spread area.

Comparing the e ects of increases in wall superheat and droplet release height on maximum spread area, it is evident once again that maximum spread area was more strongly sensitive to wall superheat than release height at superheat levels less than and equal to 20 °C. As was discussed earlier in this section, for a wall superheat change from 10 °C to 20 °C, the maximum spread area increased by approximately 150, 60 and 175% for release heights of 1.5 mm, 3.9 and 8.1 cm. By comparison, a release height increase from 1.5 mm to 3.9 cm at a superheat level of 10 °C results in an increase of approximately 110%, from 54 mm^2 to 115 mm^2, and an increase of about 33%, from 137 mm^2 to 182 mm^2, when the superheat level is increased to 20 °C. Increasing the release height from 3.9 to 8.1 yields signi cantly less area increases at both superheat levels of 10 °C and 20 °C. Clearly, the wall superheat dominates the spreading process at the lower levels. However, for superheat levels greater than 20 °C, increasing the release height from 1.5 mm to 3.9 cm dominated the e ect of increased maximum spread area. For this release height increase, the maximum spread area increased by approximately 33%, from 137 mm^2 to 182 mm^2, for a superheat of 20 °C; by approximately 10%, from 184 mm^2 to 203 mm^2, for a superheat of 30 °C; and by approximately 40%, from 158 mm^2 to 224 mm^2, for a superheat of 40 °C. In contrast, for superheat level increases from 20 to 30 °C, the spread area increased by approximately 33%, from 137 mm^2 to 184 mm^2, at a release height of 1.5 mm, but only 11%, from 182 mm^2 to 203 mm^2, at release height of 3.9 cm. For a superheat level increase of 30 to 40 °C the spread area decreased by about 14%, from 184 mm^2 to 158 mm^2, for a release height of 1.5 mm and increases by about 10%, from 203 mm^2 to 224 mm^2, for a release height of 3.9 cm. The e ect of increasing the release height to 8.1 cm was negligible in comparison.

In summary, for the 3.0 mm droplet deposited over the surface grown for 10 hours by hydrothermal synthesis, the maximum spread area increased as a function of wall superheat up to 30 °C for droplets released from 1.5 mm and 8.1 cm. Only droplets released from 3.9 cm exhibited a steady increase in maximum spread area for all superheat levels. In

general, increasing the release height resulted in an increase in maximum spread area for all superheat levels. An increase from 1.25 mm to 3.9 cm in release height generally resulted in a greater percentage increase in spread area than an increase from 3.9 to 8.1 cm. There were diminishing returns resulting from an increase in release height.

16 ga droplet - 3.9 mm diameter

For droplets of 3.9 mm diameter deposited on the ZnO nanostructured surface grown by hydrothermal synthesis for 10 hours, the greatest percentage increase in maximum spread area was due to an increase in wall superheat from 10°C to 20 °C. For a wall superheat increase of 10°C to 20 °C, the spread area increased by approximately 175%, from 90 mm^2 to 250 mm^2, for a release height of approximately 0.2 cm; by approximately 170%, from 115 mm^2 to 312 mm^2, for a release height of 3.9 cm; and by approximately 40%, from 228 mm^2 to 325 mm^2, for a release height of 8.1 cm. With the exception of an increase in maximum spread area of 97%, from 115 mm^2 to 228 mm^2, that resulted from increasing droplet release height from 3.9 cm to 8.1 cm at a wall superheat of 10°C, no other parametric change resulted in an increase of spread area greater than 40%.

In general, for this drop size, an increase in wall superheat resulted in an increase in maximum droplet spread area. As was seen for the other droplet sizes the e ect of increasing wall superheat diminished in terms of the rate of percentage increase of maximum spread area. The plateauing e ect that was observed for the smaller droplets as wall superheat levels approached 40°C was exhibited by this size droplet as well, especially for release heights of 3.9 and 8.1 cm. For droplets released from 0.2 cm, a wall superheat increase from 20 °C to 30 °C resulted in a spread area increase of about 17%, from 250 mm^2 to 295 mm^2, which is a negligible percentage increase compared with the 175% increase observed for a wall superheat increase from 10°C to 20 °C. A further increase in superheat from 30°C to 40 °C resulted in about a 15% increase in spread area from 295 mm^2 to 341 mm^2. This trend is similarly observed by droplets released from 3.9 cm and 8.1 cm for a wall superheat increase from 20 °C to 30 °C. For a wall superheat increase from 30°C to 40 °C, the maximum spread area increased by less than 2% for droplets released from 3.9 cm and 8.1 cm.

In general, incremental increases in droplet release height resulted in increases in maximum spread area. As was described earlier in this section, the greatest percentage increase in maximum spread area of approximately 97% resulted from a height increase from 3.1 cm to 8.4 cm at a wall superheat of 10°C. For this release height increase, beyond a superheat level of 10 °C, spread area percentage increases were less than 15% for all superheats, a signi cant reduction from that observed at the lowest superheat level. For release height increases from 0.2 cm to 3.9 cm, maximum spread area percentage increased from its value at a release height of 0.2 cm by approximately 25% to its value at a release height of 3.9 cm for superheats 10{30°C, whereas the spread area increased only by about 8%, from 341 mm^2 to 370 mm^2, for a wall superheat of 40°C.

As with the two smaller droplets tested, the 3.9 mm droplet maximum spread area was most sensitive to wall superheats up to 20 compared with release height. Beyond a wall

superheat level of 20°C, the effects of increasing wall superheat and droplet release height were the most balanced compared with the effects observed for the smaller droplets.

In summary, for 3.9 mm droplets deposited over a surface grown by hydrothermal synthesis for 10 hours, the greatest percentage increases in maximum spread area were observed for wall superheat increases of 10°C to 20 °C and were equivalent to approximately 175% and 170% for release heights of 0.2 cm and 3.9 cm, respectively, and about 40% for the droplet released from 8.1 cm. In fact, this was the greatest percentage increase observed for spread area in the entire parametric study, including surface geometry. For a droplet release height increase from 0.2 cm to 3.9 cm maximum spread area percentage increases were relatively constant at 25% for superheat levels between 10°C and 30 °C. A release height increase from 3.9 cm to 8.1 cm resulted in a significant percentage increase, 97%, in maximum spread area for a superheat of 10°C and quickly dropped off to below 15% for the greater superheat levels. Finally, the maximum spread area was most sensitive to changes in wall superheat below 20°C after which the effects of increasing release height and wall superheat were balanced.

4.1.5 Discussion of diminishing returns in spread area increase as a function of wall superheat

It was observed that for the two smaller droplets measuring 2.5 mm and 3.0 mm, there was a diminishing percentage increase in maximum spread area with increasing wall superheat. This indicates that there may have been mechanisms suppressing any further growth at higher superheats. Unlike the surface grown over 4 hours, the surface grown by hydrothermal synthesis for 10 hours exhibited the onset of nucleate boiling at a relatively high wall superheat level of 30–40°C. The onset of nucleate boiling was detected from video evidence only. Thus, at the highest superheat level there was nucleate boiling and some small satellite droplet ejection. It is assumed that this minimal droplet ejection is negligible compared to the relatively large volume of the 3.9 mm diameter droplet, but as was discussed before, the volume of the satellite droplets accounts for a greater volume of the 2.5 mm and 3.0 mm droplets.

It was observed that the greatest percentage increase in maximum spread area for all droplet sizes and heights resulted from a wall superheat level increase from a 10°C to 20 °C. Compared with superheat level increases from 20°C to 30 °C and 30°C to 40 °C, the increase in spread area resulting from 10°C to 20 °C increase in wall superheat was a factor of 3 to 10 greater. This suggests that there was a mechanism in the 10°C to 20 °C superheat range that triggered this rapid growth in spread area. From visual observation of the high speed recordings it was concluded that the onset of nucleate boiling was delayed to a wall superheat level between 30–40°C. For the surface grown for a period of 4 hours by hydrothermal synthesis, a significant increase in spread area was also observed in the superheat range of 10 °C to 20 °C. For that surface the onset of nucleate boiling was observed to be between 10–20 °C, which helped to explain the rapid spreading that was observed. If this theory is used to

explain the signi cant spreading that is measured between superheat levels of 10{20 °C for the surface grown for 10 hours it would contradict the visual observations that nucleation occurred only for wall superheats exceeding 30 °C.

However, SEM images of the two surfaces reveal that the geometry of the nanostructure array of the surface grown for 10 hours was noticeably di erent than that of the surface grown for 4 hours. For the surface grown for 10 hours, about 84% of the base surface area of the copper substrate was covered by ZnO nanocrystals, whereas only 40% of the substrate area nucleated nanocrystals on the surface grown for 4 hours. Furthermore, the wetted area ratio, ω of the surface grown for 10 hours was 19.3, which was about 20% greater than that of the surface grown for 4 hours, whose wetted surface area ratio was 15.6. From a thermodynamic standpoint, therefore, the surface free energy of the surface grown for 10 hours was greater than that of the surface grown for 4 hours. As a result, due to the well known Wenzel e ect, liquid deposited on the surface grown for 10 hours would be predicted to spread over a wider area compared with the surface grown for 4 hours in order to minimize the surface free energy. Indeed the surface grown for 10 hours was shown to be more wetting before and after experiments through the e ective contact angle calculations. Finally, through an adaptation of the the analysis of Ishino et al. [63] to this study, the surface grown for 10 hours was shown to exhibit the highest ratio of capillary forces to viscous forces of all the ZnO nanostructured surfaces, which further con rms its superior wetting characteristics.

4.1.6 ZnO surface - hydrothermal synthesis time = 24 hours

Results for experiments performed on the ZnO nanostructured surface grown by hydrothermal synthesis for 24 hours are depicted graphically in Figure 4.3.

In general, for this surface the maximum spread area increased with droplet volume at any given release height and wall superheat. Furthermore, for all droplet sizes, the maximum droplet spread area increased with increasing wall superheat. However, the magnitude of the increase in maximum spread area due to wall superheat also increased with droplet size. Finally, increases in the droplet release height also tended to increase the maximum spread area. These trends are consistent with those observed for the two other surfaces in this study. Based on visual observation from the video recordings, the onset of nucleate boiling occurred between superheat levels of 30 °C to 40 °C. Rippling and waviness of the liquid spreading were visually observed for all levels of superheat. Results of droplet spread area measurements, with standard deviation, on the surface grown by hydrothermal synthesis for 24 hours as a function of droplet diameter, release height and wall superheat are listed in Table 4.5. Results of estimated liquid lm thickness as a function of droplet diameter, release height and wall superheat are listed in Table 4.6.

30 ga droplet - 2.5 mm diameter

Unlike the previous surfaces analyzed in this study, for the surface grown by hydrothermal synthesis for 24 hours, the 2.5 mm droplet did not exhibit a relatively gradual percentage

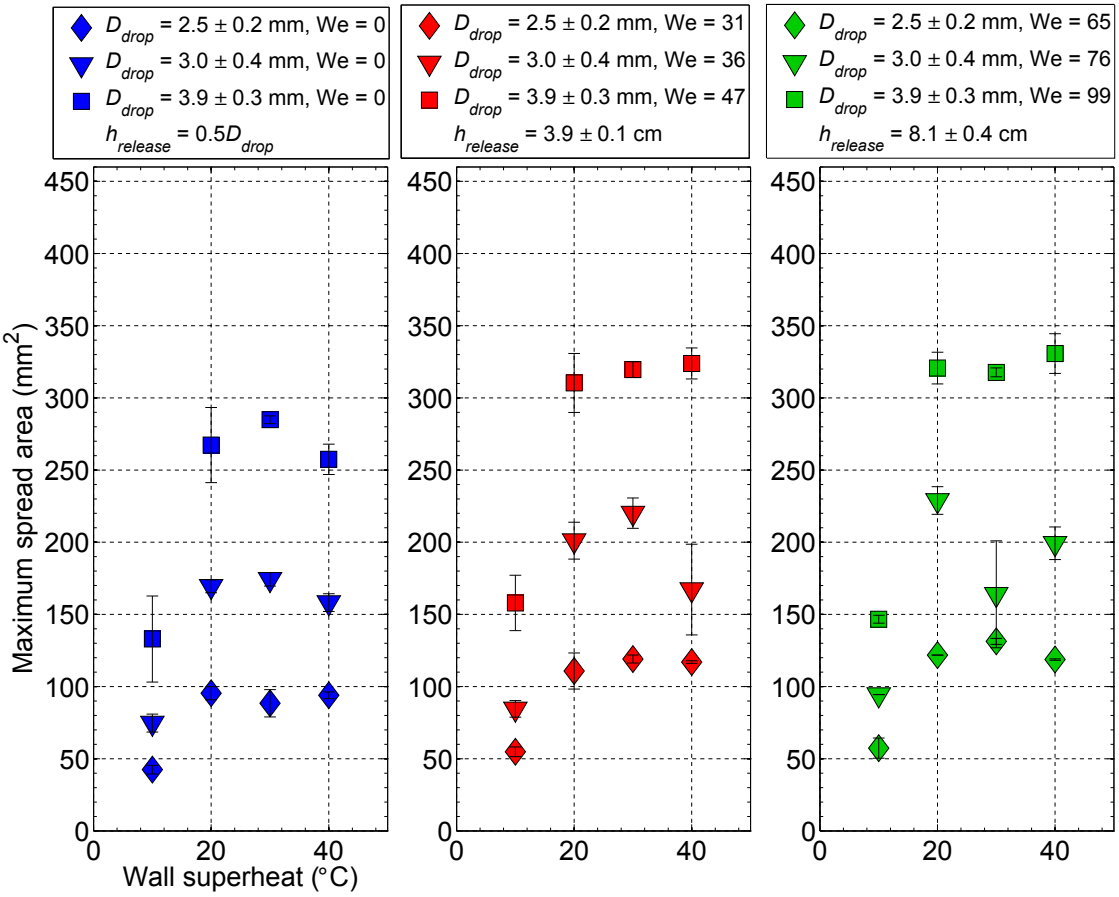

Figure 4.3: Droplet spread area as a function of wall superheat, droplet size and release height for ZnO nanostructured surface generated by hydrothermal synthesis for 24 hours.

increase as a function of superheat. On this surface, the droplet exhibited the greatest percentage increase for a wall superheat increase of 10 °C to 20 °C, which continued the trend observed for the previous surfaces. However, the spread area exhibited a much greater decrease in spreading rate beyond 20 °C. Whereas the plateauing was much more gradual on the previous surfaces, the plateauing begins immediately beyond a wall superheat of 20 °C and is more pronounced. For a wall superheat increase of 10 °C to 20 °C and a release height of 1.25 mm, the 2.5 mm droplet spread area increased by about 125%, from 43 mm^2 to 95 mm^2. Meanwhile, for a wall superheat increase of 10 °C to 20 °C and a release height of 3.9 cm, the 2.5 mm droplet spread area increased by about 100%, from 55 mm^2 to 111 mm^2. Finally, for a wall superheat increase of 10 °C to 20 °C and a release height of 8.9 cm, the 2.5 mm droplet spread area increased by about 110%, from 57 mm^2 to 122 mm^2. The

Table 4.5: Results of maximum droplet spread area measurements, with standard deviation, on surface grown for 24 hours$D$ is the droplet diameter, A is the maximum droplet spread area, H is the droplet release height and T is the wall superheat.

		T = 10 °C	T = 20 °C	T = 30 °C	T = 40 °C
D (mm)	H (cm)	A (mm^2)	A (mm^2)	A (mm^2)	A (mm^2)
2.5	0.12	42.5± 3.0	95.4± 4.5	88.5± 9.5	94.0± 2.4
2.5	3.9	54.8± 3.4	110.8± 12.5	119.1± 2.8	117.0± 0.9
2.5	8.1	57.4± 7.0	121.8± 0.0	131.3± 2.1	118.7± 0.5
3.0	0.15	74.7± 6.2	169.5± 4.5	174.4± 4.7	158.2± 6.2
3.0	3.9	84.6± 5.7	201.1± 12.8	220.2± 10.5	167.2± 31.4
3.0	8.1	94.4± 0.0	228.9± 9.6	164.0± 37.1	199.3± 11.3
3.9	0.20	133.0± 29.8	267.3± 26.0	284.9± 2.7	257.5± 10.5
3.9	3.9	157.9± 19.2	310.4± 20.4	319.6± 5.5	323.9± 10.8
3.9	8.1	146.7± 2.7	320.7± 11.0	317.7± 3.1	330.7± 13.8

Table 4.6: Estimated liquid lm thickness based on initial droplet volume and the measured maximum droplet spread area on surface grown for 24 hours$D$ is the droplet diameter, L_{film} is the lm thickness, H is the droplet release height and T is the wall superheat.

		T = 10 °C	T = 20 °C	T = 30 °C	T = 40 °C
D (mm)	H (cm)	L_{film} (μm)	L_{film} (μm)	L_{film} (μm)	L_{film} (μm)
2.5	0.12	114.2	73.0	84.1	88.5
2.5	3.9	117.0	69.4	59.6	80.3
2.5	8.1	138.4	71.2	60.5	42.8
3.0	0.15	138.4	83.4	67.7	90.1
3.0	3.9	156.6	66.4	65.9	64.4
3.0	8.1	141.6	72.7	68.0	75.3
3.9	0.20	181.8	89.9	107.6	134.4
3.9	3.9	163.0	84.0	100.2	109.7
3.9	8.1	183.4	93.1	107.9	110.3

percent increase rate plummeted to less than 8% for all surfaces for the next incremental increase of wall superheat of 20°C to 30 °C. For a release height of 1.25 mm the droplet spread area actually decreased from about 95 mm^2 to 89 mm^2 for a wall superheat increase from 20 °C to 30 °C. For a wall superheat increase from 20°C to 30 °C a drop released from 3.9 cm experienced an increase in spread area from about 111 mm^2 to 119 mm^2. For a release height of 8.1 cm and a wall superheat increase from 20°C to 30 °C the droplet spread area increased from about 122 mm^2 to 131 mm^2. For an increase in wall superheat from 30°C to

40 °C and a release height of 1.25 mm, the droplet spread area increased by only about 6% from 89 mm^2 to 94 mm^2. For a release height of 3.9 cm the spread area decreased by about 2% from 119 mm^2 to 117 mm^2. The spread area also decreased for a release height of 8.1 cm by about 10% from 131 mm^2 to 119 mm^2. Beyond, a superheat of 20°C, the maximum spread area is roughly constant, i.e. it did not continue to grow signi cantly with additional increases in wall superheat.

In general, increases in droplet release height resulted in percentage increases in maximum spread area for all superheat levels. Following the trend observed for the previous surfaces, the maximum spread area percentage increase that resulted from a release height increase from 1.25 mm to 3.9 cm generally resulted in signi cantly higher percentage increases in spread area compared with increasing release height from 3.9 to 8.1 cm. For all droplet sizes, the percentage increase in maximum spread area resulting from a release height increase from 1.25 mm to 3.9 cm was about 26% on average, for all superheat levels. For an increase in release height from 3.9 to 8.1 cm the spread area only increased by less than 10%.

The spread area increase was dominated by changes in wall superheat below 20°C. For a wall superheat increase of 10°C to 20 °C, the spread area increased by well over 100% from its value at a superheat of 10°C to its value at 20 °C for all release heights. For the wall superheat range of 10{20°C, any increase in release height resulted in less than a 30% increase in maximum spread area. However, beyond a superheat of 20°C, all spread area increases were dominated by increases in release height. Release height increases yielded a 20% increase in spread area, roughly on average, for all superheats beyond 20°C, whereas, temperature increases yielded less than an 8% increase.

In summary, for 2.5 mm droplets deposited on this surface the greatest percentage increase in maximum spread area resulted from a wall superheat increase of 10°C to 20 °C. The spread area increased from its value at 10°C to its value at 20 °C by approximately 125%, 100% and 110% for release heights of 1.25 mm, 3.9 cm and 8.1 cm, respectively. Beyond 20 °C, the percentage increases in maximum spread area were drastically reduced and were roughly constant for the higher superheat levels. Increases in droplet release height generally resulted in increases in maximum spread area. Beyond superheat levels of 20°C, increases in droplet release height dominated the e ect on increasing maximum spread area.

22 ga droplet - 3.0 mm diameter

For 3.0 mm diameter droplets deposited on the surface grown by hydrothermal synthesis for 24 hours, the greatest percentage change in maximum spread area resulted from a wall superheat increase from 10°C to 20 °C, equivalent to an approximate increase of 125%, from 74 mm^2 to 170 mm^2 for droplets released from a height of 1.5 mm, approximately 140%, from 85 mm^2 to 201 mm^2 for droplets released from 3.9 cm and 140%, from 94 mm^2 to 229 mm^2 for a release height of 8.1 cm. This single parametric change yielded the highest percentage increases in maximum spread area compared with any other parametric change for this surface. The rate of increase in spread area quickly decreased down to levels below

20% for any further increase in wall superheat. The increase in spread area peaked again at a superheat level of 30°C and decreased at a superheat level of 40°C.

With one exception, increases in droplet release height yielded a percentage increase in maximum spread area. Droplet release height increases from 1.5 mm to 3.9 cm generally resulted in greater percentage increases than did height increases from 3.9 cm to 8.1 cm. However, if the seemingly anomalous point occurring for a height increase of 3.9 cm to 8.1 cm at a superheat of 30°C is neglected, the percentage increases in spread area is approximately 15% for a release height increase from 1.5 mm to 3.9 cm as for an increase from 3.9 cm to 8.1 cm.

For wall superheat levels less than and equal to 20°C, increases in maximum spread area were most sensitive to changes in wall superheat by approximately a factor of 10 compared with increases in release height. Beyond a superheat level of 20°C, however, increases in maximum spread area were due almost entirely to increases in release height.

In summary, for 3.0 mm droplets deposited on this surface, the greatest percentage increase in maximum spread area resulted from a wall superheat increase of 10°C to 20 °C. The spread area increased from its value at 10°C to its value at 20 °C by approximately 125% for droplets released from a height of 1.5 mm and approximately 140% for droplets released from 3.9 cm and 8.1 cm. Increasing droplet release height generally resulted in increases in maximum spread area on the order of 15% for all wall superheat levels. Increases in maximum spread area were most sensitive to changes in wall superheat for superheat levels below 20 °C. For superheat levels greater than 20°C, increases in spread area were most dependent on changes in droplet release height.

16 ga droplet - 3.9 mm diameter

For 3.9 mm diameter droplets deposited on the ZnO nanostructured surface grown by hydrothermal synthesis for 24 hours the greatest percentage increase in maximum spread area resulted from an increase in wall superheat from 10°C to 20 °C. For this superheat level and a release height of 0.2 cm the spread area increased by about 100%, from 133 mm^2 to 267 mm^2. For a release height of 3.9 cm the spread area also increased by approximately 100%, from 158 mm^2 to 310 mm^2. For a release height of 8.1 cm the maximum spread area increased by about 120%, from 147 mm^2 to 321 mm^2. For a droplet released from about 0.2 cm, an increase in wall superheat from 20°C to 30 °C yielded in an increase in spread area of about 6%, from 267 mm^2 to 285 mm^2 and a decrease of about 10%, from 285 mm^2 to 278 mm^2 for a wall superheat increase to 40°C. In contrast to the other two surfaces in this study, for this surface the spread area for a 3.9 mm droplet exhibited a plateauing effect as a function of increases in wall superheat beyond 20°C.

Increases in droplet release height generally resulted in increases in maximum spread area. An increase in droplet release height from 0.2 cm to 3.9 cm resulted in an average increase in spread area of about 18% from its value at a height of 0.2 cm to its value at a height of 3.9 cm for all superheat levels. A release height increase from 3.9 cm to 8.1 cm had a negligible effect on spread area in comparison.

For superheat levels below 20°C, the maximum spread area was clearly dominated by changes in wall superheat by approximately a factor of 10 compared with changes in release height. However, for superheat levels exceeding 20°C, the maximum spread area was most sensitive to changes in release height from 0.2 cm to 3.9 cm.

In summary, for 3.9 mm droplets deposited on this surface the greatest percentage increase in maximum spread area resulted from a wall superheat increase of 10°C to 20 °C. For this increase in superheat and a release heights of 0.2 cm and 3.9 cm, the spread area increased by about 100% from its value at 10°C to 20 °C. For a release height of 8.1 cm the spread area increased by about 120% from its value at 10°C to 20 °C. The percentage increases due to a wall superheat level of 10°C to 20 °C were nearly a factor 10 greater than those due to any other parametric change for this droplet and surface combination. In general, increasing the droplet release height from 0.2 cm to 3.9 cm resulted in a spread area increase of about 18% from its value at the lower height to its value at the greater height. In comparison increasing the release height to 8.1 cm had a negligible effect on the maximum spread area. Beyond a superheat level of 20°C, the maximum spread area was most sensitive to changes in release height from 0.2 cm to 3.9 cm.

4.1.7 Comparison of spread area across all surfaces

On average, the surface which exhibited the greatest droplet spread areas for all droplet sizes, release heights and wall superheats was the surface grown by hydrothermal synthesis for 10 hours. In general, the maximum droplet spread area was achieved by releasing the droplet from the maximum test height of 8.1 cm. Ironically, the same surface which was grown for 10 hours also represents the average minimum spread area across all parameters compared with the other surfaces.

The average maximum spread area across all superheats for the surface grown for 4 hours for the 2.5 mm, 3.0 mm and 3.9 mm droplets was approximately 105 mm^2, 190 mm^2 and 290 mm^2, respectively. For the surface grown for 10 hours the average maximum spread area across all superheats for the 2.5 mm, 3.0 mm and 3.9 mm droplets was approximately 125 mm^2, 195 mm^2 and 350 mm^2, respectively. The average maximum spread area across all superheats for the surface grown for 24 hours for the 2.5 mm, 3.0 mm and 3.9 mm droplets was approximately 110 mm^2, 185 mm^2 and 280 mm^2, respectively.

The maximum spread area for 2.5 mm and 3.9 mm droplets was exhibited by the surface grown for 10 hours and corresponded to approximately 150 mm^2 and 420 mm^2, respectively, at superheats of 30°C and 40 °C, respectively, and a release height of 8.1 cm. The surface grown for 4 hours exhibited the largest spread area for a 3.0 mm droplet, approximately 240 mm^2 at a wall superheat of 30°C and a release height of 8.1 cm.

Results of the maximum spread areas for each droplet size and the corresponding release height and surface are summarized in Tables 4.7–4.9.

Although the spreading process is clearly dependent on the very specific combination of every parameter tested, on average it was found that a test surface change from one grown for 4 hours to one grown for 10 hours resulted in approximately 5% greater spread area. A

Table 4.7: Maximum values of maximum spread area for surface grown for 4 hours. D is the droplet diameter, A is the maximum spread area, H is the droplet release height and T is the wall superheat.

	T = 10 °C		T = 20 °C		T = 30 °C		T = 40 °C	
D (mm)	A (mm^2)	H (cm)	A (mm^2)	H (cm)	A (mm^2)	H (cm)	A (mm^2)	H (cm)
2.5	62.8	8.1	109.2	8.1	130.1	8.1	119.6	8.1
3.0	110.9	0.15	183.0	8.1	238.7	8.1	231.6	8.1
3.9	182.1	3.9	287.4	3.9	313.9	3.9	372.1	8.1

Table 4.8: Maximum values of maximum spread area for surface grown for 10 hours. D is the droplet diameter, A is the maximum spread area, H is the droplet release height and T is the wall superheat.

	T = 10 °C		T = 20 °C		T = 30 °C		T = 40 °C	
D (mm)	A (mm^2)	H (cm)	A (mm^2)	H (cm)	A (mm^2)	H (cm)	A (mm^2)	H (cm)
2.5	90.9	8.1	130.4	8.1	150.4	8.1	134.3	8.1
3.0	114.9	3.9	231.3	8.1	203.0	3.9	225.3	8.1
3.9	227.5	8.1	325.0	8.1	415.6	8.1	422.2	8.1

Table 4.9: Maximum values of maximum spread area for surface grown for 24 hours. D is the droplet diameter, A is the maximum spread area, H is the droplet release height and T is the wall superheat.

	T = 10 °C		T = 20 °C		T = 30 °C		T = 40 °C	
D (mm)	A (mm^2)	H (cm)	A (mm^2)	H (cm)	A (mm^2)	H (cm)	A (mm^2)	H (cm)
2.5	57.4	8.1	121.8	8.1	131.3	8.1	118.7	8.1
3.0	94.4	8.1	228.9	8.1	220.2	3.9	199.3	8.1
3.9	157.9	3.9	320.7	3.9	319.6	8.1	330.7	3.9

change from a surface grown from 10 hours to one grown for 24 hours resulted in negligible results. A negligible effect results from changing from a surface grown for 4 hours to one grown for 24 hours. The standard deviation for the average effect due to a surface change is on the order of $\pm$ 20%, so clearly there is a significant deviation from the average value. This indicates that the effect of changing parameters to influence spread area depends on the specific parametric combination to a non-negligible extent.

Furthermore, the parameter which most strongly affects the spread area across all surfaces is wall superheat. More specifically, a superheat level rise from 10 °C to 20 °C resulted in the greatest percentage increase in maximum spread area for all surfaces. Volume changes

alone, although incrementally unequal, resulted in the next greatest in uence on spread area. Finally, changing release height alone had the least e ect on spread area.

4.2 Droplet evaporation time on ZnO nanostructured surfaces

As it was shown in Section 4.1, when a liquid water droplet impinged upon the ZnO nanostructured surface the nominally spherical droplet spread into a thin lm over the surface. If it is assumed that the initial thickness of the lm is achieved when the liquid spreads to its maximum area, A_{spread}, the initial liquid lm thickness, $L_{film,i}$ can be estimated from the measurement of the initial volume of the droplet, V_{drop} and measured A_{spread}, given by,

$$L_{film,i} = \frac{V_{drop}}{A_{spread}}. \tag{4.2}$$

The energy required to evaporate the lm, Q balances the liquid-to-vapor phase change, such that,

$$Q = m_{drop}\,[h_v(T_{sat}) - h_l(T_{sat})] \tag{4.3}$$

where m_{drop} is the mass of the droplet, $h_v(T_{sat})$ and $h_l(T_{sat})$ are the enthalpies of water vapor and liquid water, respectively, at saturation. The heat requirement for evaporation, Q delivered from the surface to the liquid lm is given by,

$$Q = (\,h_{evap}A_{film} \quad T)\,t_{evap} \tag{4.4}$$

where h_{evap} is the average heat transfer coe cient for the evaporation process, which will be addressed in more detail in Section 4.3, T is the di erence between the surface temperature, T_{wall} and the liquid-vapor interface temperature, assumed to be the saturation temperature, T_{sat} and t_{evap} is the evaporation time. Balancing the heat delivery with the phase change energy gives,

$$(h_{evap}A_{spread} \quad T)\,t_{evap} = \rho_l A_{spread} L_{film,i} h_{lv} \tag{4.5}$$

where ρ_l is the liquid density, and V_{drop} has been substituted by the product of the spread area, A_{spread} and initial lm thickness $L_{film,i}$ and the enthalpy di erence between the liquid and vapor phases has been substituted by h_{lv}. Simplifying equation 4.5 and solving for the evaporation time gives,

$$t_{evap} = \frac{\rho_l L_{film} h_{lv}}{h_{evap} \quad T}. \tag{4.6}$$

Therefore, for a given heat transfer coe cient, wall superheat and droplet volume, the evaporation time is expected to decrease as the lm thickness of the spreading droplet decreases. Indeed, as will be shown in the remainder of this section, experimental results con rm the trend predicted by Equation 4.6.

In Section 4.3 it will be shown that the liquid droplets tend to evaporate by film evaporation from the surface at the lower superheat levels. For the surfaces grown by hydrothermal synthesis for 10 and 24 hours the approximate threshold for film evaporation was a superheat level less than and equal to 30°C. For the surface grown by hydrothermal synthesis for 4 hours, the threshold film evaporation spans a wider range approximately equal to 20°C to 30 °C. In either case, however, it is important to recognize that in the absence of vigorous nucleate boiling, which causes small satellite droplets to be ejected from the surface, the entire mass of the droplet is consumed in the evaporation process. Therefore the droplet evaporation times which are reported in the following section represent the total time required to evaporate the entire droplet for the superheat levels below the film evaporation thresholds. It was observed that beyond a superheat level of 40°C for all surfaces, the nucleate boiling resulted in significant ejection of small droplets such that the droplet evaporation time represented the evaporation of only a small fraction of the original volume of the droplet. As one of the goals of this study was to determine the effect of the nanostructured surfaces on film evaporation, the maximum wall superheat level tested in this study was 40 °C. The results of the effect of wall superheat, droplet size, droplet release height and surface geometry on droplet evaporation time are summarized in the following section.

4.2.1 ZnO surface - hydrothermal synthesis time = 4 hours

Results for experiments performed on the ZnO nanostructured surface grown by hydrothermal synthesis for 4 hours to determine the effect of wall superheat, droplet size, release height on evaporation time are depicted graphically in 4.4.

Results of droplet evaporation time measurements, with standard deviation, on the surface grown by hydrothermal synthesis for 4 hours as a function of droplet diameter, release height and wall superheat are listed in Table 4.10.

In general, for any given height and wall superheat level, an increase in droplet diameter, results in an increase in droplet evaporation time. For a given release height, increasing the droplet diameter from 2.5 mm by a factor of 1.2 to 3.0 mm, which is equivalent to a volumetric increase of a factor of 1.6, results in approximately 45% increase in evaporation time for superheat levels of 10{30°C. For a superheat level of 40°C, the increase in evaporation time is increased by about 33%. For a given release height, increasing the droplet diameter from 3.0 mm to 3.9 mm, a factor of nearly 1.5, leads to an increase in evaporation time of about 110%, 90%, 45% and 40% for superheat levels of 10°C, 20 °C, 30 °C and 40 °C, respectively. Thus it is evident that the effect of increasing droplet volume on increasing evaporation time is diminished as the superheat level rises.

In general, an increase in droplet release height also tended to reduce the evaporation time even as droplet volume increases, however, this effect is quite minimal compared to the effect that results from increasing wall superheat. For this surface, reductions in evaporation time are governed almost completely by changes in wall superheat and very weakly dependent on changes in droplet release height for all droplet sizes. For instance, for a wall superheat level increase from 10°C to 20 °C, a 2.5 mm droplet released from a height of 1.25 mm exhibits

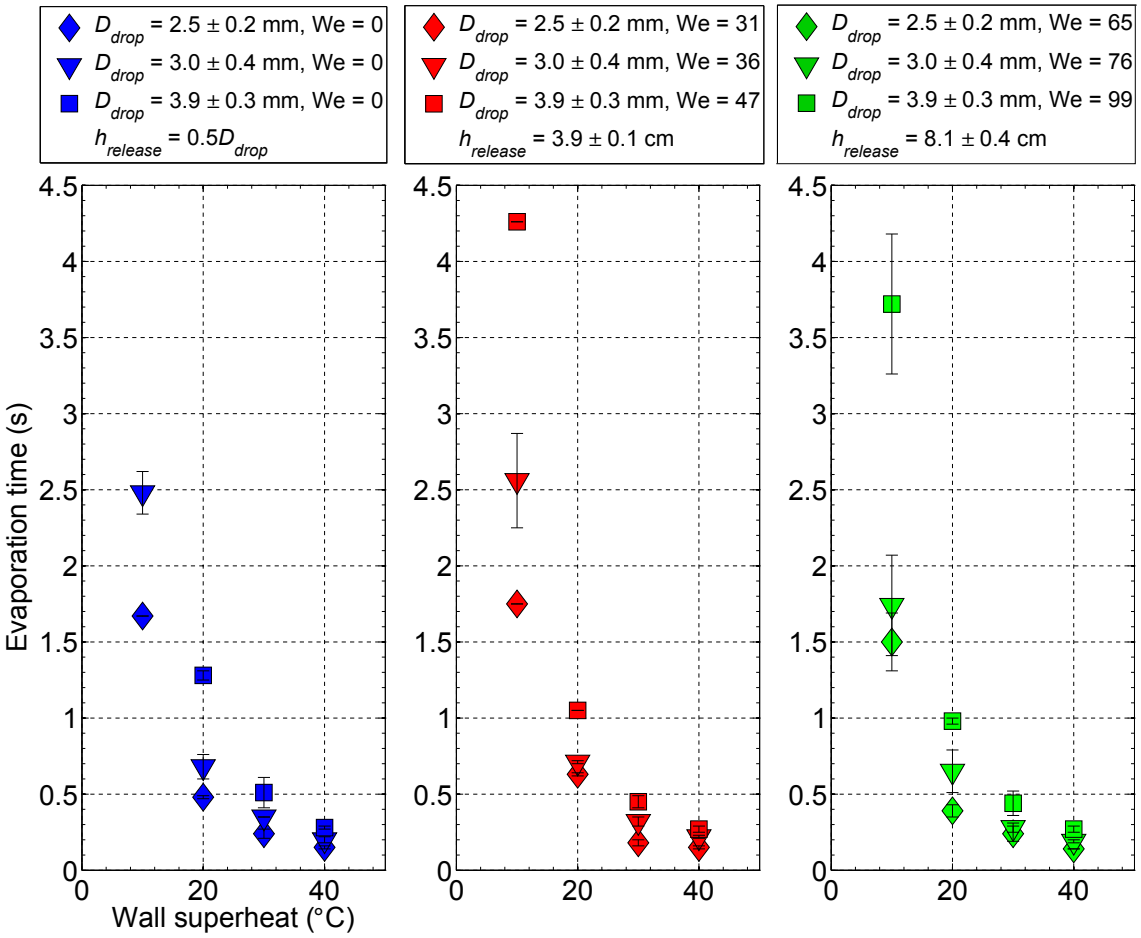

Figure 4.4: Droplet evaporation time as a function of wall superheat, droplet size and release height for the ZnO nanostructured grown by hydrothermal synthesis for 4 hours.

a reduction in evaporation time of about 70%, from 1.67 s to 0.48 s. For the same wall superheat increase, the same droplet released from a height of 3.9 cm exhibits a reduction in evaporation time of about 65%, from 1.75 s to 0.63, and a 75% reduction, from 1.50 s to 0.39 s, for a release height of 8.1 cm. In comparison, for a release height of 1.25 mm the 2.5 mm droplet exhibits a reduction in evaporation time of about 50%, from 0.48 s to 0.24 s, for a wall superheat increase from 20 °C to 30 °C, and a reduction of about 35%, from 0.24 s to 0.15, for a wall superheat increase from 30 °C to 40 °C. For a release height of 3.9 cm, the 2.5 mm droplet exhibited a reduction in evaporation time of about 70%, from 0.63 s to 0.18 s, for a wall superheat increase from 20 °C to 30 °C and about a 17% reduction, from 0.18 s to 0.15 s, for a wall superheat increase from 30 °C to 40 °C. For a release height of 8.1 cm, the 2.5 mm droplet exhibited a reduction in evaporation time of about 40%, from 0.39 s to 0.24 s, for a wall superheat increase from 20 °C to 30 °C and about a 40% reduction, from

Table 4.10: Results of droplet evaporation time measurements, with standard deviation, on the surface grown for 4 hours. D is the droplet diameter, t is the droplet evaporation time, H is the droplet release height and T is the wall superheat.

		T = 10 °C	T = 20 °C	T = 30 °C	T = 40 °C
D (mm)	H (cm)	t (s)	t (s)	t (s)	t (s)
2.5	0.12	1.67±0.00	0.48± 0.01	0.24±0.03	0.15±0.01
2.5	3.9	1.75±0.00	0.63±0.01	0.18±0.02	0.15±0.01
2.5	8.1	1.50±0.19	0.39±0.04	0.24±0.05	0.14±0.00
3.0	0.15	2.48 ± 0.14	0.68 ± 0.08	0.35 ± 0.00	0.20 ± 0.02
3.0	3.9	2.56 ± 0.31	0.71 ± 0.01	0.32 ± 0.03	0.22 ± 0.01
3.0	8.1	1.74±0.33	0.65±0.14	0.28±0.03	0.19±0.01
3.9	0.20	5.15 ± 0.24	1.28 ± 0.03	0.51 ± 0.10	0.28 ± 0.01
3.9	3.9	4.26 ± 0.00	1.05 ± 0.00	0.45 ± 0.04	0.27 ± 0.02
3.9	8.1	3.72±0.46	0.98±0.02	0.44±0.08	0.27±0.02

0.24 s to 0.14 s, for a wall superheat increase from 30 °C to 40 °C. Remarkably, for a 3.0 mm diameter droplet, for all release heights, the percentage reduction in evaporation times are about 70% from its value at a wall superheat of 10 °C to its value at 20 °C, a 50% reduction from its value at a wall superheat of 20 °C to its value at 30 °C and a 35% reduction from its value at a wall superheat of 30 °C to its value at 40 °C. The percentage reductions in evaporation time for the 3.0 mm droplet were almost identical to those observed for the 2.5 mm droplet. Finally, for the 3.9 mm diameter droplet, for all release heights, the percentage reduction in evaporation times are about 75% from its value at a wall superheat of 10 °C to its value at 20 °C, a 60% reduction from its value at a wall superheat of 20 °C to its value at 30 °C and a 40% reduction from its value at a wall superheat of 30 °C to its value at 40 °C. Therefore, for this surface, it is concluded that release height has a minimal e ect compared with wall superheat and droplet size on evaporation time.

4.2.2 ZnO surface - hydrothermal synthesis time = 10 hours

Results for experiments performed on the ZnO nanostructured surface grown by hydrothermal synthesis for 10 hours to determine the e ect of wall superheat, droplet size, release height on evaporation time are depicted graphically in Figure 4.5.

Results of droplet evaporation time measurements, with standard deviation, on the surface grown by hydrothermal synthesis for 10 hours as a function of droplet diameter, release height and wall superheat are listed in Table 4.11.

In general, for any given height and wall superheat level, an increase in droplet diameter, resulted in an increase in droplet evaporation time. As wall superheat increased, however, the e ect of increasing volume was diminished. Furthermore, for the minimum release height

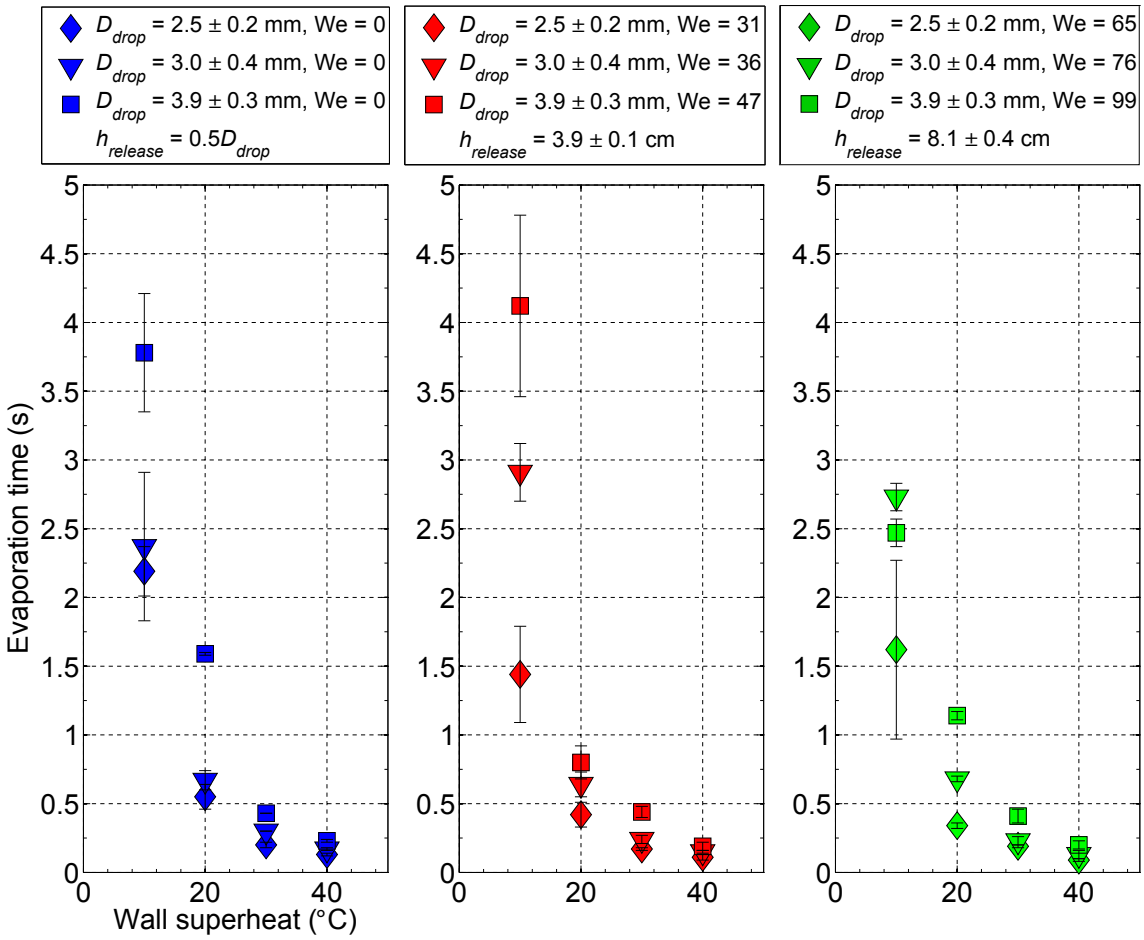

Figure 4.5: Droplet evaporation time as a function of wall superheat, droplet size and release height for the ZnO nanostructured surface generated by hydrothermal synthesis for 10 hours.

for each droplet size, increasing the droplet size from a diameter of 3.0 mm to 3.9 mm, a factor of 2.2 increase in droplet volume, resulted in a 70% increase, on average, in evaporation time across all wall superheat levels. For the minimum droplet release height, an increase in droplet size from 2.5 mm to 3.0 mm, a 1.6 times increase in volume, resulted in approximately a 34% increase in evaporation time, averaged across all wall superheat levels. For the minimum droplet release height, an increase in droplet size from 3.0 mm to 3.9 mm resulted in approximately a 70% increase in evaporation time, averaged across all wall superheat levels. For a release height of 3.9 cm, an increase in droplet size from 2.5 mm to 3.0 mm resulted in approximately a 43% increase in evaporation time, averaged over all wall superheat levels. For a release height of 3.9 cm, an increase in droplet size from 3.0 mm to 3.9 mm resulted in an almost identical increase in evaporation time, approximately 44%, averaged over all wall superheat levels. The trend was similar for a release height of

Table 4.11: Results of droplet evaporation time measurements, with standard deviation, on the surface grown for 10 hours$D$ is the droplet diameter,t is the droplet evaporation time, H is the droplet release height and T is the wall superheat.

		T = 10 °C	T = 20 °C	T = 30 °C	T = 40 °C
D (mm)	H (cm)	t (s)	t (s)	t (s)	t (s)
2.5	0.12	2.19 ± 0.18	0.55 ± 0.09	0.20 ± 0.02	0.13 ± 0.01
2.5	3.9	1.44 ± 0.35	0.42 ± 0.09	0.17 ± 0.01	0.11 ± 0.02
2.5	8.1	1.62 ± 0.65	0.34 ± 0.02	0.19 ± 0.01	0.09 ± 0.01
3.0	0.15	2.37 ± 0.54	0.67 ± 0.07	0.30 ± 0.00	0.17 ± 0.01
3.0	3.9	2.91 ± 0.21	0.64 ± 0.09	0.24 ± 0.03	0.15 ± 0.01
3.0	8.1	2.73 ± 0.10	0.68 ± 0.02	0.23 ± 0.03	0.13 ± 0.03
3.9	0.20	3.78 ± 0.43	1.59 ± 0.01	0.43 ± 0.00	0.23 ± 0.01
3.9	3.9	4.12 ± 0.66	0.80 ± 0.12	0.44 ± 0.04	0.19 ± 0.03
3.9	8.1	2.47 ± 0.10	1.14 ± 0.03	0.41 ± 0.05	0.20 ± 0.03

8.1 cm. For a release height of 8.1 cm and a droplet size increase from 2.5 mm to 3.0 mm, the evaporation time increased by approximately 45%, averaged across all wall superheat levels. For a release height of 8.1 cm and a droplet size increase from 3.0 mm to 3.9 mm, the evaporation time increased by approximately 48%, averaged across all wall superheat levels. Therefore, since the magnitude increase in evaporation time was approximately equal for most changes in droplet release height, it is concluded that the e ect of changing droplet volume dominates over the e ect of changing droplet release height.

Similar to the surface grown by hydrothermal synthesis for 4 hours, for the surface grown for 10 hours, reductions in evaporation time were much more sensitive to changes in wall superheat than droplet release height. It is remarkable to note once again that for the 2.5 mm and 3.0 mm droplets, percentage reductions in evaporation time due to wall superheat increases were approximately equal for all release heights.

For the 2.5 mm and 3.0 mm droplets, the percentage reduction in evaporation times are about 75% from its value at a wall superheat of 10°C to its value at 20 °C, a 55{60% reduction from its value at a wall superheat of 20°C to its value at 30 °C and a 40% reduction from its value at a wall superheat of 30°C to its value at 40 °C. For the 3.9 mm diameter droplet, the percentage reduction in evaporation times, across all droplet release heights, was about 65% from its value at a wall superheat of 10°C to its value at 20 °C, a 60% reduction from its value at a wall superheat of 20°C to its value at 30 °C and a 50% reduction from its value at a wall superheat of 30°C to its value at 40 °C. Thus, it is concluded for this surface that evaporation time is weakly dependent on release height.

4.2.3 ZnO surface - hydrothermal synthesis time = 24 hours

Results for experiments performed on the ZnO nanostructured surface grown by hydrothermal synthesis for 24 hours to determine the e ect of wall superheat, droplet size, release height on evaporation time are depicted graphically in Figure 4.6.

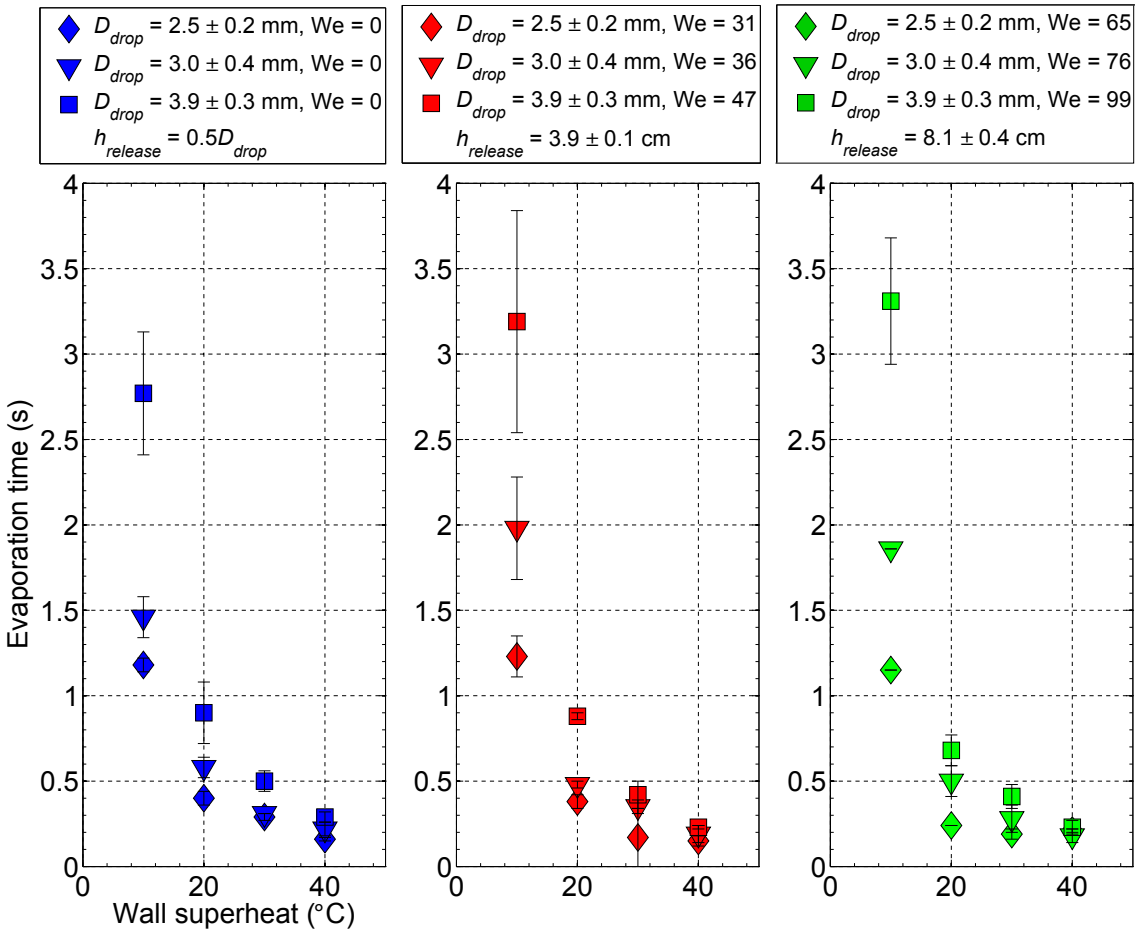

Figure 4.6: Droplet evaporation time as a function of wall superheat for surface generated by hydrothermal synthesis for 24 hours.

Results of droplet evaporation time measurements, with standard deviation, on the surface grown by hydrothermal synthesis for 24 hours as a function of droplet diameter, release height and wall superheat are listed in Table 4.12.

In general, for any given height and wall superheat level, an increase in droplet diameter, resulted in an increase in droplet evaporation time. For this surface, changes in droplet release height have a negligible e ect on evaporation time compared with those in droplet size and wall superheat. For all droplet sizes and release heights, the evaporation time was reduced by about 70% for a superheat level increase from 10 to 20 °C and by 35{45%

Table 4.12: Results of droplet evaporation time measurements, with standard deviation, on the surface grown for 24 hours$D$ is the droplet diameter,t is the droplet evaporation time, H is the droplet release height and T is the wall superheat.

		T = 10 °C	T = 20 °C	T = 30 °C	T = 40 °C
D (mm)	H (cm)	t (s)	t (s)	t (s)	t (s)
2.5	0.12	1.18 ± 0.04	0.40 ± 0.04	0.29 ± 0.04	0.16 ± 0.00
2.5	3.9	1.23 ± 0.12	0.38 ± 0.02	0.17 ± 0.17	0.15 ± 0.03
2.5	8.1	1.15 ± 0.00	0.24 ± 0.01	0.19 ± 0.03	0.21 ± 0.01
3.0	0.15	1.46 ± 0.12	0.58 ± 0.06	0.31 ± 0.00	0.22 ± 0.04
3.0	3.9	1.98 ± 0.30	0.48 ± 0.02	0.35 ± 0.04	0.19 ± 0.05
3.0	8.1	1.86 ± 0.00	0.50 ± 0.09	0.28 ± 0.08	0.18 ± 0.04
3.9	0.20	2.77 ± 0.36	0.90 ± 0.18	0.50 ± 0.06	0.29 ± 0.03
3.9	3.9	3.19 ± 0.65	0.88 ± 0.02	0.42 ± 0.08	0.23 ± 0.01
3.9	8.1	3.31 ± 0.37	0.68 ± 0.09	0.41 ± 0.07	0.23 ± 0.04

for a superheat level increase from 20°C to 30 °C. In contrast to the previous surfaces, a wall superheat increase from 30°C to 40 °C resulted in a wider spread of percentage reduction in evaporation time as a function of drop size, but not release height. For a superheat level increase of 30°C to 40 °C, a 2.5 mm droplet exhibited an average percentage reduction in evaporation time of 15%. Droplets of 3.0 mm and 3.9 mm diameter exhibited a percentage reduction in evaporation time of approximately 37% and 44%, respectively, over a wall superheat increase of 30°C to 40 °C. This illustrates once again that evaporation time is very weakly dependent on release height compared with changes in wall superheat and droplet size.

4.2.4 Comparison of droplet evaporation time across all ZnO nanostructured surfaces

The shortest evaporation time for every surface tested was exhibited for the 2.5 mm droplet deposited onto the surface at a superheat level of 40°C from a release height of 8.1 cm for the surfaces grown for 4 hours and 10 hours and from 3.9 cm for the surface grown for 24 hours. The surface grown for 10 hours exhibited the shortest evaporation time for all surfaces equivalent to approximately 0.09 s for a superheat of 40°C and a release height of 8.1 cm. The shortest evaporation time for the surface grown for 4 hours was 0.14 s. The shortest evaporation time for the surface grown for 24 hours was 0.15 s.

In contrast to the shortest evaporation time, the longest evaporation times for every surface were exhibited by the 3.9 mm droplets. The longest evaporation time was 5.15 s, exhibited by a 3.9 mm droplet deposited on a surface grown for 4 hours at a superheat level of 10°C and the minimum release height of 0.2 cm. The longest evaporation time for

the surface grown for 10 hours was 4.12 s for a droplet released from 3.9 cm. The longest evaporation time for the surface grown for 24 hours was 3.31 s for a droplet released from 8.9 cm.

Results of the minimum evaporation times for each droplet size and the corresponding release height and surface are summarized in Tables 4.13{4.15.

Table 4.13: Minimum values of evaporation time for surface grown for 4 hours. D is the droplet diameter, t is the evaporation time, H is the droplet release height and T is the wall superheat.

	T = 10 °C		T = 20 °C		T = 30 °C		T = 40 °C	
D (mm)	t (s)	H (cm)	t (s)	H (cm)	t (s)	H (cm)	t (s)	H (cm)
2.5	1.5	8.1	0.39	8.1	0.18	3.9	0.14	8.1
3.0	1.74	8.1	0.65	8.1	0.28	8.1	0.19	8.1
3.9	3.72	8.1	0.98	8.1	0.44	8.1	0.27	3.9

Table 4.14: Minimum values of evaporation time for surface grown for 10 hours. D is the droplet diameter, t is the evaporation time, H is the droplet release height and T is the wall superheat.

	T = 10 °C		T = 20 °C		T = 30 °C		T = 40 °C	
D (mm)	t (s)	H (cm)	t (s)	H (cm)	t (s)	H (cm)	t (s)	H (cm)
2.5	1.44	3.9	0.34	8.1	0.17	8.1	3.9	8.1
3.0	2.37	0.15	0.64	3.9	0.23	8.1	0.13	8.1
3.9	2.47	8.1	0.8	3.9	0.41	8.1	0.19	3.9

Table 4.15: Minimum values of evaporation time for surface grown for 24 hours. D is the droplet diameter, t is the evaporation time, H is the droplet release height and T is the wall superheat.

	T = 10 °C		T = 20 °C		T = 30 °C		T = 40 °C	
D (mm)	t (s)	H (cm)	t (s)	H (cm)	t (s)	H (cm)	t (s)	H (cm)
2.5	1.15	8.1	0.24	8.1	0.17	3.9	0.15	3.9
3.0	1.46	0.15	0.48	3.9	0.28	8.1	0.18	8.1
3.9	2.77	0.20	0.68	8.1	0.41	8.1	0.23	3.9

For each surface the e ect of increasing wall superheat from 10 °C to 20 °C had an impact of reducing evaporation time by approximately 75{80% from its value at the lower

temperature. For all surfaces the effect of increasing wall superheat from 20 °C to 30 °C resulted in evaporation time reductions of 50–70% from its value at the lower temperature. For all surfaces the effect of increasing wall superheat from 30 °C to 40 °C resulted in evaporation time reductions of 45–55% from its value at the lower temperature

The effect of increasing droplet release height affected the evaporation time to a lesser extent than changes in wall superheat. For all three surfaces an increase in height resulted in about 40–50% reduction in evaporation. There was a negligible difference in evaporation time reduction between a release height increase from the minimum droplet release height to 3.9 cm and from 3.9 cm to 8.1 cm. Therefore for the release heights tested it was found that the evaporation time was not influenced by release heights greater than 3.9 cm or Weber numbers greater than 47.

Finally increasing droplet volume had the greatest impact of all parameters for every surface. In general, the data did not reveal a trend as to whether a change from a droplet size of 2.5 mm to 3.0 mm, a factor of 1.6 in volume, or a change from 3.0 mm to 3.9 mm, a factor of 2.2 in volume, had a greater impact. However, comparing a droplet size increase from 1.5 mm to 3.9 mm, a factor of 3.6 increase in volume, did have a clear impact. On average, the surface grown for 4 hours exhibited a 67% increase in evaporation time for an increase in volume. The surface grown for 10 hours exhibited approximately a 70% increase in evaporation time for an increase in volume. The surface grown for 24 hours exhibited approximately a 65% increase in evaporation time for an increase in volume.

4.2.5 Discussion of droplet evaporation time

In general, for all of the ZnO nanostructured surfaces in this study, droplet release height had a minimal to negligible effect on evaporation time compared with wall superheat and droplet volume. Considering this result in the context of maximum droplet spread area, it is both surprising and unsurprising that release height had a minimal effect on droplet evaporation time. It was shown in Section 4.2 that a greater spread area of the droplet should reduce evaporation time. Therefore, it is unsurprising that an increase in droplet release height from 3.9 cm to 8.1 cm would yield any significant reduction in droplet evaporation time since the percentage increase in droplet spread area for all surfaces was generally unaffected by that increase in release height. However, at first glance it is surprising that an increase from the minimum droplet release height to 3.9 cm would not have a more significant impact on the evaporation time since it affected the spread area percentage increase by 20–50% depending on the surface. The reason that a change in both spread area and evaporation time due to an increase in height is hardly noticeable is that changes in droplet volume and wall superheat, to a greater extent, dominate the spreading and evaporation processes.

4.3 Heat transfer coe cient on ZnO nanostructured surfaces

So far it was shown in Section 4.1, that when a liquid water droplet impinged upon the ZnO nanostructured surface, the nominally spherical droplet spread into a thin lm over the surface. It was observed for all ZnO nanostructured surfaces that the maximum droplet spread area was most sensitive to changes in wall superheat from 10 °C to 20 °C. Beyond the a superheat level of 20 °C, spread area increases were mostly due to an increase in droplet release height and were only a small fraction of the percentage increase that was observed for the changes in the lower superheat levels. In Section 4.2 it was shown that droplet evaporation time was most strongly sensitive to changes in droplet volume and wall superheat and very weakly dependent upon changes in release height. It was observed that evaporation time increased with droplet volume increases and decreased with increasing wall superheat.

In this section, the results of a parametric study on the e ects of wall superheat, droplet size, droplet release height and surface geometry on heat transfer coe cient are explored. The heat transfer coe cient was calculated based on measurements of maximum droplet spread area and droplet evaporation time. This calculation method is described next.

4.3.1 Calculation of heat transfer coe cient

The power delivered from the test surface of the solid substrate to evaporate the droplet was calculated from knowledge of the properties of water at saturation, the measured droplet volume, maximum spread area and evaporation time. The power, q, in Watts, is given by

$$q = \frac{\rho_l V_{drop} h_{lv}}{t_{evap}} \tag{4.7}$$

where ρ_l is the saturated liquid water density at 101 kPa equivalent to 958.35 kg/m^3, V_{drop} is the liquid droplet volume, h_{lv} is the enthalpy of vaporization of water at 101 kPa equivalent to 2256.43 kJ/kg-°C, and t_{evap} is the droplet evaporation time. The heat transfer coe cient, h_{evap} is given by

$$h_{evap} = \frac{q}{A_{spread}(T_{wall} - T_{int})} \tag{4.8}$$

where A_{spread} is the maximum droplet spread area, T_{wall} is the ZnO nanostructured surface temperature and T_{int} is the liquid-gas interface temperature of the droplet surface where evaporation occurs. The droplet interface temperature is assumed to be equivalent to the saturation temperature, T_{sat} throughout the entire experiment since the sensible heat that raises the droplet temperature from approximately 20 °C at the moment of deposition to saturation temperature is only about 15% of the latent heat of vaporization. Additionally, for most of the levels of wall superheat tested, the entirety of the droplet volume was consumed in the evaporation process without the production and subsequent ejection of satellite droplets

from the surface at any time. The few cases for which negligible amounts of satellite droplets were produced as a result of nucleate boiling will be noted. Finally, since for every experiment many data points were gathered at every superheat level, the heat transfer coe cients are calculated from the calculated average of all measured d_{drop}, A_{spread} and t_{evap} at the reported wall superheat. The results of the parametric study are described in the remainder of this section.

4.3.2 Comparison to nucleate boiling correlation of Stephan and Abdelsalam

The calculated heat transfer coe cients from this study are compared to standard nucleate boiling predictions from Stephan and Abdelsalam [67]. The correlation by Stephan and Abdelsalam used to compute the heat transfer coe cient h_{SA} for comparison purposes is given by,

$$h_{SA} = \frac{\{C_1 [T_{wall} - T_{sat}]\}^{1/0.327}}{T_{wall} - T_{sat}} \tag{4.9}$$

where for water at 101 kPa, C_1 is approximately 3.85. The predicted values h_{SA} for the wall superheat levels in this study are listed in Table 4.16.

Table 4.16: Heat transfer coe cient, h_{SA} predictions by Stephan and Abdelsalam for the wall superheat levels, T in this study.

T (°C)	h_{SA} (kW/m ^{2}{°C)
10	7.1
20	29.4
30	67.7
40	122.4

4.3.3 ZnO surface - hydrothermal synthesis time = 4 hours

Heat transfer coe cients calculated from results of experiments performed on the ZnO nanostructured surface grown by hydrothermal synthesis for 4 hours are depicted graphically in Figure 4.7. The calculated heat transfer coe cients are compared to those predicted by the nucleate boiling correlation of Stephan and Abdelsalam [67].

Results of calculations of heat transfer coe cient on surface grown for 4 hours as a function of droplet diameter, release height and wall superheat are listed in Table 4.17.

In general, the heat transfer coe cient, h_{evap} increased with decreasing droplet size. The heat transfer coe cient increased with increasing wall superheat as well as with increasing droplet release height.

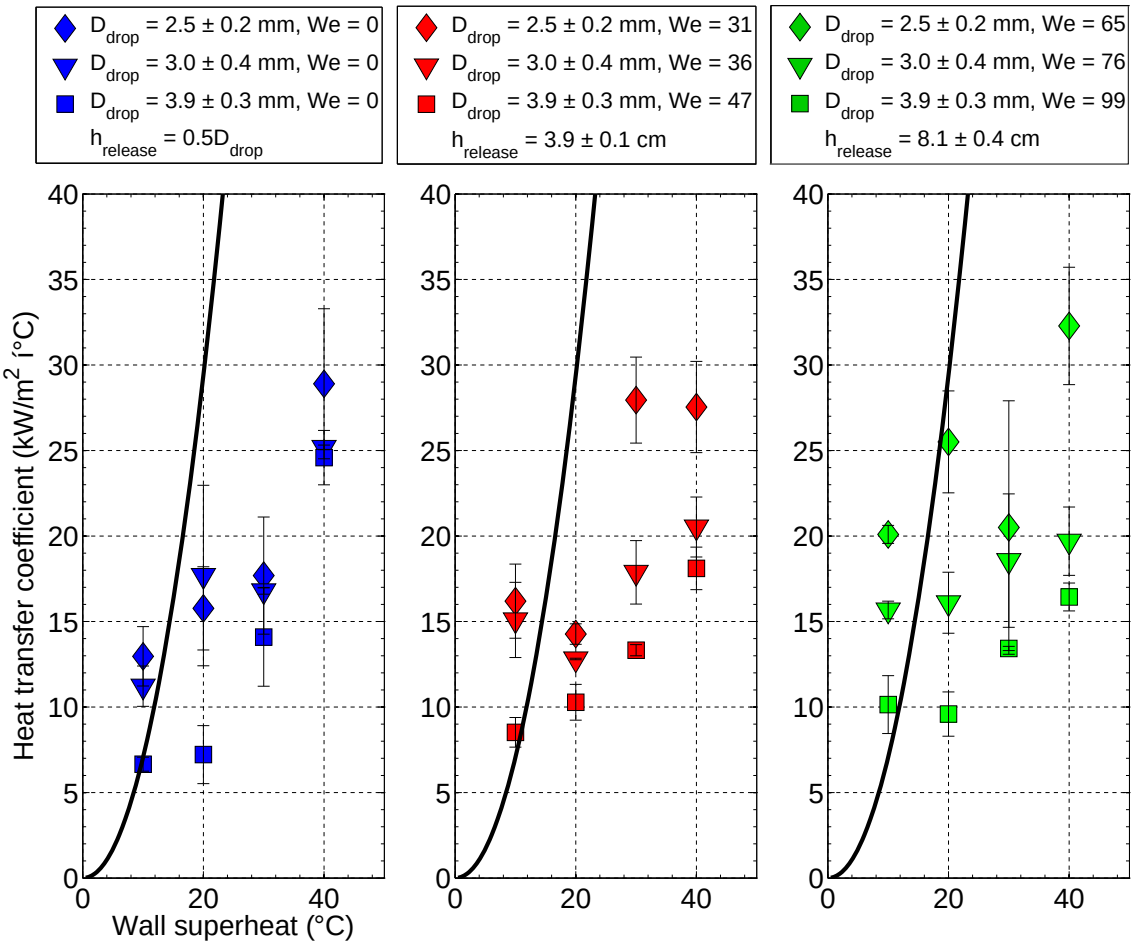

Figure 4.7: Heat transfer coe cient as a function of wall superheat, droplet size and release height for ZnO nanostructured surface generated by hydrothermal synthesis for 4 hours.

4.3.3.1 E ects of release height, droplet volume and wall superheat on heat transfer coe cient

Neglecting the prediction from Stephan and Abdelsalam for the moment, it is clear from Figure 4.7, that droplet volume and wall superheat most strongly in uence the heat transfer coe cient, h_{evap}. Focusing for the moment on droplet volume, at the minimum droplet release height, averaging the reductions in h_{evap} over all superheat levels, increasing from a droplet diameter of 2.5 mm to 3.0 mm, a factor of 1.6 in volume, resulted in an average reduction of 10% in h_{evap}. If the droplet size is increased from 3.0 mm to 3.9 mm, a factor of 2.2 times in volume, h_{evap} is reduced by nearly 30%, averaging over all superheat levels. If droplet diameter is increased from 2.5 mm to 3.9 mm, a factor of 3.6 times in volume, h_{evap} is reduced by about approximately 35%. A similar trend is exhibited for droplets released

Table 4.17: Results of calculations of heat transfer coe cient on surface grown for 4 hours. D is the droplet diameter, h_{evap} is the heat transfer coe cient and T is the wall superheat.

		T = 10 °C	T = 20 °C	T = 30 °C	T = 40 °C
D (mm)	H (cm)	h_{evap} (kW/m ^{2}{°C)	h_{evap} (kW/m ^{2}{°C)	h_{evap} (kW/m ^{2}{°C)	h_{evap} (kW/m ^{2}{°C)
2.5	0.12	13.0 ± 1.7	15.8 ± 2.4	17.7 ± 3.4	28.9 ± 4.4
2.5	3.9	16.2 ± 2.2	14.3 ± 0.6	27.9 ± 2.5	27.5 ± 2.7
2.5	8.1	20.1 ± 0.5	25.5 ± 3.0	20.5 ± 7.4	32.3 ± 3.4
3.0	0.15	11.2 ± 1.2	17.7 ± 5.3	16.8 ± 0.2	25.2 ± 0.1
3.0	3.9	15.1 ± 2.2	12.8 ± 0.0	17.9 ± 1.9	20.5 ± 1.7
3.0	8.1	15.7 ± 0.5	16.1 ± 1.7	18.6 ± 3.9	19.7 ± 2.0
3.9	0.20	6.7 ± 1.7	7.2 ± 2.4	14.1 ± 3.4	24.6 ± 4.4
3.9	3.9	8.5 ± 2.2	10.3 ± 0.6	13.3 ± 2.5	18.1 ± 2.7
3.9	8.1	10.1 ± 0.5	9.6 ± 3.0	13.4 ± 7.4	16.4 ± 3.4

from 3.9 cm and 8.1 cm. For droplets released from 3.9 cm, increasing the droplet diameter from 2.5 mm to 3.0 mm resulted in an average reduction of 20% in h_{evap}; increasing diameter from 3.0 mm to 3.9 mm resulted in a 25% reduction in h_{evap}; and increasing diameter from 2.5 mm to 3.9 mm resulted in average reductions in h_{evap} of approximately 40%, across all superheat levels. Increasing to a release height of 8.1 cm, increasing the droplet diameter from 2.5 mm to 3.0 mm resulted in an average reduction of 25% in h_{evap}; increasing diameter from 3.0 mm to 3.9 mm resulted in a 30% reduction in h_{evap}; and increasing diameter from 2.5 mm to 3.9 mm resulted in average reductions in h_{evap} of approximately 45%, across all superheat levels.

Isolating the e ect of increasing release height, for any given change in droplet size in this study, the data indicate that increasing release height by incremental steps of 4 cm in addition to the increase in droplet size resulted in approximately a 5% greater reduction in h_{evap} than changing droplet size alone. Although a 5% e ect on h_{evap} per 4 cm increase in height is almost negligible in comparison to the e ect of the other parameters, it indicates that the e ect on h_{evap} from increasing droplet height depends on the droplet size. This is visually apparent in Figure 4.7 by observing the increasing spread in value of h_{evap} between droplet sizes at one particular superheat level as the release height increases from plot to plot, left to right. This observation rea rms the signi cance of droplet size on heat transfer.

Focusing now on the e ect of increasing wall superheat on heat transfer coe cient h_{evap}, for all droplet sizes, a wall superheat increase from 10 °C to 20 °C resulted in a relatively modest increase in h_{evap} of approximately 8{15% increase. The range of percentage increase in h_{evap} expands to approximately 20{55% across all droplet sizes and heights for a wall superheat increase of 20 °C to 30 °C and 20{45% for a wall superheat increase of 30 °C to 40 °C. Therefore, for all release heights, the heat transfer coe cient increases as a simultaneous

function of increasing wall superheat and decreasing droplet volume.

4.3.3.2 Comparing experimental heat transfer coefficient to nucleate boiling predictions by Stephan and Abdelsalam

In comparing the calculated heat transfer coefficients, h_{evap} to those predicted by Stephan and Abdesalam, h_{SA} which are listed in Table 4.16 it is evident that the magnitude of h_{SA} surpassed h_{evap} by a significant factor at superheat levels of 20°C and greater for almost all droplet sizes and release heights. While h_{SA} rises steeply, roughly as T^2 as a result of nucleate boiling for increasing wall superheat, h_{evap} increased much more gradually even though nucleate boiling ensues for superheats greater than 10°C on the nanostructured surface grown for 4 hours. Even though the onset of nucleate boiling occurs at a a wall superheat of approximately 10°C, vigorous boiling is not evident until a superheat level of 40 °C is achieved. At a superheat level of 40°C, small satellite droplets were ejected from the main liquid volume. The difference in magnitude between h_{SA} and h_{evap} for all superheat levels suggests that for the nanostructured surface, nucleate boiling is not the driving heat transfer mechanism. The gradual increase in h_{evap} as a function of wall superheat, compared with h_{SA}, indicates that heat transfer from the surface was dominated more by mechanisms typical of film evaporation. Video recordings of the experiments confirmed the suggestions of the measured data that nucleate boiling was not the driving heat transfer mechanisms, but rather, that evaporation was driven by mechanisms more typical of film evaporation.

Comparing h_{evap} to h_{SA} in more quantitative detail, for a wall superheat of 10°C, h_{evap} for a 2.5 mm droplet was about 130% greater, on average across all release heights, than the value of h_{SA}, 7.1 kW/m^2{°C, at the same superheat level. Looking more closely at the individual release heights, however, reveals its subtle yet important effect in comparing h_{evap} to h_{SA}. For the same wall superheat of 10°C and minimum release height h_{evap} was 13.0 kW/m^2{°C, which was about about 85% greater than h_{SA}, which was 7.1 kW/m^2{°C at the same wall superheat. At a release height of 3.9 cm, the 2.5 mm droplet exhibited an h_{evap} of 16.2 kW/m^2{°C, which was 128% greater than the h_{SA} value of 7.1 kW/m^2{°C at a wall superheat of 10°C. For a release height of 8.1 cm, the 2.5 mm droplet exhibited an h_{evap} of 20.1 kW/m^2{°C, which was 183% greater than the h_{SA} value of 7.1 kW/m^2{°C at a wall superheat of 10°C.

For a superheat level of 10°C, this trend is observed as droplet volume increases, but to a lesser extent. For a superheat of 10°C, a 3.0 mm droplet, h_{evap} is an average of about 98% greater, on average across all release heights, than the value of h_{SA}, 7.1 kW/m^2{°C, at the same superheat level. Looking beyond the average reveals, however, that for this droplet size, the effect of increasing release height diminishes. For the minimum height of 1.5 mm, h_{evap} was 11.2 kW/m^2{°C, which was about 58% greater than the h_{SA} value of 7.1 kW/m^2{°C at the same superheat. For a release height of 3.9 cm, the 3.0 mm droplet exhibited an h_{evap} of 15.1 kW/m^2{°C, which was 127% greater than the h_{SA} value of 7.1 kW/m^2{°C at a wall superheat of 10°C. For a release height of 8.1 cm, the 3.0 mm droplet exhibited an h_{evap} of 15.7 kW/m^2{°C, which was 111% greater than the h_{SA} value of 7.1 kW/m^2{°C at

a wall superheat of 10°C. At a superheat level of 10°C, increasing the release height for a 3.9 mm droplet had a much weaker effect on the difference between h_{evap} and h_{SA} compared with that observed for the smaller droplets. For the minimum release height of 0.2 cm h_{SA} is actually greater than h_{evap} by about 5%. Increasing the release height to 3.9 cm and 8.1 cm results in h_{evap} exceeding h_{SA} by about 20% and 42%, respectively.

Beyond a superheat level of 10°C, the magnitude of h_{SA}, which increases as function of wall superheat squared, exceeded h_{evap} very quickly. At 20 °C, h_{SA} is predicted to be equivalent to 29.4 kW/m^2{°C. For a wall superheat of 20°C and droplet sizes of 2.5 mm, h_{SA}, exceeded h_{evap} by approximately 86% at the minimum release height, by approximately 105% at a release height of 3.9 cm, but only by about 15% for a release height of 8.1 cm. For a 3.0 mm droplet h_{SA}, exceeded h_{evap} by approximately 66% at the minimum release height, by approximately 130% at a release height of 3.9 cm, and by about 83% for a release height of 8.1 cm. For a 3.9 mm droplet h_{SA}, exceeded h_{evap} by approximately 307% at the minimum release height, by approximately 185% at a release height of 3.9 cm, and by about 205% for a release height of 8.1 cm. Beyond a superheat level of 20°C, h_{SA} exceeds h_{evap} by 280{650% across all droplet sizes.

4.3.4 ZnO surface - hydrothermal synthesis time = 10 hours

Heat transfer coefficients calculated from results of experiments performed on the ZnO nanostructured surface grown by hydrothermal synthesis for 10 hours are depicted graphically in Figure 4.8. The calculated heat transfer coefficients are compared to those predicted by the nucleate boiling correlation of Stephan and Abdelsalam.

Results of calculations of heat transfer coefficient on the surface grown for 10 hours as a function of droplet diameter, release height and wall superheat are listed in Table 4.18.

In general, for this surface the heat transfer coefficient, h_{evap} increases with increasing wall superheat and droplet release height as well as decreasing droplet volume. One detail that immediately stands out in Figure 4.8 is that for a wall superheat level of 10°C, every droplet size exhibits a heat transfer coefficient substantially greater than the heat transfer coefficient prediction for nucleate boiling of Stephan and Abdelsalam, h_{SA}. At a release height of 1.25 mm, the 2.5 mm droplet exhibited a heat transfer coefficient of 29.5 kW/m^2{°C, which is approximately 4.2 times greater than the h_{SA} value of 7.1 kW/m^2{°C at the same superheat level. For release heights of 3.9 cm and 8.1 cm, the 2.5 mm droplet exhibited values of h_{evap} which were approximately 4.8 and 2.6 times greater, respectively, than the h_{SA} value of 7.1 kW/m^2{°C at the same superheat level. On average across all release heights, the 2.5 mm droplet exhibited a value of h_{evap} which was about 3.9 times greater than the h_{SA} value of 7.1 kW/m^2{°C at the same superheat level. This trend is also true of the 3.0 mm and 3.9 mm droplets. At a release height of 1.5 mm, the 3.0 mm exhibited a heat transfer coefficient of 18.9 kW/m^2{°C, which is approximately 2.7 times greater than the h_{SA} value of 7.1 kW/m^2{°C at the same superheat level. For release heights of 3.9 cm and 8.1 cm, the 3.0 mm droplet exhibited values of h_{evap} which were approximately 2.6 and 3.6 times greater than the h_{SA} value of 7.1 kW/m^2{°C at the same superheat level. On average

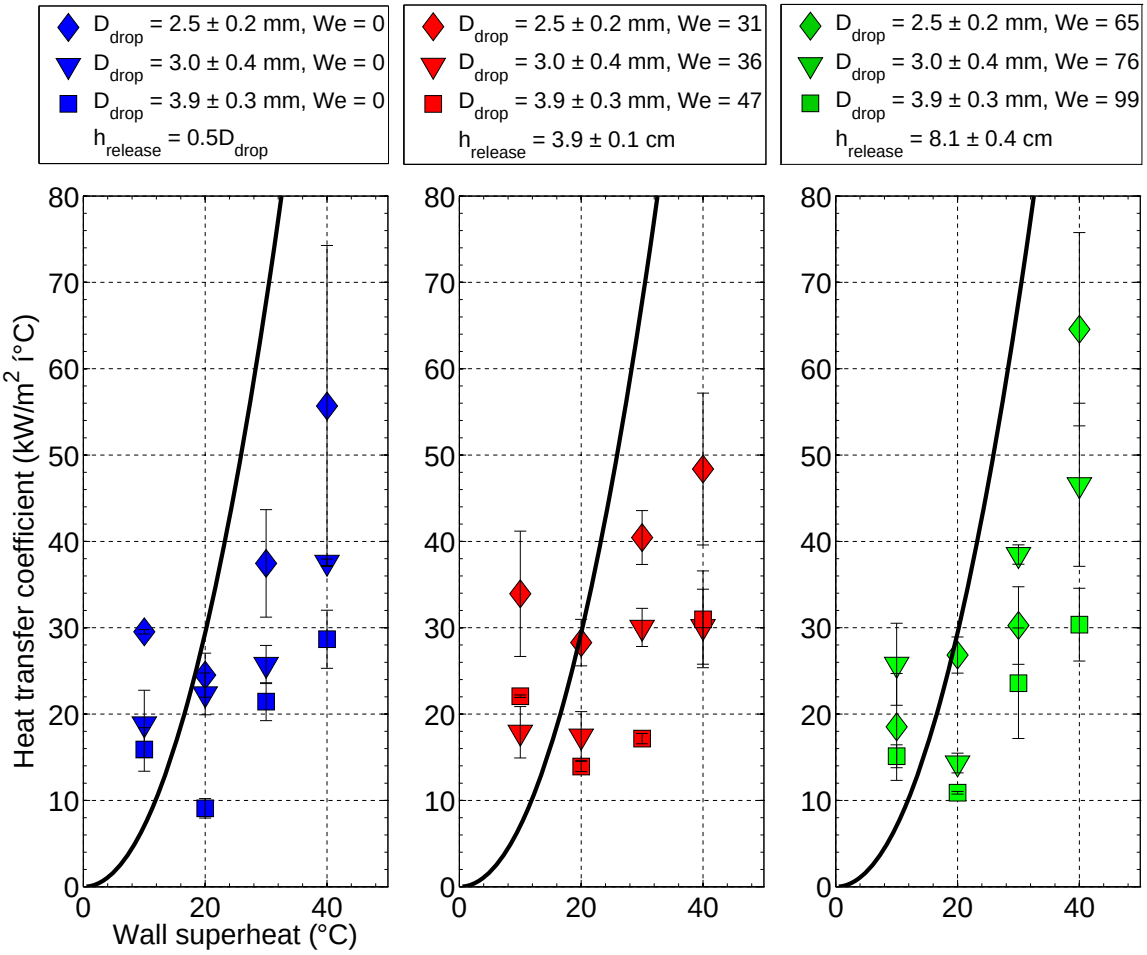

Figure 4.8: Heat transfer coe cient as a function of wall superheat, droplet size and release height for ZnO nanostructured surface generated by hydrothermal synthesis for 10 hours.

across all release heights, the 3.0 mm droplet exhibited a value of h_{evap} which was about 3.0 times greater than the h_{SA} value of 7.1 kW/m^2{°C at the same superheat level. At a release height of 0.2 cm, the 3.9 mm exhibited a heat transfer coe cient of 15.9 kW/m^2{°C, which is approximately 2.2 times greater than the h_{SA} value of 7.1 kW/m^2{°C at the same superheat level. For release heights of 3.9 cm and 8.1 cm, the 3.9 mm droplet exhibited values of h_{evap} which were approximately 3.1 and 2.1 times greater than the h_{SA} value of 7.1 kW/m ^{2}{°C at the same superheat level. On average across all release heights, the 3.9 mm droplet exhibited a value of h_{evap} which was about 2.5 times greater than the h_{SA} value of 7.1 kW/m^2{°C at the same superheat level.

In contrast, the same size droplets deposited on the surface grown for 4 hours by hydrothermal synthesis exhibited heat transfer coe cients that were greater than the nucleate boiling prediction by average factors of 2.3, 2.0 and 1.2, respectively. Similar to the nanos-

Table 4.18: Results of calculations of heat transfer coe cient on surface grown for 10 hours. D is the droplet diameter, h_{evap} is the heat transfer coe cient and T is the wall superheat.

		T = 10 °C	T = 20 °C	T = 30 °C	T = 40 °C
D (mm)	H (cm)	h_{evap} (kW/m ^{2}{°C)	h_{evap} (kW/m ^{2}{°C)	h_{evap} (kW/m ^{2}{°C)	h_{evap} (kW/m ^{2}{°C)
2.5	0.12	29.5 ± 0.3	24.5 ± 2.5	37.5 ± 6.2	55.7 ± 18.6
2.5	3.9	33.9 ± 7.3	28.3 ± 2.7	40.4 ± 3.1	48.4 ± 8.8
2.5	8.1	18.5 ± 6.2	26.8 ± 2.1	30.3 ± 4.5	64.6 ± 11.2
3.0	0.15	18.9 ± 3.9	22.3 ± 2.4	25.7 ± 2.2	37.6 ± 0.4
3.0	3.9	17.9 ± 3.0	17.4 ± 2.8	30.0 ± 2.2	30.1 ± 4.3
3.0	8.1	25.8 ± 4.7	14.3 ± 1.1	38.5 ± 1.1	46.6 ± 9.4
3.9	0.20	15.9 ± 2.5	9.1 ± 1.1	21.4 ± 2.2	28.7 ± 3.4
3.9	3.9	22.1 ± 0.1	13.9 ± 0.6	17.2 ± 0.6	31.0 ± 5.6
3.9	8.1	15.1 ± 1.3	10.9 ± 0.2	23.6 ± 6.4	30.4 ± 4.2

tructured surface grown for 4 hours, the value of h_{SA} quickly exceeded h_{evap} for superheats equal to and greater than 20°C, though by a lesser percentage for this surface.

For example, whereas for the surface grown for 4 hours h_{SA} exceeded h_{evap} by more than 200%, on average, for superheats greater than and equal to 30°C for all droplet sizes, on the surface grown for 10 hours only the h_{evap} associated with the 3.9 mm droplet at superheats of 30 °C and 40°C and the 3.0 mm droplet at 40°C were exceeded by h_{SA} by more than 200%. In any case, that h_{SA} exceeds h_{evap} by such a substantial factor indicates that heat transfer on this surface from droplet evaporation is not due to nucleate boiling. Thus the comparison between experimental results and nucleate boiling predictions helps to con rm the visual observation that the droplet evaporated by mechanisms more typical of lm evaporation.

The droplet release height had a similar e ect on heat transfer coe cient, h_{evap} as it did for the previously analyzed surface. In general, the e ect of increasing droplet release height on h_{evap} diminished with increasing wall superheat. Furthermore, for this surface there was no clear indication that an increease in release height a ected the magnitude of h_{evap} independent of droplet volume. It is noteworthy that for the 2.5 mm droplet an increase in release height from 1.25 mm to 3.9 cm accounts for the droplet exhibiting a heat transfer coe cient within 5% of the nucleate boiling prediction at a superheat level of 20°C. There were no further gains in h_{evap} for an increase in release height for the same droplet at the same superheat.

4.3.5 ZnO surface - hydrothermal synthesis time = 24 hours

Heat transfer coe cients calculated from results of experiments performed on the ZnO nanostructured surface grown by hydrothermal synthesis for 24 hours are depicted graphically

in Figure 4.9. As was done for the other two surfaces in this parametric study, the calculated heat transfer coe cients are compared to those predicted by the nucleate boiling correlation of Stephan and Abdelsalam.

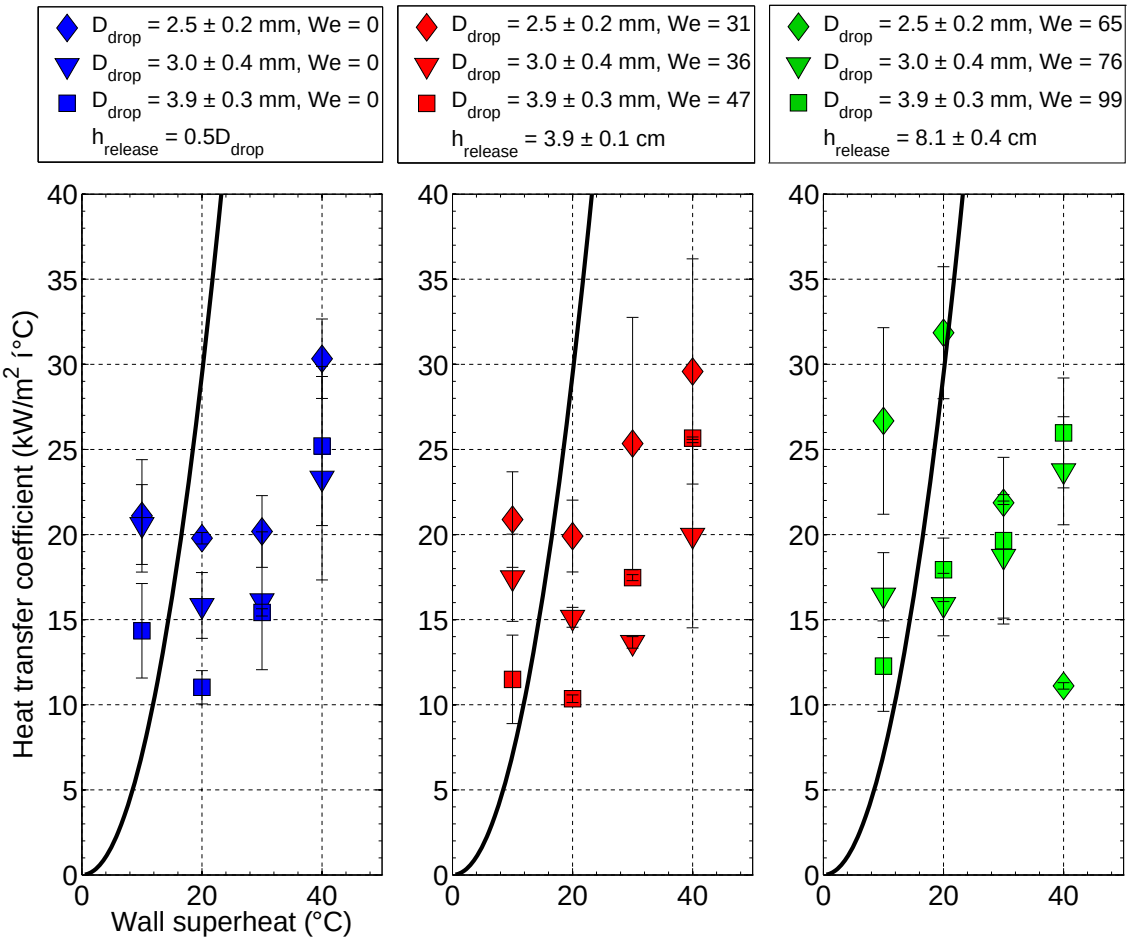

Figure 4.9: Heat transfer coe cient as a function of wall superheat, droplet size and release height for ZnO nanostructured surface generated by hydrothermal synthesis for 24 hours.

Results of calculations of heat transfer coe cient on surface grown for 24 hours as a function of droplet diameter, release height and wall superheat are listed in Table 4.19.

As was observed by the previous two surfaces, the heat transfer coe cient h_{evap} generally increases with a decrease in droplet volume. However, in comparison with the previous two surfaces analyzed in this study, this surface exhibited less predictable behavior in terms of the e ect of droplet release height and wall superheat level.

It is interesting to note that while the previous two surfaces exhibited an increase in h_{evap} for any increase in wall superheat, this surface exhibted a decrease in h_{evap} of 5{20% for an increase in wall superheat from 10°C to 20 °C, for all droplets released from the minimum

Table 4.19: Results of calculations of heat transfer coe cient on surface grown for 24 hours. D is the droplet diameter, h_{evap} is the heat transfer coe cient and T is the wall superheat.

		T = 10 °C	T = 20 °C	T = 30 °C	T = 40 °C
D (mm)	H (cm)	h_{evap} (kW/m ^{2}{°C)	h_{evap} (kW/m ^{2}{°C)	h_{evap} (kW/m ^{2}{°C)	h_{evap} (kW/m ^{2}{°C)
2.5	0.12	21.1 ± 3.3	19.8 ± 0.3	20.2 ± 2.1	30.3 ± 2.3
2.5	3.9	20.9 ± 2.8	19.9 ± 2.1	25.3 ± 7.4	29.6 ± 6.6
2.5	8.1	26.7 ± 5.5	31.9 ± 3.9	21.9 ± 0.1	11.1 ± 0.2
3.0	0.15	20.6 ± 2.3	15.8 ± 1.9	16.1 ± 4.0	23.3 ± 6.0
3.0	3.9	17.5 ± 2.6	15.1 ± 0.6	13.7 ± 0.3	20.0 ± 5.4
3.0	8.1	16.4 ± 2.5	15.9 ± 1.8	18.7 ± 3.6	23.7 ± 3.2
3.9	0.20	14.3 ± 2.8	11.0 ± 1.0	15.4 ± 0.2	25.2 ± 4.7
3.9	3.9	11.5 ± 2.6	10.4 ± 0.2	17.5 ± 0.2	25.7 ± 0.1
3.9	8.1	12.3 ± 2.7	17.9 ± 1.9	19.6 ± 4.9	26.0 ± 3.2

height and 3.9 cm. This is an unexpected result. Further increases in wall superheat result in increases in h_{evap}, except for the 2.5 mm droplet released from 8.1 cm. A 2.5 mm droplet released from 8.1 cm exhibits a 20% increase in h_{evap}, from 26.7 kW/m^2{°C to 31.9 kW/m^2{°C, as a result of a wall superheat increase from 10°C to 20 °C . However, for a wall superheat level increase up to 30°C, h_{evap} decreases by about 30%, from 31.9 kW/m^2{°C to 21.9 kW/m^2{°C, and a further increase in wall superheat to 40°C results in an even further decrease in h_{evap} by nearly 50%, down to 11.1 kW/m^2{°C. This particular example exhibits the most dramatic deviation from that of the previous surfaces, but to re-emphasize this point, a quick glance at Figure 4.9, reveals that this relatively unexpected behavior is exhibited by the other droplet sizes and release heights.

Comparing the calculated heat transfer coe cients, h_{evap} for this surface to those predicted by the nucleate boiling prediction of Stephan and Abdelsalam h_{SA} at the same superheat levels in this study, the data shown in Figure 4.9 reveal that for a superheat level of 10 °C, h_{evap} for droplets of all sizes and release heights exceeds the magnitude of the prediction, 7.1 kW/m^2{°C, by about 40{70%. At a wall superheat level of 20°C, h_{SA}, which has a value of 29.4 kW/m^2{°C, exceeds h_{evap} by 30{138% where the di erence in magnitude between h_{SA} and h_{evap} increased with increasing droplet volume. For superheat levels greater than and equal to 30°C, h_{SA} exceeds h_{evap} by 200{540% for all droplet sizes and release heights.

Droplet release height had a very minimal impact on heat transfer coe cient, especially when compared to the other two surfaces. For the 2.5 mm droplets increasing release height from 1.25 mm to 3.9 cm results in about a 5% increase in h_{evap}, whereas any further increase in height results in less than a 3% increase. The 3.0 mm droplet is impacted to lesser extent by release height than the smallest droplet. The 3.9 mm droplet exhibits a modest 10%

increase in h_{evap} for changes in release height in this study. As such it is concluded that droplet volume and wall superheat dominate the effect on h_{evap} for this surface.

4.3.6 Comparison of heat transfer coefficient across all surfaces

The maximum heat transfer coefficient, h_{evap} in this parametric study, equivalent to approximately 65 kW/m^2-°C was exhibited by a 2.5 mm droplet deposited on a surface grown for 10 hours at a superheat level of 40°C and released from a height of 8.1 cm. The minimum heat transfer coefficient in this parameteric study, equivalent to 6.7 kW/m^2-°C was exhibited by a 3.9 mm droplet deposited on a surface grown for 4 hours at a superheat level of 40°C and released from a height of 0.2 cm, the minimum release height for that size droplet. The maximum calculated heat transfer coefficient for each droplet size and the corresponding release height and surface are summarized in Tables 4.20–4.22.

Table 4.20: Maximum calculated heat transfer coefficients for surface grown for 4 hours. D is the droplet diameter, h_{max} is the maximum calculated heat transfer coefficient, H is the droplet release height and T is the wall superheat.

	T = 10 °C		T = 20 °C		T = 30 °C		T = 40 °C	
D (mm)	h_{max} (kW/m^2-°C)	H (cm)	h_{max} (kW/m^2-°C)	H (cm)	h_{max} (kW/m^2-°C)	H (cm)	h_{max} (kW/m^2-°C)	H (cm)
2.5	20.1	8.1	25.5	8.1	27.9	3.9	32.3	8.1
3.0	15.7	8.1	17.7	0.2	18.6	8.1	25.2	0.2
3.9	10.1	8.1	10.3	3.9	14.1	0.2	24.6	0.2

Table 4.21: Maximum calculated heat transfer coefficients for surface grown for 10 hours. D is the droplet diameter, h_{max} is the maximum calculated heat transfer coefficient, H is the droplet release height and T is the wall superheat.

	T = 10 °C		T = 20 °C		T = 30 °C		T = 40 °C	
D (mm)	h_{max} (kW/m^2-°C)	H (cm)	h_{max} (kW/m^2-°C)	H (cm)	h_{max} (kW/m^2-°C)	H (cm)	h_{max} (kW/m^2-°C)	H (cm)
2.5	33.9	3.9	28.3	3.9	40.4	3.9	64.6	8.1
3.0	25.8	8.1	22.3	0.15	38.5	8.1	46.6	8.1
3.9	22.1	3.9	13.9	3.9	23.6	8.1	31.0	3.9

Averaging all the maximum heat transfer coefficients, h_{evap} for each droplet size for each surface over all superheats reveals that h_{evap} increases with decreasing droplet size. For the surface grown for 4 hours, the average maximum h_{evap} across all superheats for droplets of

Table 4.22: Maximum calculated heat transfer coefficients for surface grown for 24 hours. D is the droplet diameter, h_{max} is the maximum calculated heat transfer coefficient, H is the droplet release height and T is the wall superheat.

	T = 10 °C		T = 20 °C		T = 30 °C		T = 40 °C	
D (mm)	h_{max} (kW/m^2-°C)	H (cm)	h_{max} (kW/m^2-°C)	H (cm)	h_{max} (kW/m^2-°C)	H (cm)	h_{max} (kW/m^2-°C)	H (cm)
2.5	26.7	8.1	31.9	8.1	25.3	3.9	30.3	8.1
3.0	20.6	0.15	15.9	8.1	18.7	8.1	23.7	8.1
3.9	14.3	0.20	17.9	8.1	19.6	8.1	26.0	8.1

2.5 mm, 3.0 mm and 3.9 mm is approximately 27 kW/m^2{°C, 20 kW/m^2{°C and 15 kW/m^2{°C, respectively. For the surface grown for 10 hours, the average maximum h_{evap} across all superheats for droplets of 2.5 mm, 3.0 mm and 3.9 mm is approximately 42 kW/m^2{°C, 33 kW/m^2{°C and 23 kW/m^2{°C, respectively. For the surface grown for 24 hours, the average maximum h_{evap} across all superheats for droplets of 2.5 mm, 3.0 mm and 3.9 mm was approximately 29 kW/m^2{°C, 20 kW/m^2{°C and 23 kW/m^2{°C, respectively. Thus, the maximum average heat transfer coefficients for all drop sizes across all superheats are exhibited by the surface grown for 10 hours.

Averaging across all superheats and release heights, a change in nanostructured surface from one grown for 4 hours to one grown for 10 hours, the heat transfer coefficient increased by 55{70%. A surface change from one grown for 10 hours to 24 hours resulted in a reduction in the magnitude of the heat transfer coefficient of approximately 13{30%. A surface change from one grown for 4 hours to one grown for 24 hours resulted in an average 15{30% increase in the magnitude of the heat transfer coefficient. Thus, in terms of the magnitude of the calculated heat transfer coefficient, the surface grown for 10 hours outperforms the other surfaces by a substantial factor.

The heat transfer coefficient was most sensitive to changes in wall superheat compared with changes in release height and volume. Although the specific level of wall superheat dictated the effect on heat transfer coefficient, averaging across all superheat levels it was found that a change in wall superheat across all surfaces resulted in approximately a 40{70% change in heat transfer coefficient. Changes in volume alone accounted for approximately a 30{40% difference in heat transfer coefficient, with an increase in volume generally leading to a decrease in h_{evap}. Finally, release height had the least effect on changes in heat transfer coefficient, on the order of 20-30%, where an increase in height generally lead to an increase in h_{evap}.

4.4 Comparison between ZnO nanostructured and bare metal surfaces

Droplet vaporization experiments were also performed on bare copper and aluminum surfaces. The results were compared to those from experiments on the ZnO nanostructured surfaces. Maximum droplet spread area, droplet evaporation time and calculated heat transfer coe cient were compared between surfaces as a function of wall superheat. The droplet diameter for all tests in the comparison was 3.0 mm. The droplet release height was the minimum height of 1.5 mm for this droplet size. The results of the comparison are summarized in the following section.

4.4.1 Comparison of maximum spread area between ZnO nanostructured and bare metal surfaces

The results of maximum droplet spread area measurements for all ZnO nanostructured and bare copper and aluminum surfaces are depicted graphically in Figure 4.10.

In general, for a speci ed wall superheat level, the maximum droplet spread area for the ZnO nanostructured surfaces was greater than that of the bare metal surfaces by a minimum of approximately 50%. The ZnO nanostructured surface grown for 10 hours exhibited the greatest magnitude of maximum spread area for all surfaces, equivalent to approximately 184.0 mm^2 at a superheat of 30°C. In comparison, the greatest magnitudes in maximum spread area exhibited by the copper and aluminum surfaces was about 77 mm^2 and 79 mm^2, respectively. For all surfaces in this comparison, the minimum values of maximum spread area were about 20 mm^2, exhibited by the bare metal surfaces. The surface grown for 10 hours by hydrothermal surface exhibited the minimum value in maximum spread area, equivalent to approximately 54 mm^2. For reference, the maximum and minimum values of spread area for this comparison are in Table 4.23.

Table 4.23: Maximum and minimum values of maximum spread area for all ZnO nanostructured and bare metal surfaces. $A_{spread,max}$ is the maximum value of the maximum spread area, $A_{spread,min}$ is the minimum value of the maximum spread area and T is the wall superheat. The droplet diameter for all data is 3.0 mm. The droplet release height for all data is 1.5 mm.

Surface	$A_{spread,max}$ (mm^2)	T (°C)	$A_{spread,min}$ (mm^2)	T (°C)
$t_{hydrothermal}$ = 4 hrs	170.4	30	110.52	20
$t_{hydrothermal}$ = 10 hrs	184.0	30	53.9	10
$t_{hydrothermal}$ = 24 hrs	174.4	30	74.7	10
Copper	77.3	30	19.6	10
Aluminum	79.5	30	18.8	10

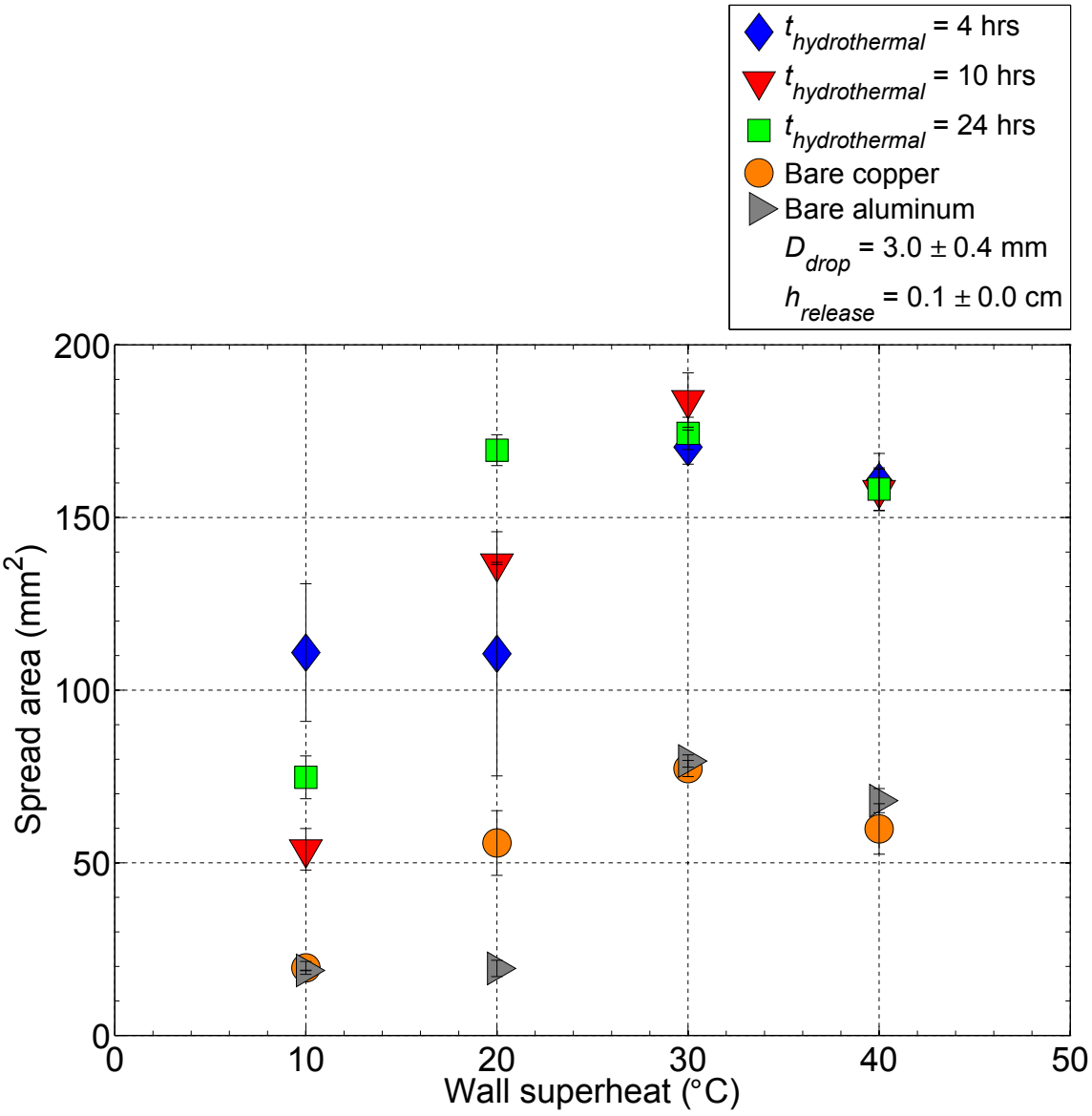

Figure 4.10: Spread area comparison between ZnO nanostructured and bare copper and aluminum surfaces.

For the nanostructured surface grown by hydrothermal synthesis for 4 hours, on average, across all superheats, the spread area was greater by about 60% in comparison to the bare copper surface and approximately 70% in comparison to the bare aluminum surface. Similarly, the surface grown for 10 hours, exhibited spread areas that were 60{66% greater, on average, than the bare metal surfaces. The surface grown for 24 hours exhibited spread areas that were 65{70% greater, on average, than the bare metal surfaces.

Clearly, the presence of the ZnO nanostructures signi cantly promoted droplet spreading compared with the metal surfaces. Whereas droplet spreading on the metallic surface appears to be enhanced only by the bene ts of an increase in its wall superheat, spreading on the nanostructured surface is aided by superheat and the geometrical and energetic advantages inherent of the nanostructures. The porosity of the nanostructure matrix is favorable for capillary e ects that aid in spreading liquid. Furthermore, the presence of the additional surface area provided by the ZnO nanostructure array requires the minimization of its surface energy and that of the liquid with which it is in contact. The result of this liquid-to-solid contact is the Wenzel wetting of the nanostructure array manifested in the spreading of the thin lm of liquid water. Finally, liquid spreading is aided on both the metal and the nanostructured surfaces by reductions in liquid viscosity and surface tensions that result from the elevated temperature of the surface.

4.4.2 Comparison of evaporation time between ZnO nanostructured and bare metal surfaces

The results of droplet evaporation time measurements for all ZnO nanostructured and bare copper and aluminum surfaces are depicted graphically in Figure 4.11.

In general, for any given superheat level, droplets deposited on the ZnO nanostructured surfaces evaporated faster, by no less than 20%, than on the bare metal surfaces. The shortest evaporation times for all surfaces were exhibited for a superheat level of 40°C. The longest evaporation times for all surfaces were exhibited for superheat level of 10°C. The shortest droplet evaporation time in this study was approximately 0.17 s and was exhibited by the ZnO surface grown for 10 hours at a superheat level of 40°C. The longest evaporation time in this study was approximately 9.67 s and was exhibited by the bare aluminum surface at a superheat of 10°C. The maximum and minimum evaporation times for all the surfaces in this study are found with the corresponding superheat level in Table 4.24.

Table 4.24: Maximum and minimum values of droplet evaporation time for all ZnO nanostructured and bare metal surfaces. t_{max} is the maximum value of the evaporation time, t_{min} is the minimum value of the evaporation time and T is the wall superheat. The droplet diameter for all data is 3.0 mm. The droplet release height for all data is 1.5 mm.

Surface	t_{max} (s)	T (°C)	t_{min} (s)	T (°C)
$t_{hydrothermal}$ = 4 hrs	2.48	10	0.20	40
$t_{hydrothermal}$ = 10 hrs	2.37	10	0.17	40
$t_{hydrothermal}$ = 24 hrs	1.46	10	0.22	40
Copper	9.70	10	0.27	40
Aluminum	9.67	10	0.68	40

In general, the bare copper surface exhibited much shorter evaporation times than the

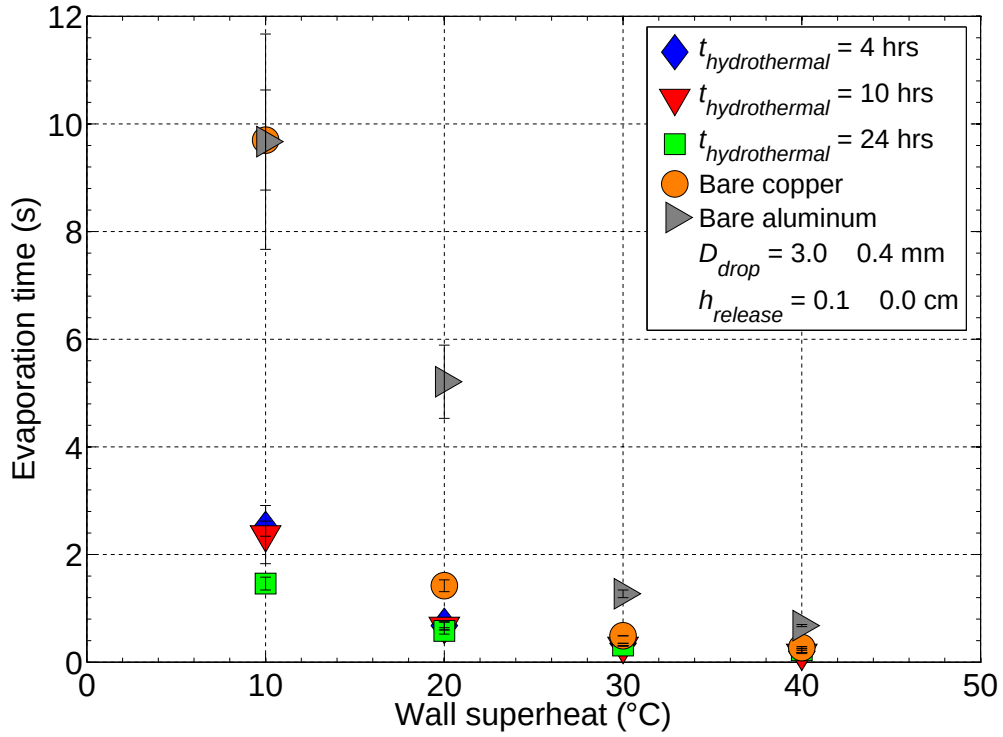

Figure 4.11: Droplet evaporation time comparison between ZnO nanostructured and bare copper and aluminum surfaces.

aluminum surface. The ZnO nanostructured surface grown for 4 hours exhibited approximately 120% shorter evaporation times than the bare copper and about 360% in comparison to the bare aluminum. The ZnO nanostructured surface grown for 10 hours exhibited approximately 135% shorter evaporation times than the bare copper and about 400% in comparison to the bare aluminum. Finally, the ZnO nanostructured surface grown for 24 hours exhibited approximately 200% shorter evaporation times than the bare copper and about 470% in comparison to the bare aluminum. Furthermore, a wall superheat level of 10°C yielded the greatest di erence in evaporation time, approximately 380% on average between all ZnO nanostructured surfaces and the bare metal surfaces.

Clearly, the presence of the ZnO nanostructures led to a reduction in the evaporation time compared with that on the bare metal surfaces. At any speci ed wall superheat, the thin lm that resulted from the droplet spreading was responsible for the shortened evaporation time as was shown in Section 4.2.

4.4.3 Comparison of heat transfer coe cient between ZnO nanostructured and bare metal surfaces

The results of the calculated heat transfer coe ecients from measurements of spread area, droplet volume and evaporation time for all ZnO nanostructured and bare copper and aluminum surfaces are depicted graphically in Figure 4.12.

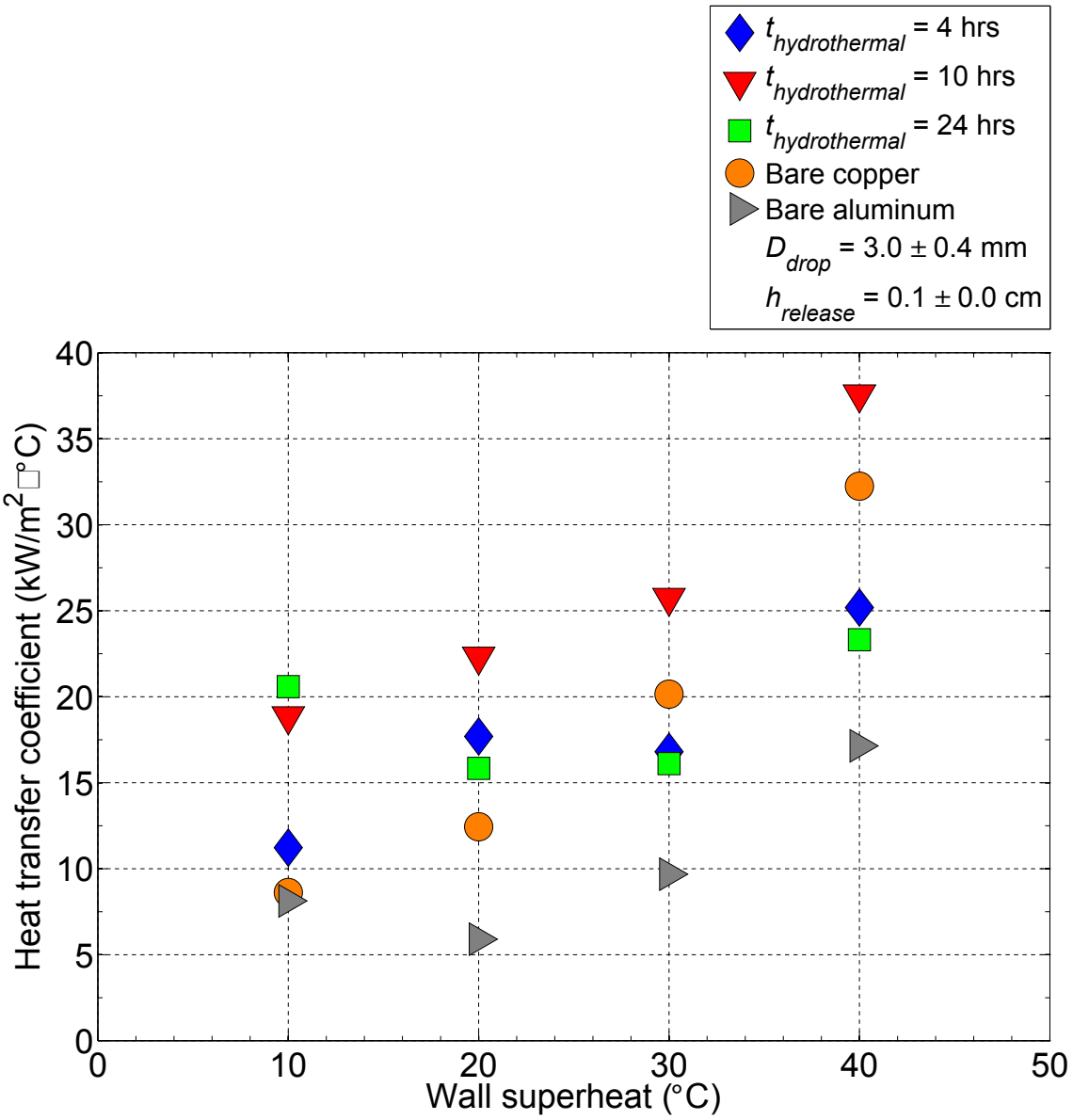

Figure 4.12: Heat transfer coe cient comparison between ZnO nanostructured and bare copper and aluminum surfaces.

In general the heat transfer coe cient for all of the surfaces tested increased with increasing wall superheat. The ZnO nanostructured surfaces exhibited heat transfer coe cients that were greater than those of the bare aluminum surface by a minimum of about 25% for all superheat levels. In fact, the bare aluminum surface exhibited the lowest heat transfer coe cients of all the surfaces at all levels of wall superheat. The ZnO nanostructured surface grown by hydrothermal synthesis for 10 hours exhibited the greatest heat transfer coe cients of all the surfaces for all superheat levels except for a superheat level of 10°C. At this superheat level the surface grown for 24 hours exhibited a heat transfer coe cient that was less than 10% greater than that exhibited by the surface grown for 10 hours.

Up to a level of 20 °C, the ZnO nanostructured surfaces exhibited heat transfer coe cients that are no less than about 20% greater than those of the bare copper surface. However, at a superheat level of 30°C, the heat transfer coe cient for the bare copper surface exceeded that of the ZnO nanostructured surfaces that were grown for 4 hours and 24 hours by hydrothermal synthesis. Only the nanostructured surface that was grown for 10 hours exhibited heat transfer coe cients that were greater than the bare copper surface for all superheats.

The maximum heat transfer coe cient for all surfaces, equivalent to approximately 38 kW/m ^{2}{°C, was exhibited by the nanostructured surface grown for 10 hours at a wall superheat of 40°C. The minimum heat transfer coe cient, equivalent to 5.9 kW/m^2{°C, was exhibited by the bare aluminum surface at a wall superheat of 20°C. The maximum and minimum calculated heat transfer coe cients for all the surfaces in this study are found with the corresponding superheat level in Table 4.25.

Table 4.25: Maximum and minimum calculated heat transfer coe cients for all ZnO nanostructured and bare metal surfaces h_{max} is the maximum calculated heat transfer coe cient, h_{min} is the minimum calculated heat transfer coe cent and T is the wall superheat. The droplet diameter for all points is 3.0 mm. The droplet release height for all points is 1.5 mm.

Surface	h_{max} (kW/m ^{2}{°C)	T (°C)	h_{min} (kW/m ^{2}{°C)	T (°C)
$t_{hydrothermal}$ = 4 hrs	25.2	40	11.2	10
$t_{hydrothermal}$ = 10 hrs	37.6	40	18.9	10
$t_{hydrothermal}$ = 24 hrs	23.3	40	15.8	20
Copper	32.2	40	8.6	10
Aluminum	17.1	40	5.9	20

On average, across all superheat levels, the bare aluminum surface exhibits heat transfer coe cients that are approximately 40{60% lower than those of all the ZnO nanostructured surfaces. The di erence in magnitude of the heat transfer coe cient between the nanostructured surfaces and the bare copper surface decreased with increasing wall superheat. For example, the ZnO nanostructured surface which was grown for 10 hours exhibited a heat transfer coe cient approximately 54% greater than that exhibited by the bare copper

surface at a wall superheat level of 10°C, but only 14% greater at a wall superheat level of 40 °C. The nanostructured surface grown for 4 hours exhibited heat transfer coefficients that were approximately 20% and 30% greater than those of the copper surface at a superheat levels of 10°C and 20 °C, respectively. However, at superheat levels of 30°C and 40 °C, the copper surface exhibited heat transfer coefficients that were 20% and almost 30% greater, respectively, than those of the nanostructured surface grown for 4 hours. Similarly, the nanostructured surface grown for 24 hours exhibited heat transfer coefficients that were approximately 60% and 20% greater than those of the copper surface at superheat levels of 10 °C and 20 °C. However, at superheat levels of 30°C and 40 °C, the copper surface exhibited heat transfer coefficients that were approximately 25% and 40% greater than the nanostructured surface grown for 24 hours.

In order to analyze the results of this comparison study, it is important to note the onset of and subsequent nucleate boiling process that was exhibited by the nanostructured and bare metal surfaces. The bare aluminum surface exhibited an onset of nucleate boiling at a wall superheat of approximately 13{19°C. However, nucleation events on this surface were quite stable and subdued until about a wall superheat of 26°C, after which there was significant satellite droplet ejection from the main droplet. This observation is consistent with the results depicted in Figure 4.12, where there is a noticeable increase in heat transfer coefficient for the aluminum surface at wall superheats greater than and equal to 30°C. The copper surface exhibited an onset of nucleate boiling at a wall superheat of approximately 10 °C. Small satellite droplets began to be ejected from the main droplet mass at superheats as low as 13°C. Satellite droplet ejection was significant at a superheat of 20°C. Nucleate boiling was vigorous and extremely explosive for superheats greater than and equal to 30°C. The increasingly vigorous boiling for both bare metal surfaces is manifested in the substantial increase in heat transfer coefficient evident in Figure 4.12 as the wall superheat increases beyond 20°C. However, while it is true that nucleate boiling results in a significant increase in heat transfer coefficient, it is very likely that the heat transfer coefficients for the bare metal surfaces depicted in Figure 4.12 are artificially high, especially for the copper surface, due to the inability to account for the mass of the significant ejection of satellite droplets with the current experimental apparatus. The heat transfer coefficient is calculated based on the assumption that the entire mass of the droplet that is deposited is evaporated from the surface. Since the experimental apparatus used in this study was not equipped to measure the mass of the satellite droplets that were ejected, the evaporation times that were measured were for a mass of liquid that was less than the original mass that was deposited on the surface. As a result, the calculated heat transfer coefficients for the bare metal surfaces are artificially higher because the calculation depends on the original mass of liquid deposited.

The onset of nucleate boiling for the ZnO nanostructured surfaces grown for 4 hours, 10 hours and 24 hours were approximately 111°C, 140 °C and 134 °C, respectively. However, the presence of the nanostructures resulted in a suppression of significant satellite droplet ejection for superheats less than and equal to 40°C for all nanostructured surfaces. So while nucleate boiling was occurring at a different wall superheat level for any one nanostructured surface, the entire mass of the droplet was evaporated from the nanostructured surface for

most experiments.

Chapter 5

Results and discussion of Leidenfrost experiments

Results for series of experiments performed to determine the e ect of surface wettability on the Leidenfrost point are shown in Figure5.3. In addition, the Leidenfrost point was determined experimentally on each surface as a function of droplet diameters spanning a range of approximately 2.5{4.0 mm, as shown in Figure 5.2.

Seven ZnO nanostructured surfaces were produced for the Leidenfrost study, one grown for 4 hours, ve grown for 10 hours and one grown for 24 hours. All syntheses were on smooth, mirror- nish copper alloy 145 of the same concave geometry which was described in Chapter 2.

Five ZnO nanostructured surfaces were grown for 10 hours by hydrothermal synthesis in order to assess the quality of the nanostructured surface with respect to reliability, durability and repeatability of the results exhibited by any one particular surface. The nanostructured surface grown for 10 hours was chosen for the the quality assessment study since it exhibited the most extreme wettability and highest Leidenfrost point of all the nanostructured surfaces. As part of this quality assessment study, extreme e orts were taken to perform identical hydrothermal syntheses on every surface. Despite these e orts, as will be seen, results for the Leidenfrost point varied from surface to surface. Nevertheless, every nanostructured surface grown for 10 hours exhibited extreme wetting conditions and resulted in signi cantly higher Leidenfrost points than the bare, smooth surfaces. Finally, since there were ve surfaces grown for 10 hours they are identi ed by a number indicating the order in which it was tested, e.g. 10-1 was the rst surface grown for 10 hours that was tested, 10-2 was the second surface grown for 10 hours that was tested and so on.

All nanostructured surfaces were subjected to many heating and cooling cycles spanning a temperature range of approximately 20C up to about 450°C. As a result, the nanostructured surfaces exhibited non-uniformities and asperities as a function of increased experiment time for each test sample. A surface was retired from testing once the non-uniformities were visible to the naked eye. Experimental times for each surface are listed in Table 5.1.

Table 5.1: Total experimental time, $t_{experimental}$ for each nanostructured surface. Surfaces are identi ed by the length of their respective hydrothermal synthesis time, $t_{hydrothermal}$.

$t_{hydrothermal}$ (hrs)	$t_{experimental}$ (hrs)
4	7.4
10-1	13.6
10-2	8.2
10-3	8.4
10-4	3.0
10-5	5.2
24	12.2

5.1 Acoustic determination of Leidenfrost point

In contrast with previous studies that employed the droplet lifetime method, the Leidenfrost point was determined in this study by measuring the acoustic signal produced during the evaporation process. By this metric, the Leidenfrost point is achieved when, after the initial deposition, the droplet hovers completely quietly above the solid surface for the entirety of the evaporation process.

The acoustic signals from two experiments are shown in screenshots of the recording software depicted in Figure 5.1 . The horizontal axis shows time in seconds while the vertical axis measures sound pressure level in decibels (dB). In both graphs, ambient fan noise from the clean room enclosure is registered as the nominally constant thick blue signal centered at 0.0 dB. Contact between the water droplet and the solid surface corresponds to the thin, tall peaks that protrude very clearly from the ambient noise signal. The Leidenfrost point is achieved or exceeded when the evaporation process is completely silent beyond the initial deposition. Once the surface temperature corresponding to the rst incidence of silent evaporation is reached, the surface is cooled and heated cyclically by progressively smaller temperature increments, generating noisy and silent evaporations, in order to narrow in on the transition point to within the range of the accuracy of the thermocouple.

The top graph displayed in Figure 5.1 corresponds to an experiment in which the Leidenfrost point is reached or exceeded. The tall, thin peaks occurring around 4 seconds correspond to the initial droplet deposition. Beyond this time there is no sound registered apart from the ambient noise. This means that for this experiment the droplet hovered completely quietly on a thin vapor lm for the duration of the evaporation process. In contrast, the graph shown on the bottom half of Figure 5.1 is for an experiment in which the surface did not reach the Leidenfrost temperature. This is evident from the tall, thin peaks registered after the initial deposition, beginning around 15 seconds. These short bursts of sound, audible to both microphone and experimenter as a brief "pop" or sizzle, indicate that the surface is not hot enough to sustain stable lm boiling which results in the droplet

wetting the surface for an instant. The resulting "pop" or sizzle is a clear indication that the Leidenfrost point has not yet been reached. Both graphs in Figure 5.1 span the droplet lifetime.

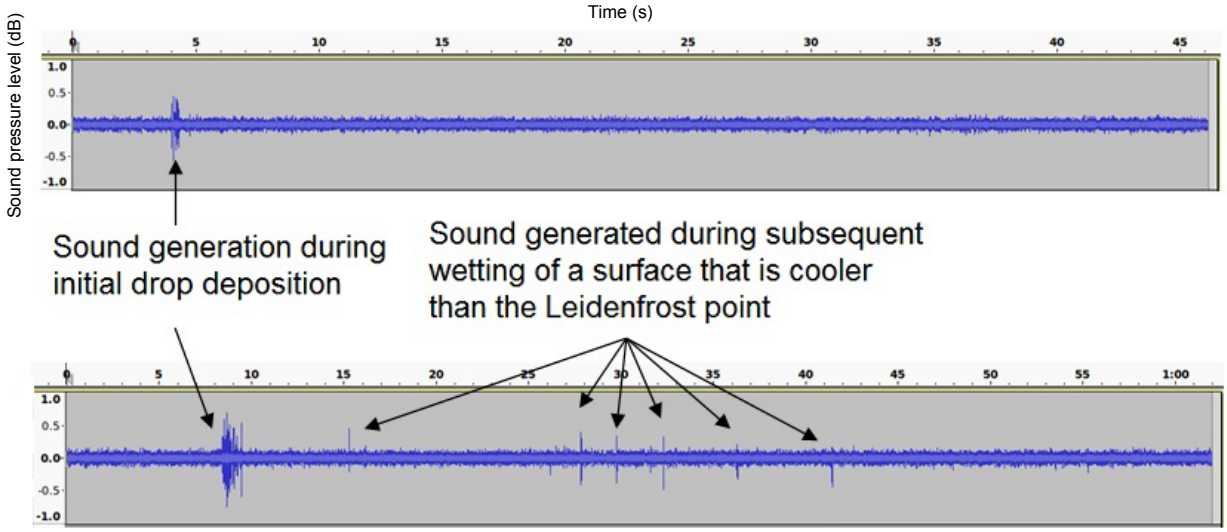

Figure 5.1: Acoustic signal recording from experiments. The signal captured in the top graph corresponds to an experiment in which the Leidenfrost point is achieved. The bottom graph corresponds to an experiment in which the surface is cooler than the Leidenfrost point.

5.2 Leidenfrost point as a function of droplet diameter

Leidenfrost transition data for each surface as a function of droplet diameter are shown in Figure 5.2 and listed in Table 5.2. The data represent Leidenfrost points spanning the entirety of the experimental lifetime of each surface. The Leidenfrost temperature, T_{Leid}, for each surface listed in Table 5.2 represent a mean of values obtained in di erent tests for each surface. The uncertainty values listed for each T_{Leid} in Table 5.2 indicate the spread of T_{Leid} obtained for each surface. The average contact angle, θ_{avg}, that is listed for each surface is the average of the contact angle measured or calculated after the second desorption and after the experiment. For convenience of presentation purposes in Figure 5.2, all of the superhydrophilic nanostructured surfaces grown for 10 hours are represented by one θ_{avg}. Furthermore, the Leidenfrost temperature was measured for each surface while it was cooling from a higher surface temperature or being heated from a lower surface temperature. In Figure 5.2, the measured Leidenfrost temperature for each surface is identi ed by whether

it was measured during a cooling or heating cycle. In the case of the surface grown for 10 hours, the Leidenfrost temperature was the same for both heating and cooling cycles.

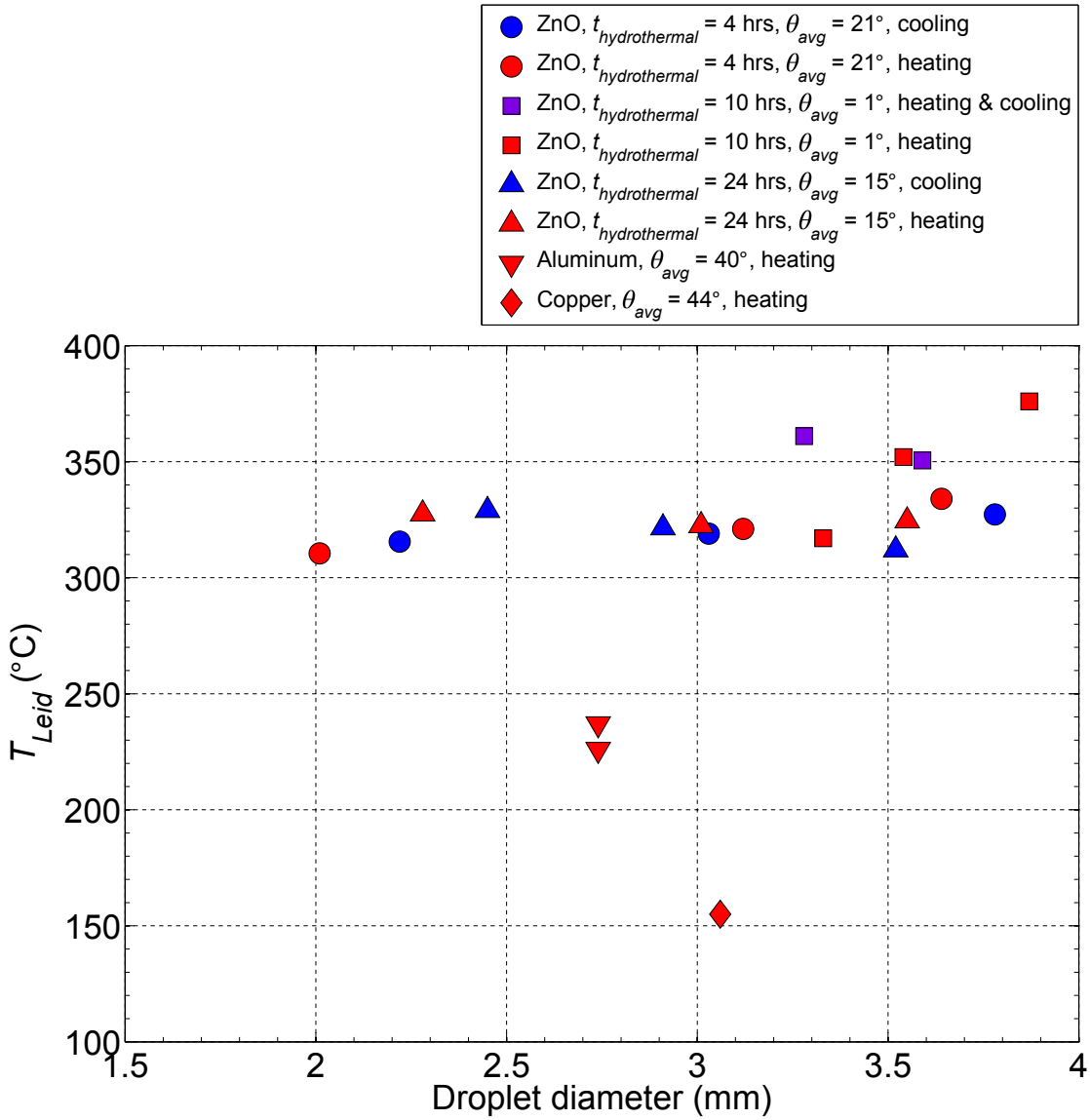

Figure 5.2: Leidenfrost point as a function of droplet diameter. The average contact angle for each surface is given by θ_{avg}

The data for the ZnO surfaces indicate that Leidenfrost point is not strongly dependent on droplet size compared with surface wettability. The variation in Leidenfrost temperature across all ZnO and metallic surfaces agree with the expected general trend that Leidenfrost

temperature increases with increasing surface wettability, characterized here by contact angle.

The surface grown by hydrothermal synthesis grown for 4 hours exhibited Leidenfrost temperatures which spanned a range of 310{334°C for droplets of 2.0{3.8 mm in diameter and an average contact angle of 15°. For this surface, T_{Leid} increased with increasing diameter. The heating or cooling cycle had a minimal effect on T_{Leid} compared with the effect of droplet diameter. Furthermore, for this surface and any given droplet diameter, it was not possible to determine the effect of the heating or cooling cycle on T_{Leid}. For droplets of 2.0{2.2 mm diameter, the heating cycle resulted in a lower T_{Leid}, 310.5°C, than the T_{Leid} of the cooling cycle, 310.5°C. However for droplets of 3.6{3.8 mm diameter, the heating cycle resulted in a higher T_{Leid}, 334.0°C, than the T_{Leid} of the cooling cycle, 327.5°C. In summary, for this surface it is concluded that the heating or cooling cycle has a negligible effect on T_{Leid}. Furthermore, an increase in droplet diameter of nearly 2 times from 2.0 mm to 3.8 mm resulted in a T_{Leid} variation of approximately 25°C, from 310{335°C.

The most wetting ZnO nanostructured surfaces were those grown by hydrothermal synthesis for 10 hours. These superhydrophilic surface exhibited an average contact angle of approximately 1° and the highest overall Leidenfrost temperatures in this study. With the exception of one of the five surfaces grown for 10 hours, the measurements of T_{Leid} for these surfaces spanned a range of 350{376°C for droplets of 3.3{3.9 mm in diameter. This surface exhibited the highest Leidenfrost point, 376°C in the entire Leidenfrost study for a droplet of 3.9 mm. This surface too exhibited increasing Leidenfrost points by increasing diameter from 3.3 mm to 3.9 mm, roughly a factor of 1.2 increase. Similar to the surface grown for 4 hours, the heating or cooling cycle did not have any apparent affect on the relative magnitude of T_{Leid}. Neglecting the lowest T_{Leid} exhibited by the surfaces grown for 10 hours, 317°C, the range of T_{Leid} was also confined to about 25°C, from 350{375°C, for droplets of 3.3{3.9 mm in diameter.

The surface grown by hydrothermal synthesis grown for 24 hours exhibited Leidenfrost temperatures which spanned a range of 312{329°C for droplets of 2.3{3.6 mm in diameter and an average contact angle of 15°. Unlike the previous two surfaces, this surface did not exhibit a trend of increasing T_{Leid} for an increase in droplet diameter. Furthermore, the heating or cooling cycle did not affect the relative magnitude of the measured T_{Leid}. The range of T_{Leid} for this surface, 312{329°C, is well within the T_{Leid} range, 310{334°C, of the surface grown for 4 hours for droplets of 2.0-3.9 mm in diameter. This is not a surprising result since the average contact angles for the two surfaces are within 6° of one another, 21° exhibited by the surface grown for 4 hours and 15° for the surface grown for 24 hours.

The bare metal surfaces were only subject to heating cycles in order to minimize the experimental time for each surface. The bare metal surfaces tend to oxidize with increased heating time. Surface oxidation tends to significantly increase the wettability of the surface [1], which was undesirable since experimental results would not reflect those of a pure metal surface if it became heavily oxidized. The Leidenfrost temperature exhibited by the copper surface was 155°C for a 3.1 mm droplet and an average contact angle of 94°. This value of T_{Leid} was quite low in comparison to the values of T_{Leid}, 226°C and 237°C, for the two

Table 5.2: Leidenfrost temperatures, T_{Leid}, as a function of droplet diameter, D_{drop}. Nanostructured surfaces are identified by their length of hydrothermal synthesis time, $t_{hydrothermal}$. The average contact angle is given by θ_{avg}. The nanostructured surfaces are listed first in order of increasing $t_{hydrothermal}$ and then in order of increasing D_{drop}.

Surface	θ_{avg}	D_{drop} (mm)	Cycle	T_{Leid} (°C)
$t_{hydrothermal}$ = 4 hrs	21°	2.0 ± 0.1	heating	310.5 ± 2.3
$t_{hydrothermal}$ = 4 hrs	21°	2.2 ± 0.1	cooling	315.5 ± 2.4
$t_{hydrothermal}$ = 4 hrs	21°	3.1 ± 0.0	heating	321.0 ± 2.4
$t_{hydrothermal}$ = 4 hrs	21°	3.0 ± 0.1	cooling	319.0 ± 2.4
$t_{hydrothermal}$ = 4 hrs	21°	3.6 ± 0.5	heating	334.0 ± 2.5
$t_{hydrothermal}$ = 4 hrs	21°	3.8 ± 0.2	cooling	327.3 ± 2.5
$t_{hydrothermal,1}$ = 10 hrs	1°	3.6 ± 0.3	heating & cooling	350.5 ± 2.6
$t_{hydrothermal,2}$ = 10 hrs	1°	3.9 ± 0.3	heating	376.0 ± 2.8
$t_{hydrothermal,3}$ = 10 hrs	1°	3.5 ± 0.3	heating	352.0 ± 2.6
$t_{hydrothermal,4}$ = 10 hrs	1°	3.3 ± 0.3	heating	317.0 ± 2.4
$t_{hydrothermal,5}$ = 10 hrs	1°	3.3 ± 0.3	heating & cooling	361.0 ± 2.7
$t_{hydrothermal}$ = 24 hrs	15.0°	2.3 ± 0.1	heating	327.5 ± 2.5
$t_{hydrothermal}$ = 24 hrs	15.0°	2.5 ± 0.1	cooling	329.0 ± 2.5
$t_{hydrothermal}$ = 24 hrs	15.0°	3.0 ± 0.0	heating	322.5 ± 2.4
$t_{hydrothermal}$ = 24 hrs	15.0°	2.9 ± 0.2	cooling	321.5 ± 2.4
$t_{hydrothermal}$ = 24 hrs	15.0°	3.6 ± 0.2	heating	324.5 ± 2.4
$t_{hydrothermal}$ = 24 hrs	15.0°	3.5 ± 0.2	cooling	312.0 ± 2.3
Copper	44.0°	3.1 ± 0.1	heating	155.0 ± 2.2
Aluminum	40.5°	2.7 ± 0.1	heating	226.0 ± 2.2
Aluminum	40.5°	2.7 ± 0.1	heating	237.0 ± 2.2

aluminum surfaces in this study which exhibited contact angles of 40.5°. The diameter of the droplets deposited on the aluminum surfaces was 2.7 mm.

Given the results exhibited by the ZnO nanostructured and bare metal surfaces, it is concluded that T_{Leid} is most strongly dependent on wettability than droplet diameter. This is most evident from the dramatic increase in T_{Leid} when comparing the bare metal and nanostructured surfaces. However, this observation is reinforced by comparing the results of the nanostructures themselves. For the nanostructured surfaces which exhibited contact angles of 15° and 21°, the Leidenfrost temperatures were in the same range, 312–329 °C and 310–334 °C, for droplet diameters spanning 2.0–3.9 mm. Meanwhile, the superhydrophilic surface grown for 10 hours exhibited an average contact angle of 1° and a significant increase in T_{Leid}, 350–376 °C, for droplet sizes of 3.3–3.9 mm. In any case, all of the nanostructured surfaces exhibited Leidenfrost temperatures that were well above those of bare and oxidized metal surfaces.

5.3 Leidenfrost point as a function of contact angle

Experimental results for Leidenfrost point as a function of contact angle are shown Figure 5.3 and listed in Table 5.3. In Figure 5.3, each surface is represented by the average of the contact angle after the second desorption, i.e. pre-experiment contact angle, $\theta_{initial}$ and the contact angle after the experiment, θ_{final}. The temperature data shown in Figure 5.3 also span the experimental lifetime of each surface. The trends observed in this figure confirm that Leidenfrost point increases with increasing surface wettability. The difference in Leidenfrost point between the nanostructured surfaces and the bare copper surface in this study is on the order of a staggering 155-221°C. The Leidenfrost points for the aluminum surfaces are consistent with findings in the literature, which span a range of 171-280°C [27]. The Leidenfrost tempeature for the copper surface in this study, 155°C is lower than that of previous studies, which span a range of 190-250°C [27]. The mostly likely reason for the difference in T_{Leid} between this study and those of others is surface roughness, cleanliness and oxidation. In general, the results depicted in Figure 5.3 and Table 5.3 indicate that the Leidenfrost point increases with decreasing contact angle, which is consistent with the findings of other studies [27]{[29]. Furthermore, this is consistent with the theory that higher wall superheats are required to de-wet and establish stable film boiling over surfaces have a higher affinity for the liquid phase [1].

The Leidenfrost temperatures reported in Table 5.3 represent the range of mean values obtained in all experiments for each surface. The error bars in Figure 5.3 represent the range of mean T_{Leid} exhibited by the surfaces listed in Table 5.3. The mean contact angle value representing all five of the ZnO surfaces grown by hydrothermal synthesis for 10 hours is approximately 1°. The highest T_{Leid}, 376 °C, was exhibited by one of the superhydrophilic nanostructured surfaces grown for 10 hours. The maximum values of T_{Leid} for the nanostructured surfaces grown for 4 and 24 hours, 334°C and 329°C, respectively, are also well above the T_{Leid} exhibited by the bare metal surfaces in this and other experimental studies [27]. Clearly, the presence of the ZnO nanostructures promotes high to extremely high wetting, manifested in low contact angles, which requires substantially higher levels of wall superheat to de-wet the surface and establish stable film boiling.

Finally, it must be reiterated that the effective contact angle calculation for the nanostructured surfaces is currently the only method used to determine surface wettability. In a future study it may be useful to compare the results of this calculation with another method for characterization of surface wettability.

5.4 Comparison with the literature

The data shown in Figure 5.3 are plotted in Figure 5.4 to compare them with findings of a very limited number of studies available in which the dependence of Leidenfrost point on surface wettability is investigated. In all of the studies cited, Leidenfrost point is determined by measuring maximum evaporation time of the droplet. Despite using a different metric to

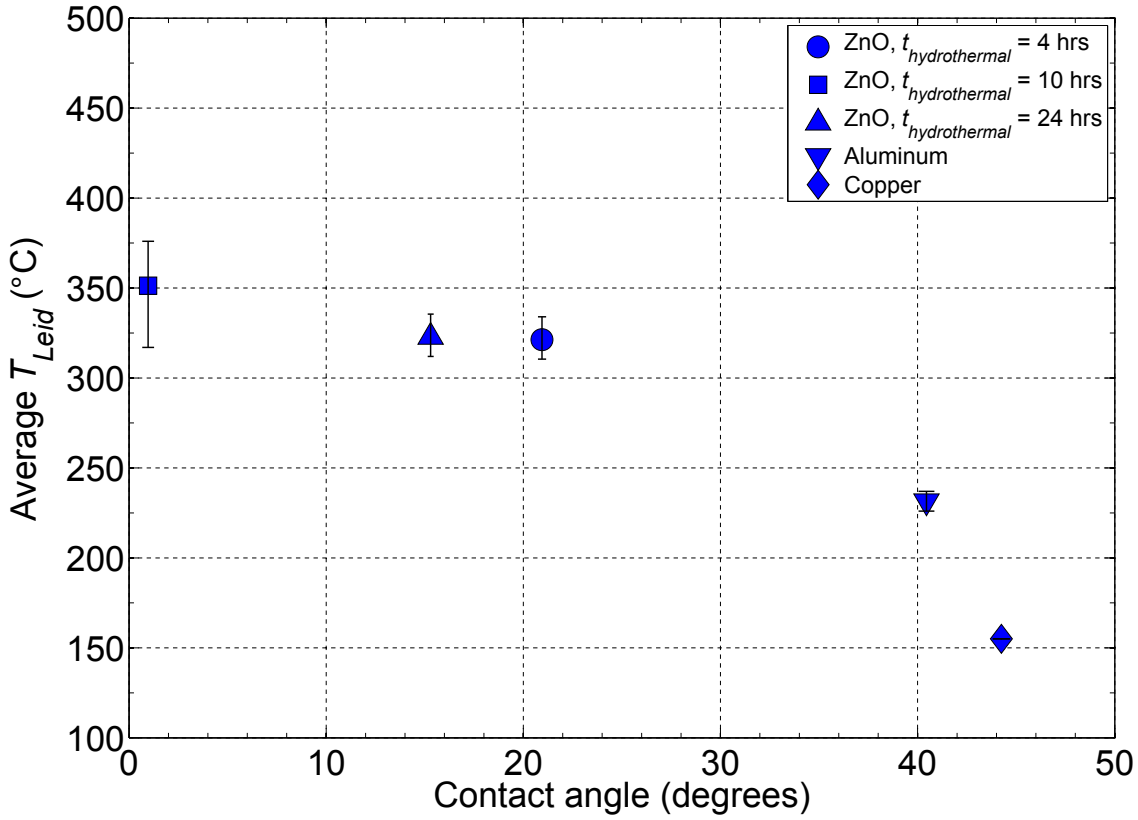

Figure 5.3: Leidenfrost point as a function of contact angle for ZnO nanostructured surfaces and bare metal surfaces. The error bars span the range of Leidenfrost points that were exhibited at each contact angle.

de ne Leidenfrost point, the results of this study fall well within the range of Leidenfrost temperatures of other highly wetting surfaces in other studies. In particular, even with the di erent metric, the bare metal control surfaces, which were tested for comparison purposes, exhibit classical behavior consistent with the Leidenfrost temperatures in the literature for similar surfaces. Furthermore, results from this study exhibit the same trend as previous studies that Leidenfrost point increases with increasing surface wettability. The maximum Leidenfrost point measured in this study corresponding to one of the ZnO nanostructured surfaces grown for 10 hours equivalent to 376°C, which is within the range of some of the highest Leidenfrost temperatures measured in the other studies highlighted in Figure 5.4 [30]{ [32]. The bare copper surface used in this study exhibits the lowest Leidenfrost temperature shown in Figure 5.4. Finally, and most importantly, the results shown in Figure 5.4 indicate that superhydrophilic surfaces can be used to elevate Leidenfrost temperatures by more than 100°C above those for surfaces exhibiting modest contact angles.

Table 5.3: Leidenfrost temperature range, T_{Leid}, as a function of average contact angle, θ_{avg}, for bare metal and nanostructured surfaces. Nanostructured surfaces are identified by their length of hydrothermal synthesis time, $t_{hydrothermal}$.

Surface	θ_{avg}	T_{Leid} (°C)
$t_{hydrothermal}$ = 4 hrs	21.0°	310.5–334.0
$t_{hydrothermal}$ = 10 hrs	1.0°	317.0–376.0
$t_{hydrothermal}$ = 24 hrs	15.0°	312.0–329.0
Copper	44.0°	155.0
Aluminum	40.5°	226.0-237.0

5.5 Theoretical discussion of Leidenfrost point exceeding the homogeneous nucleation temperature on nanostructured surfaces

The spinodal temperature, $T_{spinodal}$ of water at 101 kPa is on the order of 300°C. The spinodal temperature was measured by Skripov et al. [68] to be 309 while a correlation by Lienhard et al. [69], [70] predicts approximately 324°C. In many of the experiments in this study, the Leidenfrost temperatures measured for the ZnO nanostructured surfaces in this study exceeded the $T_{spinodal}$ significantly. Thus, it is important to explore the possible physical mechanisms that would lead to this seemingly impossible scenario.

In a recent study, Biance et al. [7] showed that for millimetric drops the vapor film thickness, L_{film} during film boiling can be estimated by

$$L_{film} \sim \left(\frac{k_v \quad T_{wall} \mu_v \rho_l g}{h_{lv} \rho_v \sigma^2} \right)^{1/3} r_{drop}^{4/3} \tag{5.1}$$

where k_v is the vapor thermal conductivity, T_{wall} is the wall superheat, μ is the vapor dynamic viscosity, ρ_l is the liquid density, g is the gravitational acceleration, h_{lv} is the enthalpy of vaporization, ρ_v is the vapor density, σ is the surface tension and r_{drop} is the droplet radius [7]. The properties of the vapor state are taken at the average film temperature, i.e. the average of T_{wall}. Therefore, as the droplet evaporates, the film thickness decreases as $r_{drop}^{4/3}$, which could result in intermittent contact between the droplet and the surface.

In another recent study, Kim et al. [30] separated the effects of surface wettability, roughness and porosity on Leidenfrost point. In this study, Kim et al. found that significant increases in the Leidenfrost point are a result of increased wetting as well as the presence of nanoporosity on the surface [Buongiorno reference]. In the experimental study, Kim et al. [30] fabricated surfaces with both nanoporosity and microposts that exhibited Leidenfrost temperatures up to 459°C for water at atmospheric pressure, which exceeded both $T_{spinodal}$ and the critical point. The nanoporosity in their experiments was established through the

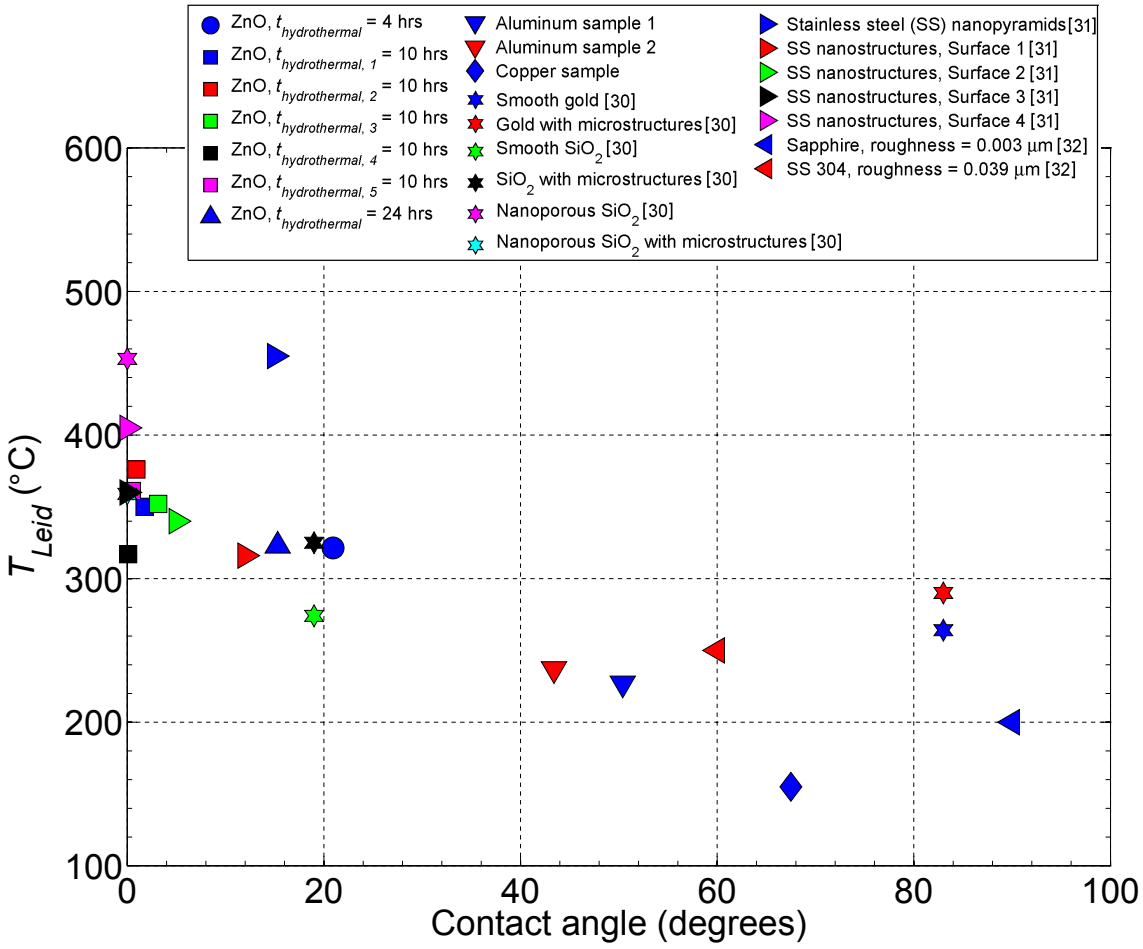

Figure 5.4: Comparison of Leidenfrost point data of this study with data in the literature. The Leidenfrost points are averaged for each surface in this study.

deposition of 23 nm silicon dioxide nanoparticles and the micropost height varied from 0 to 15 μm.

Kim et al. argued that nanoporosity initiates heterogenerous nucleation of bubbles during intermittent contact of the liquid droplet and the nanostructured surface. At temperatures approaching the Leidenfrost point, Kim et al. showed that the intermittent liquid-solid contact result in bubble nucleation events that were signi cant enough to disrupt the stable vapor lm layer that had been established by the droplet and solid nanostructured and nanoporous surface. Kim et al. argued that bubbles were nucleated from nanopores whose size permitted bubble nucleation at temperatures far less than $T_{spinodal}$ and the measured T_{Leid}. Bubble nucleation resulted in the disruption of the stable vapor lm layer that consequently shifted the heat transfer process from lm boiling to transition boiling. Therefore, even higher wall temperatures were required to establish a stable vapor lm layer throughout

the duration of the evaporation process in their experiments.

Although nanoporosity was not controlled or measured in this study, arguments similar to those of Kim et al. can still be applied to explain the findings in this study. By applying the fundamental arguments of heterogeneous nucleation theory, which combine the Clausius-Clapeyron and Young-Laplace equations [1], the minimum size, r_{min}, of a surface cavity required for it to be an active nucleation site can be predicted from

$$T_l - T_{sat}(P_l) > \frac{2\sigma T_{sat}(P_l)\nu_{lv}}{h_{lv} r_{min}}. \tag{5.2}$$

The SEM images of the nanostructured surfaces in this study reveal that the porosity was approximately 1 to 2 orders of magnitude greater than the nanoporosity achieved by Kim et al. Due to the random nature of ZnO nanocrystal nucleation on the substrate surface, it was difficult to measure an exact distance between nanocrystals. However, it was possible to estimate an approximate average distance between ZnO nanocrystals in this study to be approximately 1.0 μm, 0.5 μm and 0.1 μm for surfaces grown for 4, 10 and 24 hours, respectively. If it is assumed for the moment that the voids between the ZnO nanocrystals in this study are possible nucleation sites, cavities of 1.0 μm, 0.5 μm and 0.1 μm would be active at wall temperatures of approximately 132 °C, 165 °C and 425 °C. Therefore, as the vapor film thickness decreased in the manner predicted by Biance et al., intermittent contact between the liquid droplet and the solid nanostructures at temperatures exceeding $T_{spinodal}$ would have immediately activated surface cavities on the nanostructured surfaces. However, if the activated cavity were to have any effect on the Leidenfrost point the nucleated bubble would have to disrupt the vapor film suspending the droplet above the nanostructured surface. Carey showed that the liquid-vapor interface would be disrupted if the critical velocity of the Kelvin-Helmholtz instability was exceeded. The critical velocity of the Kelvin-Helmholtz instability is 8 m/s for water at atmospheric pressure [1]. The critical velocity, u_c is given by

$$u_c = \left[\frac{2(\rho_l - \rho_v)}{\rho_l}\right]^{1/2} \left[\frac{\sigma(\rho_l - \rho_v)g}{\rho_v^2}\right]^{1/4}. \tag{5.3}$$

Therefore, following the analysis adopted by Kim et al., assuming inertia-controlled growth of vapor bubbles, the interfacial velocity, $V_{interface}$ can be calculated from

$$V_{interface} = \left\{\frac{2}{3}\left(\frac{[T_{wall} - T_{sat}(P_l)]}{T_{sat}(P_l)}\right)\frac{h_{lv}\rho_v}{\rho_l}\right\}^{1/2}. \tag{5.4}$$

Bubbles nucleated from the 1.0 μm cavities of the surface grown for 4 hours, which are activated at 132 °C, would exhibited an interfacial velocity of approximately 9 m/s. Bubbles nucleated from the 0.5 μm cavities of the surface grown for 10 hours, which are activated at 165 °C, would exhibited an interfacial velocity of approximately 13 m/s. Therefore, if these cavities were activated during intermittent liquid-solid contact, the interfacial velocity

would be su cient to disrupt the liquid-vapor interface according to the Kelvin-Helmholtz instability threshold.

The surface grown for 4 hours exhibited Leidenfrost temperatures that spanned a range of 310{334°C, which was well within, and in some instances, exceed the predicted $T_{spinodal}$ range of 309{324°C. Therefore, given the range of Leidenfrost temperatures exhibited by this surface, it is likely that the Leidenfrost point was a ected by both heterogeneous and homogeneous nucleation events.

The surface grown for 10 hours exhibited Leidenfrost temperatures that spanned a range of 350{376°C, if we neglect the minimum value of 317°C exhibited by one of these surfaces. The temperature range of 350{376°C easily exceeds the range of the predicted $T_{spinodal}$. Therefore, it is possible that T_{Leid} was elevated well beyond $T_{spinodal}$ as a result of heterogeneous nucleation of vapor bubbles for the surface grown for 24 hours.

The surface grown for 24 hours, whose 0.1μm cavities were predicted to be active for heterogeneous nucleation at a surface temperature of approximately 425°C, exhibited Leidenfrost temperatures spanning a range of 312{329°C, which is well within, or just barely exceeding the range of the predicted $T_{spinodal}$. Since this surface did not exhibit a T_{Leid} greater than 330°C, heterogeneous nucleation cannot be attributed to nucleation events on the surface unless larger cavities were present. Therefore, nucleation events that disrupted the liquid-vapor interface could only have occurred by homogeneous nucleation or from cavities larger than 0.11μm. At a temperature of 330°C, Equation 5.2 predicts a minimum cavity size of 0.14μm. Therefore, given the temperature range of for this surface it is likely that the Leidenfrost point was a ected by both heterogeneous and homogeneous nucleation events.

5.6 Dimensionless Leidenfrost temperature and onset of nucleate boiling as a function contact angle

The results of the Leidenfrost experiments and measured onset of nucleate boiling (ONB) temperatures for the various surfaces can be consolidated to predict the relationship between wettability, characterized in this study by contact angle, and the onset of nucleate boiling and Leidenfrost temperatures. For this type of analysis, the wall superheats corresponding to either the Leidenfrost transition or ONB are normalized by the di erence between the spinodal temperature, $T_{spinodal}$ and the uid saturation temperature, T_{sat} in order to de ne a dimensionless temperature, given by,

$$= \frac{T_{wall} - T_{sat}}{T_{spinodal} - T_{sat}}. \tag{5.5}$$

The spinodal temperature, $T_{spinodal}$ was determined from the analysis by Leinhard et al. [69] and is approximately 324°C. The dimensionless temperature, can be plotted against the corresponding average contact angle for all ZnO nanostructured and bare metal surfaces in

order to t an approximate curve that could be used to predict the relationship between wettability and Leidenfrost point and ONB. The results of this analysis are shown in Figure 5.5. The approximated curve t for both the Leidenfrost transition and ONB data is a polynomial of degree 2 that is determined to be the best t in the least-squares sense. The curves for the Leidenfrost transition and ONB originate from a contact angle of 180, which corresponds to a theoretically completely non-wetting surface and are allowed to propagate according to the experimental data thereafter. The results of this analysis are depicted graphically in Figure 5.5.

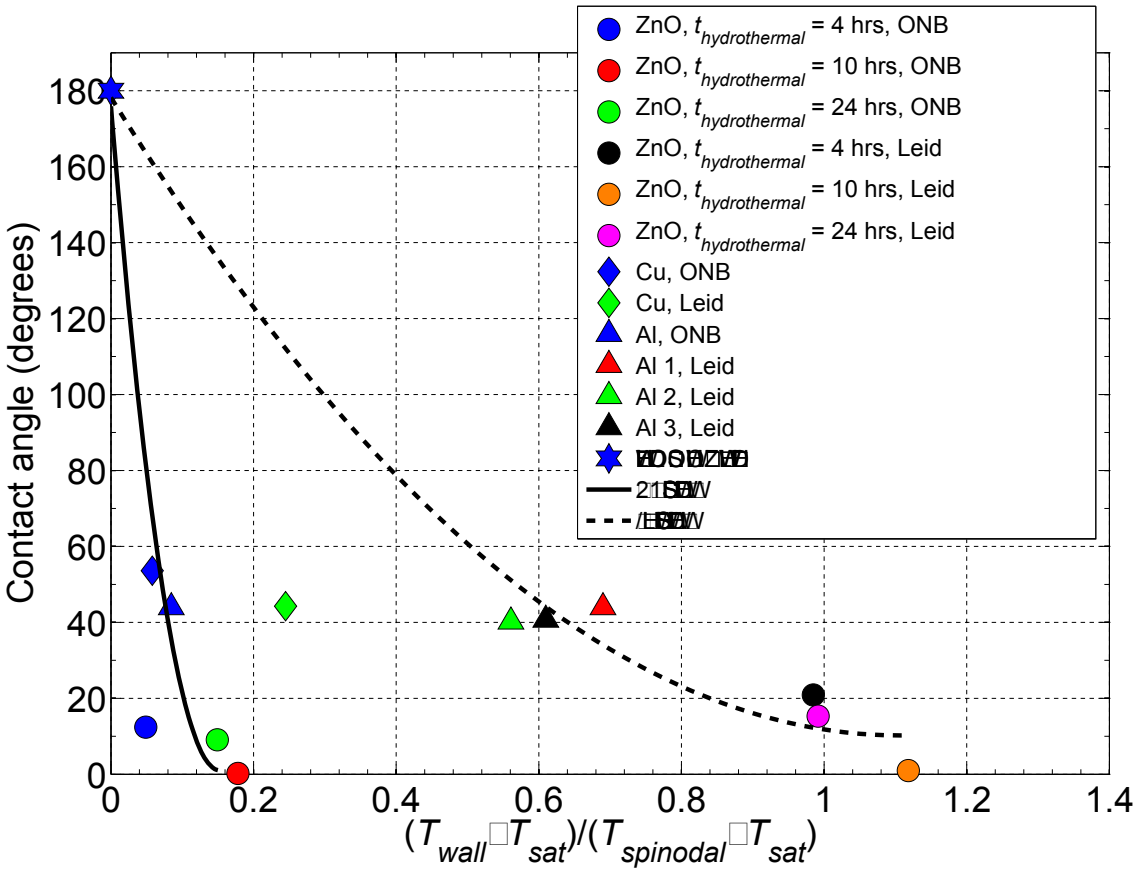

Figure 5.5: Dimensionless Leidenfrost (Leid) and onset of nucleate boiling (ONB) temperatures as a function of contact angle for every surface tested in this study.

Table 5.4: Onset of nucleate boiling for nanostructured and bare metal surfaces. The onset of nucleate boiling was detected from video recordings of the evaporation experiments.

Surface	Onset of nucleate boiling (°C)
$t_{hydrothermal}$ = 4 hrs	111
$t_{hydrothermal}$ = 10 hrs	140
$t_{hydrothermal}$ = 24 hrs	134
Copper	113
Aluminum	119

Chapter 6

Investigation summary and concluding remarks

Hydrophilic and superhydrophilic ZnO nanocrystal arrays were successfully synthesized by the hydrothermal method on a copper substrate for the purpose of determining the effect of superhydrophilicity on the Leidenfrost point and droplet vaporization at low superheat levels. This is the first known study to apply this synthesis method to generate ZnO nanostructured surfaces on copper or any metallic substrate for heat transfer applications. The results of this study may have important implications for potential heat transfer applications due to the combined use of superhydrophilic surfaces on metallic substrates.

Various nanostructured surface array geometries were produced on the copper substrate by performing the hydrothermal synthesis for 4, 10 and 24 hours.The nanostructured surfaces grown by hydrothermal synthesis for 4 and 24 hours exhibited contact angles of approximately 10°, whereas the surfaces grown for 10 hours were superhydrophilic, exhibiting contact angles less than 3°. Bare copper and aluminum surfaces exhibited average contact angles on the order of 40–50°. An effective contact angle was calculated for the nanostructured surfaces due to the difficulty associated with directly measuring contact angle on a superhydrophilic surface. The effective contact angle approach used in this study was found to provide a useful way of experimentally quantifying wettability at extremely low contact angles. This method was verified by calculating the effective contact angle of a droplet on a bare metal surface and comparing the result to that given from the ImageJ analysis of a photograph of the same droplet. In general, the two contact angle values agreed.

The geometry of the ZnO nanostructured surfaces was further characterized through SEM imaging before and after experiments. The individual nanostructures were found to be randomly-oriented and, depending on hydrothermal synthesis time, had a mean diameter of about 500-700 nm, a mean length of 1.7-3.3 μm and porosities of 0.04-0.58. The varying surface geometry of the nanostructured was responsible for the varying wettability among the nanostructured surfaces. In particular, through the adaptation of an idealized analysis from the literature, it was found that the individual nanocrystal geometry and porosity of the nanostructured surface grown for 10 hours exhibited the greatest ratio of capillary

driving forces to frictional viscous forces of all the nanostructured surfaces. Indeed, from macroscopic measurements of contact angle and droplet spread area, the nanostructured surface was extremely wetting such that it was categorized as superhydrophilic. In contrast, the nanostructured surface grown for 4 hours, exhibited a much higher porosity which was favorable for reducing viscous dissipation during liquid wetting. However, in comparison to the nanostructured surface grown for 10 hours, the high porosity also resulted in lower capillary driving forces such that the surface grown for 10 hours was much more highly wetting. The nanostructured surface grown for 24 hours, exhibited a relatively low porosity of 0.04, which is expected to be favorable for increasing capillary driving forces. However, the low porosity also resulted in relatively high viscous dissipation, such that the surface grown for 10 hours was also much more wetting in comparison. Nevertheless, the nanostructured surfaces grown for 4 and 24 hours, whose geometries were quite distinct from one another, also exhibited highly wetting qualities. It is concluded that the surface morphologies similar to those of the surface grown for 10 hours are most likely to result in superhydrophilicity.

The surface morphology of the nanostructured surfaces was shown to be conserved before and after experiments in this study through macroscopic and microscopic evaluations of the surface. However, due to their high surface energy, it was found that the nanostructured surfaces were quite susceptible to surface contamination through thin lm adsorption of foreign substances. As the presence of the unknown foreign substances tended to reduce the surface free energy, the wettability of the nanostructured surfaces was diminished as a result of contamination. Therefore a surface desorption protocol was developed in order to decontaminate the nanostructured surfaces to restore their hydrophilicity and superhydrophilicity. A nanostructured surface was subjected to a desorption cycle after the hydrothermal synthesis and immediately before an experiment. The desorption cycle consisted of heating the surface up to approximately 300°C for about 45{60 minutes. The contact angle and/or droplet spread area were measured after the substrate was allowed to cool after each desorption cycle. Remarkably, at the moment that this dissertation is being completed, many of the ZnO nanostructured surfaces are still being used in other investigations after many, many months of storage. Indeed, the ZnO nanostructured surfaces have been found to recover their highly wetting characterister immediately after one or two desorption cycles. Although a complete formal study on the durability of these types of surfaces, i.e. semiconductor nanostructures grown on a metallic substrate, has not been conducted, the results of this study and of the studies which inherited the surfaces from this study are very encouraging for their potential use in practical heat transfer applications.

In the low superheat experiments, the superhydrophilic qualities of the ZnO nanostructured surface grown for 10 hours resulted in its exhibiting the highest droplet spread area, lowest droplet evaporation time and highest heat transfer coe cients compared with nanostructured and bare metal surfaces in this study. At a superheat level of 10°C, the heat transfer coe cients on the superhydrophilic were nearly 4 times greater than those predicted from a nucleate boiling correlation at the same superheat level. In fact, at a superheat level of 10 °C, the nanostructured surfaces grown for 4 and 24 hours exhibited heat transfer coe cients that were at least 2 times greater than those predicted by a nucleate boiling correlation at

the same superheat. However, heat transfer coe cients predicted by the standard nucleate boiling correlation of Stephan and Abdelsalam, increased as a function of wall superheat squared, such that for wall superheats greater than 20°C, the heat transfer coe cient predicted by the nucleate boiling correlation exceeded those calculated for the nanostructured surfaces by a signi cant factor. In contrast, the heat transfer coe cient for the nanostructured surfaces was observed to increase relatively gradually as a function of wall superheat. This led to the conclusion that nucleate boiling was not the driving evaporation mechanism. Based on the nding of gradually increasing heat transfer coe cient, video con rmation of the absence or very limited nucleate boiling at superheat levels below 30°C and a simple analysis of heat conduction through the thin liquid lms, it is concluded that the droplets were evaporated by mechanisms typical of lm evaporation. Remarkably, despite the absence of nucleate boiling, the rapid spreading of liquid into a thin lm resulted in rapid vaporization with extremely high heat transfer coe cients at low superheat levels less than and equal to 20°C. This e ect further suggests that rapid evaporation of water droplets impinging on heated nanostructured surfaces at temperatures below saturation will also exhibit high heat transfer coe cients. Furthermore, as a result of the highly wetting capillary forces of the surface and the absence of nucleate boiling which could lead to satellite droplet ejection, the entire liquid droplet is evaporated on the ZnO nanostructured surfaces below superheat levels of 40°C. This is an extremely favorable quality for applications requiring e cient water usage such as in evaporative spray cooling.

Wall superheat and droplet size were found to have the most profound e ect on heat transfer coe cient on all nanostructured surfaces. Heat transfer coe cient was found to increase with decreasing droplet size. Heat transfer coe cient increased signi cantly as a function of wall superheat up to 20°C. For wall superheats greater than 20°C, the heat transfer coe cient increased relatively gradually. In comparison to varying droplet size and wall superheat, varying droplet release height generally resulted in minimal e ects on heat transfer coe cient. Therefore, it is concluded that the capillary wetting forces of the nanostructured arrays drive the wetting process compared with the inertial forces associated with the droplet impact on the surface.

The Leidenfrost point temperatures for the hydrophilic and superhydrophilic ZnO nanostructured surfaces considered in this study were 100-250°C higher than surfaces of modest wettability in this and other studies. Leidenfrost points for the ZnO nanostructured surfaces varied between approximately 310{376°C. The ZnO surfaces with lower contact angles generally exhibited higher Leidenfrost transition temperatures. For the surfaces tested, it was determined that Leidenfrost point was weakly dependent on droplet volume when compared to its dependence on surface wettability. The data for the ZnO surfaces and the other surfaces considered in this study indicate that the Leidenfrost point increases with increasing surface wettability as quanti ed by contact angle. This observation is consistent with the ndings of other studies. The maximum Leidenfrost temperature measured in this study was 376°C, corresponding to the superhydrophilic ZnO nanostructured surface grown for a 10 hours, which exhibited a contact angle of approximately 0°.9

The Leidenfrost transition was determined from the acoustic signal generated during the

initial droplet deposition and subsequent vaporization process. This Leidenfrost point determination method is in contrast to that used in other studies, which measured droplet evaporation time. Despite the use of a different metric, however, the results from the ZnO nanostructured surfaces of this study were well within the range of results from recent similar efforts investigating the effect of superhydrophilic surfaces on the Leidenfrost transition. Moreover, even with the different metric, the bare metal control surfaces in this study exhibited classical behavior consistent with the Leidenfrost temperatures in the literature for similar surfaces. The results of this and other studies indicate that the Leidenfrost transition temperature for nanostructured surfaces can be more than 100°C higher than surfaces of modest wettability.

Since almost all of the ZnO nanostructured surfaces exhibited a Leidenfrost point in excess of the spinodal temperature range of water at atmospheric pressure, 309–324°C, this finding was explored to a greater depth. By adapting various analyses from the literature to the findings of this study, it was found that as the droplet evaporated by film boiling, that the thickness of the vapor film suspending the droplet decreased as a function of the droplet radius, r_{drop} as $r_{drop}^{4/3}$. When the surface temperature was cooler than the Leidenfrost temperature it was then possible for the vapor film to deplete to the level that would allow contact with the surface nanostructures. The porosity of the nanostructure array was such that when the liquid droplet contacted the surface, the voids between nanostructures would act like active nucleation sites since the surface was at a temperature well in excess of that required for heterogeneous nucleation of vapor bubbles from a surface cavity with that geometry. At wall temperatures in the vicinity of the Leidenfrost transition, it was found that the nucleation events that would occur as a result of the liquid-solid contact would generate vapor bubbles whose growth would easily disrupt the vapor film and liquid droplet interphase.

Finally, the results of the Leidenfrost experiments and measured onset of nucleate boiling (ONB) temperature for all the surfaces were consolidated along with the corresponding average contact angles, to generate approximate polynomial curves that could help predict the relationship between wettability and the Leidenfrost transition and ONB.

Appendix A

Hydrothermal method for ZnO nanocrystal synthesis on smooth copper substrate

The copper surface preparation and hydrothermal method procedures are outlined in the following sections.

A.1 Surface cleaning by ultrasonic bath

1. Place copper test piece inside beaker then ll beaker with acetone until the part is completely submerged.
2. Loosely cover the beaker.
3. Place beaker inside an ultrasonic bath of distilled water
4. Activate sonicator. Permit ultrasonic bath for 15 minutes.
5. Gently remove the beaker from the ultrasonic bath.
6. Remove the copper test piece from the beaker with clean tongs and blow dry with air at room temperature.
7. Discard used acetone and rinse beaker with acetone then rinse with isopropyl alcohol.
8. Place copper test piece inside beaker then ll beaker with isopropyl alcohol until the part is completely submerged.
9. Loosely cover the beaker.
10. Place beaker inside an ultrasonic bath of distilled water

11. Activate sonicator. Permit ultrasonic bath for 15 minutes.
12. Gently remove the beaker from the ultrasonic bath.
13. Remove the copper test piece from the beaker with clean tongs and blow dry with air at room temperature.
14. Discard used isopropyl alcohol and rinse beaker with isopropyl alcohol then rinse with distilled water.
15. Place copper test piece inside beaker then ll beaker with distilled water until the part is completely submerged.
16. Loosely cover the beaker.
17. Place beaker inside an ultrasonic bath of distilled water
18. Activate sonicator. Permit ultrasonic bath for 15 minutes.
19. Gently remove the beaker from the ultrasonic bath.
20. Remove the copper test piece from the beaker with clean tongs and blow dry with air at room temperature.
21. Discard used distilled water.

A.2 Preparation of ZnO quantum dot solution

For this method, the copper substrate was seeded by drop casting with ZnO quantum dots purchased from Meliorum Technologies, approximately 6 nm, in a 30 mL ethanol solution at a concentration of approximately 0.409 M [35]. As sold, the ZnO quantum dot solution concentration is too high for the purposes of this experiment. High concentrations of seeding solution lead to non-uniform growth of ZnO nanowires [36], therefore the 0.409 M solution had to be diluted. The dilution procedure is outlined in the remainder of this section.

1. Place the container of 0.409 M solution in a beaker of distilled water, then place that beaker inside an ultrasonic bath of distilled water for 15 minutes in order to ensure that the ZnO nanoparticles are well-mixed in the ethanol solution.
2. Use a micropipette to extract 100 μL of quantum dot solution from the container of the 0.409 M solution.
3. Dilute the 100 μL of quantum dot solution to 0.0409 M by expelling the extracted 100 μL of quantum dot solution into a separate container already containing 1 mL of ethanol.

4. Loosely cover the newly diluted solution and place it inside an ultrasonic bath of distilled water for about 10 minutes to ensure adequate mixing of the nanoparticles in the diluted solution.

A.3 Drop casting ZnO nanoparticle solution on copper substrate

The diluted ZnO quantum dot solution was drop casted on the copper surface at room temperature similar to the method described in [35]{[39]. The speci c drop casting method used in this study is described in the remainder of this section.

1. Deposit 5 drops of diluted solution, each of 10 μL onto the smooth top surface of the copper test piece, i.e. the surface designated for the hydrothermal synthesis.

2. Using a pair of clean latex or nitrile glvoes, slowly and carefully rotate the copper test piece by hand, without touching the top surface, until the entire surface is coated uniformly with solution and the ethanol has completely evaporated.

3. Repeat four (4) more times so that a total of 25 drops were deposited on the surface.

4. Place the drop casted piece in an oven at 120 $^{\circ}$C for 20{25 minutes to anneal the ZnO nanoparticles to the copper surface. Place the substrate in the oven such that the seeded surface is facing upward, without physically contacting any solid surface.

A.4 Hydrothermal synthesis

ZnO nanostructures were synthesized on the copper substrate in aqueous solution by the hydrothermal method [33], [40]{[51]. The speci c method used in this study is described in the remainder of this section.

1. Prepare aqueous solution with 25 mM zinc nitrate hexahydrate [$Zn(NO_3)_2 \cdot 6\,H_2O$]and 25 mM hexamethylenetetramine [$C_6H_{12}N_4$] [34]{[39] at room temperature.

2. Mix the solution continuously with a cylindrical magnetic stir bar 1 inch long and 1/4 inch diameter at approximately 600 rpm for approximately 2 hours in a beaker. A crystallizing dish could also be used in place of a beaker.

3. Immerse the seeded substrate completely in the aqueous solution with the seeded surface facing downward. The seeded surface should be about 2 cm above the bottom surface of the beaker containing the aqueous solution.

4. Place the the beaker with immersed substrate was placed in a standard laboratory gravity convection oven at 90{95°C for desired amount of time. The surface density of nucleated nanostructures, diameter and height increase with time of hydrothermal synthesis, although not inde nitely.*

5. Remove the test piece from the solution and rinsed gently but thoroughly with distilled water at room temperature.

6. Dry the rinsed test piece in the oven for approximately 30 minutes in air at a temperature of approximately 70°C.

*For surfaces grown for longer than 12 hours, the substrates must be removed from the solution after about 12 hours, rinsed and dried and immersed into a fresh aqueous solution of the 25 mM zinc nitrate hexahydrate and 25 mM hexamethylenetetramine for the remaining length of synthesis time [35].

Appendix B

ZnO nanocrystal structure

B.1 ZnO nanocrystal structure

A Siemens D5000 X-ray di ractometer located in the Marvell Nanofabrication Laboratory at UC Berkeley was used to characterize the material properties of the ZnO nanostructures on the copper substrates. The di ractometer uses copper K-alpha (Cu$_{\alpha}$) radiation with a weighted average wavelength of 0.154184 nm (Cu$_{\alpha}$1 = 0.154056, Cu K$_{\alpha}$2 0.154439 nm). The x-ray power supply has an idling condition of 20 kV and 5 mA. Normal operating conditions during measurements are 40 kV and 30 mA. The X-ray di raction (XRD) pattern for the ZnO nanostructures grown for 10 hours by hydrothermal synthesis on a copper substrate is shown in Figure B.1. The x-ray di raction was performed after the test sample had been heated once to approximately 300°C for 60 minutes in order to evaporate any contaminants that may had adsorbed on the surface. The test sample had not yet been subjected to any distilled water droplet experiments.

The di raction peaks in Figure B.1 for the ZnO nanostructures located at approximately 32°, 34.5°, 36.5°, 47.5°, 56.5° and 63° correspond to the planes of hexagonal wurtzite ZnO, which is consistent with ndings in the literature [34]{[38], [52], [53]. The di raction peaks in Figure B.1 located at approximately 43.5, 50.6° and 74.3° correspond to the copper substrate [54]{[61].

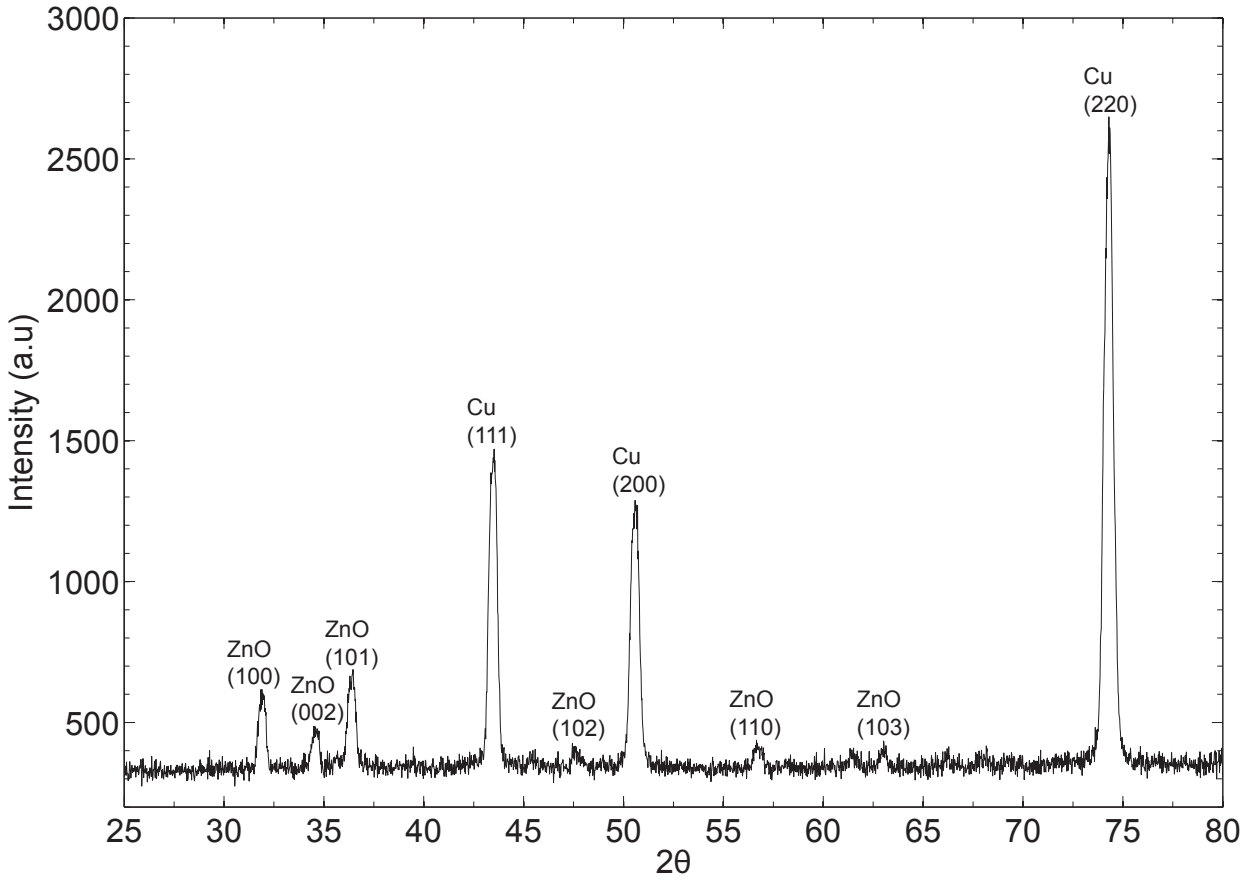

Figure B.1: XRD pattern for ZnO nanostructures grown by hydrothermal synthesis for 10 hours on a copper (Cu) substrate. The di raction peaks for the ZnO and Cu are indicated with the corresponding Miller indices in the graph individually. The angle between the projection of the X-ray source and the detector is given by$\theta 2$

.

Appendix C

Surface characteristics and experimental results: ZnO nanostructured surface grown for 4 hours

Micrographs of the ZnO nanostructured surfaces were captured before and after experiments with a LEO 1550, Schottky field emission scanning electron microscope (SEM) located in the Marvell Nanofabrication Laboratory at UC Berkeley.

C.1 SEM images and surface geometry

Micrographs for the ZnO nanostructured surfaces grown by hydrothermal synthesis for 4 hours are found in Figure C.1.

From the micrographs in Figure C.1 it was possible to measure the average nanocrystal side length, measured from substrate to tip of the nanocrystal, L_{side} and the average crystal hexagon side length, L_{hex} in order to calculate the average nanocrystal surface area, A_{ZnO} which was available to interact with the liquid droplets. For calculation purposes, the top face of an individual ZnO nanocrystal is assumed to form a regular hexagon, such that the length of all six sides are equivalent to L_{hex}. The area, A_{hex} of the top face of the ZnO nanocrystal is given by,

$$A_{hex} = \frac{3\sqrt{3}}{2} L_{hex}^2. \tag{C.1}$$

Therefore, surface area of one individual ZnO nanocrystal is given by

$$A_{ZnO} = A_{hex} + 6\, L_{hex} L_{side}. \tag{C.2}$$

Furthermore it was possible to measure the surface area of the substrate that was not covered by ZnO nanocrystals, $A_{un-nucleated}$, i.e. the base area of the substrate, $A_{substrate}$, over which

Table C.1: Average geometrical parameters with standard deviation of ZnO nanostructured surfaces grown for a hydrothermal synthesis time, t, of 4 hours. L_{hex} is the hexagon side length, L_{side} is the length of the nanocrystal measured from the substrate to the tip of the nanocrystal, A_{ZnO} is total wetted surface area of one ZnO nanocrystal and ω is wetted surface area ratio.

t (hr)	L_{hex} (μm)	L_{side} (μm)	A_{ZnO} (μm^2)	ε	ω
4	0.28 $\pm$ 0.06	1.70 $\pm$ 0.34	3.08 $\pm$ 0.98	0.58 $\pm$ 0.08	15.6

no clearly distinct ZnO nanocrystals nucleated. From these measurements it was possible to determine the porosity, ε given by

$$\varepsilon = 1 - \frac{A_{substrate} - A_{un-nucleated}}{A_{substrate}} = 1 - \frac{A_{nucleated}}{A_{substrate}} \tag{C.3}$$

where $A_{nucleated}$ is the area of the base substrate that is covered by ZnO nanocrystals. It was not possible to determine whether the un-nucleated area was bare copper or simply ZnO nanoparticles that were annealed onto the copper substrate but did not serve as a nanocrystal nucleation site. In any case, from the calculated ZnO nanocrystal surface area, A_{ZnO} and measured un-nucleated substrate surface area, $A_{un-nucleated}$, it was possible to determine the total average surface area that could potentially interact with liquid, i.e. the total average wetted surface area, $A_{wetted,total}$ given by,

$$A_{wetted,total} = \eta A_{ZnO} + A_{un-nucleated} \tag{C.4}$$

where η is the total estimated number of nanocrystals within a given substrate area, $A_{substrate}$, which is given by,

$$\eta = \frac{A_{substrate}}{A_{hex}}. \tag{C.5}$$

Therefore, per unit of substrate area, the wetted surface area ratio, ω is given by,

$$\omega = \frac{A_{wetted,total}}{A_{substrate}} = \frac{\eta A_{ZnO} + A_{un-nucleated}}{A_{substrate}}. \tag{C.6}$$

which can be simplified further to,

$$\omega = 1 + \frac{4h}{\sqrt{3}L_{hex}} + \varepsilon. \tag{C.7}$$

The geometrical measurements are listed in Table C.1.

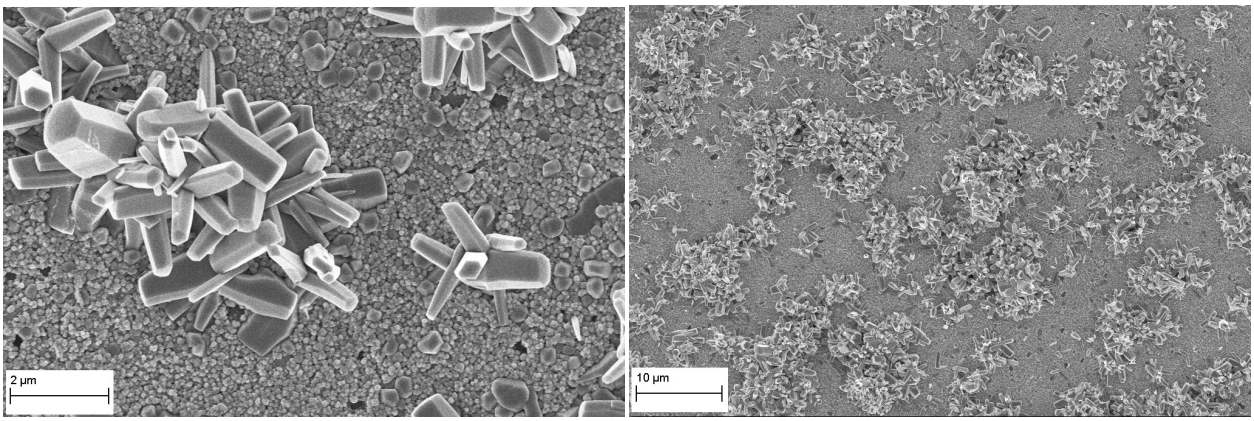

Figure C.1: SEM images of ZnO nanostructures synthesized on the smooth copper surface for 4 hours after second desorption, but before experiments. The image on the right shows the general array of the ZnO nanocrystals on the substrate. The left image is shows the hexagonal wurtzite structure of the ZnO nanocrystals.

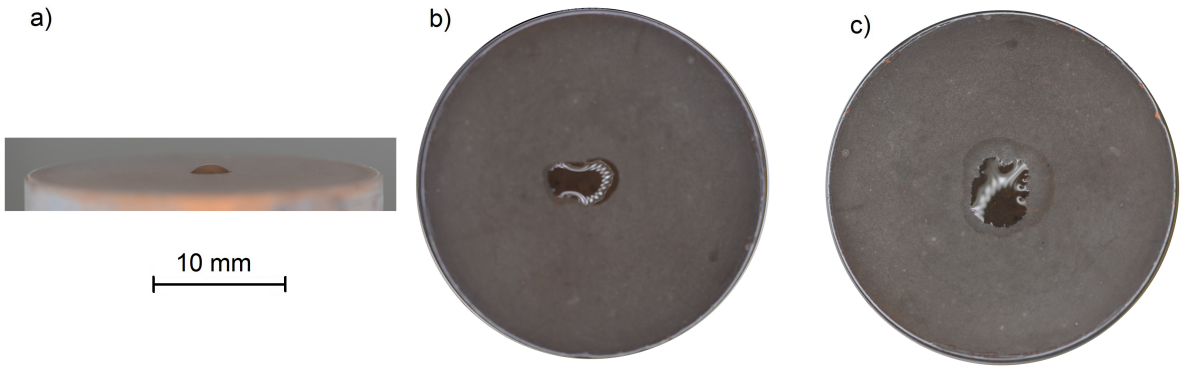

Figure C.2: Series of photographs which span one full test cycle for a nanostructured surface grown by hydrothermal synthesis for 4 hours. a)Droplet pro le after hydrothermal synthesis and rst desorption. b)Wetting after second desorption, before experiments. c)Wetting after one evaporation experiment.

C.2 Contact angle measurements and calculations for ZnO nanostructured surface grown for 4 hours

Due to the superhydrophilicity of some of the ZnO nanostructured surfaces, determining the contact angle on the ZnO nanostructured surfaces was not possible from the droplet pro le. Therefore, for all of the ZnO nanostructured surface a single 2µL distilled water droplet was gently deposited and the subsequent spreading was captured by the camera

Table C.2: Contact angles measured on ZnO nanostructured surfaces grown by hydrothermal synthesis for 4 hours for Leidenfrost experiments. θ_{inner} is the contact angle of the inner droplet, where applicable, A_{inner} is the solid-liquid contact area corresponding to the inner droplet, θ_{outer} is the calculated effective contact angle of the liquid film surrounding the inner droplet, where applicable, A_{outer} is the spread area of the film surrounding the liquid droplet. N.A. indicates that the property was not exhibited by the surface. The final column on the right indicates the moment after which the contact angle measurements were taken throughout the desorption and experiment cycles for the surface.

t (hrs)	θ_{inner}	A_{inner} (μm^2)	θ_{outer}	A_{outer} (μm^2)	Measured after...
4	44.2° $\pm$ 19.5°	8.5 $\pm$ 4.7	N.A.	N.A.	1st desorp.
4	29.9° $\pm$ 13.9°	12.3 $\pm$ 3.2	N.A.	N.A.	2nd desorp.
4	12.0° $\pm$ 3.6°	17.0 $\pm$ 3.5	N.A.	N.A.	experiment.

Table C.3: Contact angles measured on ZnO nanostructured surfaces grown by hydrothermal synthesis for 4 hours for low superheat experiments. θ_{inner} is the contact angle of the inner droplet, where applicable, A_{inner} is the solid-liquid contact area corresponding to the inner droplet, θ_{outer} is the calculated effective contact angle of the liquid film surrounding the inner droplet, where applicable, A_{outer} is the spread area of the film surrounding the liquid droplet. N.A. indicates that the property was not exhibited by the surface. The final column on the right indicates the moment after which the contact angle measurements were taken throughout the desorption and experiment cycles for the surface.

t (hrs)	θ_{inner}	A_{inner} (μm^2)	θ_{outer}	A_{outer} (μm^2)	Measured after...
4	34.4° $\pm$ 9.9°	9.0 $\pm$ 2.1	14.2° $\pm$ 0.5°	14.8 $\pm$ 1.5	1st desorp.
4	14.5° $\pm$ 0.2°	14.5 $\pm$ 1.5	12.2° $\pm$ 0.2°	16.3 $\pm$ 1.5	2nd desorp.
4	10.3° $\pm$ 1.0°	18.4 $\pm$ 1.2	3.3° $\pm$ 0.0°	39.1 $\pm$ 0.2	experiment

directly above and parallel to the test surface at 240 fps.

Complete results of measured and/or calculated contact angles for the surfaces grown for 4 hours used in the Leidenfrost experiments are found in Table C.2. Note that since there was a negligible difference between contact angles immediately before and after the experiments, it was determined that the nanostructured surface geometry was unaffected by the experiments and thus SEM images after the experiments were not taken for this surface.

Complete results of measured and/or calculated contact angles for the surfaces grown for 4 hours used in the low superheat experiments are found in Table C.3. Note that since there was a negligible difference between contact angles immediately before and after the experiments, it was determined that the nanostructured surface geometry was unaffected by the experiments and thus SEM images after the experiments were not taken for this surface.

C.3 Results of maximum droplet spread area measurements and lm thickness calculations for nanostructured surface grown for 4 hours

Results for experiments performed on the ZnO nanostructured surface grown by hydrothermal synthesis for 4 hours are depicted graphically in Figure C.3.

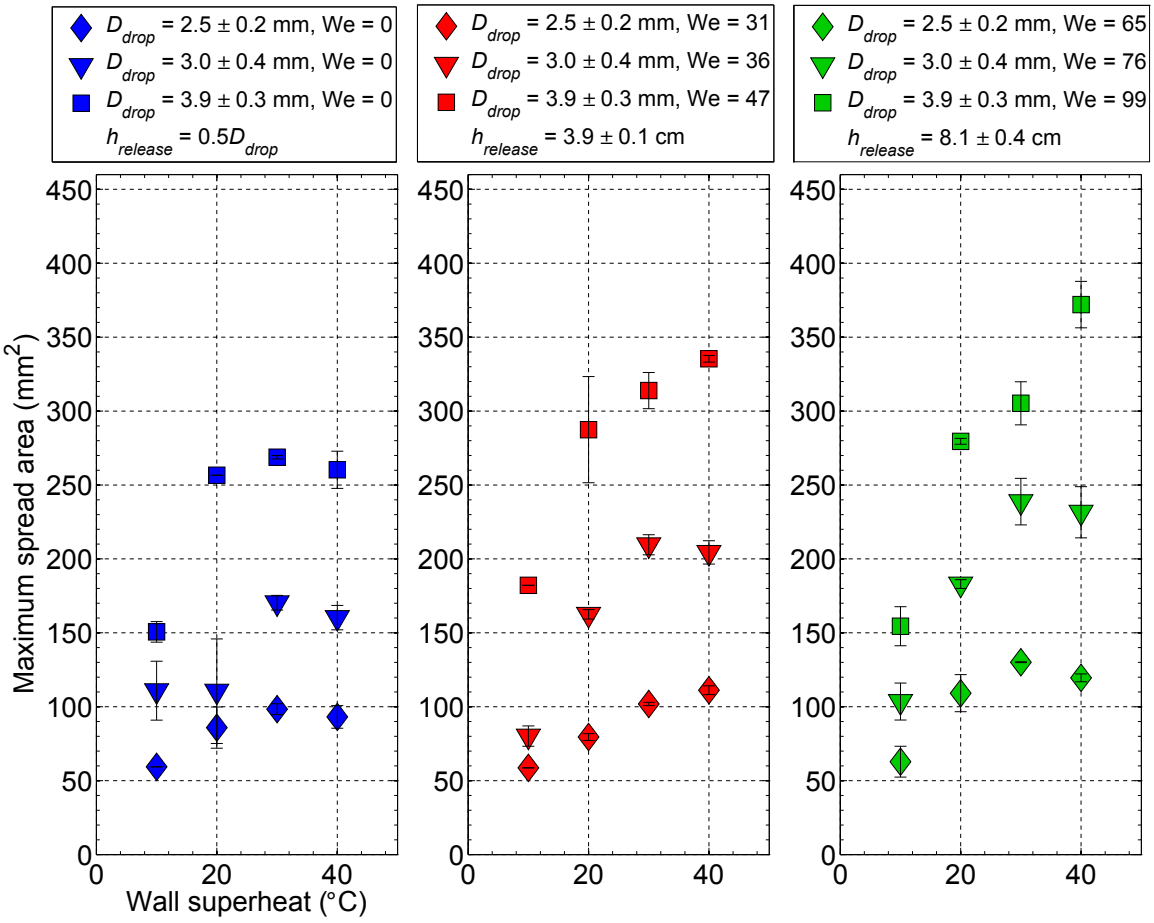

Figure C.3: Droplet spread area as a function of wall superheat, droplet size and release height for ZnO nanostructured surface generated by hydrothermal synthesis for 4 hours.

Results of droplet spread area measurements, with standard deviation, on the surface grown by hydrothermal synthesis for 4 hours as a function of droplet diameter, release height and wall superheat are listed in Table C.4. Results of estimated liquid lm thickness as a function of droplet diameter, release height and wall superheat are listed in Table C.5.

Table C.4: Results of maximum droplet spread area measurements, with standard deviation, on surface grown for 4 hours$D$ is the droplet diameter, A is the maximum droplet spread area, H is the droplet release height and T is the wall superheat.

		T = 10 °C	T = 20 °C	T = 30 °C	T = 40 °C
D (mm)	H (cm)	A (mm^2)	A (mm^2)	A (mm^2)	A (mm^2)
2.5	0.12	59.3$\pm$ 0.0	85.9$\pm$ 14.0	98.4$\pm$ 3.7	93.1$\pm$ 7.7
2.5	3.9	58.7$\pm$ 0.0	79.5$\pm$ 2.3	101.9$\pm$ 1.1	111.2$\pm$ 3.0
2.5	8.1	62.8$\pm$ 10.4	109.2$\pm$ 12.6	130.1$\pm$ 0.3	119.5$\pm$ 2.7
3.0	0.15	110.9$\pm$ 19.9	110.5$\pm$ 35.4	170.4$\pm$ 4.9	160.3$\pm$ 8.2
3.0	3.9	80.1$\pm$ 6.9	162.5$\pm$ 3.2	209.6$\pm$ 6.8	204.4$\pm$ 7.9
3.0	8.1	103.5$\pm$ 12.5	183.0$\pm$ 3.0	238.7$\pm$ 15.7	231.6$\pm$ 17.3
3.9	0.20	150.7$\pm$ 7.0	256.6$\pm$ 0.0	268.8$\pm$ 1.2	260.3$\pm$ 12.6
3.9	3.9	182.1$\pm$ 0.0	287.4$\pm$ 35.9	313.9$\pm$ 12.2	335.4$\pm$ 2.3
3.9	8.1	154.4$\pm$ 13.2	279.5$\pm$ 2.0	305.3$\pm$ 14.6	372.1$\pm$ 15.7

Table C.5: Estimated liquid lm thickness based on initial droplet volume and the measured maximum droplet spread area on surface grown for 4 hours$D$ is the droplet diameter, L_{film} is the lm thickness, H is the droplet release height and T is the wall superheat.

		T = 10 °C	T = 20 °C	T = 30 °C	T = 40 °C
D (mm)	H (cm)	L_{film} (μm)	L_{film} (μm)	L_{film} (μm)	L_{film} (μm)
2.5	0.12	110.2	136.0	92.0	91.1
2.5	3.9	144.1	74.6	81.9	53.7
2.5	8.1	172.2	101.8	100.3	65.6
3.0	0.15	141.3	158.9	146.7	112.3
3.0	3.9	151.5	156.7	142.0	98.2
3.0	8.1	163.9	156.0	130.3	97.6
3.9	0.20	127.1	93.7	103.8	128.6
3.9	3.9	151.2	109.8	82.7	92.3
3.9	8.1	170.4	95.1	83.7	80.9

C.4 Results of droplet evaporation time for nanostructured surface grown for 4 hours

Results for experiments performed on the ZnO nanostructured surface grown by hydrothermal synthesis for 4 hours to determine the e ect of wall superheat, droplet size, release height on evaporation time are depicted graphically in C.4.

Results of droplet evaporation time measurements, with standard deviation, on the sur-

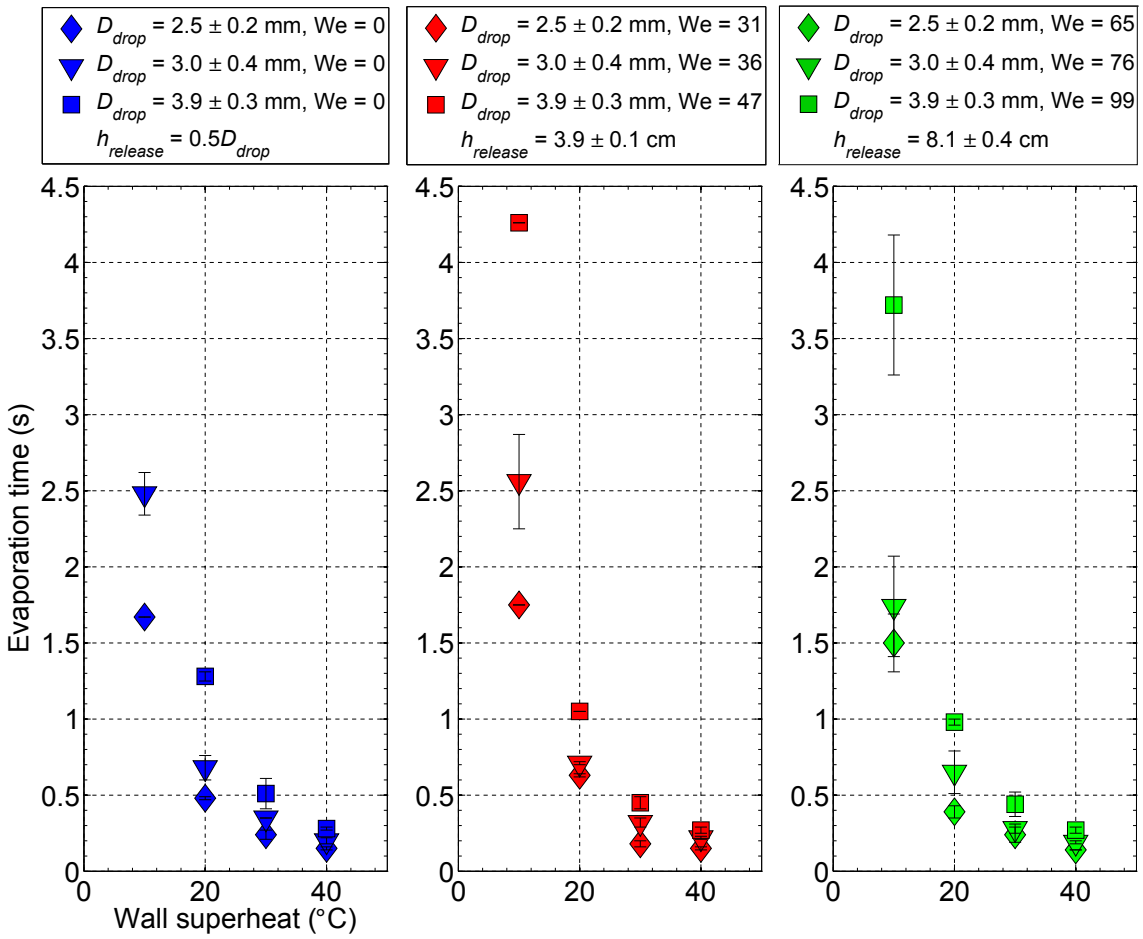

Figure C.4: Droplet evaporation time as a function of wall superheat, droplet size and release height for the ZnO nanostructured grown by hydrothermal synthesis for 4 hours.

face grown by hydrothermal synthesis for 4 hours as a function of droplet diameter, release height and wall superheat are listed in Table C.6.

C.5 Results of calculated heat transfer coe cients for nanostructured surface grown for 4 hours

Heat transfer coe cients calculated from results of experiments performed on the ZnO nanostructured surface grown by hydrothermal synthesis for 4 hours are depicted graphically in Figure C.5. The calculated heat transfer coe cients are compared to those predicted by the nucleate boiling correlation of Stephan and Abdelsalam [67].

Results of calculations of heat transfer coe cient on surface grown for 4 hours as a

Table C.6: Results of droplet evaporation time measurements, with standard deviation, on the surface grown for 4 hours$D$ is the droplet diameter,t is the droplet evaporation time, H is the droplet release height and T is the wall superheat.

		T = 10 °C	T = 20 °C	T = 30 °C	T = 40 °C
D (mm)	H (cm)	t (s)	t (s)	t (s)	t (s)
2.5	0.12	1.67±0.00	0.48± 0.01	0.24±0.03	0.15±0.01
2.5	3.9	1.75±0.00	0.63±0.01	0.18±0.02	0.15±0.01
2.5	8.1	1.50±0.19	0.39±0.04	0.24±0.05	0.14±0.00
3.0	0.15	2.48 ± 0.14	0.68 ± 0.08	0.35 ± 0.00	0.20 ± 0.02
3.0	3.9	2.56 ± 0.31	0.71 ± 0.01	0.32 ± 0.03	0.22 ± 0.01
3.0	8.1	1.74±0.33	0.65±0.14	0.28±0.03	0.19±0.01
3.9	0.20	5.15 ± 0.24	1.28 ± 0.03	0.51 ± 0.10	0.28 ± 0.01
3.9	3.9	4.26 ± 0.00	1.05 ± 0.00	0.45 ± 0.04	0.27 ± 0.02
3.9	8.1	3.72±0.46	0.98±0.02	0.44±0.08	0.27±0.02

function of droplet diameter, release height and wall superheat are listed in Table C.7.

Table C.7: Results of calculations of heat transfer coe cient on surface grown for 4 hours. D is the droplet diameter,h_{evap} is the heat transfer coe cient and T is the wall superheat.

		T = 10 °C	T = 20 °C	T = 30 °C	T = 40 °C
D (mm)	H (cm)	h_{evap} (kW/m ^{2}{°C)	h_{evap} (kW/m ^{2}{°C)	h_{evap} (kW/m ^{2}{°C)	h_{evap} (kW/m ^{2}{°C)
2.5	0.12	13.0 ± 1.7	15.8 ± 2.4	17.7 ± 3.4	28.9 ± 4.4
2.5	3.9	16.2 ± 2.2	14.3 ± 0.6	27.9 ± 2.5	27.5 ± 2.7
2.5	8.1	20.1 ± 0.5	25.5 ± 3.0	20.5 ± 7.4	32.3 ± 3.4
3.0	0.15	11.2 ± 1.2	17.7 ± 5.3	16.8 ± 0.2	25.2 ± 0.1
3.0	3.9	15.1 ± 2.2	12.8 ± 0.0	17.9 ± 1.9	20.5 ± 1.7
3.0	8.1	15.7 ± 0.5	16.1 ± 1.7	18.6 ± 3.9	19.7 ± 2.0
3.9	0.20	6.7 ± 1.7	7.2 ± 2.4	14.1 ± 3.4	24.6 ± 4.4
3.9	3.9	8.5 ± 2.2	10.3 ± 0.6	13.3 ± 2.5	18.1 ± 2.7
3.9	8.1	10.1 ± 0.5	9.6 ± 3.0	13.4 ± 7.4	16.4 ± 3.4

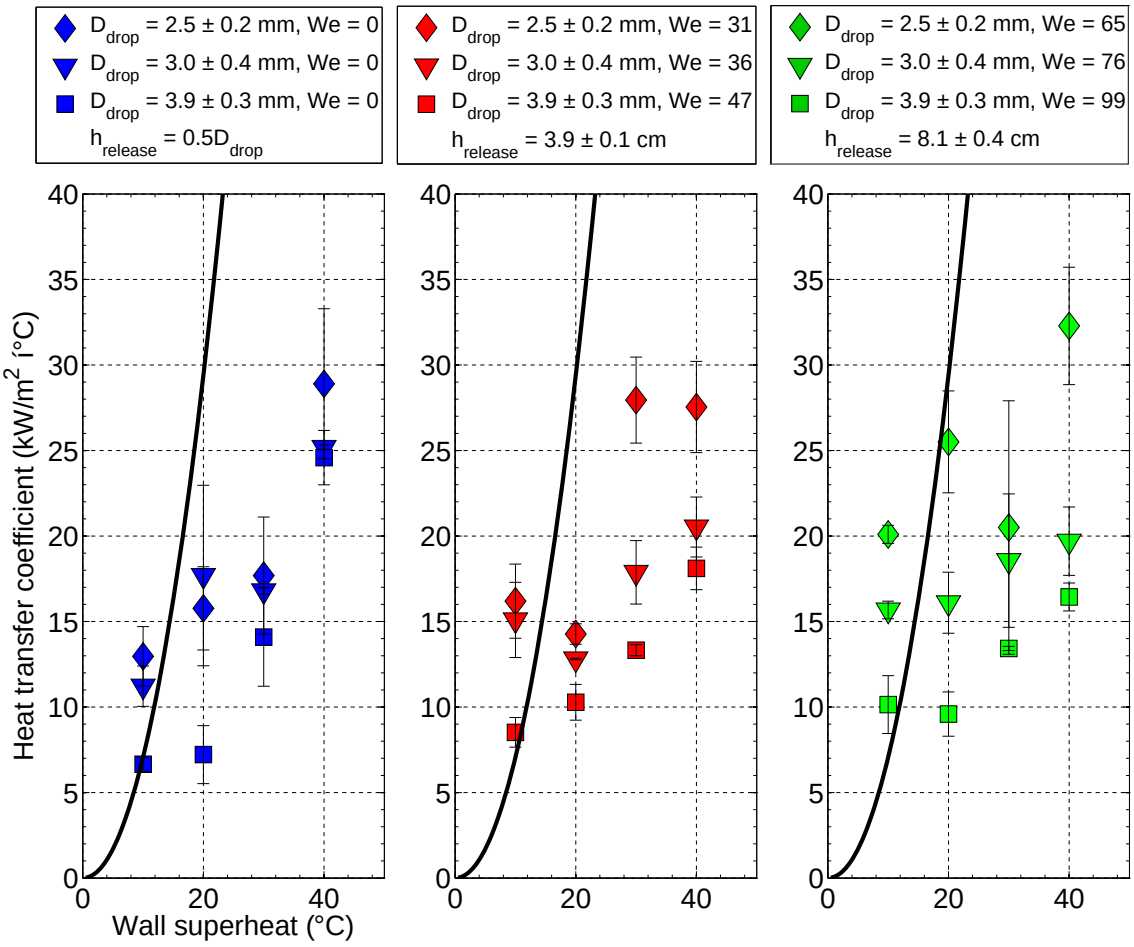

Figure C.5: Heat transfer coe cient as a function of wall superheat, droplet size and release height for ZnO nanostructured surface generated by hydrothermal synthesis for 4 hours.

C.6 Results of Leidenfrost experiments for nanostructured surface grown for 4 hours

Leidenfrost transition data for the nanostructured surface grown for 4 hours are listed in Table C.8. The data represent Leidenfrost points spanning the entirety of the experimental lifetime of each surface. The Leidenfrost temperatures, T_{Leid}, listed in Table C.8 represent a mean of values obtained in di erent tests for this surface. The uncertainty values listed for each T_{Leid} in Table C.8 indicate the spread of T_{Leid} obtained for this surface. The average contact angle, θ_{avg}, that is listed for this surface is the average of the contact angle measured or calculated after the second desorption and after the experiment.

Table C.8: Leidenfrost temperatures,T_{Leid}, as a function of droplet diameter,D_{drop} for nanostructured surface grown for at$t_{hydrothermal}$ of 4 hours. The average contact angle is given byθ_{avg}.

Surface	θ_{avg}	D_{drop} (mm)	Cycle	T_{Leid} (°C)
$t_{hydrothermal}$ = 4 hrs	21°	2.0 ± 0.1	heating	310.5± 2.3
$t_{hydrothermal}$ = 4 hrs	21°	2.2 ± 0.1	cooling	315.5± 2.4
$t_{hydrothermal}$ = 4 hrs	21°	3.1 ± 0.0	heating	321.0± 2.4
$t_{hydrothermal}$ = 4 hrs	21°	3.0 ± 0.1	cooling	319.0± 2.4
$t_{hydrothermal}$ = 4 hrs	21°	3.6 ± 0.5	heating	334.0± 2.5
$t_{hydrothermal}$ = 4 hrs	21°	3.8 ± 0.2	cooling	327.3± 2.5

Appendix D

Surface characteristics and experimental results: ZnO nanostructured surface grown for 10 hours

Micrographs of the ZnO nanostructured surfaces were captured before and after experiments with a LEO 1550, Schottky field emission scanning electron microscope (SEM) located in the Marvell Nanofabrication Laboratory at UC Berkeley.

D.1 SEM images and surface geometry

Micrographs for the ZnO nanostructured surfaces grown by hydrothermal synthesis for 10 hours are found in Figure C.1.

From the micrographs in Figure D.1 it was possible to measure the average nanocrystal side length, measured from substrate to tip of the nanocrystal, L_{side} and the average crystal hexagon side length, L_{hex} in order to calculate the average nanocrystal surface area, A_{ZnO} which was available to interact with the liquid droplets. For calculation purposes, the top face of an individual ZnO nanocrystal is assumed to form a regular hexagon, such that the length of all six sides are equivalent to L_{hex}. The area, A_{hex} of the top face of the ZnO nanocrystal is given by,

$$A_{hex} = \frac{3\sqrt{3}}{2} L_{hex}^2. \tag{D.1}$$

Therefore, surface area of one individual ZnO nanocrystal is given by

$$A_{ZnO} = A_{hex} + 6\, L_{hex} L_{side}. \tag{D.2}$$

Furthermore it was possible to measure the surface area of the substrate that was not covered by ZnO nanocrystals, $A_{un-nucleated}$, i.e. the base area of the substrate, $A_{substrate}$, over which

Table D.1: Average geometrical parameters with standard deviation of ZnO nanostructured surfaces grown for a hydrothermal synthesis time, t, of 10 hours. L_{hex} is the hexagon side length, L_{side} is the length of the nanocrystal measured from the substrate to the tip of the nanocrystal, A_{ZnO} is total wetted surface area of one ZnO nanocrystal and ω is wetted surface area ratio.

t (hr)	L_{hex} (μm)	L_{side} (μm)	A_{ZnO} (μm^2)	ε	ω
10	0.34 $\pm$ 0.10	2.66 $\pm$ 0.65	5.73 $\pm$ 2.30	0.16 $\pm$ 0.03	19.3

no clearly distinct ZnO nanocrystals nucleated. From these measurements it was possible to determine the porosity, ε given by

$$\varepsilon = 1 - \frac{A_{substrate} - A_{un-nucleated}}{A_{substrate}} = 1 - \frac{A_{nucleated}}{A_{substrate}} \tag{D.3}$$

where $A_{nucleated}$ is the area of the base substrate that is covered by ZnO nanocrystals. It was not possible to determine whether the un-nucleated area was bare copper or simply ZnO nanoparticles that were annealed onto the copper substrate but did not serve as a nanocrystal nucleation site. In any case, from the calculated ZnO nanocrystal surface area, A_{ZnO} and measured un-nucleated substrate surface area, $A_{un-nucleated}$, it was possible to determine the total average surface area that could potentially interact with liquid, i.e. the total average wetted surface area, $A_{wetted,total}$ given by,

$$A_{wetted,total} = \eta A_{ZnO} + A_{un-nucleated} \tag{D.4}$$

where η is the total estimated number of nanocrystals within a given substrate area, $A_{substrate}$, which is given by,

$$\eta = \frac{A_{substrate}}{A_{hex}}. \tag{D.5}$$

Therefore, per unit of substrate area, the wetted surface area ratio, ω is given by,

$$\omega = \frac{A_{wetted,total}}{A_{substrate}} = \frac{\eta A_{ZnO} + A_{un-nucleated}}{A_{substrate}}. \tag{D.6}$$

which can be simplified further to,

$$\omega = 1 + \frac{4h}{\sqrt{3}L_{hex}} + \varepsilon. \tag{D.7}$$

The geometrical measurements are listed in Table D.1.

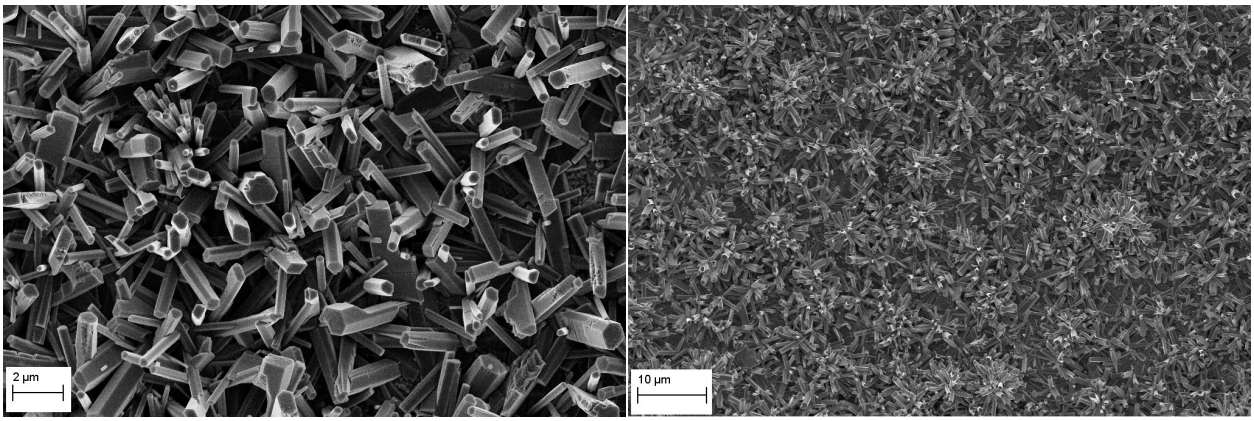

Figure D.1: SEM images of ZnO nanostructures synthesized on the smooth copper surface for 10 after second desorption, but before experiments. The image on the right shows the general array of the ZnO nanocrystals on the substrate. The left image is shows the hexagonal wurtzite structure of the ZnO nanocrystals.

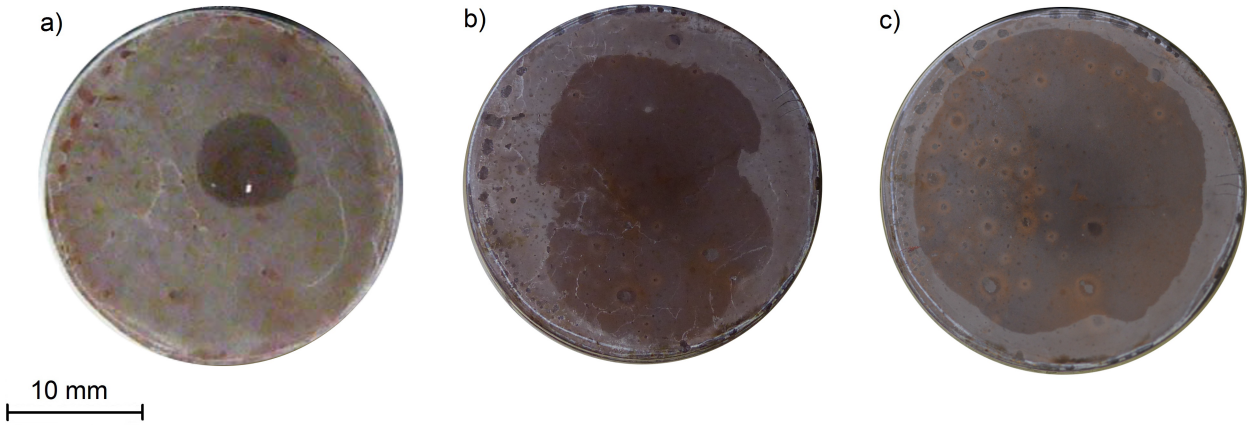

Figure D.2: Series of photographs which span one full test cycle for a nanostructured surface grown by hydrothermal synthesis for 10 hours. a)Wetting after hydrothermal synthesis and rst desorption. b)Wetting after second desorption, before experiments. c)Wetting after one evaporation experiment.

D.2 Contact angle measurements and calculations for ZnO nanostructured surface grown for 10 hours

Due to the superhydrophilicity of some of the ZnO nanostructured surfaces, determining the contact angle on the ZnO nanostructured surfaces was not possible from the droplet pro le. Therefore, for all of the ZnO nanostructured surface a single 2µL distilled water droplet was gently deposited and the subsequent spreading was captured by the camera

Table D.2: Contact angles measured on ZnO nanostructured surfaces grown by hydrothermal synthesis for 10 hours for Leidenfrost experiments. θ_{inner} is the contact angle of the inner droplet, where applicable, A_{inner} is the solid-liquid contact area corresponding to the inner droplet, θ_{outer} is the calculated effective contact angle of the liquid film surrounding the inner droplet, where applicable, A_{outer} is the spread area of the film surrounding the liquid droplet. N.A. indicates that the property was not exhibited by the surface. The final column on the right indicates the moment after which the contact angle measurements were taken throughout the desorption and experiment cycles for the surface.

t (hrs)	θ_{inner}	A_{inner} (μm^2)	θ_{outer}	A_{outer} (μm^2)	Measured after...
10-1	32.6° ± 8.4°	8.2 ± 4.5	N.A.	N.A.	1st desorp.
10-1	0.2° ± 0.0°	219.6± 5.3	N.A.	N.A.	2nd desorp.
10-1	0.2° ± 0.0°	226.1± 5.0	N.A.	N.A.	experiment
10-2	0.9° ± 0.1°	428.7± 21.0	N.A.	N.A.	experiment
10-3	3.2° ± 0.8°	40.5± 4.0	N.A.	N.A.	experiment
10-4	41.9° ± 4.6°	6.8 ± 0.6	9.7° ± 4.3°	20.3± 5.1	1st desorp.
10-4	38.4° ± 1.3°	7.3 ± 0.2	10.4° ± 0.4°	18.2± 0.5	2nd desorp.
10-4	0.1° ± 0.0°	392.0± 36.5	N.A.	N.A.	experiment
10-5	18.0° ± 6.1°	13.1± 3.2	1.3° ± 0.2°	72.5± 8.0	1st desorp.
10-5	0.5° ± 0.0°	130.7± 6.6	N.A.	N.A.	2nd desorp.
10-5	0.4° ± 0.0°	161.8± 11.8	N.A.	N.A.	experiment

directly above and parallel to the test surface at 240 fps.

Complete results of measured and/or calculated contact angles for the surfaces grown for 10 hours used in the Leidenfrost experiments are found in Table D.2. Since there were five surfaces grown for 10 hours they are simply identified by a number indicating the order in which it was tested, e.g. 10-1 was the first surface grown for 10 hours that was tested, 10-2 was the second surface grown for 10 hours that was tested and so on.

Complete results of measured and/or calculated contact angles for the surfaces grown for 10 hours used in the low superheat experiments are found in Table D.3.

D.3 Results of maximum droplet spread area measurements and film thickness calculations for nanostructured surface grown for 10 hours

Results for experiments performed on the ZnO nanostructured surface grown by hydrothermal synthesis for 10 hours are depicted graphically in Figure D.3.

Results of droplet spread area measurements, with standard deviation, on the surface grown by hydrothermal synthesis for 10 hours as a function of droplet diameter, release

Table D.3: Contact angles measured ZnO nanostructured surfaces grown by hydrothermal synthesis for 10 hours for low superheat experiments. θ_{inner} is the contact angle of the inner droplet, where applicable, A_{inner} is the solid-liquid contact area corresponding to the inner droplet, θ_{outer} is the calculated e ective contact angle of the liquid lm surrounding the inner droplet, where applicable, A_{outer} is the spread area of the lm surrounding the liquid droplet. N.A. indicates that the property was not exhibited by the surface. The nal column on the right indicates the moment after which the contact angle measurements were taken throughout the desorption and experiment cycles for the surface.

t (hrs)	θ_{inner}	A_{inner} (μm^2)	θ_{outer}	A_{outer} (μm^2)	Measured after...
10	3.7° ± 0.3°	36.5± 1.5	N.A.	N.A.	1st desorp.
10	0.2° ± 0.0°	266.0± 10.8	N.A.	N.A.	2nd desorp.
10	0.1° ± 0.0°	335.7± 11.5	N.A.	N.A.	experiment

height and wall superheat are listed in Table D.4. Results of estimated liquid lm thickness as a function of droplet diameter, release height and wall superheat are listed in Table D.5.

Table D.4: Results of maximum droplet spread area measurements, with standard deviation, on surface grown for 10 hours. D is the droplet diameter, A is the maximum droplet spread area, H is the droplet release height and T is the wall superheat.

		T = 10 °C	T = 20 °C	T = 30 °C	T = 40 °C
D (mm)	H (cm)	A (mm^2)	A (mm^2)	A (mm^2)	A (mm^2)
2.5	0.12	39.3± 3.3	67.8± 5.4	85.0± 5.2	93.4± 4.5
2.5	3.9	57.9± 1.1	99.2± 13.1	119.4± 4.1	113.1± 1.5
2.5	8.1	90.9±31.1	130.4±0.1	150.4±16.7	134.3±5.8
3.0	0.15	53.9± 6.0	136.7± 0.3	184.0± 7.9	158.0± 6.0
3.0	3.9	114.9± 16.9	182.4± 9.7	203.0± 26.4	224.3± 7.9
3.0	8.1	83.9±8.0	231.3±10.5	194.1±12.3	225.3±26.6
3.9	0.20	90.8± 7.0	250.7± 0.0	294.9± 1.2	341.1± 12.6
3.9	3.9	115.4± 0.0	311.9± 35.9	366.1± 12.2	369.7± 2.3
3.9	8.1	227.5±13.2	325.0±2.0	415.6±14.6	422.2±15.7

D.4 Results of droplet evaporation time for nanostructured surface grown for 10 hours

Results for experiments performed on the ZnO nanostructured surface grown by hydrothermal synthesis for 10 hours to determine the e ect of wall superheat, droplet size,

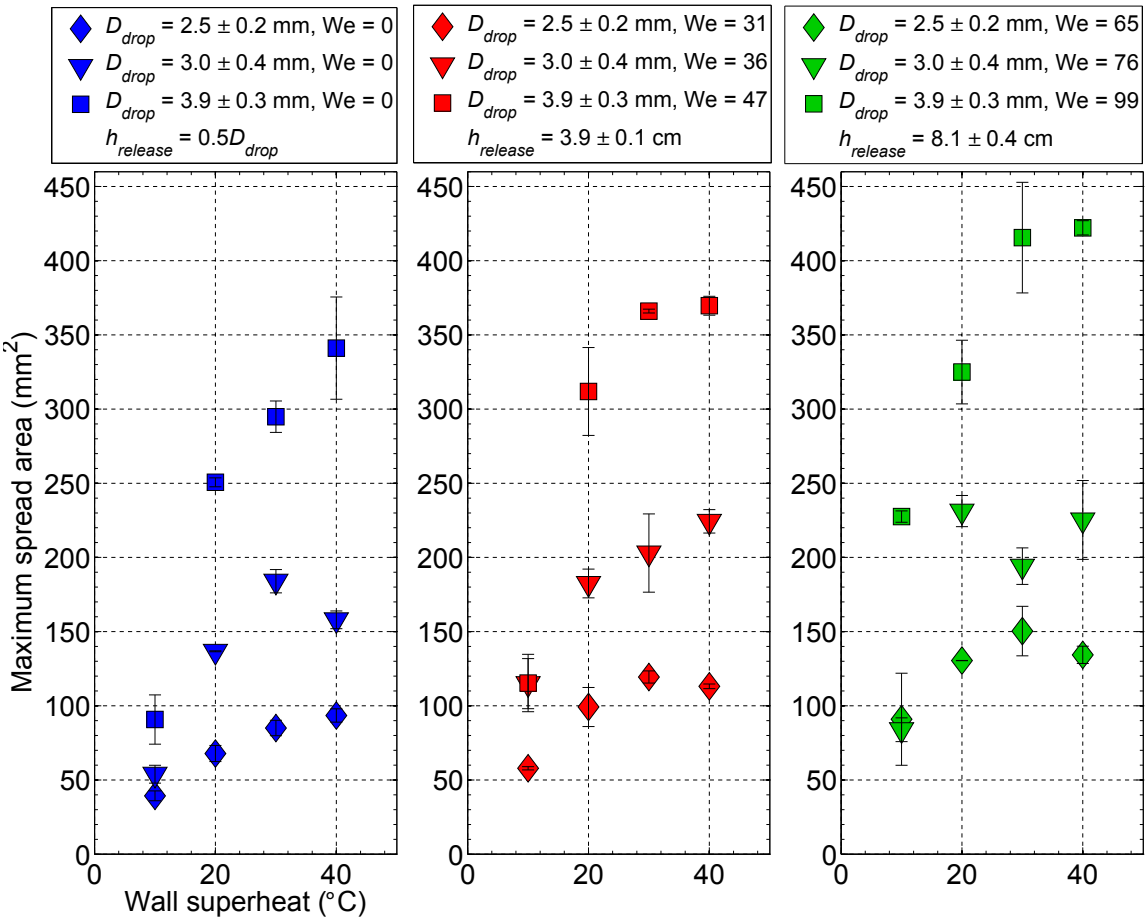

Figure D.3: Droplet spread area as a function of wall superheat, droplet size and release height for ZnO nanostructured surface generated by hydrothermal synthesis for 10 hours.

release height on evaporation time are depicted graphically in Figure D.4.

Results of droplet evaporation time measurements, with standard deviation, on the surface grown by hydrothermal synthesis for 10 hours as a function of droplet diameter, release height and wall superheat are listed in Table D.6.

D.5 Results of calculated heat transfer coe cients for nanostructured surface grown for 10 hours

Heat transfer coe cients calculated from results of experiments performed on the ZnO nanostructured surface grown by hydrothermal synthesis for 10 hours are depicted graphically in Figure D.5. The calculated heat transfer coe cients are compared to those predicted by the nucleate boiling correlation of Stephan and Abdelsalam.

Table D.5: Estimated liquid lm thickness based on initial droplet volume and the measured maximum droplet spread area on surface grown for 10 hours$D$ is the droplet diameter, L_{film} is the lm thickness, H is the droplet release height and T is the wall superheat.

		T = 10 °C	T = 20 °C	T = 30 °C	T = 40 °C
D (mm)	H (cm)	L_{film} (μm)	L_{film} (μm)	L_{film} (μm)	L_{film} (μm)
2.5	0.12	297.8	129.6	104.4	128.0
2.5	3.9	217.1	112.0	96.4	94.9
2.5	8.1	122.4	93.5	78.7	104.1
3.0	0.15	205.6	136.9	102.5	116.5
3.0	3.9	238.1	101.9	95.7	84.6
3.0	8.1	322.1	89.1	121.9	100.5
3.9	0.20	272.0	133.0	127.6	121.0
3.9	3.9	415.2	102.1	100.1	109.0
3.9	8.1	171.9	114.2	122.8	109.5

Table D.6: Results of droplet evaporation time measurements, with standard deviation, on the surface grown for 10 hours$D$ is the droplet diameter,t is the droplet evaporation time, H is the droplet release height and T is the wall superheat.

		T = 10 °C	T = 20 °C	T = 30 °C	T = 40 °C
D (mm)	H (cm)	t (s)	t (s)	t (s)	t (s)
2.5	0.12	2.19 $\pm$ 0.18	0.55 $\pm$ 0.09	0.20 $\pm$ 0.02	0.13 $\pm$ 0.01
2.5	3.9	1.44 $\pm$ 0.35	0.42 $\pm$ 0.09	0.17 $\pm$ 0.01	0.11 $\pm$ 0.02
2.5	8.1	1.62 $\pm$ 0.65	0.34 $\pm$ 0.02	0.19 $\pm$ 0.01	0.09 $\pm$ 0.01
3.0	0.15	2.37 $\pm$ 0.54	0.67 $\pm$ 0.07	0.30 $\pm$ 0.00	0.17 $\pm$ 0.01
3.0	3.9	2.91 $\pm$ 0.21	0.64 $\pm$ 0.09	0.24 $\pm$ 0.03	0.15 $\pm$ 0.01
3.0	8.1	2.73 $\pm$ 0.10	0.68 $\pm$ 0.02	0.23 $\pm$ 0.03	0.13 $\pm$ 0.03
3.9	0.20	3.78 $\pm$ 0.43	1.59 $\pm$ 0.01	0.43 $\pm$ 0.00	0.23 $\pm$ 0.01
3.9	3.9	4.12 $\pm$ 0.66	0.80 $\pm$ 0.12	0.44 $\pm$ 0.04	0.19 $\pm$ 0.03
3.9	8.1	2.47 $\pm$ 0.10	1.14 $\pm$ 0.03	0.41 $\pm$ 0.05	0.20 $\pm$ 0.03

Results of calculations of heat transfer coe cient on the surface grown for 10 hours as a function of droplet diameter, release height and wall superheat are listed in Table D.7.

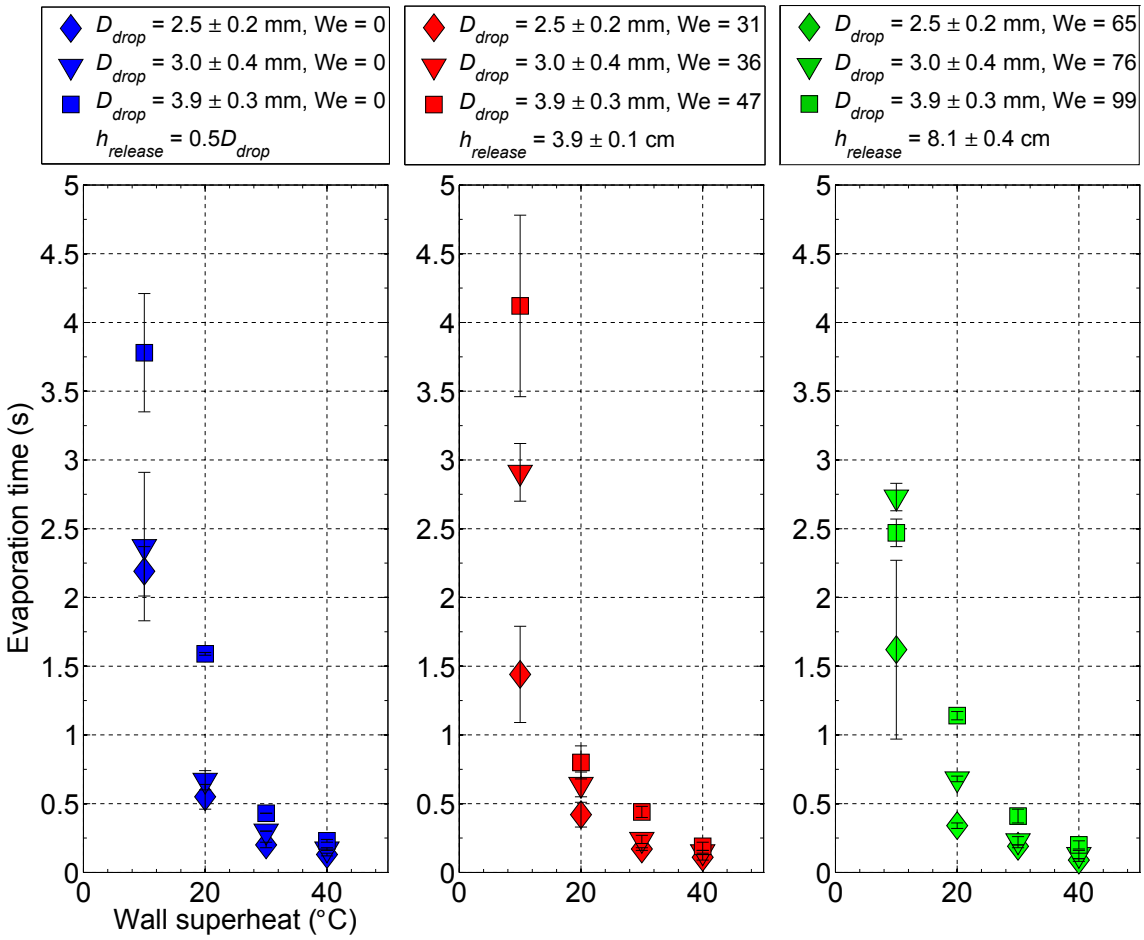

Figure D.4: Droplet evaporation time as a function of wall superheat, droplet size and release height for the ZnO nanostructured surface generated by hydrothermal synthesis for 10 hours.

D.6 Results of Leidenfrost experiments for nanostructured surface grown for 10 hours

Leidenfrost transition data for the nanostructured surface grown for 10 hours are listed in Table D.8. The data represent Leidenfrost points spanning the entirety of the experimental lifetime of each surface. The Leidenfrost temperatures, T_{Leid}, listed in Table D.8 represent a mean of values obtained in di erent tests for this surface. The uncertainty values listed for each T_{Leid} in Table D.8 indicate the spread of T_{Leid} obtained for this surface. The average contact angle, θ_{avg}, that is listed for this surface is the average of the contact angle measured or calculated after the second desorption and after the experiment.

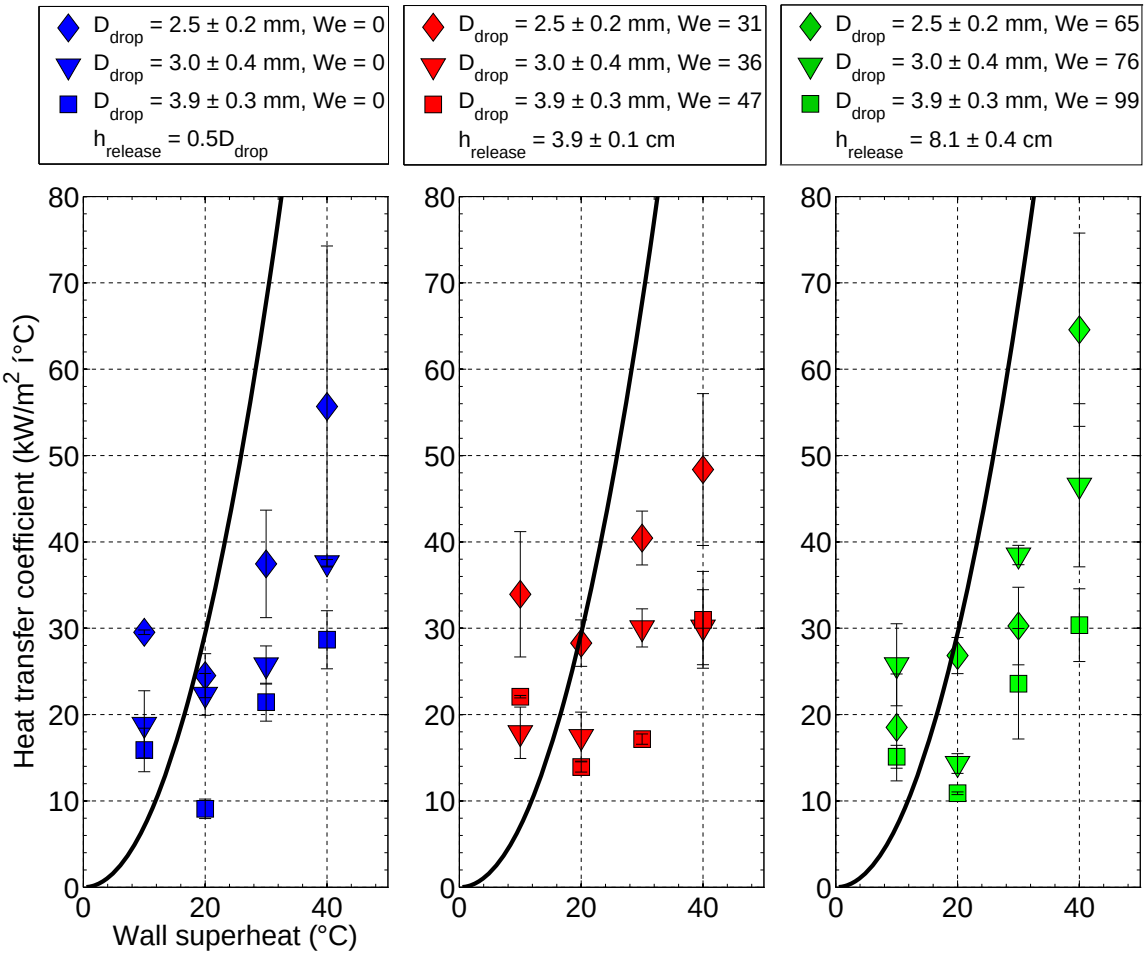

Figure D.5: Heat transfer coe cient as a function of wall superheat, droplet size and release height for ZnO nanostructured surface generated by hydrothermal synthesis for 10 hours.

Table D.7: Results of calculations of heat transfer coe cient on surface grown for 10 hours. D is the droplet diameter,h_{evap} is the heat transfer coe cient and T is the wall superheat.

		T = 10 °C	T = 20 °C	T = 30 °C	T = 40 °C
D (mm)	H (cm)	h_{evap} (kW/m ^{2}{°C)	h_{evap} (kW/m ^{2}{°C)	h_{evap} (kW/m ^{2}{°C)	h_{evap} (kW/m ^{2}{°C)
2.5	0.12	29.5 ± 0.3	24.5 ± 2.5	37.5 ± 6.2	55.7 ± 18.6
2.5	3.9	33.9 ± 7.3	28.3 ± 2.7	40.4 ± 3.1	48.4 ± 8.8
2.5	8.1	18.5 ± 6.2	26.8 ± 2.1	30.3 ± 4.5	64.6 ± 11.2
3.0	0.15	18.9 ± 3.9	22.3 ± 2.4	25.7 ± 2.2	37.6 ± 0.4
3.0	3.9	17.9 ± 3.0	17.4 ± 2.8	30.0 ± 2.2	30.1 ± 4.3
3.0	8.1	25.8 ± 4.7	14.3 ± 1.1	38.5 ± 1.1	46.6 ± 9.4
3.9	0.20	15.9 ± 2.5	9.1 ± 1.1	21.4 ± 2.2	28.7 ± 3.4
3.9	3.9	22.1 ± 0.1	13.9 ± 0.6	17.2 ± 0.6	31.0 ± 5.6
3.9	8.1	15.1 ± 1.3	10.9 ± 0.2	23.6 ± 6.4	30.4 ± 4.2

Table D.8: Leidenfrost temperatures,T_{Leid}, as a function of droplet diameter,D_{drop} for nanostructured surface grown for at$t_{hydrothermal}$ of 10 hours. The average contact angle is given by θ_{avg}.

Surface	θ_{avg}	D_{drop} (mm)	Cycle	T_{Leid} (°C)
$t_{hydrothermal,1}$ = 10 hrs	1°	3.6 ± 0.3	heating & cooling	350.5 ± 2.6
$t_{hydrothermal,2}$ = 10 hrs	1°	3.9 ± 0.3	heating	376.0 ± 2.8
$t_{hydrothermal,3}$ = 10 hrs	1°	3.5 ± 0.3	heating	352.0 ± 2.6
$t_{hydrothermal,4}$ = 10 hrs	1°	3.3 ± 0.3	heating	317.0 ± 2.4
$t_{hydrothermal,5}$ = 10 hrs	1°	3.3 ± 0.3	heating & cooling	361.0 ± 2.7

Appendix E

Surface characteristics and experimental results: ZnO nanostructured surface grown for 24 hours

Micrographs of the ZnO nanostructured surfaces were captured before and after experiments with a LEO 1550, Schottky field emission scanning electron microscope (SEM) located in the Marvell Nanofabrication Laboratory at UC Berkeley.

E.1 SEM images and surface geometry

Micrographs for the ZnO nanostructured surfaces grown by hydrothermal synthesis for 24 hours are found in Figure E.1.

From the micrographs in Figure E.1 it was possible to measure the average nanocrystal side length, measured from substrate to tip of the nanocrystal, L_{side} and the average crystal hexagon side length, L_{hex} in order to calculate the average nanocrystal surface area, A_{ZnO} which was available to interact with the liquid droplets. For calculation purposes, the top face of an individual ZnO nanocrystal is assumed to form a regular hexagon, such that the length of all six sides are equivalent to L_{hex}. The area, A_{hex} of the top face of the ZnO nanocrystal is given by,

$$A_{hex} = \frac{3\sqrt{3}}{2} L_{hex}^2. \tag{E.1}$$

Therefore, surface area of one individual ZnO nanocrystal is given by

$$A_{ZnO} = A_{hex} + 6\, L_{hex} L_{side}. \tag{E.2}$$

Furthermore it was possible to measure the surface area of the substrate that was not covered by ZnO nanocrystals, $A_{un-nucleated}$, i.e. the base area of the substrate, $A_{substrate}$, over which

Table E.1: Average geometrical parameters with standard deviation of ZnO nanostructured surfaces grown for a hydrothermal synthesis time, t, of 24 hours. L_{hex} is the hexagon side length, L_{side} is the length of the nanocrystal measured from the substrate to the tip of the nanocrystal, A_{ZnO} is total wetted surface area of one ZnO nanocrystal and ω is wetted surface area ratio.

t (hr)	L_{hex} (μm)	L_{side} (μm)	A_{ZnO} (μm^2)	ε	ω
24	0.77 $\pm$ 0.15	3.25 $\pm$ 0.96	16.73 $\pm$ 5.99	0.04 $\pm$ 0.005	10.8

no clearly distinct ZnO nanocrystals nucleated. From these measurements it was possible to determine the porosity, ε given by

$$\varepsilon = 1 - \frac{A_{substrate} - A_{un-nucleated}}{A_{substrate}} = 1 - \frac{A_{nucleated}}{A_{substrate}} \tag{E.3}$$

where $A_{nucleated}$ is the area of the base substrate that is covered by ZnO nanocrystals. It was not possible to determine whether the un-nucleated area was bare copper or simply ZnO nanoparticles that were annealed onto the copper substrate but did not serve as a nanocrystal nucleation site. In any case, from the calculated ZnO nanocrystal surface area, A_{ZnO} and measured un-nucleated substrate surface area, $A_{un-nucleated}$, it was possible to determine the total average surface area that could potentially interact with liquid, i.e. the total average wetted surface area, $A_{wetted,total}$ given by,

$$A_{wetted,total} = \eta A_{ZnO} + A_{un-nucleated} \tag{E.4}$$

where η is the total estimated number of nanocrystals within a given substrate area, $A_{substrate}$, which is given by,

$$\eta = \frac{A_{substrate}}{A_{hex}}. \tag{E.5}$$

Therefore, per unit of substrate area, the wetted surface area ratio, ω is given by,

$$\omega = \frac{A_{wetted,total}}{A_{substrate}} = \frac{\eta A_{ZnO} + A_{un-nucleated}}{A_{substrate}}. \tag{E.6}$$

which can be simplified further to,

$$\omega = 1 + \frac{4h}{\sqrt{3}L_{hex}} + \varepsilon. \tag{E.7}$$

The geometrical measurements are listed in Table E.1.

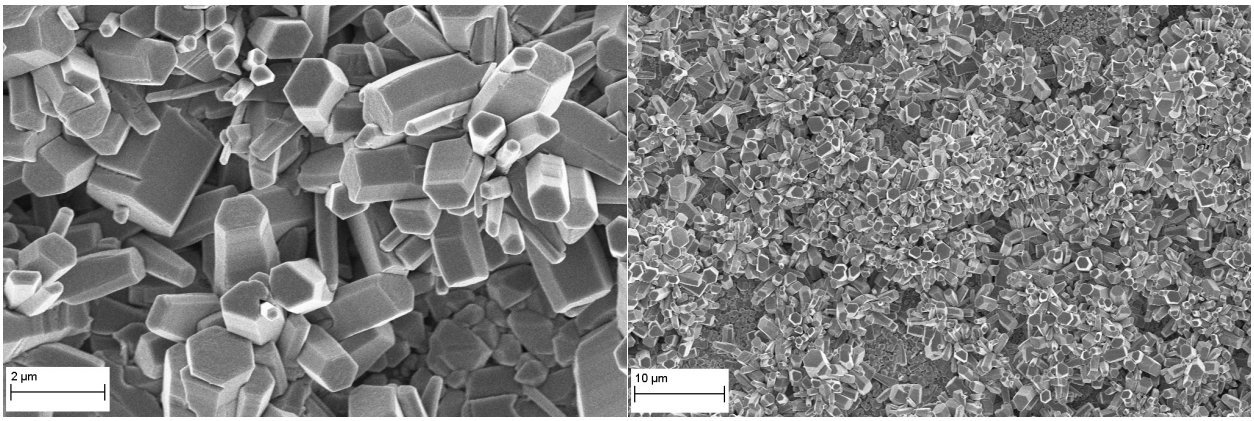

Figure E.1: SEM images of ZnO nanostructures synthesized on the smooth copper surface for 24 hours before experiments. The image on the right shows the general array of the ZnO nanocrystals on the substrate. The left image is shows the hexagonal wurtzite structure of the ZnO nanocrystals.

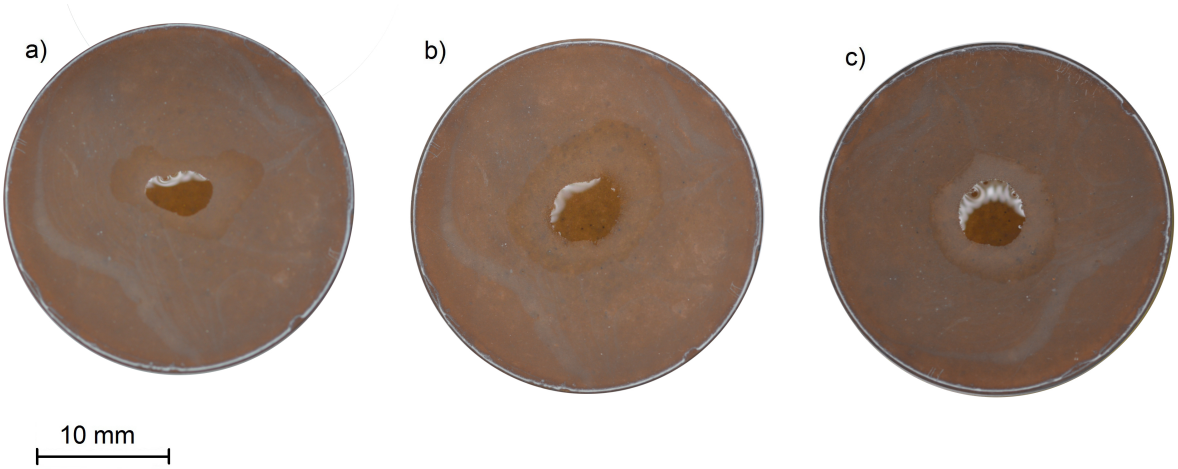

Figure E.2: Series of photographs which span one full test cycle for a nanostructured surface grown by hydrothermal synthesis for 24 hours. a)Wetting after hydrothermal synthesis and rst desorption. b)Wetting after second desorption, before experiments. c)Wetting after one evaporation experiment.

E.2 Contact angle measurements and calculations for ZnO nanostructured surface grown for 24 hours

Due to the superhydrophilicity of some of the ZnO nanostructured surfaces, determining the contact angle on the ZnO nanostructured surfaces was not possible from the droplet

Table E.2: Contact angles measured on ZnO nanostructured surfaces grown by hydrothermal synthesis for 24 hours for Leidenfrost experiments. θ_{inner} is the contact angle of the inner droplet, where applicable, A_{inner} is the solid-liquid contact area corresponding to the inner droplet, θ_{outer} is the calculated effective contact angle of the liquid film surrounding the inner droplet, where applicable, A_{outer} is the spread area of the film surrounding the liquid droplet. N.A. indicates that the property was not exhibited by the surface. The final column on the right indicates the moment after which the contact angle measurements were taken throughout the desorption and experiment cycles for the surface.

t (hrs)	θ_{inner}	A_{inner} (μm^2)	θ_{outer}	A_{outer} (μm^2)	Measured after...
24	21.2° ± 8.0°	12.9 ± 4.9	5.6° ± 1.6°	44.9 ± 36.8	1st desorp.
24	18.2° ± 4.9°	13.7 ± 3.3	4.9° ± 1.9°	31.5 ± 8.3	2nd desorp.
24	12.4° ± 1.3°	16.2 ± 1.1	3.1° ± 0.4°	41.0 ± 3.3	experiment

profile. Therefore, for all of the ZnO nanostructured surface a single 2 μL distilled water droplet was gently deposited and the subsequent spreading was captured by the camera directly above and parallel to the test surface at 240 fps.

Complete results of measured and/or calculated contact angles for the surfaces grown for 24 hours used in the Leidenfrost experiments are found in Table E.2. Note that since there was a negligible difference between contact angles immediately before and after the experiments, it was determined that the nanostructured surface geometry was unaffected by the experiments and thus SEM images after the experiments were not taken for this surface.

Complete results of measured and/or calculated contact angles for the surfaces grown for 24 hours used in the low superheat experiments are found in Table E.3. Note that since there was a negligible difference between contact angles immediately before and after the experiments, it was determined that the nanostructured surface geometry was unaffected by the experiments and thus SEM images after the experiments were not taken for this surface.

E.3 Results of maximum droplet spread area measurements and film thickness calculations for nanostructured surface grown for 24 hours

Results for experiments performed on the ZnO nanostructured surface grown by hydrothermal synthesis for 24 hours are depicted graphically in Figure E.3.

Results of droplet spread area measurements, with standard deviation, on the surface grown by hydrothermal synthesis for 24 hours as a function of droplet diameter, release height and wall superheat are listed in Table E.4. Results of estimated liquid film thickness as a function of droplet diameter, release height and wall superheat are listed in Table E.5.

Table E.3: Contact angles measured on ZnO nanostructured surfaces by hydrothermal synthesis for 24 hours for low superheat experiments. θ_{inner} is the contact angle of the inner droplet, where applicable, A_{inner} is the solid-liquid contact area corresponding to the inner droplet, θ_{outer} is the calculated e ective contact angle of the liquid lm surrounding the inner droplet, where applicable, A_{outer} is the spread area of the lm surrounding the liquid droplet. N.A. indicates that the property was not exhibited by the surface. The nal column on the right indicates the moment after which the contact angle measurements were taken throughout the desorption and experiment cycles for the surface.

t (hrs)	θ_{inner}	A_{inner} (μm^2)	θ_{outer}	A_{outer} (μm^2)	Measured after...
24	16.1° ± 7.3°	15.1 ± 6.1	2.4° ± 0.1°	48.4 ± 1.5	1st desorp.
24	8.9° ± 1.1°	20.4 ± 1.6	0.9° ± 0.1°	95.6 ± 9.5	2nd desorp.
24	9.3° ± 1.9°	19.8 ± 2.7	1.5° ± 0.1°	67.5 ± 3.1	experiment

Table E.4: Results of maximum droplet spread area measurements, with standard deviation, on surface grown for 24 hours. D is the droplet diameter, A is the maximum droplet spread area, H is the droplet release height and T is the wall superheat.

		T = 10 °C	T = 20 °C	T = 30 °C	T = 40 °C
D (mm)	H (cm)	A (mm^2)	A (mm^2)	A (mm^2)	A (mm^2)
2.5	0.12	42.5 ± 3.0	95.4 ± 4.5	88.5 ± 9.5	94.0 ± 2.4
2.5	3.9	54.8 ± 3.4	110.8 ± 12.5	119.1 ± 2.8	117.0 ± 0.9
2.5	8.1	57.4 ± 7.0	121.8 ± 0.0	131.3 ± 2.1	118.7 ± 0.5
3.0	0.15	74.7 ± 6.2	169.5 ± 4.5	174.4 ± 4.7	158.2 ± 6.2
3.0	3.9	84.6 ± 5.7	201.1 ± 12.8	220.2 ± 10.5	167.2 ± 31.4
3.0	8.1	94.4 ± 0.0	228.9 ± 9.6	164.0 ± 37.1	199.3 ± 11.3
3.9	0.20	133.0 ± 29.8	267.3 ± 26.0	284.9 ± 2.7	257.5 ± 10.5
3.9	3.9	157.9 ± 19.2	310.4 ± 20.4	319.6 ± 5.5	323.9 ± 10.8
3.9	8.1	146.7 ± 2.7	320.7 ± 11.0	317.7 ± 3.1	330.7 ± 13.8

E.4 Results of droplet evaporation time for nanostructured surface grown for 24 hours

Results for experiments performed on the ZnO nanostructured surface grown by hydrothermal synthesis for 24 hours to determine the e ect of wall superheat, droplet size, release height on evaporation time are depicted graphically in Figure E.4.

Results of droplet evaporation time measurements, with standard deviation, on the surface grown by hydrothermal synthesis for 24 hours as a function of droplet diameter, release height and wall superheat are listed in Table E.6.

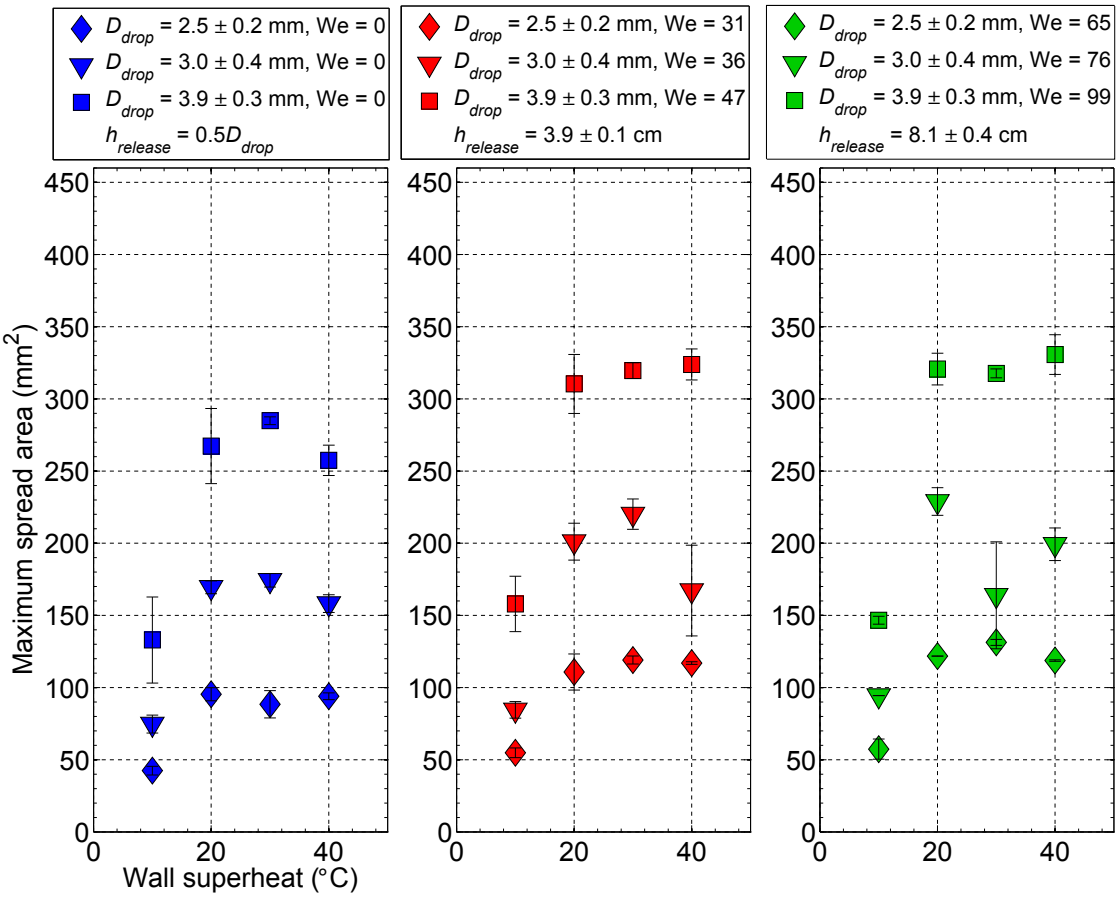

Figure E.3: Droplet spread area as a function of wall superheat, droplet size and release height for ZnO nanostructured surface generated by hydrothermal synthesis for 24 hours.

E.5 Results of calculated heat transfer coe cients for nanostructured surface grown for 24 hours

Heat transfer coe cients calculated from results of experiments performed on the ZnO nanostructured surface grown by hydrothermal synthesis for 24 hours are depicted graphically in Figure E.5. As was done for the other two surfaces in this parametric study, the calculated heat transfer coe cients are compared to those predicted by the nucleate boiling correlation of Stephan and Abdelsalam.

Results of calculations of heat transfer coe cient on surface grown for 24 hours as a function of droplet diameter, release height and wall superheat are listed in Table E.7.

Table E.5: Estimated liquid lm thickness based on initial droplet volume and the measured maximum droplet spread area on surface grown for 24 hours. D is the droplet diameter, L_{film} is the lm thickness, H is the droplet release height and T is the wall superheat.

		T = 10 °C	T = 20 °C	T = 30 °C	T = 40 °C
D (mm)	H (cm)	L_{film} (μm)	L_{film} (μm)	L_{film} (μm)	L_{film} (μm)
2.5	0.12	114.2	73.0	84.1	88.5
2.5	3.9	117.0	69.4	59.6	80.3
2.5	8.1	138.4	71.2	60.5	42.8
3.0	0.15	138.4	83.4	67.7	90.1
3.0	3.9	156.6	66.4	65.9	64.4
3.0	8.1	141.6	72.7	68.0	75.3
3.9	0.20	181.8	89.9	107.6	134.4
3.9	3.9	163.0	84.0	100.2	109.7
3.9	8.1	183.4	93.1	107.9	110.3

Table E.6: Results of droplet evaporation time measurements, with standard deviation, on the surface grown for 24 hours. D is the droplet diameter, t is the droplet evaporation time, H is the droplet release height and T is the wall superheat.

		T = 10 °C	T = 20 °C	T = 30 °C	T = 40 °C
D (mm)	H (cm)	t (s)	t (s)	t (s)	t (s)
2.5	0.12	1.18 $\pm$ 0.04	0.40 $\pm$ 0.04	0.29 $\pm$ 0.04	0.16 $\pm$ 0.00
2.5	3.9	1.23 $\pm$ 0.12	0.38 $\pm$ 0.02	0.17 $\pm$ 0.17	0.15 $\pm$ 0.03
2.5	8.1	1.15 $\pm$ 0.00	0.24 $\pm$ 0.01	0.19 $\pm$ 0.03	0.21 $\pm$ 0.01
3.0	0.15	1.46 $\pm$ 0.12	0.58 $\pm$ 0.06	0.31 $\pm$ 0.00	0.22 $\pm$ 0.04
3.0	3.9	1.98 $\pm$ 0.30	0.48 $\pm$ 0.02	0.35 $\pm$ 0.04	0.19 $\pm$ 0.05
3.0	8.1	1.86 $\pm$ 0.00	0.50 $\pm$ 0.09	0.28 $\pm$ 0.08	0.18 $\pm$ 0.04
3.9	0.20	2.77 $\pm$ 0.36	0.90 $\pm$ 0.18	0.50 $\pm$ 0.06	0.29 $\pm$ 0.03
3.9	3.9	3.19 $\pm$ 0.65	0.88 $\pm$ 0.02	0.42 $\pm$ 0.08	0.23 $\pm$ 0.01
3.9	8.1	3.31 $\pm$ 0.37	0.68 $\pm$ 0.09	0.41 $\pm$ 0.07	0.23 $\pm$ 0.04

E.6 Results of Leidenfrost experiments for nanostructured surface grown for 24 hours

Leidenfrost transition data for the nanostructured surface grown for 24 hours are listed in Table E.8. The data represent Leidenfrost points spanning the entirety of the experimental lifetime of each surface. The Leidenfrost temperatures, T_{Leid}, listed in Table E.8 represent a mean of values obtained in di erent tests for this surface. The uncertainty values listed for

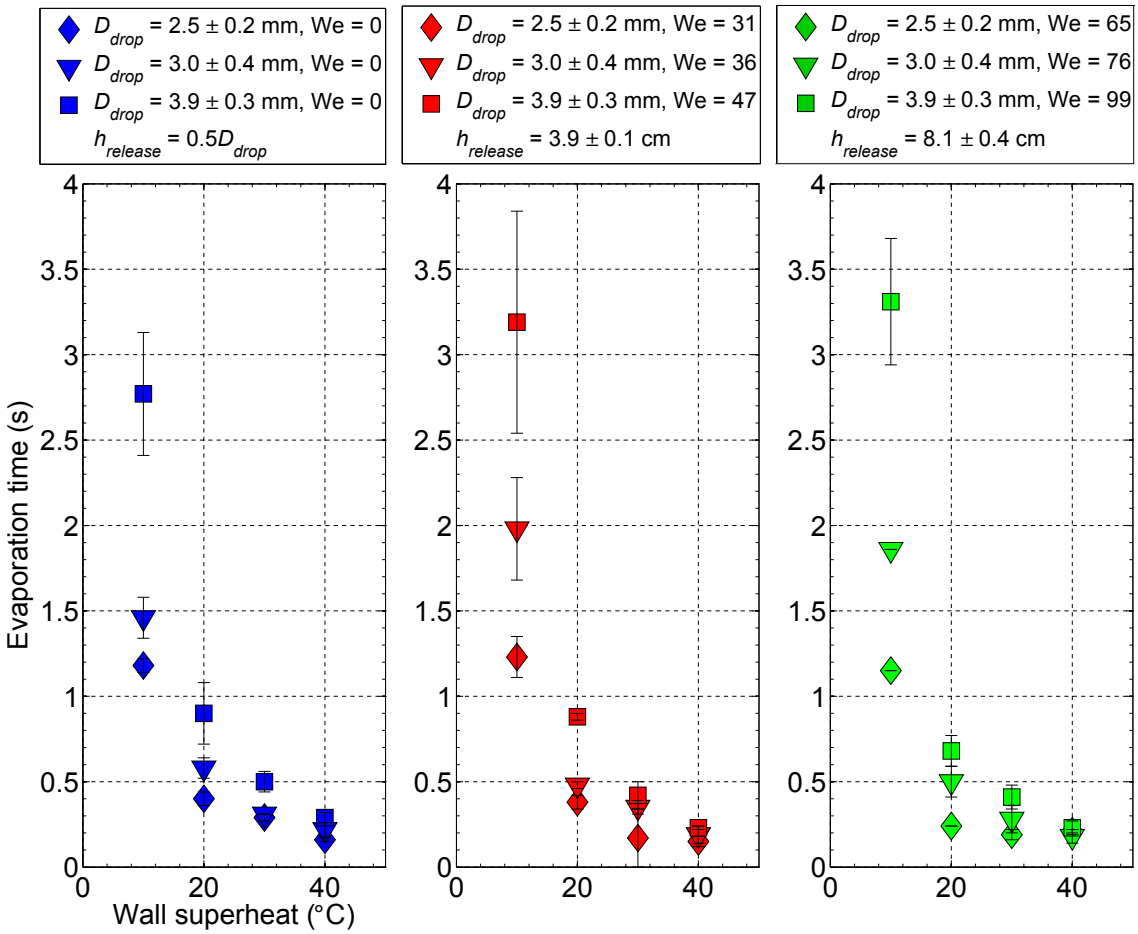

Figure E.4: Droplet evaporation time as a function of wall superheat for surface generated by hydrothermal synthesis for 24 hours.

each T_{Leid} in Table E.8 indicate the spread of T_{Leid} obtained for this surface. The average contact angle, θ_{avg}, that is listed for this surface is the average of the contact angle measured or calculated after the second desorption and after the experiment.

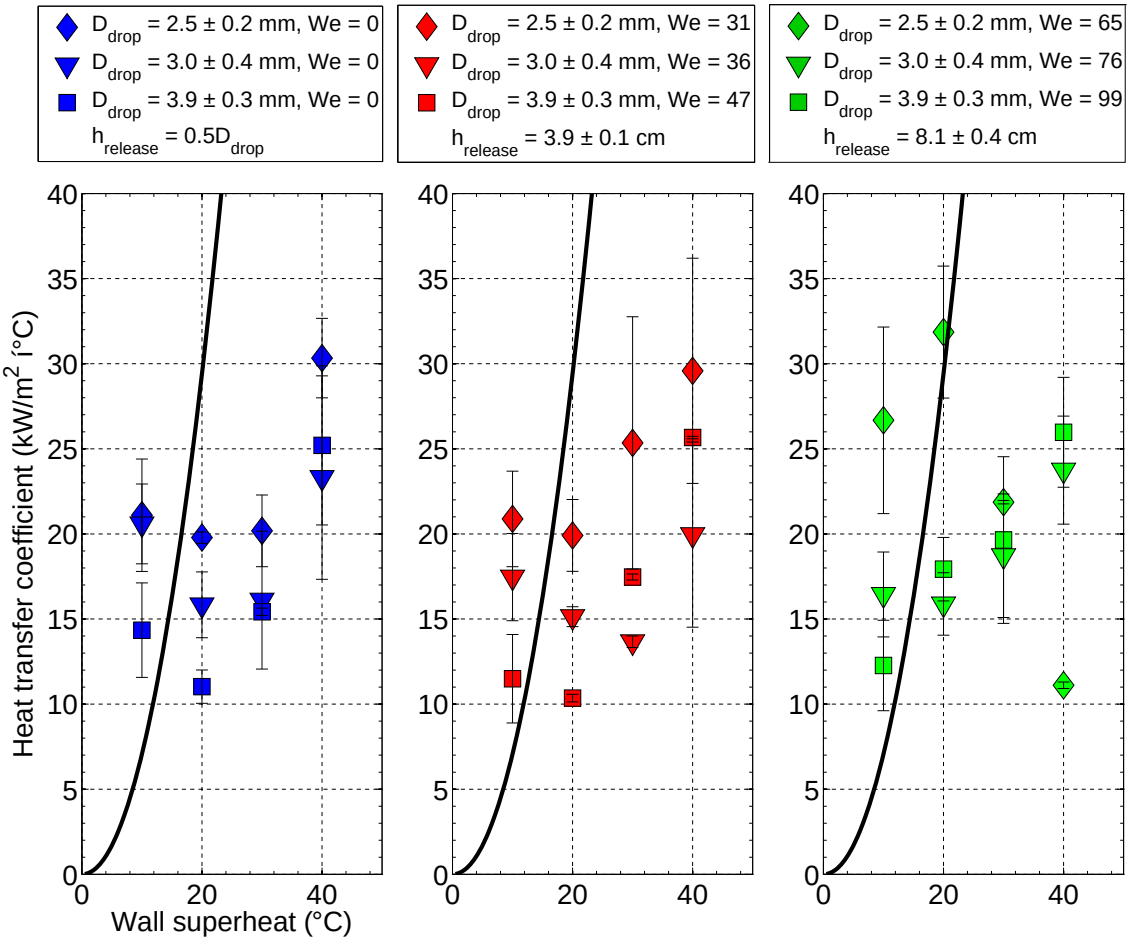

Figure E.5: Heat transfer coe cient as a function of wall superheat, droplet size and release height for ZnO nanostructured surface generated by hydrothermal synthesis for 24 hours.

Table E.7: Results of calculations of heat transfer coe cient on surface grown for 24 hours. D is the droplet diameter,h_{evap} is the heat transfer coe cient and T is the wall superheat.

		T = 10 °C	T = 20 °C	T = 30 °C	T = 40 °C
D (mm)	H (cm)	h_{evap} (kW/m ^{2}{°C)	h_{evap} (kW/m ^{2}{°C)	h_{evap} (kW/m ^{2}{°C)	h_{evap} (kW/m ^{2}{°C)
2.5	0.12	21.1 ± 3.3	19.8 ± 0.3	20.2 ± 2.1	30.3 ± 2.3
2.5	3.9	20.9 ± 2.8	19.9 ± 2.1	25.3 ± 7.4	29.6 ± 6.6
2.5	8.1	26.7 ± 5.5	31.9 ± 3.9	21.9 ± 0.1	11.1 ± 0.2
3.0	0.15	20.6 ± 2.3	15.8 ± 1.9	16.1 ± 4.0	23.3 ± 6.0
3.0	3.9	17.5 ± 2.6	15.1 ± 0.6	13.7 ± 0.3	20.0 ± 5.4
3.0	8.1	16.4 ± 2.5	15.9 ± 1.8	18.7 ± 3.6	23.7 ± 3.2
3.9	0.20	14.3 ± 2.8	11.0 ± 1.0	15.4 ± 0.2	25.2 ± 4.7
3.9	3.9	11.5 ± 2.6	10.4 ± 0.2	17.5 ± 0.2	25.7 ± 0.1
3.9	8.1	12.3 ± 2.7	17.9 ± 1.9	19.6 ± 4.9	26.0 ± 3.2

Table E.8: Leidenfrost temperatures,T_{Leid}, as a function of droplet diameter,D_{drop} for nanostructured surface grown for at $t_{hydrothermal}$ of 24 hours. The average contact angle is given by θ_{avg}.

Surface	θ_{avg}	D_{drop} (mm)	Cycle	T_{Leid} (°C)
$t_{hydrothermal}$ = 24 hrs	15.0°	2.3 ± 0.1	heating	327.5 ± 2.5
$t_{hydrothermal}$ = 24 hrs	15.0°	2.5 ± 0.1	cooling	329.0 ± 2.5
$t_{hydrothermal}$ = 24 hrs	15.0°	3.0 ± 0.0	heating	322.5 ± 2.4
$t_{hydrothermal}$ = 24 hrs	15.0°	2.9 ± 0.2	cooling	321.5 ± 2.4
$t_{hydrothermal}$ = 24 hrs	15.0°	3.6 ± 0.2	heating	324.5 ± 2.4
$t_{hydrothermal}$ = 24 hrs	15.0°	3.5 ± 0.2	cooling	312.0 ± 2.3

Appendix F

Heat transfer by lm evaporation

The results of the comparison between the calculated heat transfer coe cient h_{evap} and the heat transfer coe cient predicted by Stephan and Abdelsalam h_{SA} for all the ZnO nanostructured surfaces suggest that nucleate boiling was not the driving heat transfer mechanism. The gradual increase in h_{evap} is more typical of lm evaporation. Furthermore, experimental video evidence reveals that on the ZnO nanostructured surfaces, nucleate boiling was either absent or minimally present at superheats of 30°C or less. In order to determine whether the liquid-to-vapor phase change is driven by lm evaporation, a simple, one-dimensional heat conduction analysis is proposed. If it is assumed that lm evaporation is the driving mechanism for droplet evaporation, then heat transfer by conduction from the surface through the liquid lm, $Q_{conduction}$, for any given length of time, t_{cond}, is balanced by the liquid-to-vapor phase change such that,

$$Q_{conduction} = -\rho_l \quad V_{drop} h_{lv} \tag{F.1}$$

where ρ_l is the liquid density, V_{drop} is the change in droplet volume, V_{drop}, over the length of time of heat conduction and h_{lv} is the enthalpy of vaporization. The heat conduction, $Q_{conduction}$ is given approximately by,

$$Q_{conduction} = \frac{k_l A_{spread} \quad T}{L_{film}} \quad t_{cond} \tag{F.2}$$

where k_l is the liquid thermal conductivity, T is the wall superheat, L_{film} is the liquid lm thickness and A_{spread} is the droplet spread area. Balancing the heat conduction with the phase change energy for a given length of time gives,

$$\frac{k_l A_{spread} \quad T}{L_{film}} \quad t_{cond} = -\rho_l h_{lv} A_{spread} \quad L_{film} \tag{F.3}$$

where, V_{drop} has been substituted by the product of the spread area, A_{spread} and the change in lm thickness L_{film}. Equation F.3 can be simpli ed further by eliminating the A_{spread} term, such that,

$$\frac{k_l \quad T}{L_{film}} \quad t_{cond} = -\rho_l h_{lv} \quad L_{film}. \tag{F.4}$$

Reducing changes in time and lm thickness to in nitesimal magnitude, Equation F.4 becomes an integrable function given by,

$$\int_0^{t_{evap,cond}} dt_{cond} = -\frac{\rho_l h_{lv}}{k_l \quad T} \int_{L_{film}(0)}^{0} L_{film} dL_{film} \tag{F.5}$$

where L_{film}(0) is the liquid lm thickness calculated from,

$$L_{film}(0) = \frac{V_{drop}(0)}{A_{spread,max}} \tag{F.6}$$

where V_{drop}(0) is the initial droplet volume and $A_{spread,max}$ is the measured maximum spread area. Equation F.5 is solved for the predicted evaporation time due to heat conduction, $t_{evap,cond}$, given by,

$$t_{evap,cond} = \frac{\rho_l h_{lv}}{k_l \quad T} \frac{L_{film}^2}{2}. \tag{F.7}$$

Based on the assumption of one-dimensional conduction through the liquid lm, then, $t_{evap,cond}$ is used to calculate a heat transfer coe cient, $h_{evap,cond}$, given by

$$h_{evap,cond} = \frac{\rho_l h_{lv} L_{film}}{t_{evap,cond} \quad T} \tag{F.8}$$

which after substituting for $t_{evap,cond}$, is simpli ed to give

$$h_{evap,cond} = \frac{2k_l}{L_{film}}. \tag{F.9}$$

The predicted value of $h_{evap,cond}$ was then compared to the value of h_{evap} which was computed from the measurements of t_{evap} for every experiment in this study. The results of the comparison between h_{evap} and $h_{evap,cond}$ are depicted graphically in Figures F.1{F.3.

In general, the prediction, $h_{evap,cond}$ was less than h_{evap}. It is evident from Figures F.1{F.3 that the $h_{evap,cond}$ does not predict h_{evap} very precisely. For the surface grown for 4 hours, $h_{evap,cond}$ was within about 1{95% of h_{evap}. For the surface grown for 10 hours, $h_{evap,cond}$ was within about 5{55% of h_{evap}. For the surface grown for 24 hours, $h_{evap,cond}$ was within about 2{97% of h_{evap}. Clearly there is a wide spread of results for this analysis, but it is reassuring that the predicted trends are generally the same, with some exceptions of course. However, it is important to determine the source that results in the di erence in the magnitude of the two heat transfer coe cients. First, h_{evap} does not depend explicitly on the liquid lm thickness. Since it is determined from the measurements of V_{drop} and A_{spread}, an estimation or measurement of L_{film} is not necessary. Secondly, h_{evap} is the average heat transfer coe cient over the entire wetted area, A_{spread}. In contrast $h_{evap,cond}$ depends on knowledge of some initial lm thickness $L_{film,i}$. The initial lm thickness is estimated from a measurement of V_{drop} before the droplet impacts the surface, whereas A_{spread} is

measured when it reaches its maximum value, which occurs after the droplet impacts the surface. Therefore, the estimated $L_{film,i}$ is very likely greater than the actual lm thickness since liquid is assumed to evaporate immediately upon droplet impact on the surface. A greater $L_{film,i}$ would result in a greater $t_{evap,cond}$ which would result in a lesser heat transfer coe cient. This observation is re ected in the results of the analysis depicted in Figures F.1{ F.3. This assumption results in predicted values that deviate from experimental results even further as wall superheat increases since a higher wall superheat would evaporate more liquid before the maximum spread area was achieved than a lower wall superheat. Furthermore, the evaporation is not a one-dimensional process. It is assumed in the one-dimensional analysis that the lm thickness is uniform, whereas in reality the lm thickness varies from the edge of the wetted area, where it is thinnest, to the center, where it is thickest. The variation in lm thickness tends to accelerate the evaporation process which is another reason that h_{evap} was generally greater than $h_{evap,cond}$. Finally, the one-dimensional model does not account for e ects of liquid-to-solid surface interaction. In reality, the liquid-to-surface interactions in uence the shape of the lm which leads to lm adsorption at the edges of the wetted area and the formation of a bulk meniscus [1], [71]{[82]. These interactions can also lead to density driven ow as function of temperature gradients within the liquid lm that can have a non-negligible e ect on the heat transfer. In spite of these mechanisms, however, it is remarkable that a simple, one-dimensional heat conduction analysis predicts a heat transfer coe cient that is within 100% of the heat transfer coe cient based on experimental measurements. It is well known that lm evaporation is a complicated multi-dimensional process, which is evident in the di erence between h_{evap} and $h_{evap,cond}$. However, the results of the simple heat conduction analysis as well as the comparison to the nucleate boiling predictions lead to the conclusion that heat transfer from the nanostructured surfaces was not driven by nucleate boiling, but by mechanisms typical of lm evaporation.

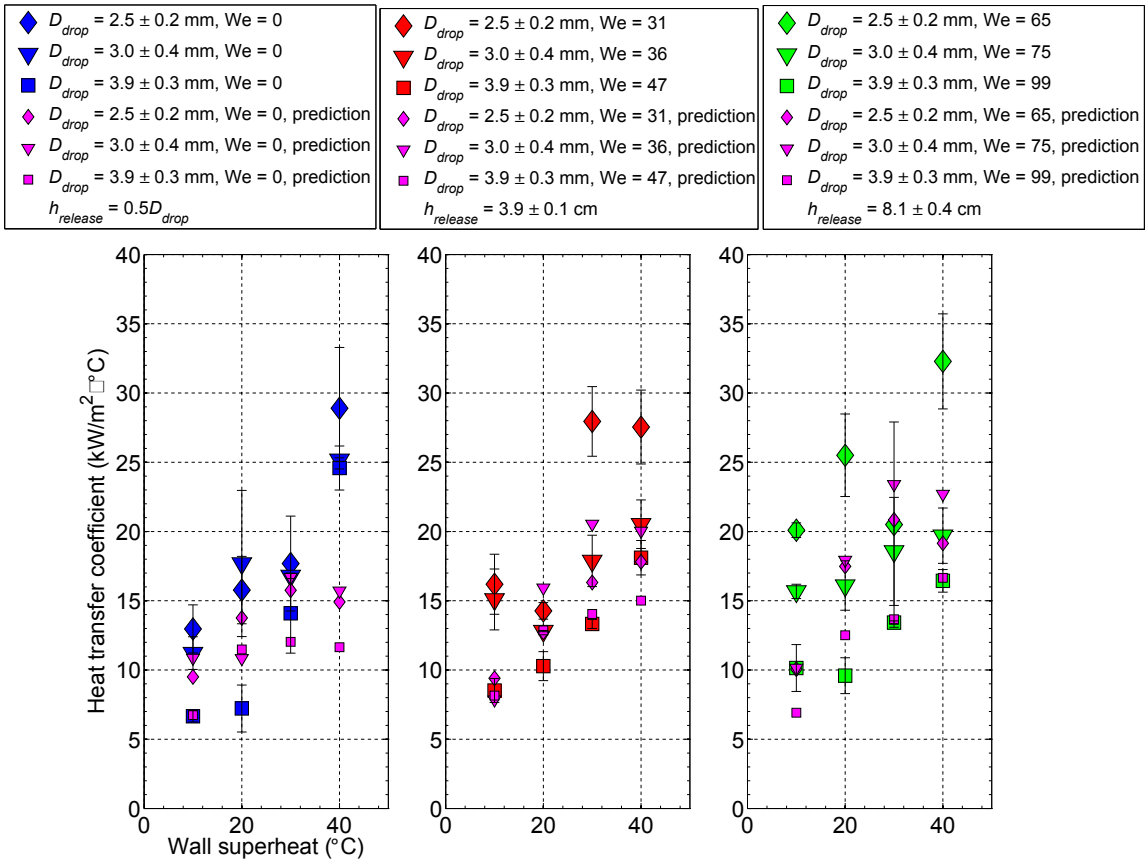

Figure F.1: Comparison between heat transfer coe cients that were calculated based on experimental measurements and heat transfer coe cients calculated from a heat conduction analysis for ZnO nanostructured surface generated by hydrothermal synthesis for 4 hours.

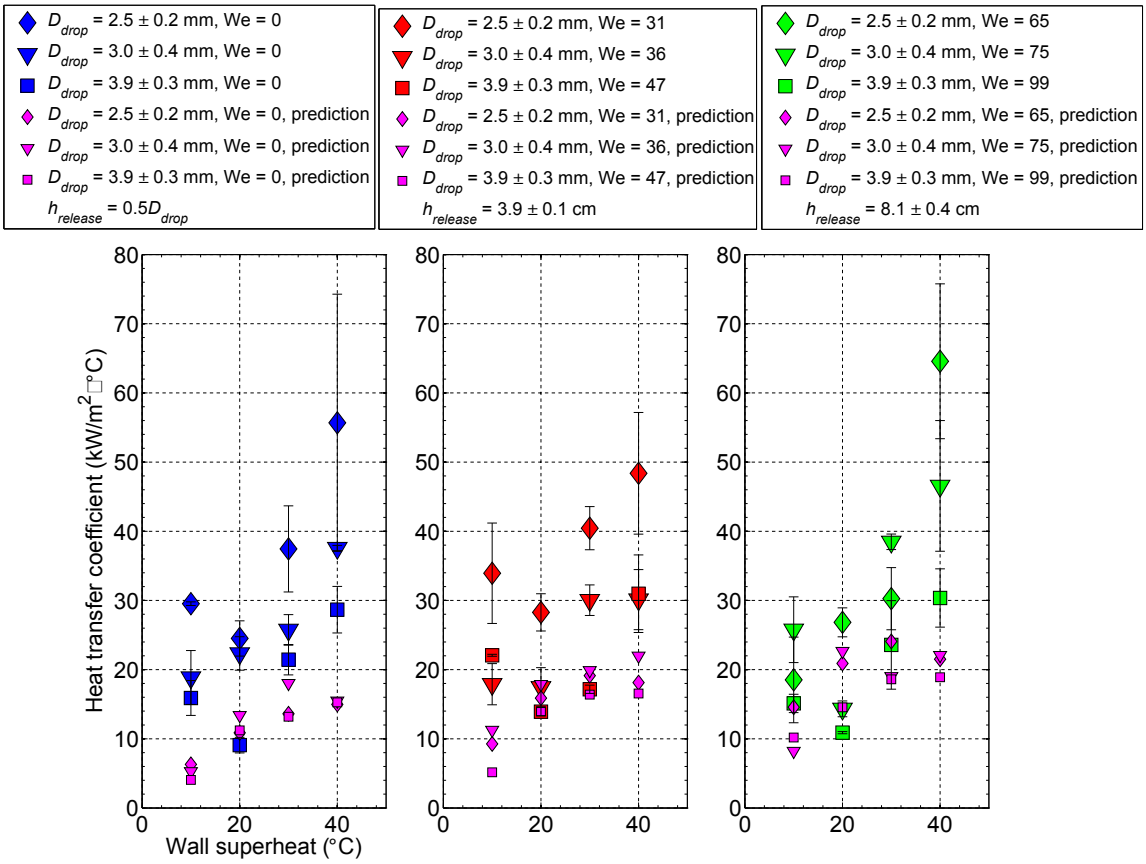

Figure F.2: Comparison between heat transfer coe cients that were calculated based on experimental measurements and heat transfer coe cients calculated from a heat conduction analysis for ZnO nanostructured surface generated by hydrothermal synthesis for 10 hours.

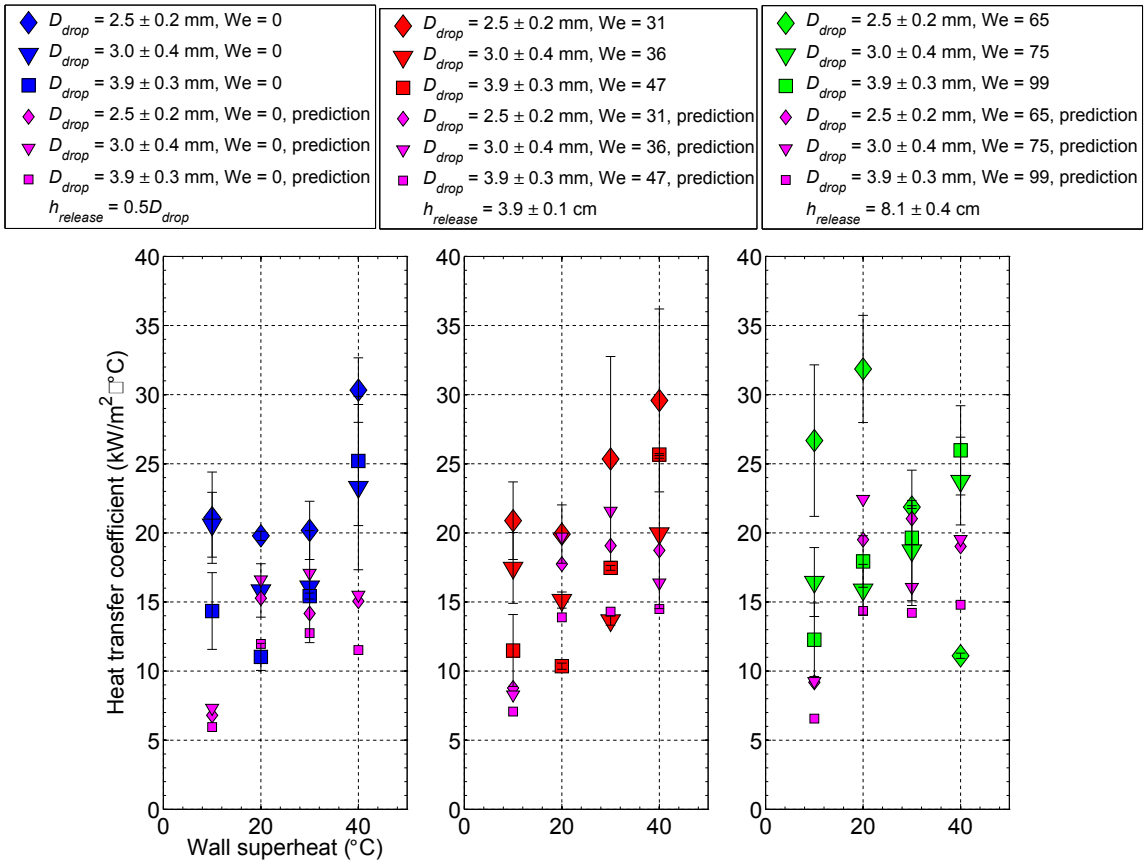

Figure F.3: Comparison between heat transfer coe cients that were calculated based on experimental measurements and heat transfer coe cients calculated from a heat conduction analysis for ZnO nanostructured surface generated by hydrothermal synthesis for 24 hours.

Bibliography

[1] V. P. Carey, *Liquid-vapor phase-change phenomena*, 2nd ed. Taylor & Francis, 2008.

[2] C. D. Stow and M. G. Had eld, \An experimental investigation of uid ow resulting from the impact of a water drop with an unyielding dry surface,"*Proc. R. Soc. London, Ser. A*, vol. 373, pp. 419{441, 1981.

[3] D. C. D.Roux and J. J. Cooper-White, \Dynamics of water spreading on a glass surface," *J. Colloid Interface Sci.*, vol. 277, no. 424, 2004.

[4] L. Wachters, H. Bonne, and H. Van Nouhuis, \The heat transfer from a horizontal plate to sessile water drops in the spheroidal state,"*Chemical Engineering Science*, vol. 21, pp. 923{936, 1966.

[5] A. L. Biance, F. Checy, C. Clanet, G. Lagubeau, and D. Quere, \On the elasticity of an inertial liquid shock," *Journal of Fluid Mechanics*, vol. 554, pp. 47{66, 2006.

[6] L. Wachters and N. Westerling, \The heat transfer from a hot wall to impinging water droplets in the spheroidal state," *Chemical Engineering Science*, vol. 21, pp. 1047{ 1056, 1966.

[7] A.-L. Biance, A.-L. Clanet, and D. Quere, \Leidenfrost drops,"*Physics of Fluids*, vol. 15, no. 6, pp. 1632{1637, 2003.

[8] C. Pedersen, \An experimental study of the dynamic behaviour and heat transfer characteristics of water droplets impinging upon a heated surface,"*Int. Journal of Heat and Mass Transfer*, vol. 13, 369{381, 1970.

[9] K. Okumura, F. Chevy, D. Richard, D. Quere, and C. Clanet, \Water spring: a model for bouncing drops," *Europhysics Letters*, vol. 62, p. 237, 2003.

[10] F. Harlow and J. Shannon, \The splash of a liquid droplet,"*Journal of Applied Physics*, vol. 38, p. 3855, 1697.

[11] D. v. Dam and C. L. Clerc, \Experimental study of the impact of an ink-jet printed droplet on a solid substrate,"*Phys. Fluids*, vol. 16, p. 3403, 2004.

[12] M. Gavaises, A. Theodorakakos, and G. Bergeles, \Modeling wall impaction of diesel sprays," *Int. J. Heat Fluid Flow*, vol. 17, p. 130, 1996.

[13] M. Fatchi and M. Kaviany, \Analysis of levitation of saturated liquid droplets on permeable surfaces,"*Int. J. Heat Mass Transfer*, vol. 33, pp. 983{994, 1990.

[14] W. Wirth, S. Storp, and W. Jacobsen, \Mechanisms controlling leaf retention of agricultural spray solutions," *Pestic. Sci.*, vol. 33, p. 411, 1991.

[15] S. Chandra and C. T. Avedisian, \On the collision of a droplet with a solid surface," *Proc. R. Soc. London*, vol. 432, p. 1341, 1991.

[16] S. Chandra and C. Avedisian, \Observations of droplet impingement on a ceramic porous surface,"*Int. J. Heat Mass Transfer*, vol. 35, pp. 3277{2388, 1992.

[17] V. Bergeron, D. Bonn, J. Y. Martin, and L. Vovelle, \Controlling droplet deposition with polymer additives," *Nature*, vol. 405, p. 772, 2000.

[18] A. L. Yarin, \Drop impact dynamics: splashing, spreading, receding, bouncing,"*Ann. Rev. Fluid Mech.*, vol. 38, p. 159, 2006.

[19] C. Josserand, L. Lemoyne, R. Troeger, and S. Zaleski, \Droplet impact on a dry surface: triggering the splash with a small obstacle,"*J. Fluid Mech.*, vol. 524, p. 47, 2005.

[20] L. Xu, W. W. Zhang, and S. R. Nagel, \Drop splashing on a dry smooth surface," *Phys. Rev. Lett.*, vol. 94, p. 184 505, 2005.

[21] I. V. Roisman, K. Horvat, and C. Tropea, \Spray impact: rim transverse instability initiating ngering and splash, and description of a secondary spray,"*Phys. Fluids*, vol. 18, p. 102 104, 2006.

[22] L. Xu, \Liquid drop splashing on smooth, rough, and textured surfaces,"*Phys. Rev. E*, vol. 75, p. 056 316, 2007.

[23] I. V. Roisman, E. Berberovic, and C. Tropea, \Inertia dominated drop collisions i. on the universal ow in the lamella," *Phys. Fluids*, vol. 21, p. 052 103, 2009.

[24] I. V. Roisman, \Inertia dominated drop collisions. ii. an analytical solution of the navierstokes equations for a spreading viscous lm,"*Phys. Fluids*, vol. 21, p. 052 104, 2009.

[25] R. D. Schroll, C. Josserand, S. Zaleski, and W. W. Zhang, \Impact of a viscous liquid drop," *Phys. Rev. Lett.*, vol. 104, p. 034 504, 2010.

[26] J. d. Ruiter, R. Pepper, and H. Stone, \Thickness of the rim of an expanding lamella near the splash threshold,"*Physics of Fluids*, vol. 22, p. 022 104, 2010.

[27] J. Bernardin and I. Mudawar, \The leidenfrost point: experimental study and assessment of existing models,"*Journal of Heat Transfer*, vol. 121, pp. 894{903, 1999.

[28] D. Quere, \Leidenfrost becomes a fakir,"*Nature Materials*, vol. 11, 2013.

[29] Y. Takata, S. Hidaka, J. Cao, T. Nakamura, H. Yamamoto, M. Masuda, and T. Ito, \E ect of surface wettability on boiling and evaporation," *Energy*, vol. 30, pp. 209{220, 2005.

[30] H. Kim, B. Truong, J. Buongiorno, and L. W. Hu, \On the e ect of surface roughness height, wettability, and nanoporosity on leidenfrost phenomena,"*Applied Physics Letters*, vol. 98, p. 083 121, 2011.

[31] C. Kruse, T. Anderson, C. Wilson, C. Zuhlke, D. Alexander, G. Gogos, and S. Ndao, \Extraordinary shifts of the leidenfrost temperature from multiscale micro/nanostructured surfaces,"*Langmuir*, vol. 29, pp. 9798{9806, 2013.

[32] N. Nagai and S. Nishio, \Leidenfrost temperature on an extremely smooth surface," *Experimental Thermal and Fluid Science*, vol. 12, pp. 373{379, 1996.

[33] P. Yang, H. Yan, S. Mao, R. Russo, J. Johnson, R. Saykally, N. Morris, J. Pham, R. He, and H. Choi, \Controlled growth of zno nanowires and their optical properties," *Advanced Functional Materials*, vol. 12, no. 5, pp. 323{331, 2002.

[34] D. Lee, T. Kim, S. Park, S. Lee, and S. Ko, \Zinc oxide nanowire forest for pool boiling heat transfer," *Japanese Journal of Applied Physics*, vol. 51, 2012.

[35] S. Ko, D. Lee, H. Kang, K. Ham, J. Yeo, S. Hong, C. Grigoropoulos, and H. Sung, \Nanoforest of hydrothermally grown hierarchical zno nanowires for a high e ciency dye-sensitized solar cell,"*Nano Letters*, vol. 11, pp. 666{671, 2011.

[36] D. Lee, \Zno nanostructure synthesis and laser direct writing process for optoelectronic devices," PhD thesis, University of California, Berkele, 2012.

[37] S. Ko, D. Lee, N. Hotz, J. Yeo, S. Hong, K. Nam, and C. Grigoropoulos, \Digital selective growth of zno nanowire arrays from inkjet-printed nanoparticle seeds on a exible substrate," *Langmuir*, vol. 28, pp. 4787{4792, 2012.

[38] S. Ko, I. Park, H. Pan, N. Misra, M. Rogers, C. Grigoropoulos, and A. Pisano, \Zno nanowire network transistor fabrication on a polymer substrate by low-temperature, all-inorganic nanoparticle solution process,"*Applied Physics Letters*, vol. 15, p. 154 102, 2008.

[39] I. Herman, J. Yeo, S. Hong, D. Lee, K. Nam, J. Choi, W. Hong, D. Lee, C. Grigoropoulos, and S. Ko, \Hierarchical weeping willow nano-tree growth and e ect of branching on dye-sensitized solar cell e ciency,"*Nanotechnology*, vol. 23, p. 194 005, 2012.

[40] M. Law, L. Greene, J. Johnson, R. Saykally, and P. Yang, \Nanowire dye-sensitized solar cells,"*Nature Materials*, pp. 455{459, 2005.

[41] L. Greene, M. Law, J. Goldberger, F. Kim, J. Johnson, Y. Zhang, R. Saykally, and P. Yang, \Low-temperature wafer-scale production of zno nanowire arrays,"*Angewandte Chemie International*, vol. 42, pp. 3031{3034, 2003.

[42] L. Greene, B. Yuhas, M. Law, D. Zitoun, and P. Yang, \Solution-grown zinc oxide nanowires,"*Inorganic Chemistry*, vol. 45, no. 19, pp. 7535{7543, 2006.

[43] M. Guo, P. Diaoc, and S. Caib, \Hydrothermal growth of well-aligned zno nanorod arrays: dependence of morphology and alignment ordering upon preparing conditions," *Journal of Solid State Chemistry*, vol. 178, pp. 1864{1873, 2005.

[44] C. Pacholski, A. Kornowski, and H. Weller, \Self-assembly of zno: from nanodots to nanorods,"*Angewandte Chemie International*, vol. 41, no. 7, pp. 1188{1191, 2002.

[45] A. Sugunan, H. Warad, M. Boman, and J. Dutta, \Zinc oxide nanowires in chemical bath on seeded substrates: role of hexamine," *Journal of Sol-Gel Science and Technology*, vol. 39, pp. 49{56, 2006.

[46] B. Sun and H. Sirringhaus, \Solution-processed zinc oxide eld-e ect transistors based on self-assembly of colloidal nanorods," *Nanoletters*, vol. 5, no. 12, pp. 2408{2413, 2005.

[47] L. Vayssieres, \Growth of arrayed nanorods and nanowires of zno from aqueous solutions," *Advanced Materials*, vol. 15, pp. 464{466, 2003.

[48] L. Vayssieres, K. Keis, L. S.E., and A. Hagfeldt, \Purpose-built anisotropic metal oxide material: 3d highly oriented microrod array of zno," *Journal of Physical Chemistry*, vol. 105, pp. 3350{3352, 2001.

[49] W. Wu, G. G. Hu, S. Cui, Y. Zhou, and H. Wu, \Epitaxy of vertical zno nanorod arrays on highly (001)-oriented zno seed monolayer by a hydrothermal route," *Crystal Growth and Design*, vol. 8, no. 11, pp. 4014{4020, 2008.

[50] Y. Zhou, W. Wu, G. Hu, H. Wu, and S. Cui, \Hydrothermal synthesis of zno nanorod arrays with the addition of polyethyleneimine," *Materials Research Bulletin*, vol. 43, pp. 2113{2118, 2008.

[51] W. Beek, M. Wienk, and R. Janssen, \E cient hybrid solar cells from zinc oxide nanoparticles and a conjugated polymer," *Advanced Materials*, vol. 16, no. 12, 2004.

[52] Z. H. Ibupoto, K. Khun, M. Eriksson, M. AlSalhi, M. Atif, A. Ansari, and M. Willander, \Hydrothermal growth of vertically aligned zno nanorods using a biocomposite seed layer of zno nanoparticles," *Materials*, vol. 6, no. 8, pp. 3584{3597, 2013.

[53] S. Talam, S. R. Karumuri, and N. Gunnam, \Synthesis, characterization, and spectroscopic properties of zno nanoparticles," *ISRN Nanotechnology*, vol. 2012, 2012.

[54] C. Fernando, L. De Silva, R. Mehra, and K Takahashi, \Junction e ects of p-cu2o photocathode with layers of hole transfer sites (au) and electron transfer sites (nio) at the electrolyte interface," *Semiconductor science and technology*, vol. 16, no. 6, p. 433, 2001.

[55] A. Rittermeier, S. Miao, M. K. Schroter, X. Zhang, M. W. van den Berg, S. Kundu, Y. Wang, S. Schimpf, E. Lo er, R. A. Fischer, *et al.*, \The formation of colloidal copper nanoparticles stabilized by zinc stearate: one-pot single-step synthesis and characterization of the core{shell particles," *Physical Chemistry Chemical Physics*, vol. 11, no. 37, pp. 8358{8366, 2009.

[56] S. Elzey, J. Baltrusaitis, S. Bian, and V. H. Grassian, \Formation of paratacamite nanomaterials via the conversion of aged and oxidized copper nanoparticles in hydrochloric acidic media," *Journal of Materials Chemistry*, vol. 21, no. 9, pp. 3162{3169, 2011.

[57] Z. Li, J. A. Larsson, P. Larsson, R. Ahuja, J. M. Tobin, J. OByrne, M. A. Morris, G. Attard, and J. D. Holmes, \Copper/molybdenum nanocomposite particles as catalysts for the growth of bamboo-structured carbon nanotubes," *The Journal of Physical Chemistry C*, vol. 112, no. 32, pp. 12 201{12 206, 2008.

[58] Q. bao Zhang, D. Xu, T. F. Hung, and K. Zhang, \Facile synthesis, growth mechanism and reversible superhydrophobic and superhydrophilic properties of non- aking cuo nanowires grown from porous copper substrates," *Nanotechnology*, vol. 24, no. 6, p. 065 602, 2013.

[59] M. d. C. A. d. Silva and S. J. G. d. Lima, \Evaluation of mechanical alloying to obtain cu-al-nb shape memory alloy," *Materials Research*, vol. 8, no. 2, pp. 169{172, 2005.

[60] S. Liu, B. Ma, M. Narayanan, S. Chao, R. Koritala, and U. Balachandran, \Improved properties of barium strontium titanate thin lms grown on copper foils by pulsed laser deposition using a self-bu ered layer," *Journal of Physics D: Applied Physics*, vol. 45, no. 17, p. 175 304, 2012.

[61] T. M. D. Dang, T. T. T. Le, E. Fribourg-Blanc, and M. C. Dang, \The in uence of solvents and surfactants on the preparation of copper nanoparticles by a chemical reduction method," *Advances in Natural Sciences: Nanoscience and Nanotechnology*, vol. 2, no. 2, p. 025 004, 2011.

[62] H. Morkoc and U. Ozgur, *Zinc oxide fundamentals, materials and device technology*, pp. 54{57, 2009.

[63] C. Ishino, M. Reyssat, E. Reyssat, K. Okumura, and D. Quere, \Wicking within forests of micropillars," *EPL (Europhysics Letters)*, vol. 79, no. 5, p. 56 005, 2007.

[64] E. W. Washburn, \The dynamics of capillary ow," *Physical review*, vol. 17, no. 3, p. 273, 1921.

[65] R. N. Wenzel, \Resistance of solid surfaces to wetting by water," *Industrial & Engineering Chemistry*, vol. 28, no. 8, pp. 988{994, 1936.

[66] A. Bar-Cohen, M. Arik, and M. Ohadi, \Direct liquid cooling of high ux micro and nano electronic components," *Proceedings of the IEEE*, vol. 94, no. 8, pp. 1549{1570, 2006.

[67] K. Stephan and M. Abdelsalam, \Heat-transfer correlations for natural convection boiling," *Int. J. Heat and Mass Transfer*, vol. 23, no. 1, pp. 73{87, 1980.

[68] V. P. Skripov, R. Kondor, and D. Slutzkin, *Metastable liquids*. Wiley New York, 1974.

[69] . J. Lienhard and A. Karimi, \Homogeneous nucleation and the spinodal line," *Journal of Heat Transfer*, vol. 103, no. 1, pp. 61{64, 1981.

[70] J. Lienhard, \Corresponding states correlations of the spinodal and homogeneous nucleation limits," *Journal of Heat Transfer*, vol. 104, no. 2, pp. 379{381, 1982.

[71] J. L. Plawsky, M. Ojha, A. Chatterjee, and P. C. Wayner Jr, \Review of the e ects of surface topography, surface chemistry, and uid physics on evaporation at the contact line," *Chemical Engineering Communications*, vol. 196, no. 5, pp. 658{696, 2008.

[72] S. J. Gokhale, J. L. Plawsky, and P. C. Wayner, \Spreading, evaporation, and contact line dynamics of surfactant-laden microdrops,"*Langmuir*, vol. 21, no. 18, pp. 8188{ 8197, 2005.

[73] J. Plawsky, A. Fedorov, S. Garimella, H. Ma, S. Maroo, L Chen, and Y Nam, \Nano- and microstructures for thin- lm evaporationa review," *Nanoscale and Microscale Thermophysical Engineering*, vol. 18, no. 3, pp. 251{269, 2014.

[74] C. Byon and S. J. Kim, \The e ect of meniscus on the permeability of micro-post arrays," *Journal of Micromechanics and Microengineering*, vol. 21, no. 11, p. 115 011, 2011.

[75] A. Jiao, R Riegler, H. Ma, and G. Peterson, \Thin lm evaporation e ect on heat transport capability in a grooved heat pipe," *Microfluidics and Nanofluidics*, vol. 1, no. 3, pp. 227{233, 2005.

[76] M. Leverett, \Capillary behavior in porous solids," *Trans. Am. Inst*, 1940.

[77] R. Ranjan, J. Y. Murthy, and S. V. Garimella, \A microscale model for thin- lm evaporation in capillary wick structures," *International Journal of Heat and Mass Transfer*, vol. 54, no. 1, pp. 169{179, 2011.

[78] N. C. Reis Jr, R. F. Gri ths, and J. M. Santos, \Parametric study of liquid droplets impinging on porous surfaces,"*Applied Mathematical Modelling*, vol. 32, no. 3, pp. 341{ 361, 2008.

[79] L. A. Richards, \Capillary conduction of liquids through porous mediums,"*Journal of Applied Physics*, vol. 1, no. 5, pp. 318{333, 2004.

[80] A. Rogacs, J. E. Steinbrenner, J. A. Rowlette, J. M. Weisse, X. L. Zheng, and K. E. Goodson, \Characterization of the wettability of thin nanostructured lms in the presence of evaporation,"*Journal of colloid and interface science*, vol. 349, no. 1, pp. 354{360, 2010.

[81] P. C. Wayner Jr, \Spreading of a liquid lm with a nite contact angle by the evaporation/condensation process,"*Langmuir*, vol. 9, no. 1, pp. 294{299, 1993.

[82] J. A. Weibel, S. V. Garimella, and M. T. North, \Characterization of evaporation and boiling from sintered powder wicks fed by capillary action,"*International Journal of Heat and Mass Transfer*, vol. 53, no. 19, pp. 4204{4215, 2010.